International Journal of
Applied Sciences and Smart Technologies

Volume 05, Issue 02, December 2023

Production and Characterization of Bio-Briquettes from Coconut Leaves and Cassava Peels
Gema Fitriyano, Ismiyati , Irfan Purnawan, Raihan Fajar Ramadhan

The Effectiveness of Exhaust Fan Rotation with Microcontroller for Indoor CO_2 Gas Concentration Control System
Sri Hartanto, Tri Ongko Priyono, Triono

Numerical Beamforming and Parametric Descriptions of Laguerre-Gaussian Vortex Beams
Dicky Januarizky Silitonga, Devia Gahana Cindi Alfian

Traditional Cultural Learning System for Batak Toba Wedding Using Multimedia Approach
Ridha Sefina Samosir, Varian Adriel

Analysis of Blasting Geometry on Blasting Production Results at PT Semen Bosowa Maros
Abdul Salam Munir, Nur Asmiani, Nurliah Jafar, Muhamad Hardin Wakila, Jihan Fitri Ramdita Putri Gouw

Cloud Quantum Coin-Tossing Gambling
Jose C. Moreno

Evolution of The Generalized Coordinates ofPendulum-Spring System
N. W. Rini, J. Saefan

Evaluation of The Current Level of Knowledge of The Residents of Dhaka City Regarding Earthquake Hazard
Saif Ahmed Santo, Akhi Sultana Fariha, Md. Rakib Hossain, Syed Emon Shah

A Deep Learning Model for Identical National Flag Recognition in Selected African Countries
Halleluyah Oluwatobi Aworinde, Oladosu Oladimeji, Segun Adebayo, Akinwale Akinwunmi, Aderonke B. Sakpere, Olayanju Oladimeji

A Detailed Review on The Denial of Service (DoS) and Distributed Denial of Service (DDoS) Attacks in Software Defined Networks (SDNs) and Defense Strategies
Elvis Tamakloe, Benjamin Kommey, Emmanuel Akowuah, Daniel Opoku

Resources Estimation of Laterite Nickel Using Ordinary Kriging Method at PT Mahkota Semesta Nikelindo District Wita Pond Morowali District
Alfian Nawir, Alam Budiman Thamsi, Harta Sanjaya, Muhammad Aswadi

Developing A Robot to Improve The Accuracy of Ring Retrieval And Throwing at The Abu Robocon Indonesia Robot Competition
Agus Siswoyo

Finitely Generated Simple Graphs
Burcu Nişancı Türkmen, Gülçin Karaca

Cultivation Investigation of Brazilian Spinach Through Indoor Hydroponic System
M. Prayadi Sulistyanto, Ronny Dwi Agusulistyo

Analysis of Spiral Pump Discharge Based on Simulation of Fluid Flow in Hoses
Hengky Luntungan, Stenly Tangkuman, I Nyoman Gede

p-ISSN 2655-8564 & e-ISSN 2685-9432

International Journal of Applied Sciences and Smart Technologies

Volume 5, Issue 2, page i-ii

p-ISSN 2655-8564, e-ISSN 2685-9432

CONTENTS

CONTENTS i

EDITORIAL BOARD iii

PREFACE iv

Production and Characterization of Bio-Briquettes from Coconut Leaves and Cassava Peels 145–156
Gema Fitriyano, Ismiyati, Irfan Purnawan and Raihan Fajar Ramadhan

The Effectiveness of Exhaust Fan Rotation with Microcontroller for Indoor CO2 Gas Concentration Control System 157–172
Sri Hartanto, Tri Ongko Priyono and Triono

Numerical Beamforming and Parametric Descriptions of Laguerre-Gaussian Vortex Beams 173–180
D. Silitonga and D. G. C. Alfian

Traditional Cultural Learning System for Batak Toba Wedding Using Multimedia Approach 181–194
Ridha Sefina Samosir and Varian Adriel

Analysis of Blasting Geometry on Blasting Production Results at PT Semen Bosowa Maros 195–212
Abdul Salam Munir, Nur Asmiani, Nurliah Jafar, Muhamad Hardin Wakila, Jihan Fitri Ramdita Putri Gouw

Cloud Quantum Coin-Tossing Gambling 213–228
Jose C. Moreno

Evolution of The Generalized Coordinates of Pendulum-Spring System 229–240
N. W. Rini and J. Saefan

Evaluation of The Current Level of Knowledge of The Residents of Dhaka City Regarding Earthquake Hazard 241–254
Saif Ahmed Santo, Akhi Sultana Fariha, Md. Rakib Hossain, Syed Emon Shah

A Deep Learning Model for Identical National Flag Recognition in Selected African Countries 255-270
Halleluyah Oluwatobi Aworinde, Oladosu Oladimeji, Segun Adebayo, Akinwale Akinwunmi, Aderonke B. Sakpere, Olayanju Oladimeji

International Journal of Applied Sciences and Smart Technologies

Volume 4, Issue 1, page i-ii

p-ISSN 2655-8564, e-ISSN 2685-9432

A Detailed Review on The Denial of Service (DoS) And Distributed Denial of Service (DDoS) Attacks in Software Defined Networks (SDNs) and Defense Strategies 271-302
Elvis Tamakloe, Benjamin Kommey , Emmanuel Akowuah, Daniel Opoku

Resources Estimation of Laterite Nickel Using Ordinary Kriging Method at PT Mahkota Semesta Nikelindo District Wita Pond Morowali District 303-314
Alfian Nawir, Alam Budiman Thamsi, Harta Sanjaya, Muhammad Aswadi

Developing A Robot to Improve The Accuracy of Ring Retrieval and Throwing at The ABU Robocon Indonesia Robot Competition 315-334
Agus Siswoyo

Finitely Generated Simple Graphs 335-344
*Burcu Nişancı Türkme*n, Gülçin Karaca

Cultivation investigation of Brazilian Spinach through Indoor Hydroponic System 345-354
M. Prayadi Sulistyanto and Ronny Dwi Agusulistyo

Analysis of Spiral Pump Discharge Based on Simulation of Fluid Flow in Hoses 355-364
Hengky Luntungan, Stenly Tangkuman, I Nyoman Gede

AUTHOR GUIDELINES 365-366

International Journal of Applied Sciences and Smart Technologies

Volume 5, Issue 2, page iii

p-ISSN 2655-8564, e-ISSN 2685-9432

EDITORIAL BOARD

Editor in Chief
Dr. I Made Wicaksana Ekaputra (Sanata Dharma University, Yogyakarta, Indonesia)
Email: made@usd.ac.id

Associate Editor
Dr. Pham Nhu Viet Ha (Vietnam Atomic Energy Institute, Hanoi, Vietnam)
Dr. Hendra Gunawan Harno (Gyeongsang National University, Jinju, The Republic of Korea)
Dr. Mukesh Jewariya (National Physical Laboratory, New Delhi, India)
Dr. Mongkolsery Lin (Institute of Technology of Cambodia, Phnom Penh, Cambodia)
Dr. Yohanes Baptista Lukiyanto (Sanata Dharma University, Yogyakarta, Indonesia)
Dr. Apichate Maneewong (Thailand Institute of Nuclear Technology, Bangkok, Thailand)
Prof. Dr. Sudi Mungkasi (Sanata Dharma University, Yogyakarta, Indonesia)
Dr. Pranowo (Universitas Atma Jaya Yogyakarta, Yogyakarta, Indonesia)
Dr. Monica Cahyaning Ratri (Sanata Dharma University, Yogyakarta, Indonesia)
Dr. Mahardhika Pratama (Nanyang Technological University, Singapore)
Prof. Dr. Leo Hari Wiryanto (Bandung Institute of Technology, Bandung, Indonesia)
Dr. Ranggo Tungga Dewa (Universitas Pertahanan, Bogor, Indonesia)

Editorial Assistant
Rosalia Arum Kumalasanti, M.T. (Sanata Dharma University, Yogyakarta, Indonesia)
Vittalis Ayu, M.Cs. (Sanata Dharma University, Yogyakarta, Indonesia)

Contact us
International Journal of Applied Sciences and Smart Technologies
Faculty of Science and Technology
Sanata Dharma University
Kampus III Paingan, Maguwoharjo, Depok, Sleman
Yogyakarta, 55282
Phone : +62 274883037 ext. 523110, 52320
Fax : +62 272886529
Email : editorial.ijasst@usd.ac.id
Website : http://e-journal.usd.ac.id/index.php/IJASST

IJASST is an open-access peer-reviewed journal that mediates the dissemination of research and studies conducted by academicians, researchers, and practitioners in science, engineering, and technology.

International Journal of Applied Sciences and Smart Technologies

Volume 5, Issue 2, page iv

p-ISSN 2655-8564, e-ISSN 2685-9432

PREFACE

Dear readers, we are delighted to serve you Volume 5, Issue 2 of International Journal of Applied Sciences and Smart Technologies (IJASST), which is managed and published by the Faculty of Science and Technology, Sanata Dharma University. IJASST is an open-access peer-reviewed journal that mediates the dissemination of research and studies conducted by academicians, researchers, and practitioners in science, engineering, and technology. Its scope also includes basic sciences which relate to technology, such as applied mathematics, physics, and chemistry.

In this edition, we have fifteen papers authored by researchers from Indonesia, Ghana, Nigeria, United State of America, Bangladesh, and Turkey. Submitted papers are reviewed fairly using the open journal system (OJS) of IJASST. After the review process, accepted papers of the journal are publicly available for free at the website of IJASST. For future issues, we are looking forward to your contributions to IJASST.

Dr. I Made Wicaksana Ekaputra
Editor in Chief
IJASST

International Journal of Applied Sciences and Smart Technologies

Volume 5, Issue 2, pages 145–156

p-ISSN 2655-8564, e-ISSN 2685-9432

Production and Characterization of Bio-Briquettes from Coconut Leaves and Cassava Peels

Gema Fitriyano [1, *], Ismiyati [1], Irfan Purnawan [1] and Raihan Fajar Ramadhan [1]

[1] Chemical Engineering Department, Universitas Muhammadiyah Jakarta, Jakarta, 10510, Indonesia.
[*]Corresponding Author: gema.fitriyano@umj.ac.id

(Received 19-12-2022; Revised 06-02-2023; Accepted 11-02-2023)

Abstract

Bio-briquettes from a mixture of coconut leaves charcoal and cassava peel charcoal have been produced and characterized in this study. The analysis carried out included density, burning rate, water content, ash content, and calorific value. Bio-briquette samples were produced with composition variations between coconut leaves charcoal and cassava peel charcoal with mass percentage ratios of 100:0, 75:25, 50:50, 25:75 and 0:100. The mixture used to produce briquettes with a ratio of tapioca flour, water and charcoal as raw materials is 1.5:1.5:2. The results of the study show that the density and calorific value of bio-briquettes increases with the increase in the amount of cassava peel in the briquette content. The optimum bio-briquette product from this research was found in variations of coconut leaves and cassava peel with a ratio of 75:25. The density is 0.96 g/ml, the burning rate is 0.190 g/min, the water content is 3%, the ash content is 18.81%, and the calorific value is 3521.47 Cal/g.

Keywords: bio-briquette, coconut leaves, cassava peels, bioenergy, biomass

1 Introduction

The potential for an energy crisis can be caused by various factors. Not only experienced by the least developed countries, but this condition also has the potential to occur in developed countries. In the least developed countries, it is easy to understand that there are many factors that cause energy crisis that these countries often face.

Developing countries have different potential causes of energy crisis, including dependence on technology, fuel prices and fuel supply. For example, in South America, there was an energy crisis caused by the unpreparedness of technology related to the lack

This work is licensed under a Creative Commons Attribution 4.0 International License

Volume 5, Issue 2, pages 145–156
p-ISSN 2655-8564, e-ISSN 2685-9432

of stored hydropower, which resulted in the length of construction of hydropower plants [1].

In developed countries, the occurrence of an energy crisis can be caused by a country's dependence on one type of energy source, as happened in several countries in Europe due to dependence on gas and not ready to transfer technology when a crisis occurs.

To overcome the energy crisis, research and development has been carried out on various types of energy sources including solar, wind, biomass, geothermal, tidal, and hydro. Problems with renewable energy include the high cost of technology and regulations that do not support its mass use [2].

The unpreparedness of technology transfer during a crisis makes it difficult to mitigate these problems. The use of non-fossil energy is still minimal in many countries, The portion of its production worldwide is around 20-30% of all energy production. This is also related to energy dependence and the difficulty of implementing technology transfer, so it becomes an obstacle in reducing the potential for an energy crisis [3], [4].

Technology in the production of non-fossil energy such as solar panels, vertical wind turbines, sea wave turbines which are still undergoing development cause the production costs to be relatively more expensive than some other alternative technologies such as waste-to-energy.

Energy technology from waste already existed and was operated in the early 1980s. But this technology was considered a failure because it has not been able to reduce the environmental impact of combustion in the form of residual solids and gases. This has caused this technology to disappear from the energy market, although its operation has the potential to be used in several pioneer industries that use waste energy, such as cement factories and coal-fired power plants [5].

The use of all types of waste that is directly burned using an incinerator to become heat energy does cause environmental pollution. It is because the combustion products contain various chemical elements because they do not come from one type of waste.

To overcome this, waste-to-energy technology has the potential to be used if it uses similar waste and is always produced. For example, waste from the agro industry which harvests every time. Agro-industrial waste that have the potential to become

Volume 5, Issue 2, pages 145–156
p-ISSN 2655-8564, e-ISSN 2685-9432

energy sources that have been studied previously are tuber peels, fruit peels, straw, husks, plant stems and leaf midribs [6].

Industrial waste through waste-to-energy technology can show potential as a non-fossil energy source, The use of this waste can be an alternative mitigation route when facing an energy crisis. Agro-industrial waste whose crops are harvested throughout the year is highly preferred. This is because it is able to ensure the availability of materials in a sustainable manner. Agro-industrial wastes included in this criterion include cassava peels and coconut leaf.

Cassava peel has been studied and has shown satisfactory characterization results, namely the calorific value of 5126 Cal/g with a mixture of 20% adhesive mass and 80% charcoal, where the adhesive is made from a mixture of water and tapioca flour with a ratio of 9:1 [7].

It is known that dried coconut leaves contain energy, so they are often used as a fire starter for bonfires. However, coconut leaves have not been widely studied regarding the use of energy as raw material for bio-briquette charcoal. The composition used in several previous studies provides a high calorific value but has a weakness, namely the bio-briquette product which is brittle when printed. This is because of the adhesive content that does not bind the entire charcoal mixture.

In this study, data were searched regarding the characteristics of bio-briquettes including density, burning rate, moisture content, ash content and calorific value of a mixture of coconut leaf charcoal and cassava peel charcoal. It is hoped that the results of this study will obtain a composition with optimum characteristics.

2 Research Methodology

The materials used in this study include coconut leaves charcoal, cassava peel charcoal, tapioca flour, and water. Coconut leaves that have fallen naturally are taken from coconut trees in the park. Cassava peel comes from traditional market waste, unbranded bulk tapioca flour and tap water is used. The equipment used includes digital balance, blender, plastic container, porcelain dish, cube briquette molds, oven, furnace and Leco AC600 calorimeter.

Volume 5, Issue 2, pages 145–156
p-ISSN 2655-8564, e-ISSN 2685-9432

The experimental stages consist of handling raw materials, making charcoal blending and molding bio-briquettes. The handling of coconut leaves is done by removing it from the midrib, reducing its size to about 20 cm to fit in the furnace. Meanwhile, the cassava peel is washed to clean it from impurities such as soil, then dried in the sun for a day to dry before being processed in the furnace.

After the material is ready, then the carbonization process is carried out using a furnace at temperatures of 400, 500, 600, 700 and 800^{o}C for 1 hour, which aims to determine the optimum temperature in the formation of charcoal.

After the process of forming charcoal with a furnace, each charcoal from coconut leaves and cassava peels is mashed using a blender separately. Mixing materials to produce bio-briquettes using variations in mass composition is shown in Table 1.

Table 1. Mass variation of bio-briquette composition

No	Ratio	TF (g)	W (g)	CL (g)	CP (g)
1	100:0	15	15	20	0
2	75:25	15	15	15	5
3	50:50	15	15	10	10
4	25:75	15	15	5	15
5	0:100	15	15	0	20

Annotation : **Ratio** is mass percentage ratio of coconut leaves charcoal and cassava peels charcoal, **TF** is tapioca flour, **W** is water, **CL** is coconut leaves charcoal, **CF** is cassava peel charcoal.

The bio-briquette sample molding process was carried out using a mold with hand pressure to produce a cube-shaped sample with dimensions of 2.5 cm x 2.5 cm x 2.5 cm. After the molding process is carried out, the sample is then dried in a room exposed to direct sunlight for 1 day so that the sample becomes hard and does not change its shape.

The analytical parameters tested on the sample include density, moisture content, ash content and calorific value. The density test is carried out by weighing the sample with dimensions 2.5 cm x 2.5 cm x 2.5 cm, then record the results of the weighing and calculate the density with the equation 1 [8], [9].

$$Density = \frac{briquette\ \ mass\ (g)}{briquette\ volume\ (cm^3)} \quad (1)$$

International Journal of Applied Sciences and Smart Technologies
Volume 5, Issue 2, pages 145–156
p-ISSN 2655-8564, e-ISSN 2685-9432

Water content analysis was carried out by weighing the sample and recording the initial mass, heating it in an oven at 115^{o}C for 3 hours. After the heating time is complete, then place the briquettes in a desiccator until the sample reaches room temperature, weigh the sample after it has room temperature, then record the weighing results and calculate the water content with equation 2.

$$Water\ content = \frac{initial\ mass - final\ mass}{initial\ mass} \times 100\% \quad (2)$$

Ash content analysis was carried out by weighing the sample and recording the initial mass, then placing the sample in a furnace at 800^{o}C for 2 hours. After the time is over, the sample is placed in a desiccator at room temperature. Weigh the sample after it reaches room temperature and record the mass of the weighing result, then calculate the ash content using equation 3 [10].

$$Ash\ content = \frac{final\ mass}{initial\ mass} \times 100\% \quad (3)$$

The method of calorie analysis with a calorimeter is done by putting the sample inside the combustion vessel, which is pressurized with oxygen. The sample is ignited and the temperature of the bucket and jacket water is measured by an electrical thermometer with a resolution of 0.0001 of a degree. A measurement of the water temperature inside the bucket and jacket is collected every second. Calorific values are determined by a simple maximum temperature rise of the bucket [11].

3 Results and Discussions

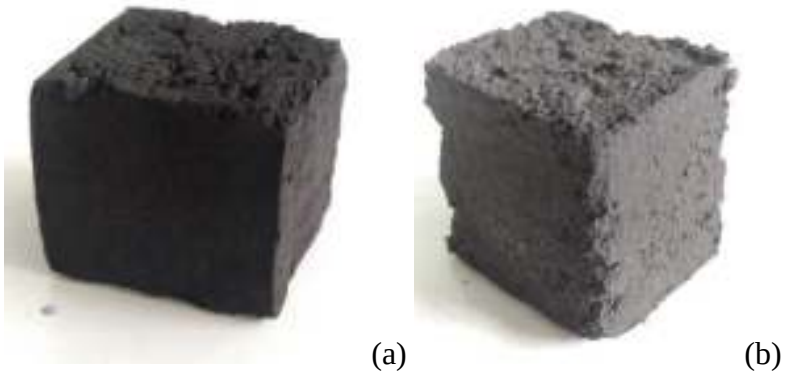
In the production of coconut leaf charcoal and cassava peel charcoal, temperature variations are carried out in the carbonization process at a temperature of 400 to 800^{o}C. The results showed that at a temperature of 400^{o}C the material was still in the form of black charcoal. There was a slight visible ash formed. Meanwhile, both coconut shells and banana peels turn into the form of completely gray ash at a temperature of 500, 600, 700 and 800^{o}C.

Based on the results of charcoal formation, a temperature of 400^{o}C was chosen to produce coconut leaf charcoal and cassava peel charcoal samples. Figure 1 shows the

Volume 5, Issue 2, pages 145–156

p-ISSN 2655-8564, e-ISSN 2685-9432

appearance of bio-briquettes produced from charcoal with a carbonization temperature of 400^{o}C compared to commercial bio-briquettes.



(a) (b)

Figure 1. The appearance of commercial bio-briquettes (a) and sample (b)

Based on its appearance, the commercial bio-briquettes look darker than the bio-briquettes samples from this study. This is due to the large amount of tapioca adhesive in the sample. Bio-briquette samples have been characterized to compare their properties with commercial sample properties, as shown in Table 2.

Table 2. Properties of bio-briquette made of coconut leaves and cassava peels compared to commercial sample

Parameter	Commercial sample properties	Mass percentage ratio of coconut leaves charcoal and cassava peels charcoal				
		100:0	**75:25**	**50:50**	**25:75**	**0:100**
Density (g/ml)	0.97	0.84	0.96	0.99	1.05	1.14
Burning rate (g/min)	0.136	0.307	0.190	0.357	0.441	0.318

The characteristics of the sample results from the study compared to commercial samples showed that the higher the content of cassava peel, the higher the density. The density value that is close to the value of the commercial sample is a ratio of 75:25 with a density of 0.96 g/ml and 50:50 of 0.99 g/ml.

International Journal of Applied Sciences and Smart Technologies

Volume 5, Issue 2, pages 145–156

p-ISSN 2655-8564, e-ISSN 2685-9432

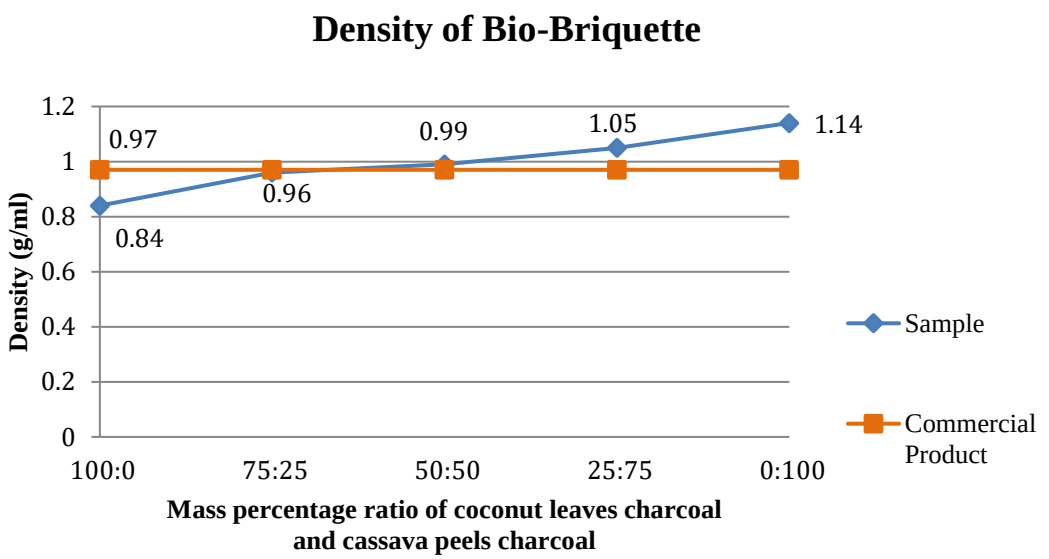


Figure 2. The effect of sample composition on density

The burning rate shows that the smaller the value, the longer the bio-briquette will burn. This is indicated by the commercial sample value as a reference of 0.136 g/min. Samples that are close to this value are in the composition of coconut leaves and cassava peels 75:25 with a burning rate of 0.190 g/min.

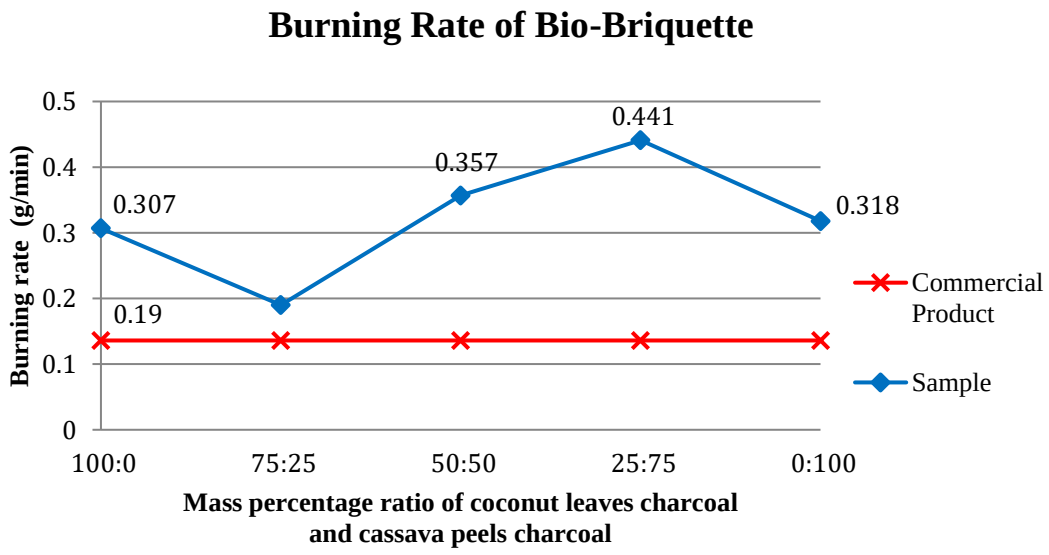


Figure 3. The effect of sample composition on burning rate

Volume 5, Issue 2, pages 145–156
p-ISSN 2655-8564, e-ISSN 2685-9432

The homogeneity and size distribution of the materials have an impact on the density of bio-briquettes. The density of a commercial bio-briquette has a value of 0.97 g/ml. If the density is greater than this value, it will require more raw materials for one piece of product [12]. The burning rate of a commercial bio-briquette has a value of 0.136 g/min. The higher the combustion rate, the faster the bio-briquette burn out. The lower the burning rate, the longer the bio-briquettes burn. Its impact on the increasing amount of heat generated.

So, for these two parameters, the sample with a mass percentage ratio of 75:25 gives the optimum analysis result. Further on Table 3, it shows bio-briquette samples properties compared with Indonesian national standards (SNI 01-6535-2000).

Table 3. Properties of bio-briquette made of coconut leaves and cassava peels compared to Indonesian national standards

Parameter	Indonesian national standard	Mass percentage ratio of coconut leaves charcoal and cassava peels charcoal				
		100:0	75:25	50:50	25:75	0:100
Water content (%)	8	11	3	3	3	3
Ash content (%)	8	18.01	18.81	18.32	19.35	17.02
Calorific value (Cal/g)	5000	3040.91	3521.47	3420.27	3199.28	3976.89

From Table 3, comparisons are made to the parameters water content, ash content, and calorific value. The results of the water content analysis show only samples with a ratio of 100:0 that do not meet the standards.

The ash content of the sample has a range of 17.03 to 18.81, where this value does not meet the standard. This can be caused by too much tapioca adhesive added in this study, which is around 40%. In several previous studies, the amount of tapioca that produced ash content values that met the standards was between 5 to 30% with an ash content range of 0.84% to around 6.42% [13]–[17].

Similar to the ash content, the calorific value of the bio-briquette sample did not meet the standard value. The optimum value obtained from the sample with a ratio of 0:100 is 3976.89 Cal/g. From several previous studies, bio-briquettes made from cassava peel charcoal have a fairly high calorific value, reaching 7669 Cal/g [16].

The second highest calorific value was obtained from the sample with a ratio of 75:25 of 3521.47 Cal/g. The lower calorific value than the standard is due to the low amount of charcoal used in this research sample, which is around 60%.

Samples with a ratio of 0:100 have a high calorific value but have a weakness, namely a high burning rate compared to commercial samples. This can cause the bio-briquettes to burn out quickly.

Suggestions for further research are to experiment with the amount of adhesive between 5 – 30% so that a higher calorific value and lower ash content can be obtained. It is also hoped that the durability analysis of the sample will be carried out so that the results of the analysis are more comprehensive.

4 Conclusions

In this study, bio-briquette production was carried out using coconut leaves and cassava peel as raw materials, where the two materials are included in the category of agro-industry waste, which has the potential as waste-to-energy. This research was conducted to determine the characteristics of bio-briquettes from coconut leaves and their mixture with cassava peel. The optimum bio-briquette product from this research was found in variations of coconut leaves and cassava peels with a ratio of 75:25. The density is 0.96 g/ml, the burning rate is 0.190 g/min, the water content is 3%, the ash content is 18.81%, and the calorific value is 3521.47 Cal/g.

Acknowledgements

The author would like to thank LPPM Universitas Muhammadiyah Jakarta as the provider of research and publication of research papers funds with contract number 324/R-UMJ/VI/2022 dated June 24th, 2022. And thanks to the Chemical Engineering Department UMJ as a place for conducting research.

References

[1] J. D. Hunt, D. Stilpen, and M. A. V. de Freitas, A Review of the Causes, Impacts and Solutions for Electricity Supply Crisis in Brazil, (2022).

Volume 5, Issue 2, pages 145–156

p-ISSN 2655-8564, e-ISSN 2685-9432

[2] O. Ellabban, H. Abu-Rub, and F. Blaabjerg, Renewable energy resources: Current status, future prospects and their enabling technology, Renew. Sustain. Energy Rev., 39 (2014) 748–764.

[3] D. Maradin, Advantages and Disadvantages of Renewable Energy Sources Utilization, Int. J. Energy Econ. Policy, 11(3) (2021) 176–183.

[4] International Energy Agency, Global Energy Review 2020 Renewables, (2020).

[5] K. E. Lorber and A. Ragoßnig, Solid recovered fuels 2.0 – 'what's new?', Waste Manag. Res., 30 (4) (2012) 333– 334.

[6] P. K. Sadh, S. Duhan, and J. S. Duhan, Agro-industrial wastes and their utilization using solid state fermentation: a review, Bioresour. Bioprocess, 5 (1) (2018) 15.

[7] F. E. Hirniah, Analisis Energi dalam Pembuatan Briket Arang dari Kulit Singkong dengan Tepung Tapioka Sebagai Perekat, Jember, (2020).

[8] O.A. Oyelaran, O. Balogun, A.O. Ambali, and J. K. Abidoye, Characterization of Briquette Produced from Tannery Solid Waste, J. Mater. Eng. Struct., 4 (2017) 79–86.

[9] S. Anggraeni, S. N. Hofifah, A. B. D. Nandiyanto, And M. R. Bilad, Effects Of Particle Size And Composition Of Cassava Peels And Rice Husk On The Briquette Performance, J. Eng. Sci. Technol., 16 (1) (2021) 527–542.

[10] BSN, SNI 01-6235-2000 tentang Briket Arang Kayu. Badan Standar Nasional, Jakarta, (2000) 8.

[11] Leco, AC600 Isoperibol Calorimeter. Semi-Automatic Gross Calorific Content Analyzer, (2022). [Online]. Available: https://www.leco.com/product/ac600. [Accessed: 09-Sep-2022].

[12] D Nurba, M Yasar, Mustaqimah, R. Fadhil, S P Sari, and C V Mysa, Performance of Corncobs and Wood Charcoal Briquette as Heat Energy Sources in In-Store Dryer, IOP Conference Series: Earth and Environmental Science 365 (2019) 1–10.

[13] Ropiudin and K. Syska, Analisis Kualitas Biobriket Karbonisasi Tempurung Kelapa dan Kulit Singkong dengan Perekat Tepung Singkong, J. Agric. Biosyst. Eng. Res., 3 (1) (2022) 19–38.

[14] F. T. Aprilia, The Use of Sengon (Albizia Chinensis) Wood and Cassava Peel in Making Briquettes, Politeknik Negeri Jember, Jember, (2022).

Volume 5, Issue 2, pages 145–156

p-ISSN 2655-8564, e-ISSN 2685-9432

[15] J. T. Oladeji and O. R. Oyetunji, Investigations into Physical and Fuel Characteristics of Briquettes Produced from Cassava and Yam Peels, J. Energy Technol. Policy, 3 (7) (2013) 40–46.

[16] U. E. Terhider and O. E. Ediba, Investigation of The Combustion Characteristics of Briquettes Produced from Cassava Peels, Mango Nuts and Orange Peels, Int. Res. J. Mod. Eng. Technol. Sci., 3 (10) (2021) 736–742.

[17] L. Rumiyanti, A. Irnanda, and Y. Hendronursito, Analisis Proksimat pada Briket Arang Limbah Pertanian, J. Fis. dan Apl., 3 (1) (2018) 15–22.

International Journal of Applied Sciences and Smart Technologies

Volume 5, Issue 2, pages 145–156

p-ISSN 2655-8564, e-ISSN 2685-9432

This page intentionally left blank

International Journal of Applied Sciences and Smart Technologies

Volume 5, Issue 2, pages 157-172

p-ISSN 2655-8564, e-ISSN 2685-9432

The Effectiveness of Exhaust Fan Rotation with Microcontroller for Indoor CO_2 Gas Concentration Control System

Sri Hartanto[1, *], Tri Ongko Priyono[1] and Triono[2]

[1]Department of Electrical Engineering, Universitas Krisnadwipayana, Jakarta, Indonesia

[2]Research and Development Department, PT Delamita Bilano, Jakarta, Indonesia

[*]Corresponding Author: srihartanto@unkris.ac.id

(Received 09-02-2023; Revised 26-02-2023; Accepted 27-02-2023)

Abstract

A dangerous gas that is harmful to human health and is generally found in the room is carbon dioxide (CO_2) gas, which is produced from the accumulation of cigarette smoke. In order to overcome the CO_2 gas concentration in the room, it is necessary to develop a device that can control the CO_2 gas concentration in the room and that processes the CO_2 gas detection results from the MQ-2 sensor. In this research, a device simulation was created that can control the CO_2 gas concentration produced by accumulated cigarette smoke in a simulation room measuring 15 cm long, 20 cm wide, and 15 cm high with two CO_2 gas release ventilation holes, each with a diameter of 3.5 cm, using the exhaust fan rotation and a microcontroller type Arduino UNO as the control unit. The effectiveness of using a microcontroller of the type Arduino UNO to process the CO_2 gas detection results from the MQ-2 sensor can be seen in how the exhaust fan works to release CO_2 gas from the simulation room. From the results of this research, it can be seen that the effectiveness of the exhaust fan rotation in controlling the CO_2 gas concentration detected by the MQ-2 sensor looks good where the CO_2 gas concentration can be controlled under 350 ppm.

Keywords: CO_2 gas; cigarette smoke; microcontroller; exhaust fan rotation, MQ-2 sensor

1 Introduction

The health of people is impacted by air quality. Cigarette smoke is one of the many elements that can lower air quality [1]. The primary component of cigarette smoke is a particle that is less than 1 micron in size, and it could even be as small as 0.1 micron [2]. The smoke inhalation cycle follows a recognizable rhythm that includes a puff, smoke inhalation, and smoke expiration [3].

This work is licensed under a Creative Commons Attribution 4.0 International License

Volume 5, Issue 2, pages 157-172
p-ISSN 2655-8564, e-ISSN 2685-9432

IoT becomes a utility as sensing, actuation, communications, control, and knowledge extraction from massive amounts of data grow more sophisticated [4]. Data will be gathered, exchanged, and analyzed by IoT to get important knowledge about the interactions between things [5, 6]. The IoT's fundamental components include sensors and actuators [7, 8] to control systems [9]. The control unit shows the smoke unit in the display area receives a signal from the smoke detector when it detects smoke within the house [10]. One sensor that can find CO_2 gas is the MQ series gas sensor [11]. MQ-2 was chosen because, in addition to its high sensitivity, it is inexpensive and suitable for a wide range of applications [12]. The MQ-2 gas sensor has the ability to detect gas leakage such as LPG, i-butane, methane, alcohol, hydrogen, smoke, etc. [13]. The gas sensor will be configured via Open CR like a microcontroller of the type Arduino UNO [14]. The microcontroller of the type Arduino UNO program was created utilizing this smoke sensor input to determine the presence of cigarette smoke [15]. The microcontroller of the type Arduino UNO serves as the controller and signal processor for the MQ-2 sensor that detects cigarette smoke [16, 17].

Therefore, in this research, a device simulation was created that can control the CO_2 gas concentration produced by accumulated cigarette smoke in the room using the exhaust fan rotation and a microcontroller type Arduino UNO as the control unit. The indoor CO_2 gas control system is simulated in the room measuring 15 cm long, 20 cm wide, and 15 cm high with two CO_2 gas release ventilation holes, each with a diameter of 3.5 cm, wherein the CO_2 gas concentration from cigarette smoke is gradually increased by lighting one to five cigarettes. This research is expected to determine the effectiveness of exhaust fan rotation in controlling the CO_2 gas concentration detected by the MQ-2 sensor.

2 Research Methodology

This research was conducted in several phases, as seen in Figure 1, as follows:

International Journal of Applied Sciences and Smart Technologies

Volume 5, Issue 2, pages 157-172

p-ISSN 2655-8564, e-ISSN 2685-9432

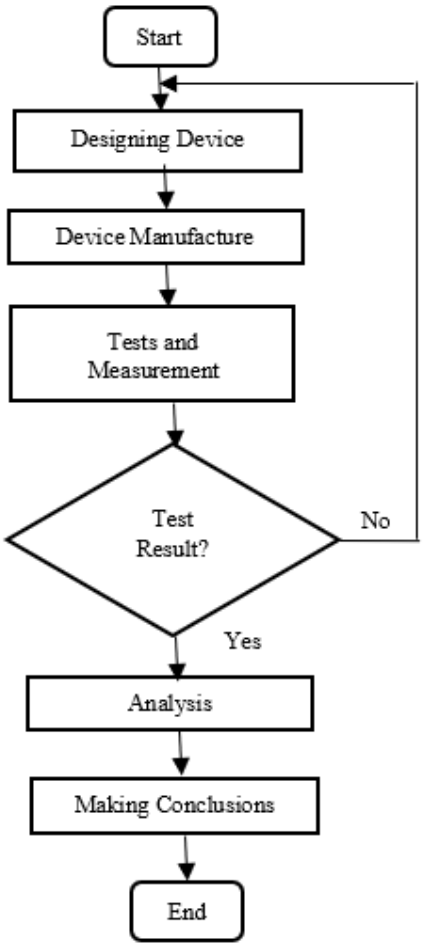


Figure 1. Flowchart of Research Method

The method used in this research refers to a sequential algorithm, where the research steps are carried out sequentially [18, 19, 20]. The research begins by collecting data on the components that make up the device used to examine controlling system the CO_2 gas concentration to detect cigarette smoke in a room. In this step, the research was carried out by designing an indoor CO_2 gas concentration control circuit with the MQ-2 sensor using QElectroTech software, which was then controlled by the microcontroller of the type Arduino UNO version 1.6.11 microcontroller and issued an electrical voltage used to drive the exhaust fan and display a warning on the LCD display screen. The block diagram of the indoor CO_2 gas concentration control circuit design is shown in Figure 2. Then, those processing results are used to adjust the exhaust fan rotation.

International Journal of Applied Sciences and Smart Technologies
Volume 5, Issue 2, pages 157-172
p-ISSN 2655-8564, e-ISSN 2685-9432

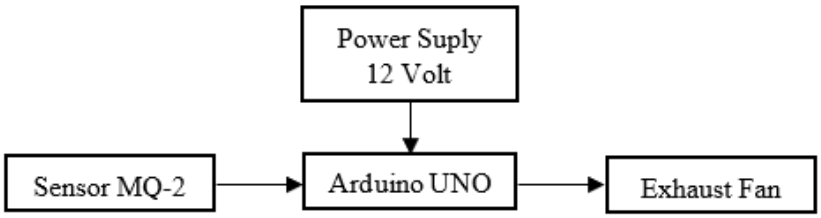


Figure 2. Circuit Block Diagram

The design of an indoor CO_2 gas control system consists of two steps, namely the design of the electronic circuit (hardware) and the design of the microcontroller program (software). The design of an electronic circuit for controlling CO_2 gas in a room using the MQ-2 sensor and exhaust fan rotation made using the QElectroTech software is shown in Figure 3. The MQ-2 sensor [21, 22, 23] will send a signal to the microcontroller of the type Arduino UNO via pin A0, when the MQ-2 sensor detects cigarette smoke. The data from the MQ-2 sensor is then processed by the microcontroller of the type Arduino UNO. When the microcontroller of the type Arduino UNO processes, the voltage data from the MQ-2 sensor is transmitted to pin A0. The results of data processing will be displayed on the LCD and run the exhaust fan at medium and high conditions. As a display of smoke conditions, the LCD display will display the specified conditions. As shown in Figure 3, to display smoke conditions on the LCD using pins 12, 11, 10, 9, 8, 7 of a microcontroller of the type Arduino UNO. The LED connected to pins 4, 5, 6 of a microcontroller of the type Arduino UNO will turn on according to the conditions that have been determined. The exhaust fan rotation release smoke to the outer room.

International Journal of Applied Sciences and Smart Technologies

Volume 5, Issue 2, pages 157-172

p-ISSN 2655-8564, e-ISSN 2685-9432

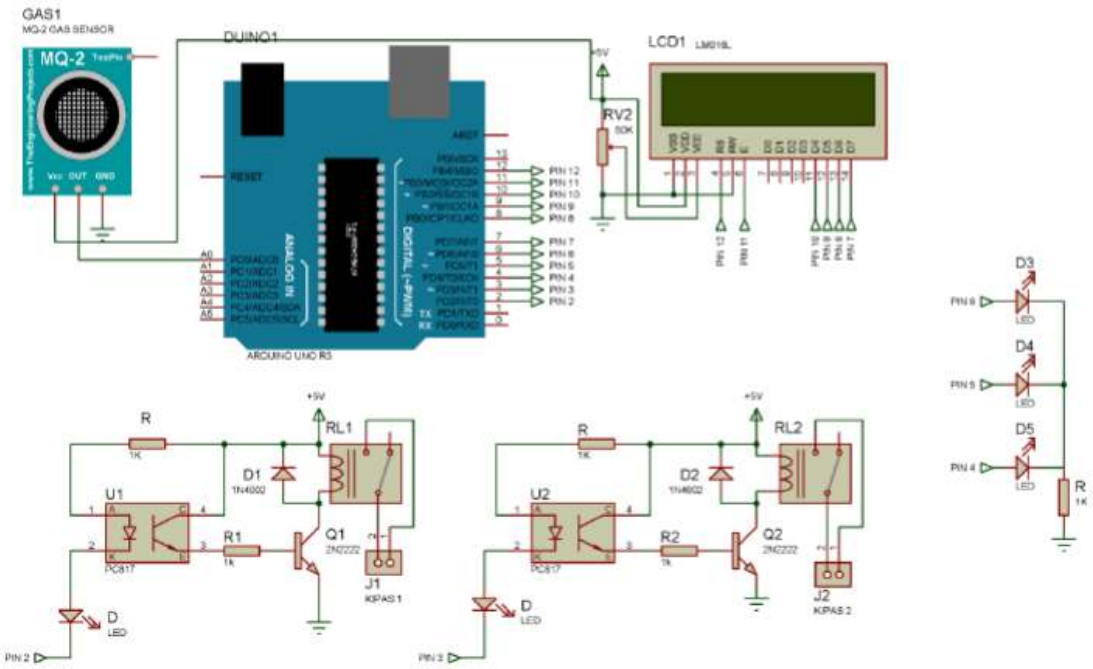


Figure 3. Electronic Circuit Design

In the device manufacture step, the layout of the PCB [26] for the design of an electronic indoor CO_2 gas concentration control device is made in accordance with the component diagram contained in the electronic indoor CO_2 gas concentration control circuit, which includes the constituent components that connect the MQ-2 sensor, the microcontroller of the type Arduino UNO circuit, and an output device in the form of an LCD display panel and an exhaust fan. The circuit that has been made is then put into a simulation room made of mica with a length x width x height of 15 cm x 20 cm x 15 cm. Finally, the microcontroller of the type Arduino UNO is programmed using the microcontroller of the type Arduino UNO IDE software version 1.6.11 [24, 25]. The embodiment of the electronic circuit design for indoor CO_2 gas concentration control device can be seen in Figure 4.

In the tests and measurement step, the MQ-2 sensor-equipped indoor CO_2 gas concentration control device is tested, and its output is controled and measured using a measuring device such as a multimeter. Cigarettes, from one to five that are burned simultaneously, are burned in order to measure the operation of the MQ-2 sensor and

Volume 5, Issue 2, pages 157-172
p-ISSN 2655-8564, e-ISSN 2685-9432

exhaust fan. The output on the LCD is then scrutinized to ascertain the MQ-2 sensor's sensitivity to detecting cigarette smoke. The exhaust fan's inlet and outlet voltage were then controled to determine how well it worked to clear the room of cigarette smoke.



Figure 4. Indoor CO_2 Gas Concentration Control Device

In the analysis step, from the results of observations and performance measurements of the indoor CO_2 gas concentration control device with the MQ-2 sensor, it is analyzed to know the effectiveness of exhaust fan rotation in controlling the CO_2 gas concentration detected by the MQ-2 sensor.

In the final step, conclusions are made from the analysis of performance measurements of the indoor CO_2 gas concentration control device with the MQ-2 sensor.

3 Results and Discussions

The process of detecting smoke using the MQ-2 sensor which is shown in Figure 5. First, the device is turned on. The next step is initialization, which involves checking the readiness of the program and device system circuits. Furthermore, the MQ-2 sensor detects cigarette smoke, which is then transmitted to the Arduino UNO microcontroller for processing and sends an output signal to the output devices, LCD screen, LED light, and the exhaust fan. When the MQ-2 sensor output is less than 1 volt (< 1 V), the Arduino

Volume 5, Issue 2, pages 157-172

p-ISSN 2655-8564, e-ISSN 2685-9432

UNO microcontroller will turn on the green LED light and LCD Display shows "Low". When the MQ-2 sensor output is greater than 1 volt and less than 3 volt (1 V < MQ-2 sensor output < 3 V), the Arduino UNO microcontroller will turn off the green LED light, turn on the yellow LED light, turn on the exhaust fan 1 and LCD Display shows "Medium". When the MQ-2 sensor output is greater than 3 volt (> 3 V), the Arduino UNO microcontroller will turn off the yellow LED light, turn on the red LED light, turn on the exhaust fan 1 and 2 and LCD Display shows "High" (in this condition, both the exhaust fan will turn on).

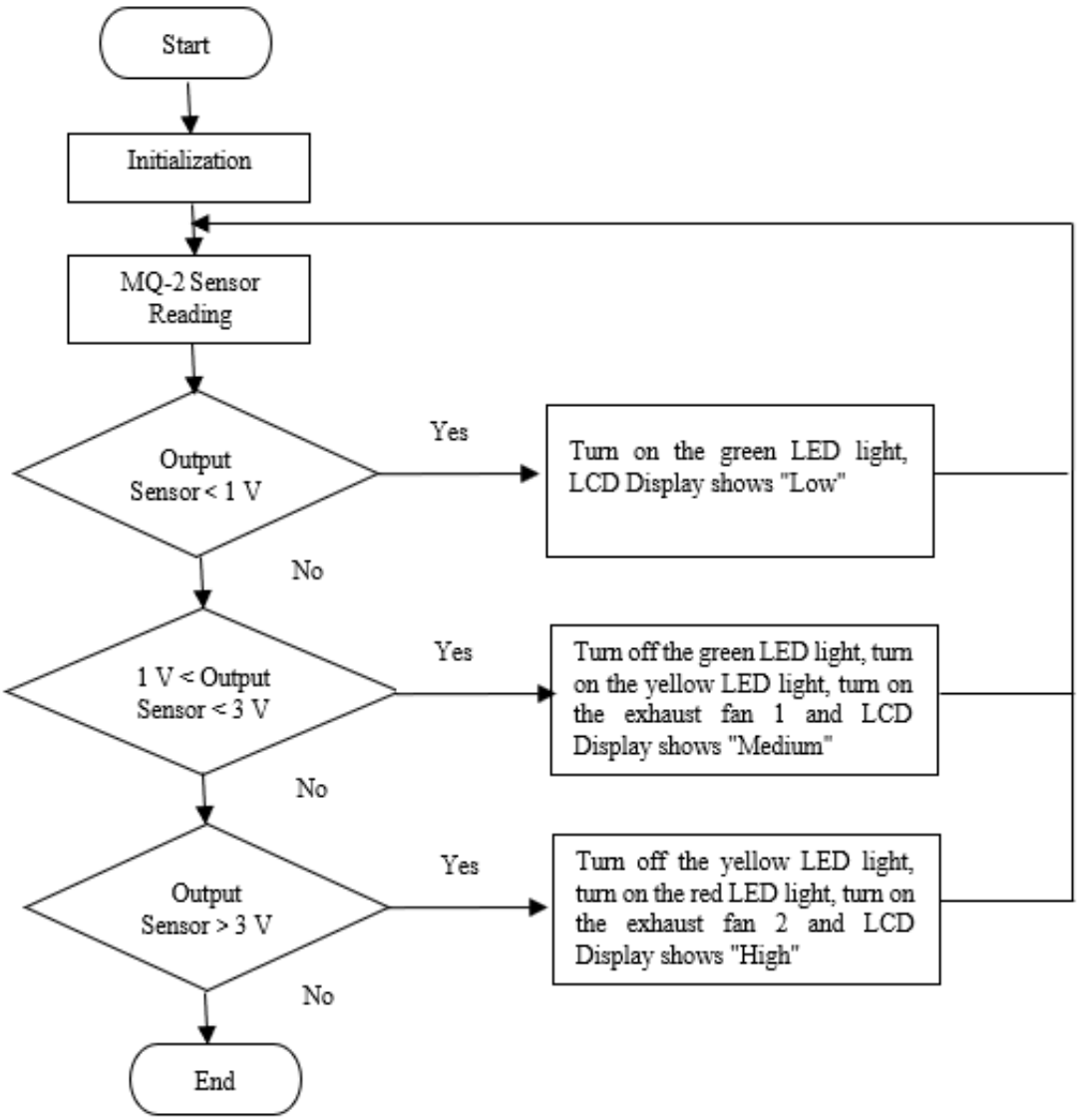


Figure 5. Process of Detecting Smoke Using the MQ-2 Sensor

Volume 5, Issue 2, pages 157-172
p-ISSN 2655-8564, e-ISSN 2685-9432

Overall circuit testing in the design of this device as shown in Figure 6 ensure the equipment functions as designed. First, testing the whole circuit starts with the MQ-2 sensor sending a signal to the microcontroller if it detects smoke. When the Arduino UNO microcontroller gets a signal from the MQ-2 smoke sensor, it will process the program and send signals to the LEDs and relays. The relay will connect the exhaust fan to the electric current so that the exhaust fan rotates when the Arduino UNO microcontroller sends a low, medium, or high condition signal. The LED will turn on when it gets a signal from the microcontroller. The LCD will display the voltage value from the MQ-2 smoke sensor and the condition if it gets a signal from the Arduino UNO microcontroller.



Figure 6. Indoor CO_2 Gas Control System Test

The sequence of steps for the LED lighting condition described as follows. The first step of testing a cigarette smoke detection device is to burn one cigarette with a length of 80 mm and a diameter of 7 mm, which is placed on an ashtray and put into the simulation room. At the beginning of the experiment, before the sixth minute, the LED lights off and the LCD display does not display smoke condition information. In the sixth minute, the green LED lights up and the LCD display displays "Low". At the tenth minute, the green LED is off, the yellow LED is on, the LCD display displays "Medium" and the left exhaust fan is on.

In the second experiment, two cigarettes were burned, then placed on an ashtray and put into the simulation room. At the beginning of the experiment, before the fourth

Volume 5, Issue 2, pages 157-172
p-ISSN 2655-8564, e-ISSN 2685-9432

minute, the LED lights off and the LCD display does not display smoke condition information. In the fourth minute, the green LED lights up and the LCD display displays "Low". At the seventh minute, the green LED is off, the yellow LED is on, the LCD display displays "Medium" and the left exhaust fan is on. In the twelfth minute, the yellow LED light is off, the red LED is on, the LCD display displays "High" and both exhaust fan are on.

In the third experiment, three cigarettes were burned, then placed on an ashtray and put into the simulation room. At the beginning of the experiment, before the third minute, the LED lights off and the LCD display does not display smoke condition information. In the third minute, the green LED lights up and the LCD display displays "Low". In the fifth minute, the green LED is off, the yellow LED is on, the LCD display displays "Medium" and the left exhaust fan is on. In the eighth minute, the yellow LED light is off, the red LED is on, the LCD display displays "High" and both exhaust fan are on.

In the fourth experiment, four cigarettes were burned, then placed on an ashtray and put into the simulation room. At the beginning of the experiment, before the second minute, the LED lights off and the LCD display does not display smoke condition information. In the second minute, the green LED lights up and the LCD display displays "Low". In the third minute, the green LED is off, the yellow LED is on, the LCD display displays "Medium" and the left exhaust fan is on. In the fifth minute, the yellow LED is off, the red LED is on, the LCD display displays "High" and both exhaust fan are on.

In the fifth experiment, five cigarettes were burned, then placed on an ashtray and put into the simulation room. At the beginning of the experiment, before the first minute, the LED lights off and the LCD display does not display smoke condition information. In the first minute, the green LED lights up and the LCD display displays "Low". In the second minute, the yellow LED light is on, the LCD display displays "Medium" and the left exhaust fan is on. In the third minute, the yellow LED is off, the red LED is on, the LCD display displays "High" and both exhaust fan are on.

In the five experiments conducted, the performance of the CO_2 gas concentration control system controlled by the Arduino UNO microcontroller can be analyzed through the output displayed by the LCD screen, LED light, and exhaust fan. The analysis is based

Volume 5, Issue 2, pages 157-172
p-ISSN 2655-8564, e-ISSN 2685-9432

on measuring the voltage at the output electrode of the MQ-2 sensor. With the increase in the amount of cigarette smoke in a simulation room measuring length x width x height of 15 cm x 20 cm x 15 cm, which is provided with a ventilation hole of 3.5 cm in diameter, the output voltage of the MQ-2 sensor is increasing, which is indicated by a higher voltage value. The Arduino UNO microcontroller turns on the LED light, with the green color indicating low smoke concentration in the simulation room, the yellow indicating medium smoke concentration in the simulation room, and the red indicating high smoke concentration in the simulation room. In addition, the voltage value given by the MQ-2 sensor to the Arduino UNO microcontroller can make the Arduino UNO microcontroller process the display on the LCD display according to the smoke conditions in the simulation room, which displays "Low" information for low smoke concentration in the simulation room, "Medium" information for the smoke concentration currently in the simulation room, and "High" information for high smoke concentration in the simulation room. In addition to the LCD display, the voltage value given by the MQ-2 sensor to the Arduino UNO microcontroller can make the Arduino UNO microcontroller able to turn on one exhaust fan in the condition when the simulation room is quite thick with smoke, which is generally indicated by the green light off and the yellow light on, and turn on the two exhaust fan in the condition when the simulation room is very thick with smoke, which is generally indicated by the yellow light off and the red light on.

The measurement results on the Arduino UNO microcontroller pin A0 connected to the MQ-2 sensor are shown in Table 1. Measurement of the output voltage of the MQ-2 sensor using a multimeter connected to the Arduino UNO microcontroller's A0 pin, where previously the Arduino UNO microcontroller's A0 pin was extended through the use of a conductor rod soldered to the Arduino UNO microcontroller's A0 pin and extended (approximately 25 cm) to the output through ventilation holes that can make it easier for the multimeter pin to be connected to carry out voltage measurements, resulting in changes in voltage values as the smoke concentration increases in the simulation room. Based on the measurement results, it was found that the smallest voltage value that can be measured is 300 millivolt in Experiment 1 when one cigarette is burned to the sixth minute, and the largest voltage value that can be measured is 3620 millivolt in Experiment 5 when five cigarettes are burned to the fifteenth minute. Based on the MQ-2 sensor

Volume 5, Issue 2, pages 157-172
p-ISSN 2655-8564, e-ISSN 2685-9432

datasheet, the maximum voltage value of which is 5.0 V ± 0.1 V, the test in this research has not yet reached the maximum output voltage of the MQ-2 sensor, which can still be tolerated.

Table 1. MQ-2 Sensor Output Voltage

Time (in minutes)	Vout MQ-2 Experiment 1 (in mV)	Vout MQ-2 Experiment 2 (in mV)	Vout MQ-2 Experiment 3 (in mV)	Vout MQ-2 Experiment 4 (in mV)	Vout MQ-2 Experiment 5 (in mV)
1	0	0	0	0	900
2	0	0	0	900	1300
3	0	0	560	1200	2600
4	0	320	750	2700	3120
5	0	460	1210	3080	3140
6	300	870	2300	3120	3190
7	450	1140	2350	3220	3230
8	630	1220	3140	3310	3250
9	860	1910	3220	3360	3290
10	1230	2320	3340	3380	3340
11	1560	2720	3350	3420	3420
12	1780	3140	3380	3440	3450
13	1820	3230	3400	3460	3480
14	1850	3360	3420	3480	3500
15	1910	3410	3440	3490	3620

The voltage measurement in Experiment 1 resulted in the smallest voltage value above 0 millivolt of 300 millivolt in the sixth minute and the largest voltage of 1910 millivolt in the fifteenth minute. The voltage measurement in Experiment 2 produces the smallest voltage value above 0 millivolt of 320 millivolt in the fourth minute and the largest voltage of 3410 millivolt in the fifteenth minute. The voltage measurement in Experiment 3 produces the smallest voltage value above 0 millivolt of 560 millivolt in the third minute and the largest voltage of 3440 millivolt in the fifteenth minute. The

Volume 5, Issue 2, pages 157-172
p-ISSN 2655-8564, e-ISSN 2685-9432

voltage measurement in Experiment 4 produces the smallest voltage value above 0 millivolt of 900 millivolt in the second minute and the largest voltage of 3490 millivolt in the fifteenth minute. The voltage measurement in Experiment 5 produces the smallest voltage value above 0 millivolt of 900 millivolt in the sixth minute and the largest voltage of 3620 millivolt in the fifteenth minute. With the results of voltage measurements in five experiments, information was obtained that the more cigarettes were burned, which produced smoke in the simulation room, the voltage value issued by the MQ-2 sensor increased.

The CO_2 gas concentration in the simulation room was measured using a CO_2 gas meter [26, 27, 28] in each experiment. The results of measuring CO_2 gas concentrations are shown in Figure 7.

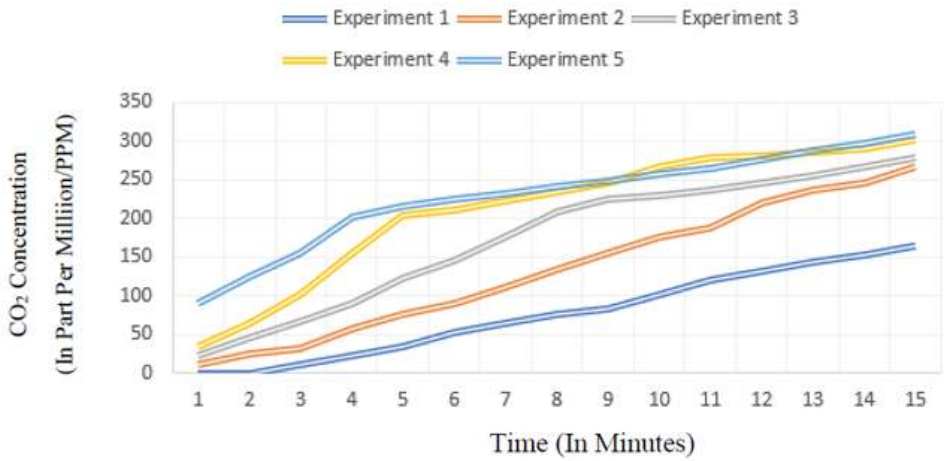


Figure 7. The CO_2 Gas Concentration

In Figure 7, the low concentration of CO_2 gas on the y-axis in the range of 50 to 100 ppm is indicated by a green LED turning on. This occurred between minutes 1 and 10 in Experiment 1, between minutes 1 and 6 in Experiment 2, between minutes 1 and 4 in Experiment 3, between minutes 1 and 3 in Experiment 4, and in minute 1 of Experiment 5. A yellow LED turning on indicates a medium concentration of CO_2 gas on the y-axis in the range of 100 to 200 ppm. This occurred in Experiment 1, between minutes 10 and 15 in Experiment 2, between minutes 7 and 15 in Experiment 3, between minutes 3 and 5 in Experiment 4, and between minutes 2 and 4 in Experiment 5. When the red LED turns on, there is a high concentration of CO_2 gas on the y-axis, in the range of 200 to 370

ppm. This occurred between minutes 12 and 15 in Experiment 2, between minutes 8 and 15 in Experiment 3, between minutes 6 and 15 in Experiment 4, and from minutes 5 to 15 in Experiment 5.

4 Conclusions

This research produces a conclusion about controlling the CO_2 gas concentration when detecting cigarette smoke in a simulation room. With the increase in the amount of cigarette smoke in a simulation room, the output voltage of the MQ-2 sensors is increasing. The CO_2 gas concentration rises in the simulation room as the amount of cigarette smoke increases. It can be concluded that as the number of cigarettes burned in the simulation room increases, the amount of cigarette smoke in the room increases, which causes the CO_2 gas concentration to increase and increases the voltage of the MQ-2 sensors required by the microcontroller to rotate the exhaust fan to control the CO_2 gas concentration. Based on Figure 7, the effectiveness of the exhaust fan rotation in controlling the CO_2 gas concentration detected by the MQ-2 sensor looks good where the CO_2 gas concentration can be controlled under 350 ppm.

Acknowledgements

Sri Hartanto is the main contributor to this paper, whose role is in designing electronic circuit, conceptualization, formal analysis, while Tri Ongko Priyono and Triono help in investigation and data validation. Thanks to all those who have helped with this research.

References

[1] J. B. Sanger, L. Sitanayah, and V. D. Kumenap, Detection System for Cigarette Smoke, Proc. 4th International Conference on Information Technology, Information Systems and Electrical Engineering (ICITISEE), (2019) 145-149.

Volume 5, Issue 2, pages 157-172

p-ISSN 2655-8564, e-ISSN 2685-9432

[2] S. Panpaeng, P. Phanpeang, E. Metharak, Cigarette Smoke Detectors for Non-Smoking Areas in the Building, Proc. International Computer Science and Engineering Conference (ICSEC), (2018) 1-4.

[3] Prajakta B, Volkan Y S, Masudul H I, Stephen T, and Edward S, Computation of Cigarette Smoke Exposure Metrics from Breathing, IEEE Transactions on Biomedical Engineering, 67(8) (2020) 1-5.

[4] J. A. Stankovic, Research Directions for the Internet of Things, IEEE Internet of Things Journal, 1(1) (2014) 3-9.

[5] H. Ping, J Wang, Z. Ma, Y. Du, Mini-review of application of IoT technology in controlling system agricultural products quality and safety, International Journal of Agricultural and Biological Engineering, 11(5) (2018) 35-45.

[6] M. Muntjir, M. Rahul, H. A. Alhumyani, An Analysis of Internet of Things (IoT): Novel Architectures, Modern Applications, Security Aspects and Future Scope with Latest Case Studies, International Journal of Engineering Research & Technology (IJERT), 6(6) (2017) 422-448.

[7] I. B. G. Purwania, I N. S. Kumara, and M. Sudarma, Application of IoT-Based System for Controlling system Energy Consumption, International Journal of Engineering and Emerging Technology, 5(2) (2020) 81-93.

[8] C. Wang, M. Daneshmand, M. Dohler, X. Mao, R. Q. Hu, and H. Wang, Guest Editorial - Special issue on the internet of things (IoT): Architecture, protocols, and services, IEEE Sensor Journal, 13(10) (2013) 3505–3508.

[9] R. A. Mouha, Internet of Things (IoT), Journal of Data Analysis and Information Processing, 9 (2021) 77-101.

[10] R. Singh, A. K. Thakur, A. Gehlot, Akhilesh, Internet Of Things Based On Home Automation For Intrusion Detection, Smoke Detection, Smart Appliance And Lighting Control, International Journal of Scientific & Technology Research 8(12) (2019) 3702-3707.

[11] M. A. Buchari, K. Exaudi, Rendyansyah, Aditya PP. Prasetyo, R. Zulfahmi, R. Passarella, Detection of Carbon Dioxide Levels in Smoker's Body, Proc. International Conference on Informatics, Multimedia, Cyber and Information System (ICIMCIS), (2019) 103-109.

Volume 5, Issue 2, pages 157-172

p-ISSN 2655-8564, e-ISSN 2685-9432

[12] S. Z. Yahaya, M. N. Mohd Zailani, Z. H. Che Soh, K. A. Ahmad, IoT Based System for Controlling system and Control of Gas Leaking, Proc. 1st International Conference on Information Technology, Advanced Mechanical and Electrical Engineering (ICITAMEE), (2020) 122-127, 2020.

[13] T. S. Gunawan, I. R. H. Yaldi, M. Kartiwi, H. Mansor, Performance Evaluation of Smart Home System using Internet of Things, International Journal of Electrical and Computer Engineering (IJECE) 8(1) (2018) 400~411.

[14] I. K. N. Trisnawan, A. N. Jati, N. Istiqomah, and I. Wasisto, Detection of Gas Leaks Using The MQ-2 Gas Sensor on the Autonomous Mobile Sensor, Proc. International Conference on Computer, Control, Informatics and its Applications, (2019) 177-180.

[15] Somantri, R. F. Ridwanullah, Hendra, D. Safitri, Cigarette Smoke Detection System for Non-Smoking Areas Based on IoT and Face Recognition, Proc. 6th International Conference on Computing Engineering and Design (ICCED), (2020) 1-6.

[16] S. Khan, K. Muhammad, S. Mumtaz, S. W. Baik, V. Hugo C. de Albuquerque, Energy-Efficient Deep CNN for Smoke Detection in Foggy IoT Environment, IEEE Internet of Things Journal, 6(6) (2019) 1-9.

[17] M. Jin, N. Bekiaris-Liberis, K. Weekly, C. J. Spanos, and A. M. Bayen, Occupancy Detection via Environmental Sensing, IEEE Transactions on Automation Science and Engineering Journal, 15(2) (2018) 443–455.

[18] I. Deshko, V. Tsvetkov, Sequential Methods and Algorithms, Journal of Physics Conference Series 2388(1) (2022) 1-5.

[19] S. N. Rodionov, A Sequential Algorithm for Testing Climate Regime Shifts, Geophysical Research Letters, 31(L09204) (2004) 1-4.

[20] S. A Ritonga, Syahwin, T. Haramain, Penerapan Algoritma Sekuensial pada Penyiraman Tanaman Otomatis Berbasis Arduino Uno R3, Blend Sains Jurnal Teknik, 1(1) (2022) 62-68.

[21] Keshamoni, K., Hemanth, S, Smart Gas Level Monitoring, Booking & Gas Leakage Detector over IoT, Proc. IEEE 7th International Advance Computing Conference (IACC), (2017) 330-332.

[22] Anoname, MQ-2 Semiconductor Sensor for Combustible Gas.

Volume 5, Issue 2, pages 157-172

p-ISSN 2655-8564, e-ISSN 2685-9432

[23] Montoya, J. M., and Chilo, J, RealTime Wireless Monitoring System of CO2 and CH4 in Juliaca-Perú, Proc. 10th IEEE International Conference on Intelligent Data Acquisition and Advanced Computing Systems: Technology and Applications (IDAACS), (2019) 464-467.

[24] A. S. Ismailov, Z. Jo`rayev, Andijan, Study of Arduino Microcontroller Board, Science and Education" Scientific Journal, 3(3) (2022) 172-179.

[25] L. Louis, Working Principle of Arduino and Using it as a Tool for Study and Research, Proc. International Journal of Control, Automation, Communication and Systems (IJCACS), (2018) 21-29.

[26] A. Abdurrachman, I. Chandra, R. A. Salam, Rancang Bangun Alat Ukur Konsentrasi Gas CO2 dan NO2 untuk Pengamatan Emisi dari Pembakaran Sampah Rumah Tangga, e-Proceeding of Engineering, 7(1) (2020) 1342-1349.

[27] S. Handayani, L. Umar, R. Setiadi, Pengembangan Deteksi Online Gas Karbondioksida Menggunakan CO2 Meter Voltcraft Cm-100, JOM FMIPA, 2(2) (2015) 1-10.

[28] Anoname, User's Guide CO2 Monitor Model CO200, Extech Instruments Corporation (a FLIR company).

International Journal of Applied Sciences and Smart Technologies

Volume 5, Issue 2, pages 173-180

p-ISSN 2655-8564, e-ISSN 2685-9432

Numerical Beamforming and Parametric Descriptions of Laguerre-Gaussian Vortex Beams

D. Silitonga[1, *], D. G. C. Alfian[1]

[1]Department of Mechanical Engineering, Sumatera Institute of Technology, Lampung, Indonesia

[*]Corresponding Author: dicky.silitonga@ms.itera.ac.id

(Received 31-03-2023; Revised 24-04-2023; Accepted 27-04-2023)

Abstract

Vortex beams are beams with a helical wavefront that have found applications in optical or acoustic tweezers to manipulate microscopic particles. Vortex beam imposes torque or force to particles, allowing them to trap the object within the beam's field and induce motion or displacement in a non-contact manner. One type of such beam is a Laguerre-Gaussian beam, where the solution of a Gaussian wave is modified by the Laguerre polynomial term that determines the pattern and helical characteristic of the beam. In this paper, a numerical method based on the mathematical expression of the Laguerre-Gaussian beam is implemented to describe how the parameters change the physical behavior of the beam. This work has shown that a straightforward numerical method is capable of producing this kind of beam. Therefore, this approach can be used for generating vortex beams for physical emissions, complex numerical simulations, or demonstrations for teaching purposes.

Keywords: vortex beam, laguerre-gaussian beam, numerical beamforming

1 Introduction

Vortex beam, characterized by the twisting of its phase as it propagates, has been investigated for its potential in the engineering field. This helical type of beam may prevail in the acoustical and optical form. One of the attractive properties of this kind of wave is that it carries angular momentum, which in turn can be transferred into the medium. Therefore, it is possible to take advantage of this feature to introduce motions to the particles within the beam envelope, creating optical or acoustic tweezers which not only traps particles but also manipulates their motion and position in a contactless manner. Practically, the tweezers can be implemented to hold position and control

This work is licensed under a Creative Commons Attribution 4.0 International License

Volume 5, Issue 2, pages 173-180
p-ISSN 2655-8564, e-ISSN 2685-9432

orientation of molecules or cells for microscopy [1]. It has also been demonstrated that a tweezer is capable of stretching microparticles to evaluate their viscoelastic property [2,3]. Both acoustic and optical tweezers have already been implemented in various research areas involving micro-sized objects such as in the biomedical and nanomaterial fields.

Multiple methods have been developed to generate vortex beams. In acoustic beamforming, a common method involves an array of piezoelectric transducers by modulating the phase and amplitude of each transducer within the array in order to form the beam [4]. Recently, Zhou et. al. proposed another method using a spiral diffraction grating and worked out theoretical and numerical investigations to reveal its feasibility [5]. On the other hand, various methods also exist to generate optical vortex, some of which are by employing laser with diffraction grating [6], spatial light modulator [7], and deformable mirror [8]. With various beam forming methods available and being developed, research on the vortex beam will advance to broaden its application in the industrial or scientific domains.

The aim of this paper is to demonstrate the principal properties of the acoustic vortex beam by visualizing the shape of the beam as it propagates along the medium and to describe theoretically the role of parameters in the mathematical expression of the Laguerre-Gaussian vortex beam. This paper isolates the study solely on the nature of the propagation of the ideal beam in a lossless medium. Physical phenomena related to the interaction of waves with the medium such as viscosity effects, damping and other external forces are not considered in this paper.

Vortex beams studied in this work are formed as Laguerre-Gaussian beams. It is a Gaussian function with Laguerre polynomial term which determines the radial and azimuthal pattern of the beam.

2 Research Methodology

Mathematical expression that describes the solution of a Laguerre-Gaussian beam in cylindrical coordinates as a function of the radius (r), azimuthal angle (φ) and propagation distance (z) can be described by [9]:

International Journal of Applied Sciences and Smart Technologies

Volume 5, Issue 2, pages 173-180

p-ISSN 2655-8564, e-ISSN 2685-9432

$$u(r,\phi,z) = A_0 \left(\sqrt{2}\frac{r}{w(z)}\right)^l L_p^l \left(2\frac{r^2}{w(z)^2}\right) \frac{w_0}{w(z)} \, exp\left[-i\varphi_{pl}(z)\right] exp\left[i\frac{k}{2q(z)}r^2\right] exp(il\phi) \quad (1)$$

where A_0 is a constant and L_p^l is the associated Laguerre polynomial of the argument that follows, i.e. the $\left(2\frac{r^2}{w(z)^2}\right)$. The associated Laguerre polynomials $L_p^l(x)$ satisfy the following differential equation:

$$x\frac{d^2L_p^l}{dx^2} - (l+1-x)\frac{dL_p^l}{dx} + pL_p^l = 0 \quad (2)$$

The beam waist and the beam width at the distance z is denoted by w_0 and w(z), respectively. Gouy phase shift $\varphi_{pl}(z)$ is given by:

$$\varphi_{pl}(z) = (2p + l + 1)tan^{-1}(z/z_0) \quad (3)$$

In the case of parameter p and l both equal to zero, a fundamental Gaussian beam will appear. The Rayleigh length z_0, which is the distance from the beam focus where the beam area doubles, can be found by knowing the wavelength (λ) or wavenumber (k) through:

$$z_0 = \frac{\pi {w_0}^2}{\lambda} = \frac{k{w_0}^2}{2} \quad (4)$$

The Laguerre-Gaussian beam is modeled in MATLAB 2020b by developing a code to solve the mathematical expression as discussed above. An advantage of using MATLAB 2020b is that the associated Laguerre polynomial term can be simply obtained by a built-in function laguerreL(p,l,x) [10]. Here, the p and l inputs are set as integers to represent the modes and the x input is fed by the $\left(2\frac{r^2}{w(z)^2}\right)$ term. The program loop iterates in the increment of radial and angular positions to determine the solution at each node throughout the specified area of square with the sides of 4λ. That iteration can then be repeated at different distance in front of the source plane (planes at z > 0) to reveal the angular displacement of intensity peaks.

This study attempts to examine the effect of varying physical parameters that can be adjusted by the setting of the wave source or transducer, namely the frequency (f). The excited frequency determines the beam's wavelength (λ) depending on the speed of sound

International Journal of Applied Sciences and Smart Technologies

Volume 5, Issue 2, pages 173-180

p-ISSN 2655-8564, e-ISSN 2685-9432

(c) as an intrinsic property of the medium of propagation, via the well-known relation of λ = c/f.

3 Results and Discussions

Different modes of LG beams can be described by the parameter p and l in the $L_p^l(x)$ associated Laguerre polynomial. There, p and l represent the radial (center to periphery direction) and azimuthal (angular-wise direction) variation of the beam, respectively. Several examples are presented in Figure 1, depicting the amplitude field in the beam source plane (z = 0) for p and l from 0 to 4. It can be observed that the radial pattern of the beam, which is simply the repetition of each beam's azimuthal pattern towards the radial direction, is described by the parameter p (the degree of the associated Laguerre polynomial). Meanwhile, the azimuthal pattern itself is related to the integer l. For brevity, the mode will be further designated as LG_{pl}. An LG_{00} mode has zeroes on both p and l which results in a standard Gaussian beam, having a single peak at the center. The other LG modes with one or both non-zero p and l values have multiple peaks in azimuthal and/or radial direction. The regularity extends in the same fashion for any integer values of p and l.

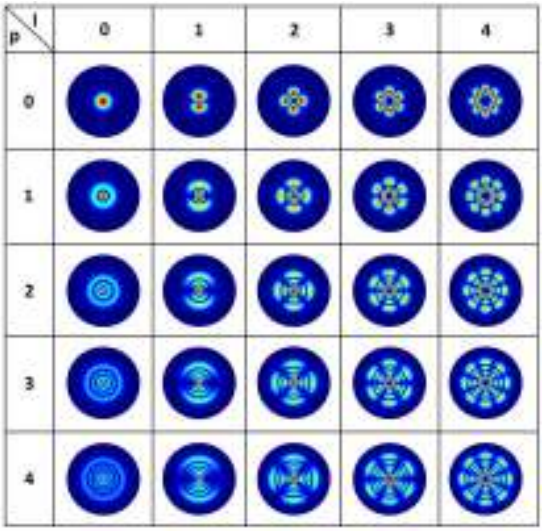


Figure 1. Amplitude pattern of various modes of LG beam at the source plane (z = 0), described by the p and l parameter of the associated Laguerre polynomials.

Volume 5, Issue 2, pages 173-180

p-ISSN 2655-8564, e-ISSN 2685-9432

On the plane of the beam source (at z = 0), the amplitude distribution of each mode is described by the p and l parameters of the associated Laguerre polynomials. Varying p and l results in the donut or segmented shapes with different numbers of layers of amplitude peaks in the radial direction. However, the total amplitude across the surface is independent of the LG modes if the other variables remain constant, as expected from the expression in Equation 1. Accordingly, the mode only specifies how the amplitude distributes within the plane orthogonal to the propagation direction.

The amplitude patterns as shown in Figure 1 consist of multiple lobes or peaks, with an exception for the LG_{00} mode that has only central peak following a standard Gaussian distribution. Note that the amplitude is plotted as absolute value, hence the maxima can be either positive or negative with the main purpose of indicating the pattern of intensity strength relative to zero, neglecting the phase evolution. The phase-dependent shape, however, can be investigated in Figure 2, where actually at a particular time, the peak may be directed towards the positive or negative sign. Take an example of mode LG_{02} that corresponds to 2D image with p = 0 and l = 2 in Figure 1 and 3D plot in Figure 2(d). In Figure 1, LG_{02} shows 4 symmetric lobes meanwhile in reality the 4 peaks consist of 2 lobes in positive direction and other 2 in negative.

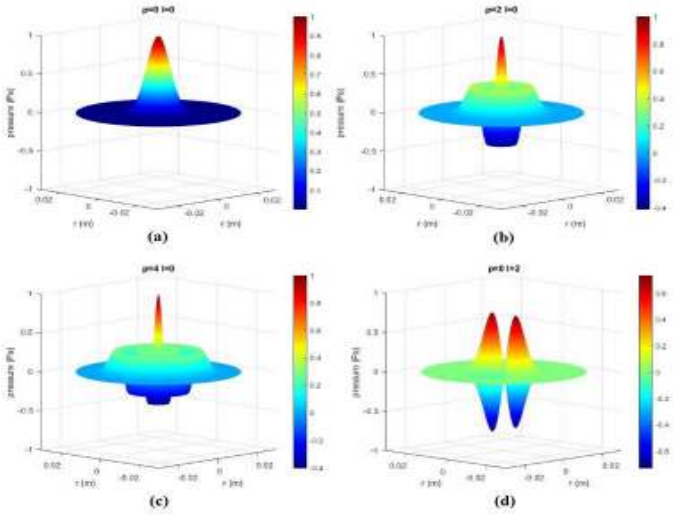


Figure 2. Implementation on acoustic beam: pressure amplitude profile at a given phase for (a) LG_{00}; (b) LG_{20}; (c) LG_{30}; (d) LG_{22}

A case study is carried out in acoustic setup by implementing the numerical method, where snapshots of pressure distribution that occurs at a certain phase for select

Volume 5, Issue 2, pages 173-180

p-ISSN 2655-8564, e-ISSN 2685-9432

modes are shown in Figure 2. Several instances of LG modes: LG_{00}, LG_{20}, LG_{40} and LG_{02} are presented. The beam in this case is simulated as an acoustic perturbation at the frequency of 1 MHz with the velocity of 1490 m/s, resembling sound propagation in water, hence the wavelength is 1.49 mm. Beam waist is set as 4 times wavelength, or equals to 5.96 mm in this case. The simulation is limited to observe the area within the radius of 20 times the wavelength or equals to 29.8 mm radially outward from the beam's axis. That envelope is considered sufficient to capture far field region without exaggerating computational requirements. The figures reveal that in a higher polynomial degree of LG mode, for example LG_{20} and LG_{40}, there exist valleys and peaks which appear in an alternating fashion along the radial direction. In addition, the same behavior of alternating peaks and valleys also prevails in the azimuthal direction. Taking the LG_{02} mode as an example, the peaks and valleys take place alternatingly every 90^o azimuthal angle, as demonstrated in Figure 2(d) Without the need to elaborate the other examples, this alternating patterns in both radial and azimuthal direction persist for other modes as well.

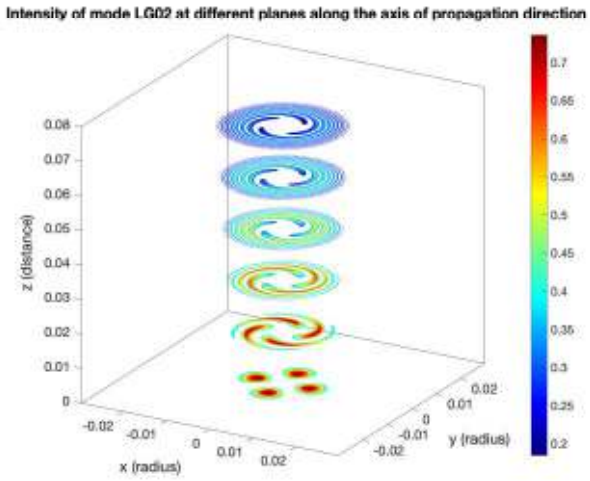


Figure 3. Amplitude field of LG_{02} on different planes at different positions downstream the source, showing spirals that indicates twisting behavior of the beam.

The use of different frequencies or mediums, which means different wave velocity, does not affect the shape of amplitude distribution at the beam source plane. That being said, all the preceding results and visualizations in Figure 1 and Figure 2 regarding the in-plane pressure distribution at $z=0$ remain identical regardless of the

Volume 5, Issue 2, pages 173-180
p-ISSN 2655-8564, e-ISSN 2685-9432

frequency and wave velocity settings, provided the same diameter of beam waist w_0 is maintained.

Rotational behavior of the Laguerre-Gaussian beam is observable down the propagation path, as presented in Figure 3. The amplitude fields on planes at different z-position form spiral shapes which indicates angular displacement of the beam as the amplitude peak moves in azimuthal direction. The field radius expands as the waves propagate further from the source plane, and at the same time the overall amplitude decreases as indicated by the corresponding color scale.

4 Conclusions

This work has demonstrated a numerical method to visualize a Laguerre-Gaussian beam. The physical implication of each parameter and terms in the mathematical expression has been discussed, where the radial and azimuthal patterns are determined by the Laguerre polynomial parameters. On the other hand, other wave parameters such as frequency, wavelength, beam width and amplitude do not affect the peak distribution and angular displacement pattern. The vortex behavior has also been visualized by depicting the field on planes at different positions ahead of the beam source which shows spiral shapes.

Acknowledgements

The authors would like to appreciate Institut Teknologi Sumatera for providing the access to MATLAB 2020b software and other computing/IT resources employed in this work.

References

[1] J.C.T. Lee, S.J. Alexander, S.D. Kevan, S. Roy, B.J. McMorran, Laguerre–Gauss and Hermite–Gauss soft X-ray states generated using diffractive optics, Nat. Photonics. 13 (2019) 205–209.

Volume 5, Issue 2, pages 173-180

p-ISSN 2655-8564, e-ISSN 2685-9432

[2] N.M. Geekiyanage, E. Sauret, S.C. Saha, R.L. Flower, Y.T. Gu, Deformation behaviour of stomatocyte, discocyte and echinocyte red blood cell morphologies during optical tweezers stretching, Biomech. Model. Mechanobiol. 19 (2020) 1827–1843.

[3] A. Magazzù, C. Marcuello, Investigation of Soft Matter Nanomechanics by Atomic Force Microscopy and Optical Tweezers: A Comprehensive Review, Nanomaterials. 13 (2023) 963.

[4] S. Mohanty, R.-J. Fidder, P.M. Matos, C.M. Heunis, M. Kaya, N. Blanken, S. Misra, SonoTweezer: An Acoustically Powered End-Effector for Underwater Micromanipulation, IEEE Trans. Ultrason. Ferroelectr. Freq. Control. 69 (2022) 988–997.

[5] H. Zhou, J. Li, K. Guo, Z. Guo, Generation of acoustic vortex beams with designed Fermat's spiral diffraction grating, J. Acoust. Soc. Am. 146 (2019) 4237–4243.

[6] Y. Zhuang, Q. Yang, P. Wu, W. Zhang, Y. Ren, H. Liu, Vortex beam array generated by a volume compound fork grating in lithium niobite, Results Phys. 24 (2021) 104083.

[7] K. Peng, X. Shen, F. Huang, Vortex Beam Generation Method based on Spatial Light Modulator, IOP Conf. Ser. Earth Environ. Sci. 440 (2020) 042082.

[8] S. Scholes, L. Mohapi, J. Leach, A. Forbes, A. Dudley, Experimentally simulating the beam shaping capabilities of piston-type deformable mirrors using a liquid crystal spatial light modulator, Appl. Phys. B. 129 (2023) 45.

[9] Q. Zhan, Cylindrical vector beams: from mathematical concepts to applications, Adv. Opt. Photonics. 1 (2009) 1–57.

[10] Generalized Laguerre Function and Laguerre Polynomials - MATLAB laguerreL, (n.d.). https://www.mathworks.com/help/symbolic/sym.laguerrel.html (accessed March 31, 2023).

International Journal of Applied Sciences and Smart Technologies

Volume 5, Issue 2, pages 181-194

p-ISSN 2655-8564, e-ISSN 2685-9432

Traditional Cultural Learning System for Batak Toba Wedding Using Multimedia Approach

Ridha Sefina Samosir[1], Varian Adriel[2]

[1]Faculty of Computer Science and Design, Institute Technology and Business Kalbis, Pulomas Selatan-East Jakarta, 13210, Indonesia

[*]Corresponding Author: ridha.samosir@kalbis.ac.id

(Received 29-03-2023; Revised 27-04-2023; Accepted 28-04-2023)

Abstract

Indonesia is a country with diverse cultures. Indonesia comprises numerous tribes, including Batak Toba. The Batak Toba people actively practice their traditional rituals, including wedding ceremonies. Their traditional wedding ceremony involves several rituals, symbols, and attributes with different meanings. Today, learning resources for traditional rituals, attributes, and others can be accessed through experts' knowledge, video tutorials, and scientific journal. However, all sources have failed to attract attention. Thus, only a few generations are concerned and interested in studying culture. And threatens the dissappear of cultural experts. The research objective is to develop a system based on a multimedia approach that provides learning materials about the traditional rituals of the Batak Toba wedding ceremony. The multimedia development life cycle method is used for system development. Based on the research result show that 90% responded easier to understand the content.

Keywords: Traditional, culture, Batak Toba, wedding, multimedia

1 Introduction

Indonesia is a country with diverse cultures. This cultural diversity includes different ethnicities, religions, and local languages. Indonesia comprises numerous ethnic groups, such as the Javanese, Bataknese, Baduy, Asmat, Mentawai, and Minang Kabau. Each ethnic group has specific and complex attributes for celebrations, such as weddings, births, and funerary rituals [1]. For example in Batak Toba wedding always involve a traditional shawl [2] called ulos (weaving).

The Batak Toba people are one of the tribes in North Sumatera, Indonesia. Apart from the Batak Toba, other tribes make up the region, namely, the Batak Simalungun,

This work is licensed under a Creative Commons Attribution 4.0 International License

Volume 5, Issue 2, pages 181-194
p-ISSN 2655-8564, e-ISSN 2685-9432

Batak Karo, Batak Pakpak, Batak Angkola, and Batak Mandailing. The Batak Toba people represent 50% of all Batak tribes in North Sumatera. Batak culture is based on the behavioral values of the people's ancestors. All the tribes in the Batak lands have a distinct language; however, a few similarities in writing and pronunciation exist. Moreover, each Batak tribe uses a different script, though the variants do not differ considerably [3]. Geographically, the Batak Toba tribe lives around Lake Toba [4]. Generally, the Batak Toba people believe and follow the dalihan na tolu philosophy. Dalihan na tolu is advice deriving from ancestors. Specifically, the dalihan na tolu philosophy represents three social community groups, namely, the dongan sahuta (friends from same village), hula-hula (a man in our mother family), and boru (daughter). Dalihan na tolu is considered an important set of rules for every ceremonial event, including wedding ceremonies. All the symbols and supporting attributes involved have important meanings for the bride, the bride's family, and everyone around them [5]. Often, the meanings of the symbols or attributes are religious [6][7]. Some attributes used in the wedding ceremony are traditional cloth called an ulos, a cuisine called arsik (goldfish), cooked rice called indahan na las, water called aek sitio-tio, betel leaf called napuran, a sarong called mandar hela, money called tuhor, rice called si pir ni tondi, and meat called jambar. By protocol, each attribute is called by a different name during the ceremony. The Batak Toba wedding ceremony consists of three stages, namely, the pre-wedding, wedding, and post-wedding stages. The pre-wedding stage consist of mangalua, marhusip, marhata sinamot, pudun saut, martumpol, and martonggo raja. Then, the wedding ceremony consists of manjalo pasu-pasu, pesta unjuk, and daulat ni si panganon. Last is the post-wedding which consists of paulak une, manjahe, and maningkir tangga. Each stage has different meanings and different supporting attributes. In addition, the duration of each stage also different. According to the dalihan na tolu philosophy, the completion of the three stages is called the full ritual or adat na gok [8]. Some Batak Toba people believe that not being able to practice their cultural rituals would be disastrous.

All of the rituals or ceremonies above is an interested object for tourists. It can often attract and motivate tourists to visit any place in Indonesia. Many tourists are interested in purchasing the miniature of the attributes. They are also interested in studying about the culture for a long time.

Volume 5, Issue 2, pages 181-194
p-ISSN 2655-8564, e-ISSN 2685-9432

Unfortunately, their enthusiasm does not accord with the enthusiasm of Batak youth in learning their culture. The complexity of the processes and rituals attributes of wedding ceremonies just attracting only a few of Batak Toba youth to learn. A lot of Batak youth people also choose to move to other city even other country for studying or leaving. Moreover, owing to current habits, most people prefer to learn things instantly and only subjects that are beneficial to them. Thus, knowledge transfer is poor, and few people understand traditional ceremonies. Finding a person who is knowledgeable related to all rituals, attributes, and process above is difficult. It is hard to imagine someday when the ceremonial rituals cannot be performed because no more expert of it.

Many communities are trying to maintain and preserve all these cultural rituals in every celebration. They try to organize sharing knowledge periodically from the expert to other people, transfer knowledge through directly communication between expert and interested people. Another method is to record the knowledge in a book or scientific journal or video tutorials. However, all of methods are ineffective for the following reasons.

a. Knowledge transfer is difficult when only a few experts exist, and such experts have poor communication skills. Communication skills are essential for transferring knowledge.
b. Finding literature or scientific journals that address the topic is difficult. Such references are often expensive, and a very limited number of journals focus on Bata Toba wedding rituals.
c. Video tutorials is good but can not cover all process or attributes because it will be boring if the duration is too long.

Based on literature reviews, several researchers conducted relevant studies. This first research develops a multimedia system for Hindu wedding ceremonies that could be accessed via mobile phones. The system consists of different types of Hindu weddings, Hindu wedding rituals, prerequisites of Hindu weddings, and the objectives of Hindu weddings[9]. Moreover, the project is an interactive multimedia system for learning the culture of Indonesia. In addition, the research aimed to increase children knowledge about Indonesia culture [10]. Other researcher developed mobile platforms with augmented reality technology for learning media the traditional houses in North Sumatera of

Volume 5, Issue 2, pages 181-194
p-ISSN 2655-8564, e-ISSN 2685-9432

Indonesia. The learning media are used for kids. This augmented reality (AR) technology aimed to visualize traditional houses [11]. Meanwhile, another study used AR as learning media for Papua cultures based on a website. Specifically, the researcher developed a website for children showing the art and culture of the province of Papua[12].

The problems above motivates us to involves information technology. Information technology plays an important role in people's lives. It's enables everything, including learning media. One information technology support to solve the problems above is the multimedia system. Therefore, this research proposes to develop a multimedia-based system that contains information about the wedding ceremony rituals of the Batak Toba. Finally, the output of this research is an information technology that present information or knowledge about traditional rituals of Batak Toba wedding.

2 Research Methodology

The objective of this research is to develop a computer system based on a multimedia approach to help anybody learn about the traditional rituals of the Batak Toba wedding. The systems contain information about the process, attributes, symbols, and techniques of the Batak Toba wedding from scientific literature and from experts related to traditional rituals. Researchers collect information from experts through several Batak communities/organizations in Indonesia. The data collection process was done directly through interviews with community representatives who are experts on traditional Batak wedding processions and direct observation of several traditional wedding events.

Research activities are carried out in sequence, including problem identification, literature study, problem formulation, data and information collection, and the system development stage using the multimedia development life cycle (MDLC) method, and conclude.

The multimedia development life cycle (MDLC) method was used for system development. In addition, observation and interviews were conducted to collect the required data. Subsequently, the research team used the black box method to evaluate the system. Multimedia is defined as a collection or combination of different types of media.

Volume 5, Issue 2, pages 181-194

p-ISSN 2655-8564, e-ISSN 2685-9432

Moreover, multimedia involves only the sense of sight and hearing. However, this definition has continuously changed and developed. Other researchers stated that multimedia is a computer-based system for interactive communication capable of creating, storing, presenting, and accessing text, graphics, animation, image, and video information [13]. Therefore, if one of these components is absent in a system, the system cannot be interpreted as multimedia Numerous system development methods exist. However, not all can be applied to create multimedia systems. An approach that can be used for multimedia systems is Luther's method. Luther's approach consists of six stages: concept, design, material collection, development, testing, and distribution [14].

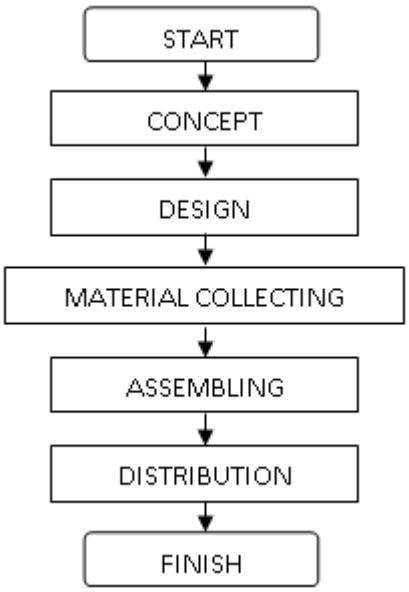


Figure 1. Multimedia Development Life Cycle Research Flow

Concept denotes the process of determining research objectives, user candidates, and the type of system required. Meanwhile, the design aims to arrange the system specifications, user interfaces, system architecture, and materials needed for the system. The material collection involves the accumulation of the necessary data. Generally, this stage is carried out in parallel with assembly. Assembly denotes developing the multimedia system, which involves all the related objects. A system is developed based on the design results and the collected materials. When the system is ready, it is tested using a system evaluation approach. This step involves the detection of bugs in the

Volume 5, Issue 2, pages 181-194
p-ISSN 2655-8564, e-ISSN 2685-9432

system. Finally, the system can be installed on a computer when all the bugs are detected. Thus, a user can utilize the system continuously. Figure 1 presents all steps in MDLC.

3 Results and Discussions

The output of this research is a multimedia learning system that can help users learn about traditional rituals of Batak Toba wedding. The system was developed using the MDLC method and contains all the processes or attributes involved in the Batak Toba wedding ceremony. Result from each step of the MDLC method are discussed below.

a. Concept

The observation and interview results show that the objective of the system is to help users understand Batak Toba wedding rituals. Thus, the users of the system are the public, especially parents planning to celebrate their children's wedding. To meet this need, the application is developed based on interactive multimedia. All data regarding traditional marriages' processes, attributes, and symbols come from interviews with experts, observations with Batak organizations/communities, and participation in several traditional wedding events.

b. Design

The outputs of this step are a use-case diagram, storyboard, navigation structure, and system user interface. A use-case diagram is a type of unified modeling language (UML) diagram. UML is graphical notation for system developments. UML comprises numerous diagrams with different functions such as use case diagram, activity diagram, and others [15][16]. The use-case diagram describes the interaction between a user (named actor) and a system. It's describe how a system works. [17]. Figure 2 is the use case diagram for the system proposed.

International Journal of Applied Sciences and Smart Technologies

Volume 5, Issue 2, pages 181-194

p-ISSN 2655-8564, e-ISSN 2685-9432

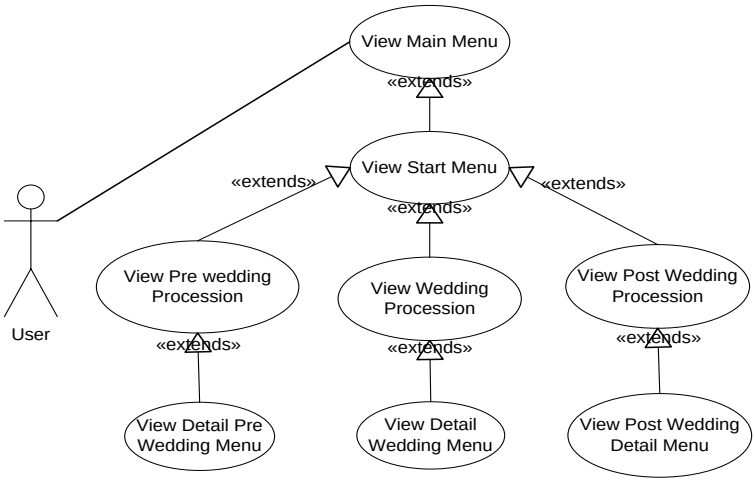


Figure 2. Usecase Diagram Multimedia Proposed System

Besides the use case diagram, the design step generates the navigation structure. It serves as a guide for operating the system, specifically where it starts and finishes. Figure 3 shows the navigation structure of the proposed system.

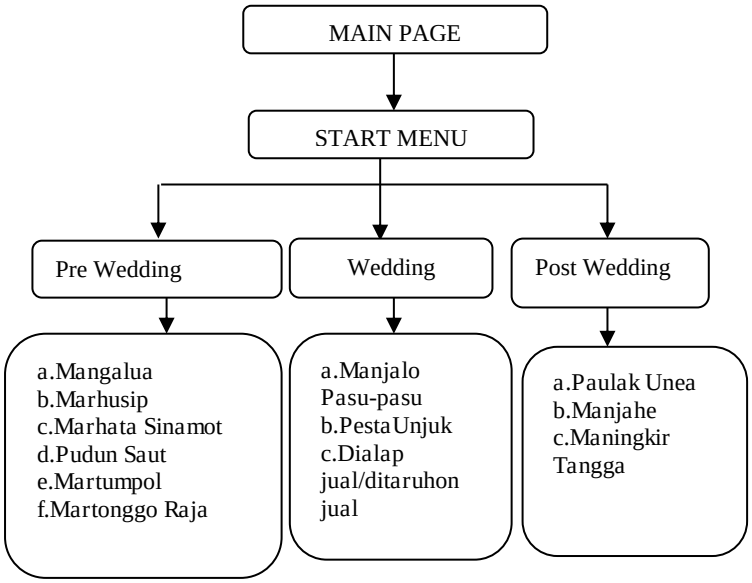


Figure 3. Navigation Structure

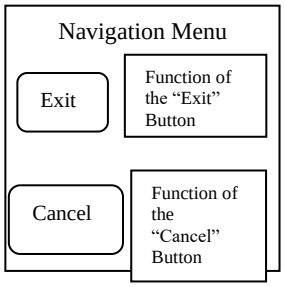
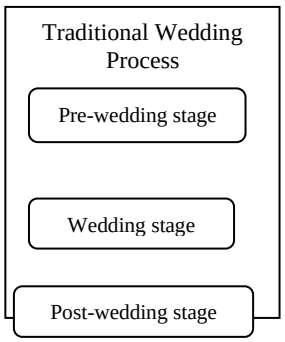
The following design is a storyboard. A storyboard can help convey a story quickly. Storyboards are widely used for making short films. However, storyboards can also be used in the system development life cycle (SDLC). In the SDLC, storyboards are used for

Volume 5, Issue 2, pages 181-194

p-ISSN 2655-8564, e-ISSN 2685-9432

multimedia-based systems [18][19]. Table 1 presents the story board design for the proposed system.

Table 1. Storyboard of System Proposed

Scene	Board	Story
1		This scene will show the main menu of the system
2		This scene will present explanations for the functions of buttons in each menu
3		This scene will present the process of each stage of the traditional Batak Toba wedding. All scenes involve multimedia attributes: images, animation, audio, and videos.

Last design is a user interface. It is a mockup design to help system developers build a system easily, as it provides access to actual descriptions of a system before development. The navigation structure design is clarified by the graphic user interface. The user interface of the proposed system starts on the menu of the main page. Subsequently, the start menu contains the three stages representing the main ritual. Finally, the detailed menu shows the processes of the Batak Toba wedding ceremony. This user interface design is simple to meet user requirements. All the processes include several images, audio, and animation.

Volume 5, Issue 2, pages 181-194
p-ISSN 2655-8564, e-ISSN 2685-9432

c. Material Collection

In this stage, the materials collected for the system are information or knowledge about the Batak Toba ceremony and supporting images relevant to the system, including animation and audio related to the wedding rituals. The system requirements obtained from observations and interviews are presented below.

- The system should be easy to use and have navigation symbols for users.
- The system should include text, images, audio, animation, and videos. Such media will help users understand the system easily.
- Supporting attributes should be relevant to the Batak Toba traditional wedding ceremony. In other words, all the materials should represent the rituals.
- Colors and symbols used should represent the actual colors and symbols used in traditional Batak Toba wedding rituals. Dominant colors of the Batak Toba ethnic group are red, blue, yellow, and black. All colors have different and distinct meanings.

Based on the explanation above, the necessary materials include images, animation, videos, textual information, symbols, colors, and buttons related to traditional Batak Toba wedding rituals. Certain collected images depict a goldfish, meat, rings, and a Batak Toba wedding couple. Several animated elements, made by the research team, are included in the system.

d. Assembly

In this section, the system is developed using Macromedia Flash with an action script programming language. This system does not involve the database because all of data just for displaying or no relation among all data. According to all process also attributes, system presents all of that completely and exactly. System displays 3 (three) big menu/window/layout that's describe 3 stage rituals of the wedding ceremony. Each window shows attributes through image, text, or video. Figure 4 is window for the first wedding stages (pre-wedding).

International Journal of Applied Sciences and Smart Technologies

Volume 5, Issue 2, pages 181-194

p-ISSN 2655-8564, e-ISSN 2685-9432



Figure 4. Pre-Wedding Stages Menu

Figure 4 explains the stages of pre-wedding. According to the previous explanation, the pre-wedding stage includes several stages, namely mangalua, marhusip, marhata sinamot, finally matonggoraja. At each stage, attributes are signs, such as rings to bind them, betel leaves during processions and other attributes.

e. Testing

The system is evaluated as a functional system using black box method. This method identifies and match system requirements with the features provided. The black box method is focuses on identifying whether a program meets the requirements mentioned in the specification. To test this evaluation approach, units or models in a system are executed and observed to determine whether the results correspond to the business process. If certain units or features generate unsuitable outputs, a second test, namely, the white box test, is employed [20][21]. Table 1 presents the evaluation results of the system using the black box method.

Table 2. Black Box Methodology Results

Menu	Information Displayed	Information Will be Displayed	Result
Main Menu	• System Title • Image as which represents Batak Toba Wedding Ceremony	• System Title • Image for Main Menu • Navigation Button	Matching

	• "NEXT" and "CANCEL" Button		
Start Menu	• Menu contained three stages of Batak Toba Wedding Ceremony • Multimedia supporting attribute relate to the topic • Navigation Button	• 3 Stage of Batak Toba Wedding Ceremony • Navigation Button • Multimedia supporting Attribute	Matching
Navigation Menu	• A guidance to operate the system • Explanation about all the button in navigation menu	• A menu contain explanation how to operate the system. • Explanation about the button function.	Matching
Pre Wedding Procession Menu	• All procession detail in pre wedding stage • All supporting attribute used (image, audio, video, etc) • Navigation button	• Show all detail procession for pre wedding stage • All menu equipped with easy navigation button. • All menu equipped with multimedia attribute relates to the topic.	Matching
Wedding Procession Menu	• All procession in wedding ceremony, • Supporting attribute based on multimedia (image, audio, video, etc) • Navigation button	• Show all details process in wedding procession • Each menu equipped with easy navigation button. • Each menu is equipped with multimedia supporting attribute relates to the stages	Matching
Post Wedding Menu Procession	• All procession in Post wedding • Multimedia Supporting Atrribute • Navigation button	• Show all detailsprocess in post wedding stage • Each menu equipped with easy naviagation menu • Each menu equipped with multimedia supporting attribute	Matching

Volume 5, Issue 2, pages 181-194
p-ISSN 2655-8564, e-ISSN 2685-9432

4 Conclusions

In summary, based on the research output, multimedia components, such as images, audio, videos, and animation, can help make learning materials easy to understand. Subjective testing through direct interviews with 30 respondents as system users showed that 27 people easier understood the content through a multimedia-based system. Moreover, they become interested in wanting to learn about their traditional culture. It means, multimedia components can help make a system interactive and interesting. Finally, multimedia learning system can be a solution to the problems faced such as the scarcity of experts, lack of user interest in learning, and very little amount of literature related to the problem domain raised. Future research should develop a mobile system to grant access to users anytime and anywhere.

Acknowledgements

Thank you for all team members such as our research partner (Batak Toba Community) and institution for funding the research.

References

[1] R. Asfina and R. Ovilia, Be Proud of Indonesian Cultural Heritage Richness and Be Alert of Its Preservation Efforts in the Global World, Humanus, 5(2) (2017) 195.

[2] J. Hardori, J. Rajagukguk, P. Randy, N. Sinaga, and H. Ruben, Studi Teologi Kontekstual terhadap pemberian Ulos dalam pernikahan adat Batak, MATHEO J. Teol., 9(1) (2019) 39–56.

[3] M. A. Lubis, Revitalisasi Nilai-Nilai Kearifan Lokal Masyarakat Hukum Adat Batak Toba Dalam Melindungi Eksistensi Danau Toba Di Mata Dunia (Kajian Hukum Progresif), J. Darma Agung, 27(3) (2020) 1234.

[4] O. C. Nindyaputra, Identifikasi pola permukiman Tradisional Desa Meat, Toba, Pros. Semin. Nas. Desain dan Arsit., 2 (2019) 394–400.

Volume 5, Issue 2, pages 181-194

p-ISSN 2655-8564, e-ISSN 2685-9432

[5] Y. Octavianna, R. Sibarani, H. Situmorang, and N. H. Hasibuan, The impact of Marpaniaran 'traditional dance of women' of Toba Batak wedding ceremony for women's physical and mental health, Gac. Sanit., 35 (2021) S537–S539.

[6] W. Purboyo, Dalihan Na Tolu Sebagai Konsep Dasar Rancangan Jembatan Tano Ponggol (Studi Kelayakan Jembatan Tano Ponggol),Widyakala J. Pembang. Jaya Univ., 8(2) (2021) 78.

[7] E. N. Butarbutar, Perlindungan Hukum terhadap Prinsip Dalihan Natolu sebagai Hak Konstitusional Masyarakat Adat Batak Toba, J. Konstitusi, 16(3) (2019) 488.

[8] O. Situmorang and R. Sibarani, Tradisi Budaya Dan Kearifan Lokal Paulak Une Dan Maningkir Tangga Pada Pernikahan Batak Toba Di Desa Sigapiton Kecamatan Ajibata: Kajian Antropolinguistik, Kompetensi, 14 (2) (2021) 82–91.

[9] S. S. D. I G. A. Agung, I. G. W. Sudatha, and A. I. W. L. Y. Sukmana, Pengembangan Multimedia Pembelajaran Interaktif Berorientasi Pendidikan Karakter Mata Pelajaran Bahasa Bali, J. Educ. Technol., 3(3) (2019) 190–195.

[10] U. Maria, A. Rusilowati, W. Hardyanto, C. Tengah, and J. Tengah, Interactive Multimedia Development in The Learning Process of Indonesian Culture Introduction Theme for 5-6 Year Old Children Article Info, J. Prim. Educ., 8 (3) (2019) 344–353,

[11] P. D. Silitonga, D. Gultom, and I. Sri Morina, Pengenalan Rumah Adat Sumatera Utara Menggunakan Augmented Rality Berbasis Android, J. ICT Inf. Commun. Technol., 19(2) (2021) 82–86,

[12] A. R. Dayat and L. Angriani, Perancangan Aplikasi Pengenalan Kebudayaan Khas Papua Berbasis Augmented Reality, JISKa, 5(1) (2020) 42–55.

[13] D. Septian, Y. Fatman, S. Nur, U. Islam, and N. Bandung, Implementasi Mdlc (Multimedia Development Life Cycle) Dalam Pembuatan Multimedia Pembelajaran Kitab Safinah Sunda, J. Comput. Bisnis, 15(1) (2021) 15–24.

[14] I. Y. Sumendap, V. Tulenan, S. Diane, and E. Paturusi, Pembuatan Animasi 3 Dimensi Menggunakan Metode Multimedia Development Life Cycle (Studi Kasus : Tarian Dana Dana Daerah Gorontalo), J. Tek. Inform., 14(2) (2019) 227–234.

Volume 5, Issue 2, pages 181-194

p-ISSN 2655-8564, e-ISSN 2685-9432

[15] T. Ahmad, J. Iqbal, A. Ashraf, D. Truscan, and I. Porres, Model-based testing using UML activity diagrams: A systematic mapping study, Comput. Sci. Rev., 33 (2019), 98–112.

[16] A. Rajab et al., UCLAONT: Ontology-Based UML Class Models Verification Tool, Appl. Sci., 12(3) (2022) 1–17.

[17] H. Koç, A. M. Erdoğan, Y. Barjakly, and S. Peker, UML Diagrams in Software Engineering Research: A Systematic Literature Review, MDPI, (2021) 13.

[18] Y. Rasheed, F. Azam, M. W. Anwar, and H. Tufail, A model-driven approach for creating storyboards of web based user interfaces, ACM Int. Conf. Proceeding Ser., (2019) 169–173.

[19] K. R. Chandu, E. Nyberg, and A. W. Black, Storyboarding of recipes: Grounded contextual generation, ACL 2019 - 57th Annu. Meet. Assoc. Comput. Linguist. Proc. Conf., (2020) 6040–6046.

[20] D. Ateşoğulları and A. Mishra, White Box Test Tools: a Comparative View, Int. J. Inf. Technol. Secur. 3 (2019).

[21] Z. A. K. Hamza and M. Hammad, Testing approaches for Web and mobile applications: An overview, Int. J. Comput. Digit. Syst., 90(4) (2020) 657–664.

International Journal of Applied Sciences and Smart Technologies

Volume 5, Issue 2, pages 195-212

p-ISSN 2655-8564, e-ISSN 2685-9432

Analysis of Blasting Geometry on Blasting Production Results at PT Semen Bosowa Maros

Abdul Salam Munir[1*], Nur Asmiani[1], Nurliah Jafar[1], Muhamad Hardin Wakila[1], Jihan Fitri Ramdita Putri Gouw[1]

[1] Department of Mining Engineering, Faculty of Industrial Technology, Universitas Muslim Indonesia, Makassar, 90242, Indonesia
*Corresponding Author: salammunir@umi.ac.id

(Received 23-05-2023; Revised 13-06-2023; Accepted 22-06-2023)

Abstract

Limestone mining for cement plants uses a blasting method to break the material. Blasting production is considered successful when it can achieve production targets based on tonnage of uncovered rock, efficient use of explosives, grain size or rock fragmentation, and environmental impact. This research aims to analyze the blasting geometry on the production results at the research location by knowing the initial design, the actual blasting geometry, and the geometry recommendation using the C.J. Konya method. In addition, researchers also know the explosives used, the production results in the form of material fractionation using the Kuz-Ram method, and the tonnage of uncovered rocks. The initial design with a burden of 3.4 m, spacing of 3.4 m, hole depth of 5.9 m, and ANFO explosives per hole of 33 kg produced 147.31 tonnages. The actual geometry with a burden of 1.7 m, spacing of 3.5 m, hole depth of 6.0 m, and ANFO explosives per hole of 26.73 kg produced a 77.11 tonnage. The actual geometry resulted in a blasting production of 6,941 tonnes per day, which did not meet the company's production target of 10,639. The fragmentation calculation results obtained an average size in the field of 15.29 cm, which meets the required screening or sieve criteria of 0.80 - 1.00 m. The size of the fragments also follows the sieve calculation using the Kuz-Ram method, with a 100 cm sieve passing only 0.01 %. Based on this, the company is recommended to make geometry changes to achieve the production tonnage target that has been set.

Keywords: blasting, geometry, fragmentation, tonnage

1 Introduction

In mining activities, blasting is one of the methods that can be used for material dismantling. Blasting production is considered successful when it can achieve production targets based on tonnage of uncovered rock [1], efficient use of explosives [2], grain size or rock fragmentation [3], and environmental impact [4]. Blasting activities aim to

This work is licensed under a Creative Commons Attribution 4.0 International License

Volume 5, Issue 2, pages 195-212
p-ISSN 2655-8564, e-ISSN 2685-9432

destroy rocks to facilitate and facilitate the excavation process with an excavator. Blast planning in the form of blast geometry and the use of explosive quantity affect the blast result [5].

The results of explosions, called explosive eruptions, range from the smallest size, such as pebbles, to boulders. Chunks formed during the explosion are called oversize. To prevent the formation of chunks or to obtain a uniform size according to the needs of the crusher, it is necessary to adjust the geometry of the explosive to the rock fragmentation caused by the explosion [6] [7]. The production of rock fragmentation is a prerequisite for successful blasting, which requires the proper use of explosives to prepare to fire holes, handle explosives, load explosives, and assemble detonators [8].

Increased production results must be done to meet the cement plant's needs. One of the things that can affect these results is the blasting activity itself. Therefore, an analysis of blasting geometry on blasting production results needs to be done to meet the increased blasting production target. Based on this, the author conducted this research to provide recommendations for increasing blasting yields to meet factory needs at PT Semen Bosowa Maros.

2 Research Methodology

a. Measurement of blasting geometry

Data collection began with measuring the diameter of the blast hole resulting from drilling, the depth of the blast hole resulting from drilling, the burden, borehole spacing, and the amount of explosive charge in the blast hole by measuring with a rolling meter. Figures 1 and 2 show the blasting geometry and explosive charge measurements.



Figure 1. Blasting geometry measurement

International Journal of Applied Sciences and Smart Technologies

Volume 5, Issue 2, pages 195-212

p-ISSN 2655-8564, e-ISSN 2685-9432



Figure 2. Filling and measuring of explosive contents

b. Explosive Identification

Explosive data was obtained from company data and directly observed explosives processing at the explosives warehouse. Processing is mixing ammonium nitrate and fuel oil explosives into ANFO which will be used in blasting activities. Figure 3 shows the mixing of the explosives used.



Figure 3. Mixing of the explosives used

c. Measurement of blasting production output

Blasting production data in mining activities was obtained from company data at the mine planning division of PT Semen Bosowa Maros. In addition, the author also directly observed the blasting results in the mining pit and the fragmentation of the blasting results at the mouth (hopper) of the crusher. Figure 4 shows the mining pit and crusher hopper.

International Journal of Applied Sciences and Smart Technologies

Volume 5, Issue 2, pages 195-212

p-ISSN 2655-8564, e-ISSN 2685-9432



Figure 4. Mining pit and crusher hopper

d. Rock Sampling

The last activity in the field was the collection of rock samples at the research site to identify the physical and mechanical properties of rocks associated with blasting activities. Rock samples are taken in the form of chunks that meet the test requirements using the tool shown in Figure 5 below.



Figure 5. Sampling equipment and rock samples

e. Preparation and Testing of Physical Properties and Mechanical Properties

The samples obtained from the field were then brought to the laboratory for testing. The testing process begins with preparing the sample in advance according to the test requirements. Sample in the boulder form is first drilled using a drilling machine and cut according to the Geomechanics Laboratory of Universitas Muslim Indonesia provisions. Figure 6 shows the drilling and cutting of rock samples.

International Journal of Applied Sciences and Smart Technologies

Volume 5, Issue 2, pages 195-212

p-ISSN 2655-8564, e-ISSN 2685-9432



Figure 6. Drilling and cutting of rock sample

Testing of physical and mechanical properties uses testing standards according to the International Rock Mechanics Society (IRMS). The prepared samples were then tested for physical properties by weighing the weight of natural samples, the weight of saturated samples, the weight of saturated samples suspended in water, and the weight of dry rock samples. After that, mechanical properties testing was carried out with the uniaxial compressive strength (UCS) test type to determine the compressive strength value of the rock. Figure 7 shows physical properties and mechanical properties testing (UCS).



Figure 7. Physical properties and mechanical properties testing (UCS)

The field and laboratory testing data are then processed and analyzed. The data processing includes blasting production calculation, rock fragmentation calculation using the Kuz-Ram method, and explosive usage recommendation and blasting geometry calculation using the C.J. Konya method.

International Journal of Applied Sciences and Smart Technologies

Volume 5, Issue 2, pages 195-212

p-ISSN 2655-8564, e-ISSN 2685-9432

3 Results and Discussions

PT Semen Bosowa Maros uses an open pit mining system with a quarry mining method with the help of blasting to break the material before excavation or retrieval of mining material which is the raw material for the company's cement factory. The rock found at the research site is limestone with physical properties: average density of 2.16 tonnes/m^3, porosity of 4.12 %, and uniaxial compressive strength of 25.73 MPa. The rocks at the study site are categorized as soft rock according to the classification of rocks based on material strength, according to Bienieawski (1973) [9] and the International Society for Rock Mechanics (1981) [10].

3.1. Initial Blasting Design Parameters

Every company that will use the blasting method in dismantling its mining material must conduct a study to obtain an initial design of the geometry and explosives that will be applied later by the Ministry of Energy and the Mineral Resources Republic of Indonesia Regulation No. 1827 K/30/MEM/2018 concerning Guidelines for the Implementation of Good Mining Engineering Principles [11]. The following are the parameters of the initial design of blasting activities at the research site.

a) Blasting Geometry

The design geometry is a geometry that PT Semen Bosowa Maros has calculated. The following Table 1 shows the results of the design geometry calculation:

Table 1. Initial geometry of the blast design

Geometry Parameters	Geometry Values
Diameter of blast hole (De)	4.5 Inch / 114.3 mm
Burden (B)	3.4 meters
Spacing (S)	3.4 meters
Borehole depth (L)	6.2 meters
Stemming (T)	2.2 meters
Fill-in column (PC)	4.0 meters
Bench height (H)	5.9 meters
Subdrilling (J)	0.3 meters
Specify gravity (SG)	0.81 tonnes/BCM
Rock Density	2.16 tonnes/m^3

Volume 5, Issue 2, pages 195-212
p-ISSN 2655-8564, e-ISSN 2685-9432

b) The volume of Rock Blasted Per blast hole

The blasting volume results from the blasting geometry of an open pit mine that generally applies bench blasting or bench blasting depending on the load, spacing, and height of the bench. The planned volume obtained is 147.32 tonnes in each hole. This value is derived from the three parameters above multiplied by the rock density of 2.16 tons/m^3.

c) Loading Density

Loading density is the amount of explosive charge per meter length of the charge column that will be inserted into the blast hole. The design loading density value is 8.25 kg/m.

d) Number of Explosives

The explosive design uses ammonium nitrate and fuel oil or ANFO, whose value is obtained by multiplying the loading density by the length of the filling column to obtain the number of blast holes per hole of 33.00 kg.

e) Powder Factor

The powder factor is one of the important parameters in blasting activities that shows the amount of material uncovered by a certain amount of explosives. The design powder factor is 0.18 kg/m^3.

3.2. Actual Blasting Parameters

The design produced before the blasting activity becomes the reference in conducting the blasting activity. However, these parameters often differ from those applied [12] [13]. The following are the actual parameters of blasting activities the company applies at the research site.

a) Blasting Geometry

The actual geometry is the geometry applied by PT Semen Bosowa Maros. Table 2 shows the company's actual geometry after drilling and inserting explosives. The following is the actual geometry applied:

Volume 5, Issue 2, pages 195-212

p-ISSN 2655-8564, e-ISSN 2685-9432

Table 2. Actual geometry after blast hole drilling

Geometry Parameters	Geometry Values
Diameter of blast hole (De)	4.5 Inch / 114.3 mm
Burden (B)	1.7 meters
Spacing (S)	3.5 meters
Borehole depth (L)	6.0 meters
Stemming (T)	2.4 meters
Fill-in column (PC)	3.24 meters
Bench height (H)	6.0 meters
Subdrilling (J)	0.0 meters
Specify gravity (SG)	0.81 tonnes/BCM
Rock Density	2.16 tonnes/m^3

b) Volume of Rock Blasted Per blast hole

The volume of blasting results from the blasting geometry in the open pit mine obtained based on the actual geometry applied by the company. The volume of rock is 77.11 tonnes in each hole. The volume was obtained using a burden of 1.7 m and a distance of 3.5 m between blast holes.

c) Loading density

The loading density used in the actual blasting activity was the same as the initial design, with a value of 8.25 kg/m.

d) Number of Explosives

Similarly, the amount of explosive used in one hole is the same as the design value, which is 26.73 kg with an explosive fill length of 3.24 m.

e) Powder Factor

The powder factor is still the same as the 0.75 kg/m^3 design parameter.

f) Explosives

Explosives have different characters, whether they are general or industrial explosives. Different types of explosives will produce different material explosions. The greater the explosive's energy, the greater the effect on the rock and surrounding area. PT Semen Bosowa Maros uses ANFO explosives. ANFO is an explosive that consists of a mixture of ammonium nitrate from PT Dahana and fuel oil in a 94.2 : 5,8% ratio. The average detonation speed for this explosive is 4170 m/sec.

Volume 5, Issue 2, pages 195-212
p-ISSN 2655-8564, e-ISSN 2685-9432

These explosives are generally used in dry blast-hole conditions. However, suppose it rains and causes the blast hole to fill with water. In that case, the company removes the water from the blast hole with a pump, and then the ANFO explosives are put into linear plastic so that the explosives do not dissolve in water or wet blast hole walls, after which the blast hole is closed with stemming.

3.3. Fragmentation of Blasted Material

Rock fragmentation or grain size of the blasted rock is one of the most important factors in assessing the success of blasting activities expressed by the size of the material or rock following the standards or design of the company [14]. The success of blasting can increase the yield of the production target [15], increase productivity [16], reduce haulage costs [17] and reduce secondary blasting, which can lead to over-utilization of the cost [18]. The rock fragmentation size required by PT Semen Bosowa Maros is 0.80-1.00 meters to meet the capability of the hopper crusher. Figure 8 shows rock Fractionation in the Hopper Crusher.



Figure 8. Rock Fractionation in the Hopper Crusher

Rock fragmentation in the field is calculated by first identifying rock conditions using the rock mass weighting method for blasting (Table 3). The following is the calculation of rock fragmentation using the Kuz-Ram method using actual blasting parameter data.

Volume 5, Issue 2, pages 195-212

p-ISSN 2655-8564, e-ISSN 2685-9432

Table 3. The blastability index parameters for PT Semen Bosowa blasting

Rock Mass Description (RMD)	
Blocky	20
Joint Plane Spacing (JPS)	
Wide (spacing > 1 m)	50
Joint Plane Orientation (JPO)	
Dip into face	40
Specific Gravity Influence (SGI)	4
Hardness (H)	3

a) Rock Factor

The factor that affects the rock factor value comes from the blast ability index, which shows the condition of the rock to be blasted. Previous researchers have calculated blast ability with rock mass description, which is blocky with a value of 20, joint plane spacing, which is wide with a value of 50, joint plane orientation, which is dip into the face with a value of 40, specific gravity influence worth four and hardness or hardness worth three [19]. This data shows the rock factor value of 6.42.

b) Average Size of Rock Fragmentation

The average rock fragmentation is obtained using the equation from Kuz-Ram, which is useful to determine the average size of the blasting results and becomes a determining factor in determining the geometry of the recommendation so that the rock can fit the size of the crusher hopper opening. The average size of the resulting rock fragmentation results from the volume of uncovered rock, the number of explosives in each hole drilled, and the relative weight strength of the explosives used, namely, ANFO. Based on this, the average fragmentation size in the field is 15.29 cm.

c) Index of Uniformity (n)

The uniformity index shows the distribution of similarity of grain size or fragmentation of blasting results based on blasting design parameters, including the standard deviation of drilling activities, especially the depth of the borehole. A small standard deviation value indicates minimal borehole non-uniformity [20]. The uniformity index of rock fragmentation at the study site is 1.81. This value is within the generally accepted range of values between 0.8 and 2.2.

Volume 5, Issue 2, pages 195-212
p-ISSN 2655-8564, e-ISSN 2685-9432

d) Rock Size Characteristics

Rock size characteristics are based on the average grain size, and uniformity index values show that the smaller these characteristics, the more uniform the blasted rock. The characteristic value of rock size at the research location is 18.72 cm.

e) Fragmentation Size Distribution of Retained Rocks

This distribution shows the rock size distribution on several sizes of sieving material, which is a means of assessing grain size after blasting activities. Each sieve has a different size. The distribution of rock size obtained will be smaller if the sieve used is larger. In this study, an increase in sieve size is used every 10 cm so that the percentage of material that does not pass on the sieve can be known. The following Table 4 is the fragmentation size distribution.

Table 4. Distribution of fragmentation retained on the sieve

Material Sieving Size (cm)	**Fragmentation Distribution** (%)
R 10	38,04
R 20	14,47
R 30	5,51
R 40	2,09
R 50	0,80
R 60	0,30
R 70	0,12
R 80	0,04
R 90	0,02
R 100	0,01

In calculating the percentage of material retained on the sieve, the results show that the material retained on the 10 cm size sieve is 38.04%, the 20 cm size sieve is 14.47%, the 30 cm size sieve is 5.51%, the 40 cm size sieve is 2.09%, the 50 cm size sieve is 0.80%, the 60 cm size sieve is 0.30%, the 70 cm size sieve is 0.12%, the 80 cm size sieve is 0.04%, the 90 cm size sieve is 0.02%, and the 100 cm size sieve is 0.01%.

f) Fragmentation Size Distribution of Unretained Rocks

Volume 5, Issue 2, pages 195-212
p-ISSN 2655-8564, e-ISSN 2685-9432

The percentage of rock grain size distribution that passes or is not retained on each sieve must also be known. The method used to obtain the value of the material pass rate from the blasting process with various sizes on the sieve was used, namely the Kuz-Ram method. Although this method has shortcomings, it needs to consider several external factors in its calculations, such as delay time settings, free fields, and the potential presence of water in the blasting hole [19]. Table 5 below shows the distribution of unretained rock fragmentation.

Table 5. Distribution of fragmentation not retained on the sieve

Material Sieving Size (cm)	**Fragmentation Distribution** (%)
R 10	61,96
R 20	85,53
R 30	94,49
R 40	97,91
R 50	99,20
R 60	99,70
R 70	99,88
R 80	99,96
R 90	99,98
R 100	99,99

In calculating the percentage of material that passes on the sieve, the results show that the material that passes on the 10 cm size sieve is 61.96%, the 20 cm size sieve is 85.53%, the 30 cm size sieve is 94.49%, the 40 cm size sieve is 97.91%, the 50 cm size sieve is 99.20%, the 60 cm size sieve is 99.70%, the 70 cm size sieve is 99.88%, the 80 cm size sieve is 99.96%, the 90 cm size sieve is 99.98%, and the 100 cm size sieve is 99.99%.

PT Semen Bosowa Maros production target is 323,614 tonnes per month or 10,639 tonnes per day. The realization obtained is 243,433 tonnes per month or 80.03 tonnes per day. This value is certainly quite far from the target set by the company. As a consideration, the blasting target can be adjusted to the blasting conditions and equipment capabilities used by the company. The blasting target can use an equation based on the burden, blast-hole spacing, and borehole depth parameters [21].

Volume 5, Issue 2, pages 195-212
p-ISSN 2655-8564, e-ISSN 2685-9432

Based on these calculations, the realistic targets that the company can use are the volume target per hole, which is 35.70 m^3 /hole, the volume target per day, which is 3,213 m^3 /BCM or 6,941 tonnes/day, and the target per month, which is 208,203 tonnes/month. These results are quite different from PT Semen Bosowa Maros planning in 2021 of 323,614 tonnes per month or 10,639 tonnes per day. This happens because the use of geometry obtained from the results of research data in the field needs to follow the planning that the company determines. This is enough to give insignificant results with planning, such as geometry and production targets that still need to be achieved. So it is an option for the company to change the geometry or reduce the production target.

3.4. Recommended Blasting Parameters C.J. Konya Method

Based on the above research results, companies can get the expected blasting results by changing the blasting geometry or reducing the production target. So the author provides recommendations for blasting parameters using the C.J. Konya method, as follows.

a) Blasting Geometry

Here is the recommended geometry:

Table 6. Actual geometry after blast hole drilling

Geometry Parameters	Geometry Values
Diameter of blast hole (De)	4.5 Inch / 114.3 mm
Burden (B)	3.12 meters
Spacing (S)	4.1 meters
Borehole depth (L)	6.9 meters
Stemming (T)	2.2 meters
Fill-in column (PC)	4.7 meters
Bench height (H)	6.0 meters
Subdrilling (J)	0.9 meters
Specify gravity (SG)	0.81 tonnes/BCM
Rock Density	2.16 tonnes/m^3

Theoretical geometry calculations calculated using the equation with the provisions of C.J. Konya obtained results (Table 6), namely the diameter of the blast hole of 4.5 inches or 114.3 mm, the burden of 3.12 meters, spacing of 4.1 meters, stemming of 2.2

Volume 5, Issue 2, pages 195-212
p-ISSN 2655-8564, e-ISSN 2685-9432

meters, sub drilling of 0.9 meters, borehole depth of 6.9 meters, bench height of 6 meters, length of the fill column of 4.7 meters, specify gravity or relative density of explosives of 0.81 tons/BCM, and rock density of 2.16 tons/m^3.

b) Volume of Rock Blasted Per blast hole

The recommended geometry above gives a value for the volume of rock that can be blasted in each hole 166.320 tonnes.

c) Loading density

The recommended loading density remains the same at 8.25 kg/m.

d) Number of Explosives

Due to the change in geometry above, the number of explosives has also changed to match the change, which is 39 kg with an explosive fill length of 4.7 m.

e) Powder Factor

The change in the amount of explosives caused the powder factor to change to 0.51 kg/m^3.

The actual geometry and recommended geometry significantly differ from the results of the company's design geometry planned by PT Semen Bosowa Maros. This significant difference occurs because the application of geometry is not as planned or determined by PT Semen Bosowa Maros, so the results are far from planned. This also affects the blasting fragmentation results and blasting production targets.

The design geometry set by the company is a blast hole diameter of 4.5 inches or 114.3 mm, a burden of 3.4 meters, a spacing of 3.4 meters, a borehole depth of 6.2 meters, stemming of 2.2 meters, a fill column length of 4 meters, a level height of 5.9 meters, and sub drilling of 0.3 meters. The blasting parameters of initial geometry are the relative density or specific gravity of explosives of 0.81 tonnes/BCM, rock density of 2.16 tonnes/m^3, loading density of each blast hole is 8.25 g/m, the amount of explosives in each hole is 33 kg, and the powder factor is 0.18 kg/m^3. The initial geometry designs and blasting parameters produce the volume of blasted rock of 147.321 tonnes per blast hole.

The actual geometry obtained from the results of field research, namely the diameter of the blast hole of 4.5 inches or 114.3 mm, a burden of 1.7 meters, a spacing of 3.5 meters, a borehole depth of 6.0 meters, stemming of 2.4 meters, a fill column length

Volume 5, Issue 2, pages 195-212
p-ISSN 2655-8564, e-ISSN 2685-9432

of 3.24 meters, a level height of 6.0 meters, and sub drilling of 0 meters. The blasting parameters of initial geometry are the relative density or specific gravity of explosives of 0.81 tonnes/BCM, rock density of 2.16 tonnes/m^3, loading density of each blast hole is 8.25 g/m, the amount of explosives in each hole is 26.73 kg, and the powder factor is 0.75 kg/m^3. The actual geometry and blasting parameters produce the volume of blasted rock of 77.112 tonnes per blast hole.

Blasting parameter recommendations obtained using the method of C.J. Konya obtained results, namely the diameter of the blast hole of 4.5 inches or 114.3 mm, a burden of 3.12 meters, a spacing of 4.1 meters, stemming of 2.2 meters, sub-drilling of 0.9 meters, a borehole depth of 6.9 meters, a level height of 6 meters, a fill column length of 4.7 meters, specify gravity or relative density of explosives of 0.81 tonnes/BCM, rock density of 2.16 tonnes/m^3, loading density for each blast hole is 8.25 kg/m, the amount of explosives per blast hole is 39 kg, and the powder factor obtained is 0.51 kg/m^3. The geometry and blasting parameter recommendations produce the volume of blasted rock of 166.320 tonnes per blast hole.

Based on these recommendations, blasting activities can produce 374,200 tons per month or 14,968.8 tons per day of limestone with an average number of blast holes of 90 per day and blasting for 25 days per month. This is more than PT Semen Bosowa's blasting production target of 323,614 tons per month or 10,639 tons per day. Blasting activities do not affect the quality of the limestone produced because the limestone at PT Semen Bosowa has a large thickness so that blasting drilling can be controlled not to penetrate other types of rocks or pass through the limestone layer itself.

4 Conclusions

Based on the analysis of blasting geometry on blasting production results at PT Semen Bosowa Maros. The following are the conclusions obtained from the results.

1. There are differences in parameters between the design and the actual, both in the amount of explosives and the actual geometry. This can prevent achieving the blasting production target set by the company.

2. The fragmentation produced in the blasting activity meets the set requirements of 0.8-1.0 meters with almost 100% fragmentation results.
3. The company is recommended to choose between changing the geometry and the number of explosives by changing the blasting production target. For example, the length of the fill column becomes 4.7 meters, the burden 3.12, the spacing 4.1, and the number of explosives 39 kg.

Acknowledgements

We sincerely thank PT Semen Bosowa Maros Indonesia. This research project was financed by the Faculty Development Fund (DPF) of the Faculty of Industrial Technology, University Muslim of Indonesia Makassar.

References

[1] R. Susanti and T. A. Cahyadi, Kajian teknis operasi peledakan untuk meningkatkan nilai perolehan hasil peledakan di Tambang Batubara Kab. Kutai Kartanegara Provinsi Kalimantan Timur, in Seminar Nasional Kebumian 2011, (2011).

[2] A. Pomasoncco-Najarro, C. Trujillo-Valerio, L. Arauzo-Gallardo, C. Raymundo, G. Quispe, and F. Dominguez, Pre-split blasting design to reduce costs and improve safety in underground mining, Energy Reports, 8 (2022).

[3] R. M. Bhatawdekar, D. Kumar, S. Changtham, D. Pathak, S. TrilokNath, and E. T. Mohamad, Intelligent Technique for Prediction of Blast Fragmentation Due to the Blasting in Tropically Weathered Limestone, in Lecture Notes in Civil Engineering, (2022).

[4] A. Nurwaskito, R. A. Putra, and A. S. Munir, Analisis Penggunaan Balldeck pada Kegiatan Peledakan untuk Meminimalisir Flyrock, Geomine, 100(2) (2022) 280–291.

Volume 5, Issue 2, pages 195-212

p-ISSN 2655-8564, e-ISSN 2685-9432

[5] S. Ramadana and R. Kopa, Analisis Geometri Peledakan Guna Mendapatkan Fragmentasi Batuan yang Diinginkan untuk Mencapai Target Produktivitas Alat Gali Muat Kalimantan Utara, Bina Tambang, (2018).

[6] Herman, Widodo S, and Waskito AN, Analisis Pengaruh Kedalaman Lubang Ledak, Burden, dan Spacing Terhadap Perolehan Fragmentasi Batugamping, Jurnal Geomine, 3(1) (2015) 184–188.

[7] A. A. Budiman, Analisis Powder Factor Dan Fragmentasi Hasil Ledakan Menggunakan Perhitungan Kuz-Ram Pada Tambang Batubara Di Provinsi Kalimantan Timur, Jurnal Geomine, 4(2) (2016).

[8] H. A. Saputra, S. Widodo and A. Nurwaskito, Analisis Pengaruh Powder Faktor Terhadap Hasil Fragmentasi Peledakan Pada PT Semen Bosowa Maros Provinsi Sulawesi Selatan, Jurnal Geomine, 3(1) (2015).

[9] Z. T. Bieniawski, Engineering Classification of Jointed Rock Masses, Civ Eng S Afr, 15(12) (1973) 90924-3.

[10] S. Saptono, Sistem Klasifikasi Massa Batuan untuk Tambang Terbuka, 1st ed. Yogyakarta: LPPM UPN Veteran Yogyakarta, (2021).

[11] Kementrian ESDM RI, Keputusan Menteri ESDM RI No. 1827 K/30/MEM/2018 tentang Pedoman Pelaksanaan Kaidah Teknik Pertambangan yang Baik, 1(4) (2018).

[12] F. A. Ramadhan, Yuliadi, and N. F. Isniarno, Pengaruh Geometri Peledakan Terhadap Getaran Tanah dan Fragmentasi Batuan pada PT. Gunung Kulalet, Kecamatan Baleendah Kabupaten Bandung, Provinsi Jawa Barat, Bandung Conference Series: Mining Engineering, 2(2) (2022) 2925.

[13] A. Nurwaskito, Studi Teknis Pengaruh Penggunaan Sekam Padi terhadap Aktivitas Peledakan di PT Semen Bosowa Maros Provinsi Sulawesi Selatan, Jurnal Geomine, 1(1) (2016).

[14] S. A. Vokhmin, A. A. Kytmanov, G. P. Erlykov, E. V. Shevnina, G. S. Kurchin, and A. K. Kirsanov, Prediction and Actual Oversized/Undersized Fragmentation in Underground Blasting, Journal of Mining Science, 57(2) (2021).

[15] M. Z. F. Rahman, Calculation of The Cost of Underground Mining Activities on Tunnel 9 PT. Allied Indo Coal Jaya, Georest, 1(1) (2022).

Volume 5, Issue 2, pages 195-212

p-ISSN 2655-8564, e-ISSN 2685-9432

[16] A. A. M. A. Ansari, V. Seervi, N. Kishore, and N. P. Singh, An Investigation into the Effect of Rain on Fragmented Coal: A Case Study, Journal of The Institution of Engineers (India): Series D, (2023).

[17] N. Slyambekov, Review of the use of advanced technologies in drilling and blasting, Geo-Technical Mechanics, 159 (2021) 108–114.

[18] B. Ke et al., Parameter Optimization and Fragmentation Prediction of Fan-Shaped Deep Hole Blasting in Sanxin Gold and Copper Mine, Minerals, 12 (7) (2022).

[19] A. Milwadi, Rancangan Peledakan untuk Memenuhi Target Produksi dan Estimasi Biaya Produksi Peledakan pada PT Semen Bosowa Maros Kabupaten Maros Provinsi Sulawesi Selatan, Universitas Papua, Manokwari, (2017).

[20] S. Dhiyauddin, Teknik Pengamatan dan Analisis Fragmentasi Hasil Peledakan Batuan Andesit Pada Tambang PT. Gunung Mas Jaya Indah, UIN Syarif Hidayatullah Jakarta, Jakarta, (2022).

[21] W. Sundari, Analisis Lubang Ledak dan Geometri Peledakan dengan Menggunakan Metode Anderson untuk Mencapai Target Produksi pada PT. Andesit Lumbung Sejahtera di Desa Bandar Dalam Kecamatan Sidomulyo Kabupaten Lampung Selatan Provinsi Lampung, Jurnal Ilmiah Teknologi FST Undana, 15 (1) (2021) 43–52.

International Journal of Applied Sciences and Smart Technologies

Volume 5, Issue 2, pages 213-228

p-ISSN 2655-8564, e-ISSN 2685-9432

Cloud Quantum Coin-Tossing Gambling

Jose C. Moreno[1*]

[1]New American Quantum Education Society Operations (NAQESO)
1340 Reynolds Ave. #116-1070, Irvine, CA 92614, USA
*Morenj13@alumni.uci.edu

(Received 18-05-2023; Revised 30-05-2023; Accepted 08-06-2023)

Abstract

Quantum computers are an alternative way to create multipartite probabilities for a game as a function of participant's inputs. In some situations, quantum gambling could be an improvement over the predictability of certain types of random number generators. However, NISQ computers require a protocol whose expected statistical gains (losses) can be confirmed empirically given the participants' inputs. A zero-sum coin-tossing protocol with Nash equilibrium [1] is tested with a quantum computer where hypothetical players enter parameters, in their respective qubits, and are compensated 1 or R coin(s) after each outcome. In theory, independently of R, the protocol implies that there is no gain improvement for a player when the other maintains the equilibrium parameter; gain is zero or better for the player maintaining it. However, outcomes obtained with several setting combinations imply Nash equilibrium only when R is a small fraction. For $R \gg 1$, given thousands of outcomes, there is Nash-like equilibrium such that a player may not improve gain significantly by changing the parameter if the other maintains it, that is, losses (gains) are considerably minimized with the parameter. The data suggests that gains (losses) would be expected statistical functions of the participants' choices if two played in this manner.

Keywords: NISQ computer, Nash equilibrium, coin-tossing game

1 Introduction

Given the availability of quantum computers through the cloud and their current development, there are tasks that are realizable with a few qubits, such as generating multipartite probabilities as a function of remote inputs. Such a task is the case in quantum gambling protocols [2],[3],[4]. A gambling protocol with a quantum computer provides essentially probabilistic outcomes as a function of the parameters entered by participants. Certainly, quantum gambling can be an alternative to other types of RNGs [5],[6],[7] needed to create multipartite probabilities, and perhaps be an improvement over the predictability of those other types in some situations [8],[9],[10],[11]. On the other hand,

This work is licensed under a Creative Commons Attribution 4.0 International License

Volume 5, Issue 2, pages 213-228
p-ISSN 2655-8564, e-ISSN 2685-9432

games with NISQ computers require evaluation from the participants. “Errors” in the output are expected [12]. External factors can influence outcomes significantly [13]. Theoretical probabilities do not inform the number of repetitions required to verify them. In this way, players must be able to confirm that the gains (losses) result significantly from expected probabilities defined by the player’s choices.

The protocol presented is a variant of two-player coin tossing quantum gambling [14],[15] with Nash equilibrium [1] adapted to a cloud IBM superconducting quantum computer [16] where each participant could operate on one qubit of a two-qubit entanglement. Such a protocol could be realized with actual remote players operating on two qubits. In the present version of the game, the input of both players is required, measurements of the qubits are not performed at the same time, as shown in Fig. 1, and there are Nash equilibrium parameters, selected independently by each player, for which there is zero average gain per game (which will be referred simply as “gain”), or it may be improved, for the one that maintains the corresponding parameter regardless of what the other does, that is, there is no gain improvement for a player if the other is maintaining it. As shown in Fig. 1, The protocol is as follows: player-q[0] “splits” $|0\rangle_{q[0]}$ into a superposition $|\psi\rangle_{q[0]} = \cos\frac{\alpha}{2}|0\rangle_{q[0]} + \sin\frac{\alpha}{2}|1\rangle_{q[0]}$, concealing parameter α. Then, Player-q[1] also “splits” qubit $|0\rangle_{q[1]}$ into two parts, also maintaining the parameter unknown to the other, creating $|\psi\rangle_{q[1]} = \cos\frac{\beta}{2}|0\rangle_{q[1]} + \sin\frac{\beta}{2}|1\rangle_{q[1]}$, but only with $|1\rangle_{q[0]}$, which means that both form

$$\cos\frac{\alpha}{2}|0\rangle_{q[0]} \otimes |0\rangle_{q[1]} + (\sin\frac{\alpha}{2}|1\rangle_{q[0]}) \otimes \left(\cos\frac{\beta}{2}\left|0\rangle_{q[1]} + \sin\frac{\beta}{2}\right| 1\rangle_{q[1]}\right), \qquad (1)$$

and the first measurement is on $q[1]$. The rules for the game are as follow:

1) If the outcome is $|1\rangle_{q[1]}$, then player-q[1] receives one coin,

2) if not, the state of $q[0]$ is projected on a verification state $|\phi^+(\gamma)\rangle$ where γ is always decided by the two players before starting the game. If the state is verified, then player-q[0] receives R coin(s) ($R > 0$); otherwise, player-q[1] receives them.

International Journal of Applied Sciences and Smart Technologies

Volume 5, Issue 2, pages 213-228

p-ISSN 2655-8564, e-ISSN 2685-9432

Quantum Computer game protocol

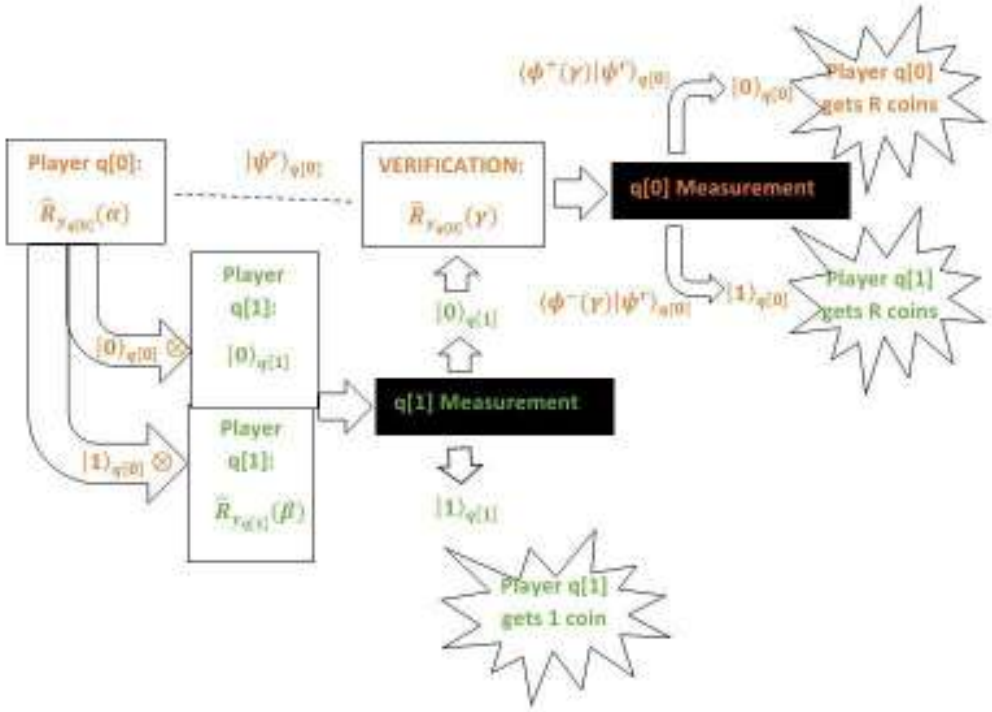


Figure 1. First, the parameter for α is entered on q[0] by one player; then the other enters β on q[1]. Both parameters lead to y-rotations. An entanglement is formed in such a way that the tensor product of $|0\rangle_{q[0]}$ and $|0\rangle_{q[1]}$ form a state, or $|1\rangle_{q[0]}$ and the state of q[1] after its rotation. The player of q[1] gets one coin if it is $|1\rangle_{q[1]}$; otherwise, another y-rotation is applied on q[0] which is now $|\psi^r\rangle_{q[0]}$. The operation is equivalent to projecting $|\psi^r\rangle_{q[0]}$ on $\langle\phi^+(\gamma)|$ or $\langle\phi^-(\gamma)|$. The former gives $|0\rangle_{q[0]}$, resulting in R coin(s) for the player of q[0]; the latter gives $|1\rangle_{q[0]}$ which means that q[1] receives the R coin(s).

International Journal of Applied Sciences and Smart Technologies

Volume 5, Issue 2, pages 213-228

p-ISSN 2655-8564, e-ISSN 2685-9432

Table 1. All possible ways to earn coins for $R > 0$ within the range shown. Notice that if the player of q[0] selects $\alpha = 0$, the average loss per game is minimized (to zero) for player-q[0] (and player-q[1]) no matter what the other player selects; the same is true for the player of q[1] when $\beta = \pi$ with the additional possibility of earning coins if $\alpha \neq 0$. There is no gain improvement for one player when the other sets the corresponding equilibrium parameter. In this way, $\alpha = 0$, $\beta = \pi, \gamma = \pi/2$, is a Nash equilibrium point in the given range. Because it is a zero-sum game, the equivalent table for the player of q[0] is the negative of each of the gains (losses) for the player of q[1].

Table for the average gains per game for the player of q[1].
$R > 0, \gamma = \pi/2$

		q[1]		
		$\frac{\pi}{2} \leq \beta < \pi$	$\beta = \pi$	$\frac{3\pi}{2} \geq \beta > \pi$
	$-\frac{\pi}{2} \leq \alpha < 0$	Depends on $R, \alpha,$	q[1] earns	Depends on R, α, β
q[0]	$\alpha = 0$	zero	zero	zero
	$\frac{\pi}{2} \geq \alpha > 0$	Depends on $R, \alpha,$	q[1] earns	Depends on R, α, β

In general, both players could follow different strategies to increase the likelihood of earning as many coins as possible, not knowing each other's specific settings. The strategy for player-q[0] is not only to diminish the likelihood of $|1\rangle_{q[0]}$, (to make sure the other does not get one coin) but also not to create a state that cannot be verified. For player-q[1], the goal is to "split" the state $q[1]$ enough to increase the likelihood of $|1\rangle_{q[1]}$, but not so much that it allows the other player to verify the remaining state of $q[0]$ if $|1\rangle_{q[1]}$ does not take place. On the other hand, there is Nash equilibrium when $\gamma = \frac{\pi}{2}, \alpha = 0, \beta = \pi$, within the range shown in Table 1. If player-q[0] changes α', either positively or negatively, there is gain for player-q[1] if $\beta = \pi$. If player-q[0] does not change the parameter, but the other does, the game remains zero-gains for both players. Thus, there is no gain improvement for the player that changes the parameter if the other does not.

International Journal of Applied Sciences and Smart Technologies

Volume 5, Issue 2, pages 213-228

p-ISSN 2655-8564, e-ISSN 2685-9432

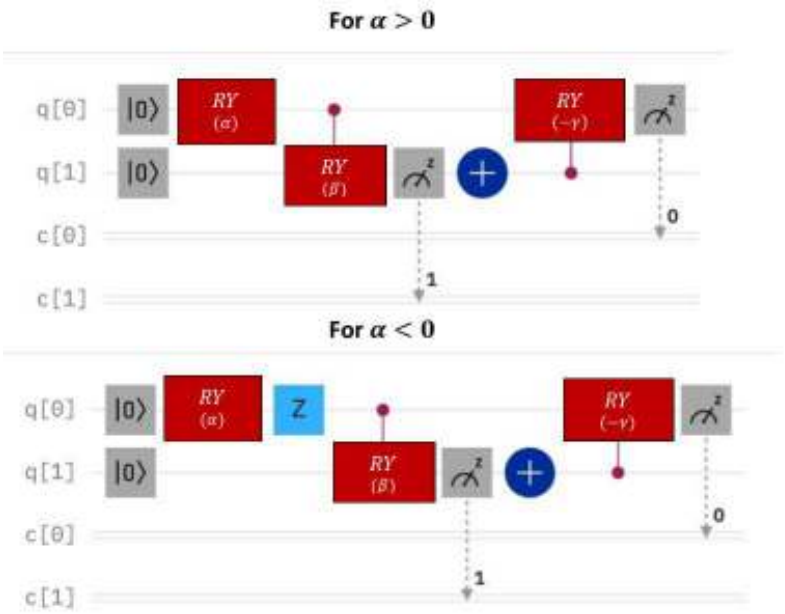


Figure 2. The upper circuit was used for $\alpha \geq 0$; the one below for $\alpha < 0$; in this way, only $|\alpha|$ was used given that $\hat{Z}\hat{R}y(|\alpha|)|0\rangle = \hat{R}y(-|\alpha|)|0\rangle$. The circuits were implemented in the IBM quantum computer "Oslo". For all the data, $\gamma = \pi/2$.

It is important to mention that no actual remote players were used to gather data; however, all data was acquired with an IBM superconducting quantum computer in the cloud. The circuit for the protocol is shown in fig. 2. Each program run determines the hypothetical player that earns coins in one "shot"; however, also thousands of continuous "shots" were obtained in one program run, repeated three times, to calculate the average and standard deviation.

The results coincide with the theoretical Nash equilibrium for $0 < R \ll 1$, and with the theoretical maximum gains (losses) when $R \gg 1$, after thousands of outcomes with a specific set of discrete parameters within the range of Table 1. Nevertheless, based on additional results, such a Nash equilibrium probably could also be confirmed with at least 20 repetitions of each setting, also letting R be a small fraction of a coin. For $R \gg 1$, given thousands of outcomes, the data suggests that if a player maintains $\alpha = 0$ or $\beta =$

Volume 5, Issue 2, pages 213-228
p-ISSN 2655-8564, e-ISSN 2685-9432

π, when the other does not, that player considerably minimizes loss, that is, a player cannot guarantee significant gain improvement by changing the parameter when the other does not, implying Nash-like equilibrium. In this manner, all the data implies that the gains (losses) that would result from the implementation of the protocol in the NISQ device with two remote players, with the specific set of discrete parameters, would be considerably expected functions of those parameters decided by the players.

The protocol presented differs from the cryptographic goal of common quantum coin-flipping protocols presented in the literature [17]. Originally, quantum coin-tossing was conceived as a solution to a "telephone" coin-toss with distrustful parties [18]. Sharing quantum information back and forth between the parties is a solution to the quandary and there have been demonstrations of such [19]. In contrast, the protocol presented in this paper requires a trustful connection to a quantum computer if two played in the cloud. Our protocol is a different paradigm that suggests to use the quantum computer as a true source of entropy as an alternate to other forms of generating multipartite probabilities rather than a secure cryptographic exchange between two parties, although a known cryptographic protocol is being tested.

2 Research Methodology

To initiate a game, two players decide R, such that $R > 0$, and impose a rotation parameter to define a verification state; then, they make concealed y-rotations on their respective qubits and perform measurements to determine the one that earns coins. The matrix representation for the y-rotation is,

$$\hat{R}_{y_{q[0]}}(\gamma) = \begin{pmatrix} \cos\left(\frac{\gamma}{2}\right) & -\sin\left(\frac{\gamma}{2}\right) \\ \sin\left(\frac{\gamma}{2}\right) & \cos\left(\frac{\gamma}{2}\right) \end{pmatrix}, \tag{2}$$

which can be written,

$$\hat{R}_{y_{q[0]}}(-\gamma) = |0\rangle_{q[0]}\langle\phi^{+}(\gamma)|_{q[0]} + |1\rangle_{q[0]}\langle\phi^{-}(\gamma)|_{q[0]} \tag{3}$$

such that

$$\langle\phi^{+}(\gamma)| = \cos\left(\frac{\gamma}{2}\right)\langle 0|_{q[0]} + \sin\left(\frac{\gamma}{2}\right)\langle 1|_{q[0]} \tag{4}$$

in the z-basis $\{|0\rangle, |1\rangle\}$, and

International Journal of Applied Sciences and Smart Technologies

Volume 5, Issue 2, pages 213-228

p-ISSN 2655-8564, e-ISSN 2685-9432

$$\langle \phi^{-}(\gamma)| = -\sin\left(\frac{\gamma}{2}\right)\langle 0|_{q[0]} + \cos\left(\frac{\gamma}{2}\right)\langle 1|_{q[0]}; \quad (5)$$

both eq. (4) and (5) will be projected on the state of $q[0]$ so that its measurement reveals whether it ends up in $\langle \phi^{+}(\gamma)|$ (verification state) or $\langle \phi^{-}(\gamma)|$ (non-verification state). However, before such a projection, Player-q[0] performs a y-rotation of $|0\rangle_{q[0]}$ with angle α, resulting in $|\psi(\alpha)\rangle_{q[0]} = \cos(\frac{\alpha}{2})|0\rangle_{q[0]} + \sin(\frac{\alpha}{2})|1\rangle_{q[0]}$ which is allowed to interact with $|\psi(\beta)\rangle_{q[1]} = \cos(\frac{\beta}{2})|0\rangle_{q[1]} + \sin(\frac{\beta}{2})|1\rangle_{q[1]}$ where player-q[1] decides β after player-q[0]. The entanglement that results from their interaction is

$$\begin{aligned} |E\rangle = \cos\left(\frac{\alpha}{2}\right)|0\rangle_{q[0]} \otimes |0\rangle_{q[1]} + \sin\left(\frac{\alpha}{2}\right)\cos\left(\frac{\beta}{2}\right)|1\rangle_{q[0]} \otimes |0\rangle_{q[1]} \\ + \sin\left(\frac{\alpha}{2}\right)\sin\left(\frac{\beta}{2}\right)|1\rangle_{q[0]} \otimes |1\rangle_{q[1]}. \end{aligned} \quad (6)$$

Now, if the measurement on $q[1]$ indicates $|1\rangle_{q[1]}$ then Player-q[1] earns one coin (Player-q[0] loses one). In case $q[1]$ is $|0\rangle_{q[1]}$, the state of q[0] that remains from eq. (6), that is $|\psi^{r}\rangle_{q[0]}$ such that

$$|\psi^{r}\rangle_{q[0]} = N \cdot [\cos\left(\frac{\alpha}{2}\right)|0\rangle_{q[0]} + \sin\left(\frac{\alpha}{2}\right)\cos\left(\frac{\beta}{2}\right)|1\rangle_{q[0]}] \quad (7)$$

where

$$N = \sqrt{\frac{1}{\left(\cos\left(\frac{\alpha}{2}\right)\right)^2 + \left(\sin\left(\frac{\alpha}{2}\right)\right)^2\left(\cos\left(\frac{\beta}{2}\right)\right)^2}}, \quad 8)$$

is projected on the verification (non-verification) state: if $|\psi^{r}\rangle_{q[0]}$ ends up in $\langle \phi^{+}(\gamma)|$ then Player-q[0] earns R coin(s) (Player-q[1] loses R coin(s)); otherwise, Player-q[1] earns them (Player-q[0] loses R coin(s)). Thus, the goal for Player-q[0] is not only that $|\psi(\alpha)\rangle_{q[0]}$ increases the likelihood that $|\psi^{r}\rangle_{q[0]}$ will be verified, but also that $|1\rangle_{q[0]}$ is unlikely. Player-q[1] must make $|\psi(\beta)\rangle_{q[1]}$ such that the one coin can be earned, but not that $|\psi^{r}\rangle_{q[0]}$ can be verified. Both will try to pick values that will minimize the gain of the opponent.

As stated in the previous section, $\gamma' = \frac{\pi}{2}, \alpha' = 0, \beta' = \pi$ is a Nash equilibrium point. If $G_{q[1]}$ and $G_{q[0]}$ are the average gain (or loss) per round of the game for Player-q[1] and Player-q[0] respectively, then

Volume 5, Issue 2, pages 213-228

p-ISSN 2655-8564, e-ISSN 2685-9432

$$G_{q[1]} = -G_{q[0]}; \tag{9}$$

thus, calculating the optimal gain for one of the players implies necessarily the loss for the other. In particular,

$$G_{q[1]} = P_1 + R(P_2 - P_3) \tag{10}$$

where P_1 is the probability that $q[1]$ is in state $|1\rangle_{q[1]}$, P_2 the probability that $|\psi^r\rangle_{q[0]}$ is not verified, and P_3 that it is verified. Eq. (9) can be used to write the expression for $G_{q[0]}$. The probabilities satisfy the condition

$$P_1 + P_2 + P_3 = 1. \tag{11}$$

Consequently, if $q[1]$ is not in state $|1\rangle_{q[1]}$ there is the possibility that $|\psi^r\rangle_{q[0]}$ will be verified, or not, such that

$$P_3 = (1 - P_1) \cdot \left(\langle\phi^+|\psi^r\rangle_{q[0]}\right)^2 \tag{12}$$

or

$$P_2 = (1 - P_1) \cdot \left(\langle\phi^-|\psi^r\rangle_{q[0]}\right)^2. \tag{13}$$

From eq. (10), (11), (12), and (13) follows that

$$G_{q[1]} = P_1 + R(1 - P_1)\left[1 - 2\left(\langle\phi^+|\psi^r\rangle_{q[0]}\right)^2\right]. \tag{14}$$

Explicitly using eq. (4), (7) and (8),

$$\begin{aligned} G_{q[1]}(\alpha,\beta,\gamma) = {} & \left(\sin\left(\frac{\alpha}{2}\right)\right)^2 \left(\sin\left(\frac{\beta}{2}\right)\right)^2 \\ & + R\left[1 - \left(\sin\left(\frac{\alpha}{2}\right)\right)^2 \left(\sin\left(\frac{\beta}{2}\right)\right)^2\right] \\ & \cdot \left\{1 - \frac{2\left(\cos\frac{\gamma}{2}\cos\frac{\alpha}{2} + \sin\frac{\gamma}{2}\sin\frac{\alpha}{2}\cos\frac{\beta}{2}\right)^2}{\left(\cos\frac{\alpha}{2}\right)^2 + \left(\sin\left(\frac{\alpha}{2}\right)\right)^2 \left(\cos\left(\frac{\beta}{2}\right)\right)^2}\right\}. \end{aligned} \tag{15}$$

for

$$\alpha' = 0,\ \beta' = \pi,\ \gamma' = \frac{\pi}{2}, \tag{16}$$

follows that $G_{q[1]}(\alpha',\beta',\gamma') = 0$; changing either α or β in eq. (15) while the other player maintains either β' or α' does not improve the average gain per game for any player, as illustrated in Fig. 3 (consistent with Table 1), when $-\frac{\pi}{2} \le \alpha \le \frac{\pi}{2}$ or $\frac{\pi}{2} \le \beta \le \frac{3\pi}{2}$. Independently of R, (α',β',γ') is a Nash equilibrium point within the range of Fig. 3.

Now, to assess the quantum computer, data was obtained from "Oslo" with two types of specific choices for each qubit using the circuit shown in Fig. 2. In the type-$\pi/3$

International Journal of Applied Sciences and Smart Technologies

Volume 5, Issue 2, pages 213-228

p-ISSN 2655-8564, e-ISSN 2685-9432

games, the choices for the hypothetical player operating $q[0]$ are $\left\{\frac{\pi}{3}, 0, -\frac{\pi}{3}\right\}_\alpha$, and $\left\{\frac{2\pi}{3}, \pi, \frac{4\pi}{3}\right\}_\beta$ for q[1]; for the type-$\pi/2$ games, $\left\{\frac{\pi}{2}, 0, -\frac{\pi}{2}\right\}_\alpha$ and $\left\{\frac{\pi}{2}, \pi, \frac{3\pi}{2}\right\}_\beta$ respectively. The upper qubit in Fig. 2 is q[0], the one below is q[1]. The parameter for the verification was $\gamma = \frac{\pi}{2}$ (on the right of fig. 2). One "shot" was obtained for each setting combination, but the process was repeated twenty times. The possible output after each repetition was $|1\rangle_{q[0]} \otimes |1\rangle_{q[1]}$, $|1\rangle_{q[0]} \otimes |0\rangle_{q[1]}$, or $|0\rangle_{q[0]} \otimes |0\rangle_{q[1]}$; respectively, each outcome was used to calculate P_1, P_2, and P_3 in eq. (10), that is, their frequencies divided by twenty. The results were compared to eq. (15). The probability for the "erroneous" state $|0\rangle_{q[0]} \otimes |1\rangle_{q[1]}$ was calculated. In addition, 1000 "shots" for each of the setting combinations were performed in one program run, repeated 3 times, to obtain an average and the standard deviation.

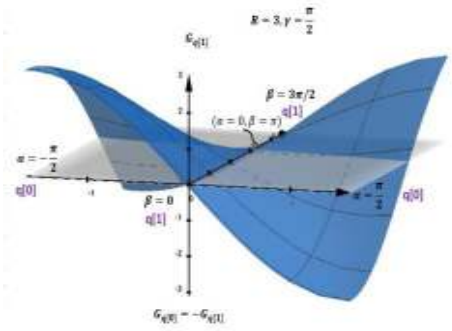


Figure 3. An illustration of Nash equilibrium for $R = 3$: if the player of q[0] moves through the equilibrium point $(\alpha = 0, \beta = \pi)$, that is, on the gray-plane and parallel to the α-axis, then there is positive gain for the player of q[1]. Doing the same along the β-axis, does not change the gain or loss for any of the players. Thus, it is a point where there is no improvement in gain for a player when the other keeps the equilibrium parameter constant. The four quadrants surrounding the equilibrium point show that, without knowing the parameter from the other, gains can be either positive or negative.

3 Results and Discussions

Table 2,3 and 4 below summarize all the results. The first two present the measured gains (losses) for the two types of games. The last one presents theoretical calculations and the "erroneous" state probability.

International Journal of Applied Sciences and Smart Technologies

Volume 5, Issue 2, pages 213-228

p-ISSN 2655-8564, e-ISSN 2685-9432

Table 2. $G_{q[1]}(\alpha,\beta,\gamma) = P_1 + R(P_2 - P_3)$, where P_1, P_2, and P_3 are the average probabilities obtained from the circuit in fig. 2 with three repetitions of 1000 "shots" each one. The standard deviations of each average were used to estimate the measurement errors. In this way, those thousands of "shots" were obtained continuously in one program run rather than one in each program run as it would be in a game.

The average of three program runs of 1000 shots in each one for $\boldsymbol{\gamma' = \pi/2}$ (Type-$\frac{\pi}{3}$ game)

	$\boldsymbol{\beta = 2\pi/3}$	$\boldsymbol{\beta = \pi}$	$\boldsymbol{\beta = 4\pi/3}$
$\boldsymbol{\alpha = -\frac{\pi}{3}}$	$G_{q[1]}(-\frac{\pi}{3},\frac{2\pi}{3},\gamma') = (0.362 \pm 0.027)(R) + (0.178 \pm 0.016)$	$G_{q[1]}(-\frac{\pi}{3},\pi,\gamma') = (-0.011 \pm 0.027)(R) + (0.215 \pm 0.007)$	$G_{q[1]}(-\frac{\pi}{3},\frac{4\pi}{3},\gamma') = (-0.379 \pm 0.036)(R) + (0.182 \pm 0.009)$
$\boldsymbol{\alpha = 0}$	$G_{q[1]}(0,\frac{2\pi}{3},\gamma') = (0.011 \pm 0.020)(R) + (0.015 \pm 0.004)$	$G_{q[1]}(0,\pi,\gamma') = (-0.021 \pm 0.020)(R) + (0.023 \pm 0.001)$	$G_{q[1]}(0,\frac{4\pi}{3},\gamma') = (-0.049 \pm 0.039)(R) + (0.014 \pm 0.004)$
$\boldsymbol{\alpha = \frac{\pi}{3}}$	$G_{q[1]}(\frac{\pi}{3},\frac{2\pi}{3},\gamma') = (-0.392 \pm 0.031)(R) + (0.165 \pm 0.008)$	$G_{q[1]}(\frac{\pi}{3},\pi,\gamma') = (-0.026 \pm 0.021)(R) + (0.241 \pm 0.021)$	$G_{q[1]}(\frac{\pi}{3},\frac{4\pi}{3},\gamma') = (0.307 \pm 0.016)(R) + (0.191 \pm 0.002)$

The average of three program runs of 1000 "shots" in each one for $\boldsymbol{\gamma' = \frac{\pi}{2}}$ (Type-$\frac{\pi}{2}$ game)

	$\boldsymbol{\beta = \pi/2}$	$\boldsymbol{\beta = \pi}$	$\boldsymbol{\beta = 3\pi/2}$
$\boldsymbol{\alpha = -\frac{\pi}{2}}$	$G_{q[1]}(-\frac{\pi}{2},\frac{\pi}{2},\gamma') = (0.588 \pm 0.017)(R) + (0.238 \pm 0.013)$	$G_{q[1]}(-\frac{\pi}{2},\pi,\gamma') = (-0.012 \pm 0.014)(R) + (0.469 \pm 0.014)$	$G_{q[1]}(-\frac{\pi}{2},\frac{3\pi}{2},\gamma') = (-0.627 \pm 0.015)(R) + (0.239 \pm 0.008)$
$\boldsymbol{\alpha = 0}$	$G_{q[1]}(0,\frac{\pi}{2},\gamma') = (-0.035 \pm 0.019)(R) + (0.015 \pm 0.002)$	$G_{q[1]}(0,\pi,\gamma') = (-0.021 \pm 0.020)(R) + (0.023 \pm 0.001)$	$G_{q[1]}(0,\frac{3\pi}{2},\gamma') = (-0.063 \pm 0.025)(R) + (0.012 \pm 0.003)$
$\boldsymbol{\alpha = \frac{\pi}{2}}$	$G_{q[1]}(\frac{\pi}{2},\frac{\pi}{2},\gamma') = (-0.663 \pm 0.020)(R) + (0.220 \pm 0.010)$	$G_{q[1]}(\frac{\pi}{2},\pi,\gamma') = (-0.032 \pm 0.026)(R) + (0.460 \pm 0.006)$	$G_{q[1]}(\frac{\pi}{2},\frac{3\pi}{2},\gamma') = (0.589 \pm 0.011)(R) + (0.245 \pm 0.008)$

International Journal of Applied Sciences and Smart Technologies

Volume 5, Issue 2, pages 213-228

p-ISSN 2655-8564, e-ISSN 2685-9432

Table 3. $G_{q[1]}(\alpha,\beta,\gamma) = P_1 + R(P_2 - P_3)$, where P_1, P_2, and P_3 are respectively the frequencies of $|1\rangle_{q[0]} \otimes |1\rangle_{q[1]}$, $|1\rangle_{q[0]} \otimes |0\rangle_{q[1]}$, and $|0\rangle_{q[0]} \otimes |0\rangle_{q[1]}$ divided by 20. Data was obtained from the circuit in fig. 2 with one "shot" for each run of the program but repeated 20 times. This is how the outcomes for an actual game are obtained.

$G_{q[1]}$ for 20 program runs of one "shot" in each one for $\gamma' = \frac{\pi}{2}$(Type-$\frac{\pi}{3}$ game)

	$\beta = 2\pi/3$	$\beta = \pi$	$\beta = 4\pi/3$
$\alpha = -\frac{\pi}{3}$	$G_{q[1]}(-\frac{\pi}{3},\frac{2\pi}{3},\gamma') = 0.4(R) + 0.15$	$G_{q[1]}(-\frac{\pi}{3},\pi,\gamma') = -0.1(R) + 0.4$	$G_{q[1]}(-\frac{\pi}{3},\frac{4\pi}{3},\gamma') = -0.45(R) + 0.5$
$\alpha = 0$	$G_{q[1]}(0,\frac{2\pi}{3},\gamma') = -0.1(R)$	$G_{q[1]}(0,\pi,\gamma') = 0.05(R) + 0.05$	$G_{q[1]}(0,\frac{4\pi}{3},\gamma') = 0$
$\alpha = \frac{\pi}{3}$	$G_{q[1]}(\frac{\pi}{3},\frac{2\pi}{3},\gamma') = -0.45(R) + 0.25$	$G_{q[1]}(\frac{\pi}{3},\pi,\gamma') = 0.25$	$G_{q[1]}(\frac{\pi}{3},\frac{4\pi}{3},\gamma') = -0.10(R) + 0.25$

$G_{q[1]}$ for 20 program runs of one "shot" in each one for $\gamma' = \pi/2$

(Type-$\frac{\pi}{2}$ game)

	$\beta = \pi/2$	$\beta = \pi$	$\beta = 3\pi/2$
$\alpha = -\frac{\pi}{2}$	$G_{q[1]}(-\frac{\pi}{2},\frac{\pi}{2},\gamma') = 0.75(R) + 0.25$	$G_{q[1]}(-\frac{\pi}{2},\pi,\gamma') = 0.30$	$G_{q[1]}(-\frac{\pi}{2},\frac{3\pi}{2},\gamma') = -0.65(R) + 0.3$
$\alpha = 0$	$G_{q[1]}(0,\frac{\pi}{2},\gamma') = -0.1(R)$	$G_{q[1]}(0,\pi,\gamma') = 0.05(R) + 0.05$	$G_{q[1]}(0,\frac{3\pi}{2},\gamma') = -0.25(R)$
$\alpha = \frac{\pi}{2}$	$G_{q[1]}(\frac{\pi}{2},\frac{\pi}{2},\gamma') = -0.35(R) + 0.35$	$G_{q[1]}(\frac{\pi}{2},\pi,\gamma') = -0.15(R) + 0.40$	$G_{q[1]}(\frac{\pi}{2},\frac{3\pi}{2},\gamma') = 0.45(R) + 0.25$

International Journal of Applied Sciences and Smart Technologies

Volume 5, Issue 2, pages 213-228

p-ISSN 2655-8564, e-ISSN 2685-9432

Table 4. Measured average gain per game for the player-q[1] using the circuit in figure 2, and also calculated using eq. (15). $G_{q[1]} = P_1 + R(P_2 - P_3)$ where P_1 is the probability to obtain $|1\rangle_{q[0]} \otimes |1\rangle_{q[1]}$, P_2 and P_3 are those that correspond to $|1\rangle_{q[0]} \otimes |0\rangle_{q[1]}$ and $|0\rangle_{q[0]} \otimes |0\rangle_{q[1]}$ respectively. Also, the probability of the "erroneous" state $|0\rangle_{q[0]} \otimes |1\rangle_{q[1]}$ was calculated for the 20 program runs of one "shot" in each one (left column) and the average of 3 program runs of 1000 "shots" in each one (right column).

Measured $G_{q[1]}$ vs. theoretical $G_{q[1]}$ for $\gamma' = \pi/2$

Type- $\pi/3$				
Settings $(q[0], q[1])$	**From "Oslo", 20 program runs of one "shot" in each one** $G_{q[1]} =$	**Theoretical** $G_{q[1]} =$	**Prob. Of** $\|0\rangle_{q[0]} \otimes \|1\rangle_{q[1]}$ (Not used in Table 3)	**Prob. Of** $\|0\rangle_{q[0]} \otimes \|1\rangle_{q[1]}$ (Not used in Table 2)
$(\pi/3,2\pi/3)$	$-0.45(R) + .25$	$-0.4331(R) + .1875$	0.00	0.038 ± 0.003
$(\pi/3,4\pi/3)$	$-0.10(R) + .25$	$+0.4331(R) + .1875$	0.05	0.026 ± 0.007
$(-\pi/3, 2\pi/3)$	$+0.4(R) + 0.15$	$+0.4331(R) + .1875$	0.05	0.033 ± 0.007
$(-\pi/3,4\pi/3)$	$-0.45R + 0.05$	$-0.4331(R) + .1875$	0.00	0.036 ± 0.002
$(0, 4\pi/3)$	0	0	0.00	0.030 ± 0.003
$(\pi/3, \pi)$	.25	.25	0.05	0.030 ± 0.010
$(0, 2\pi/3)$	$-0.10(R)$	0	0.00	0.025 ± 0.002
$(-\pi/3, \pi)$	$-0.10(R) + 0.4$	.25	0.00	0.038 ± 0.002

Type- $\pi/2$				
Settings $(q[0], q[1])$	**From "Oslo", 20 program runs of one "shot" in each one,** $G_{q[1]} =$	**Theoretical** $G_{q[1]} =$	**Prob. Of** $\|0\rangle_{q[0]} \otimes \|1\rangle_{q[1]}$ (Not used in Table 3)	**Prob. Of** $\|0\rangle_{q[0]} \otimes \|1\rangle_{q[1]}$ (Not used in Table 2)
$(-\pi/2,3\pi/2)$	$-0.65(R) + .30$	$-0.7072(R) + 0.25$	0.05	0.029 ± 0.002
$(-\pi/2, \pi/2)$	$+0.75(R) + .25$	$+.7072(R) + 0.25$	0.00	0.026 ± 0.006
$(\pi/2, 3\pi/2)$	$+0.45(R) + 0.25$	$+0.7072(R) + 0.25$	0.00	0.029 ± 0.003
$(\pi/2, \pi/2)$	$-0.35R + 0.35$	$-0.7072(R) + 0.25$	0.00	0.029 ± 0.010
$(0, 3\pi/2)$	$-0.25(R)$	0	0.05	0.040 ± 0.007
$(\pi/2, \pi)$	$-0.15(R) + 0.40$	0.5	0.05	0.054 ± 0.012
$(0, \pi/2)$	$-0.10(R)$	0	0.00	0.030 ± 0.005
$(-\pi/2, \pi)$	0.3	0.5	0.10	0.048 ± 0.009
N.E.				
$(0, \pi)$	$+0.05(R) + 0.05$	0	0.00	0.034 ± 0.007

Volume 5, Issue 2, pages 213-228

p-ISSN 2655-8564, e-ISSN 2685-9432

The results for the two types of games with one "shot" per program run, as it would be in an actual game, repeated 20 times, show that the Nash equilibrium point coincides with theory for a limited range of R. The point $(\alpha' = 0, \beta' = \pi, \gamma' = \frac{\pi}{2})$ at the centers of Type-$\pi/2$ and Type-$\pi/3$ data in Table 3 become the Nash equilibrium shown in Table 1 if

(i) a. $G_{q[1]}\left(-\frac{\pi}{3}, \pi, \gamma'\right)$ & $G_{q[1]}\left(\frac{\pi}{3}, \pi, \gamma'\right) \geq G_{q[1]}(0, \pi, \gamma')$,

b. $G_{q[1]}\left(-\frac{\pi}{2}, \pi, \gamma'\right)$ & $G_{q[1]}(\frac{\pi}{2}, \pi, \gamma') \geq G_{q[1]}(0, \pi, \gamma')$,

(ii) a. $G_{q[1]}(0, \pi, \gamma') \geq G_{q[1]}\left(0, \frac{2\pi}{3}, \gamma'\right)$ & $G_{q[1]}\left(0, \frac{4\pi}{3}, \gamma'\right)$,

b. $G_{q[1]}(0, \pi, \gamma') \geq G_{q[1]}\left(0, \frac{\pi}{2}, \gamma'\right)$ & $G_{q[1]}(0, \frac{3\pi}{2}, \gamma')$.

Given the data in Table 3, if $R > 0$ in the inequalities (i) & (ii), then $(0, \pi. \gamma')$ is a Nash equilibrium point when $0 \leq R \leq 2.3$, for Type-$\pi/3$ games, and $0 \leq R \leq 1.75$ for Type-$\pi/2$. In theory, $(0, \pi. \gamma')$ is a Nash equilibrium point without restrictions in R. Eq. (15) implies that the coefficients of R, in the center rows and columns corresponding to the two types of games in Table 3, are zero (theoretical gains are shown in Table 4); however, this is not the case in Table 3. The coefficients of R (as well as the constant terms) have variations which imply an even narrower range to confirm the theoretical Nash equilibrium point reliably. On the other hand, R is selected by the players. The closer they select R to zero the more likely that they can verify the Nash equilibrium point with a few games (assuming the error in the constant term does not fluctuate considerably when playing a small number of games). Diminishing R necessarily makes its coefficient less significant in the center rows and columns as expected in theory.

Table 2 also shows that R can be a small fraction to confirm that $(0, \pi. \gamma')$ is the Nash equilibrium point. Considering all the measurement errors and the inequalities (i) & (ii), the point is reliably the equilibrium after thousands of outcomes for $0 < R \leq 0.041$ in type-$\pi/3$ games. In type-$\pi/2$ games, the same can be concluded for $0 < R \leq 0.20$. These are the ranges implied by the most extreme measurement error fluctuations possible. In this way, these can be the ranges from which players select R from the start, even for a few games, if players seek a theoretical Nash equilibrium.

Volume 5, Issue 2, pages 213-228
p-ISSN 2655-8564, e-ISSN 2685-9432

On the other hand, for $R \gg 1$, the gains (losses) in the corners of the matrices corresponding to the two types of games in Table 2 are much greater than those in the center rows and columns as predicted by theory. If $\left|\Delta G_{q[1]}^{C}\right|$ is the absolute change in gain (loss) from a non-corner one to a corner one, and $\left|\Delta G_{q[1]}^{N}\right|$ is the absolute change from one that is a non-corner one to another non-corner one, then $\left|\Delta G_{q[1]}^{C}\right| \gg \left|\Delta G_{q[1]}^{N}\right|$ for all data in Table 2 for $R \gg 1$. In other words, in this R range, the gains (losses) when at least one player maintains the equilibrium parameter, regardless of the other's selection, are notably less than those corresponding to the other parameter combinations given thousands of "shots". Considering the measurement errors in Table 2, there may not be significant gain improvement for a player changing the equilibrium parameter when the other maintains it. Consequently, in this case, a player does not have a strong incentive to change the parameter when the other does not change it; a player considerably minimizes the losses (gains) by keeping it constant regardless of the other's selection. $(0, \pi. \gamma')$ is a Nash-like equilibrium point for $R \gg 1$ given a large number of games.

4 Conclusions

The results suggest that two players can confirm reliably that $(0, \pi, \gamma')$ is a Nash equilibrium point for two qubits of the game protocol shown in Fig. 1, with the circuits in Fig. 2, when R is a small fraction of a coin, testing thousands of times each of the setting combinations from either type-$\pi/3$ or type-$\pi/2$ games; also, the data shows that it is probable that the same could be confirmed with at least 20 repetitions. Now, consistent with theory, for $R \gg 1$, given thousands of "shots", the notably greatest gains (losses) correspond to those when both players do not set their equilibrium parameters, which means that a player can considerably minimize the losses (gains) by not changing it. In this case, there may not be significant gain improvement for the one that changes the equilibrium parameter if the other does not; consequently, there is no strong incentive for a player to change it when the other is maintaining it, suggesting Nash-like equilibrium. Thus, under the same restrictions for R after more than 20 games with the same set of setting combinations, the gains (losses) would be expected functions of participants' choices if two played remotely in the cloud. In the future, as NISQ devices

Volume 5, Issue 2, pages 213-228
p-ISSN 2655-8564, e-ISSN 2685-9432

improve, it is likely that a Nash-equilibrium point can be attained with less restrictions if two played the protocol introduced.

References

[1] Zhang P., Zhou XQ, Wang YL, et al. Quantum gambling based on Nash-equilibrium. npj Quantum inf. 3 (24) (2017).

[2] Lu Zhou, Xin Sun, Chunhua Su, Zhe Liu, Kim-Kwang, Raymond Chou, Game theoretic security of quantum bit commitment, Information Science 479 (2019).

[3] Daniel Centeno, German Sierra, General quantum chinos game, 6 (7).

[4] Yuyang Han, Cheat-sensitive coin flipping and quantum gambling, Quantum information Processing 21(170) (2022).

[5] Luyao Wang, Hai Cheng, Pseudo-Random number generator based on logistic chaotic system, Entropy 21(10), 960 (2019).

[6] Fei Yu, Lixiang Li, Qiang Tang, Shuo Cai, Yun Song, Quan Xu, A survey on true random number generator base on chaos, discrete Dynamics in nature and society, (2019).

[7] U. Ansari, A. K. Chaudhary and S. Verma, True Random Number Generator (TRNG) Using Sensors for low Cost IoT Applications, 2022 International Conference on Communication, Computing and Internet of Things (IC3IoT), Chennai, India, (2022) 1-6.

[8] Christina Chamon, Shahriar Ferdous, and Laszlo B. Kish, Deterministic random number generator attack against the kirchhoff-law-Johnson-Noise secure key exchange protocol, Fluctuation and Noise Letters, 20(5) (2021) 2150046.

[9] Yutaka Shikano, Unpredictable random number generator, AIP Conference Proceedings 2286 (2020) 040004.

[10] Miguel Herrero-Collantes, Juan Carlos Garcia-Escartin, Quantum random number generators, Rev. Mod. Phys. 89 (2017) 015004.

[11] Jaideep Patnak, Brian Hunt, Michelle Girvan, Zhixin Lu, Edward Ott, Model-free prediction of Large spatiotemporally chaotic system from Data: A reservoir computing approach. Phys. Rev. Lett. 120 (2018) 024102

[12] John Preskill, Quantum Computing in the NISQ era and beyond, Quantum 2, 79 (2018)

Volume 5, Issue 2, pages 213-228

p-ISSN 2655-8564, e-ISSN 2685-9432

[13] McEwen, M., Faoro, L., Arya, K. et al. Resolving catastrophic error bursts from cosmic rays in large arrays of superconducting qubits. Nat Phys. 18 (2022) 107-111.

[14] Lior Goldenberg, Lev Veidman, and Stephen Wiesner, Quantum gambling, Phys. Rev. Lett. 82 (1999) 3356.

[15] Ireneuz Pokula, Quantum gambling using mesoscopic ring qubits Physica Status Solidi (b) Vol. 244(7) (2007) 2513-2515.

[16] Davide Castelvecchi, IBM's quantum cloud computer goes commercial, Nature 543 (7644) (2017).

[17] Charles H. bennett, Gilles Brassard, Quantum cryptopgraphy: Public Key distribution and coin tossing, Theoretical computer Science Volume 560, Part 1, 4 (2014).

[18] Blum, Manuel Coin flipping by telephone a protocol for solving impossible problems. ACM SIGACT News 15(1) 23-27.

[19] Anna Pappa, Paul Jouguet, Thomas Lawson, Andre Chailloux, Matthieu Lagre, Patrick Trinkler, Lordanis Kernidis, Eleni Diamanti, Experimental plug and play quantum coin flipping, Nature Communications 5(3717) (2014).

International Journal of Applied Sciences and Smart Technologies

Volume 5, Issue 2, pages 229-240

p-ISSN 2655-8564, e-ISSN 2685-9432

Evolution of The Generalized Coordinates of Pendulum-Spring System

N. W. Rini* and J. Saefan

Department of Physics Education, University of PGRI Semarang, Semarang 50232, Indonesia

**Corresponding Author: rininurwidya@gmail.com*

(Received 13-06-2023; Revised: 10-08-2023; Accepted: 19-08-2023)

Abstract

The pendulum-spring system studied using Hamilton equations consists of three generalized coordinates. The coordinates are the swing angle of the rod, the swing angle of the spring, and the length extension. In this case, the total Hamiltonian is complicated because of the complicated mechanical system. Six equations of motion are obtained from the Hamilton equations. The visualization of the generalized coordinates with respect to time is illustrated. In the visualization, the spring constant and the initial swing angle of the rod were varied. These variations obtained the harmonic and non-harmonic motion. The motion of such a complex system was usually sensitive to the initial values. Solving the mechanical problems with Hamiltonian formalism could familiarize students with a branch of physics with numerous indispensable applications to other branches.

Keywords: Hamiltonian, spring-pendulum, equation of motion

1 Introduction

Hamiltonian mechanics were first stated by William Rowan Hamilton in 1833 as a formulation of Lagrangian mechanics in a different way. Hamiltonian mechanics reformulated mechanics into a momentum rather than the velocity phase space approach [1].

This work is licensed under a Creative Commons Attribution 4.0 International License

In Hamiltonian mechanics, the state of the system was described in terms of the generalized coordinates and momenta. Hamiltonian mechanics is an energy-based theory that seeks to describe and explain mechanical systems [2].

The Hamiltonian description is a stepping stone to other areas of modern physics, such as phase space and Lioville's theorem. Poisson brackets and time translation with the Hamiltonian have analogies in quantum mechanics, and Hamiltonian-Jacobi theory leads to a more general formulation of mechanics.

The equation of motion for the mechanical system of the spring-pendulum has been decomposed using the Euler-Lagrange equation [3]. There are three equations of motion obtained. The number of equations obtained corresponds to the total number of generalized coordinates within the system in the form of second-order ordinary differential equations. In this case, the generalized coordinates used are the swing angle of the rod, the swing angle of the spring, and the extension of the spring length denoted as θ_1, θ_2, x, respectively. In more detail, Figure 1 illustrates the described system. This mechanical system will be reviewed further by looking for the Hamilton equation, a formal transformation commonly used in dynamics systems. The Hamilton equation that will be obtained is twice the number of generalized coordinates in the form of the first-order ordinary differential equation.

The solution for mechanical cases involving such a pendulum must generally be oscillatory motion. Oscillatory cases involving the back-and-forth motion of a physical system are always interesting to discuss. Those physical systems can arise from existing phenomena or mathematical modeling. [4] works on the design of the simulation of a simple pendulum. While Yazid presented mathematical modeling of a moving planar payload pendulum on an elastic portal framework [5].

Complex oscillatory in the form of simple harmonic motion yield intriguing patterns in the depiction and interpretation of the variables associated with the system. Often such a system will be sensitive to the changes in the initial value of a given system.

Biglari et al. and Stachowiak et al. analyzed the dynamics of the double pendulum system numerically using Lagrangian and Hamiltonian formalism [6, 7]. They found out that a set of coupled non-linear ordinary differential equations governs the system. In another research, [8] studied the Hamiltonian equation on a double pendulum with axial forcing constraint to obtain the equation of motion.

International Journal of Applied Sciences and Smart Technologies
Volume 5, Issue 2, pages 229-240
p-ISSN 2655-8564, e-ISSN 2685-9432

This paper aims to derive the Hamilton equation based on the Lagrangian, which has been obtained in the previous research [3]. Based on previous research, the Euler-Lagrange equation obtained has three degrees of freedom in the form of a second-order differential equation, so the Hamilton equation to be obtained is six equations equal to twice the degrees of freedom in the form of a first-order differential equation. Afterward, the behavior of the solution to this equation will be analyzed, considering the potential for complex oscillations from an evolutionary perspective over time.

1.1 Pendulum-Spring System

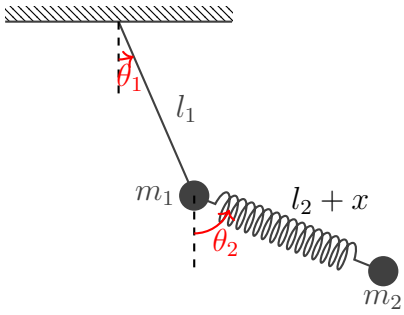


Figure 1. Pendulum-spring system

The Pendulum-Spring system consisted of two masses illustrated in Figure 1. The string l_1 connected to the mass m_1 was considered massless and inextensible. The second mass m_2 is connected to the spring with the length l_2, and the spring extends the length by x. The swing angles θ_1 and θ_2 were the swing angles each pendulum makes with respect to the vertical line. The chosen generalized coordinates are θ_1, θ_2, and x. We set the potential energy equal to zero at the point m_1.

The concrete steps to get the equations of motion using the Hamiltonian method was writing down the Lagrangian. How to obtain this Lagrangian for this system has been described by [3]. Furthermore, the Hamiltonian of this system can be directly determined by adding the kinetic energy T and the potential energy V.

The interest in solving the pendulum-spring problem using Hamiltonian is not to gain the equation of motion in efficiency. However, it could familiarize students with a branch of physics with numerous indispensable applications to other branches. Hamiltonian formalism is extremely helpful for calculating anything useful in other physics branches,

such as statistical mechanics and quantum mechanics.

1.2 Hamilton Equation

The Hamiltonian H oh the system equals to the total energy, that is,

$$H = T + V, \tag{1}$$

where T is the kinetic energy and V is the potential energy. The generalized momenta p_i corresponding to each generalized coordinate q_i is given

$$p_i = \frac{\partial L}{\partial \dot{q}_i}, \tag{2}$$

where $\dot{q}_i = dq_i/dt$. By using the standard prescription for a Legendre transformation, we define H of the system written in terms of the Lagrangian

$$H = \sum_i p_i \dot{q}_i - L \tag{3}$$

Calculating the partial derivative of the equation (3) with respect to the generalized coordinate q_i obtains [9]

$$\frac{\partial H}{\partial q_i} = -\dot{p} \quad \text{and} \quad \frac{\partial H}{\partial p_i} = \dot{q}. \tag{4}$$

2 Research Methodology

The method used in this theoretical research was transformed $L(q, \dot{q}, t) \rightarrow H(p, q, t)$ without losing any information. The first step was calculating T and V, then writing down the Lagrangian, $L = T - V$, in terms of coordinates q_i and their derivatives $\dot{q}_i$. Then, calculate $p_i = \frac{\partial L}{\partial \dot{q}_i}$ for each of the N coordinates. Furthermore, the expressions for the Np_i inverted to solve for the $N\dot{q}_i$ in terms of the q_i and p_i^2. Write down the Hamiltonian, $H = (\sum p_i \dot{q}_i) - L$, and then eliminate all the $\dot{q}_i$ in favor of the q_i and p_i. Write down Hamilton's equations for each of the N coordinates. Solve the Hamiltonian equations; the usual goal is to obtain the N functions $q_i(t)$. This process generally involves eliminating the p_i in favor of the $\dot{q}_i$. This will turn the $2N$ first-order differential Hamilton's equations into N second-order differential equations. These will be equivalent, in one way or another, to what we obtained if we had written down the Euler-Lagrange equations after the first step.

International Journal of Applied Sciences and Smart Technologies
Volume 5, Issue 2, pages 229-240
p-ISSN 2655-8564, e-ISSN 2685-9432

The solution of this kind of complex system is very sensitive to the initial value. The equation of motion will be solved numerically using the fourth-order Runge-Kutta method in Python. However, this paper focuses on the results only. Several dynamics related to changes in the initial values will be analyzed. First, the initial value to be varied is the spring constant k value, while other variables are constant. The next step is to vary the initial angle and keep the other variables constant.

3 Results and Discussions

The Lagrangian for the pendulum-spring system is written in [3] according to

$$\begin{aligned}\mathcal{L} &= T - V \\ &= \frac{1}{2}m_1(l_1^2\dot{\theta_1}^2) + \frac{1}{2}m_2\Big(l_1^2\dot{\theta_1}^2 + (l_2+x)^2\dot{\theta_2}^2 + \dot{x}^2 \\ &\quad +2l_1(l_2+x)\dot{\theta_1}\dot{\theta_2}\cos(\theta_1-\theta_2) - 2l_1\dot{x}\dot{\theta_1}\sin(\theta_1-\theta_2)\Big) \\ &\quad +(m_1+m_2)gl_1\cos\theta_1 + m_2g(l_2+x)\cos\theta_2 - \frac{1}{2}kx^2, \end{aligned} \tag{5}$$

where $\dot{\theta}_1 = d\theta_1/dt$, $\dot{\theta}_2 = d\theta_2/dt$, and $\dot{x} = x/dt$.

The generalized momenta related to the system are $p_{\theta_1}, p_{\theta_2}, p_x$. Decomposing these momenta to the equation (5) yields

$$\begin{aligned} p_{\theta_1} = \frac{\partial L}{\partial \dot{\theta_1}} &= (m_1+m_2)l_1^2\dot{\theta_1} + m_2l_1(l_2+x)\cos(\theta_1-\theta_2)\dot{\theta_2} \\ &\quad -m_2l_1\sin(\theta_1-\theta_2)\dot{x} \end{aligned} \tag{6}$$

$$p_{\theta_2} = \frac{\partial L}{\partial \dot{\theta_2}} = m_2l_1(l_2+x)\cos(\theta_1-\theta_2)\dot{\theta_1} + m_2(l_2+x)^2\dot{\theta_2} \tag{7}$$

$$p_x = \frac{\partial L}{\partial \dot{x}} = -m_2l_1\sin(\theta_1-\theta_2)\dot{\theta_1} + m_2\dot{x}. \tag{8}$$

The following expression then gives the H

$$\begin{aligned} H &= \frac{1}{2}m_1(l_1^2\dot{\theta_1}^2) + \frac{1}{2}m_2\Big(l_1^2\dot{\theta_1}^2 + (l_2+x)^2\dot{\theta_2}^2 + \dot{x}^2 \\ &\quad +2l_1(l_2+x)\dot{\theta_1}\dot{\theta_2}\cos(\theta_1-\theta_2) - 2l_1\dot{x}\dot{\theta_1}\sin(\theta_1-\theta_2)\Big) \\ &\quad -(m_1+m_2)gl_1\cos\theta_1 - m_2g(l_2+x)\cos\theta_2 + \frac{1}{2}kx^2. \end{aligned} \tag{9}$$

From the H of the pendulum-spring system, a set of equations of motion was obtained, which are equivalent to the Euler-Lagrange equations

$$\frac{\partial H}{\partial \theta_1} = -\dot{p}_{\theta_1}, \quad \frac{\partial H}{\partial \theta_2} = -\dot{p}_{\theta_2}, \quad \frac{\partial H}{\partial x} = -\dot{p}_x, \quad \frac{\partial H}{\partial p_{\theta_1}} = \dot{\theta}_1, \quad \frac{\partial H}{\partial p_{\theta_2}} = \dot{\theta}_2, \quad \frac{\partial H}{\partial p_x} = \dot{x}. \tag{10}$$

International Journal of Applied Sciences and Smart Technologies
Volume 5, Issue 2, pages 229-240
p-ISSN 2655-8564, e-ISSN 2685-9432

H as a function of the variables θ_1, θ_2, x, p_{θ_1}, p_{θ_2} and p_x were required to solve the equation (10), so $\dot{\theta}_1$, $\dot{\theta}_2$, $\dot{x}$, and L were determined in terms of these variables. Gauss-Jordan Elimination method was used to get the first derivation of θ_1, θ_2 and x from equation (6)-(8), yield

$$\dot{\theta}_1 = \frac{m_1+m_2}{m_1^2 l_1^2}\mathbf{p_{\theta_1}} - \frac{\cos(\theta_1-\theta_2)}{m_1 l_1(l_2+x)})\mathbf{p_{\theta_2}} + \frac{m_1\sin(\theta_1-\theta_2)}{m_1^2 l_1}\mathbf{p_x} \quad (11)$$

$$\dot{\theta}_2 = -\frac{\cos(\theta_1-\theta_2)}{m_1 l_1(l_2+x)})\mathbf{p_{\theta_1}} + \frac{m_1+m_2\cos^2(\theta_1-\theta_2)}{m_1 m_2(l_2+x)^2}\mathbf{p_{\theta_2}} - \frac{\sin 2(\theta_1-\theta_2)}{2m_1(l_2+x)}\mathbf{p_x} \quad (12)$$

$$\dot{x} = \frac{m_1\sin(\theta_1-\theta_2)}{m_1^2 l_1}\mathbf{p_{\theta_1}} - \frac{\sin 2(\theta_1-\theta_2)}{2m_1(l_2+x)}\mathbf{p_{\theta_2}} + \frac{m_1+m_2\sin^2(\theta_1-\theta_2)}{2m_1 m_2}\mathbf{p_x}. \quad (13)$$

Then the equation (11), (12), and (13) substituted into equation (9) yields the H in terms of θ_1, θ_2, x, p_{θ_1}, p_{θ_2} and p_x according to

$$\begin{aligned} H = {} & \frac{1}{2m_1^2 l_1^2}\mathbf{p_{\theta_1}^2} + \frac{m_1+m_2\cos^2(\theta_1-\theta_2)}{2m_1 m_2(l_2+x)^2}\mathbf{p_{\theta_2}^2} + \frac{m_1+m_2\sin^2(\theta_1-\theta_2)}{2m_1 m_2}\mathbf{p_x^2} \\ & + \frac{-\cos(\theta_1-\theta_2)}{m_1 l_1(l_2+x)})\mathbf{p_{\theta_1}p_{\theta_2}} + \frac{m_1\sin(\theta_1-\theta_2)}{m_1^2 l_1}\mathbf{p_{\theta_1}p_x} \\ & - \frac{\sin(\theta_1-\theta_2)\cos(\theta_1-\theta_2)}{m_1(l_2+x)}\mathbf{p_{\theta_2}p_x} \\ & - (m_1+m_2)gl_1\cos\theta_1 - m_2 g(l_2+x)\cos\theta_2 + \frac{1}{2}kx^2. \end{aligned} \quad (14)$$

Equation (14) used on equation (10) to obtain the Hamiltonian equations of the pendulum-spring system, yield

$$\begin{pmatrix} \dot{\theta}_1 \\ \dot{\theta}_2 \\ \dot{x} \\ \dot{p}_{\theta_1} \\ \dot{p}_{\theta_2} \\ \dot{p}_x \end{pmatrix} = \begin{pmatrix} \frac{\alpha_1}{l_1}\left(2\gamma_1 p_{\theta_1} - 2m_2 l_1 p_{\theta_2} + l_1 A p_x\right) \\ \frac{\alpha_1}{(l_2+x)}\left(-2\gamma_1 p_{\theta_1} + 2l_1\beta_1 p_{\theta_2} - 2Bp_x\right) \\ \alpha_1\left(Ap_{\theta_1} - m_2\alpha_2 p_{\theta_2} + 2\beta_2\gamma_2 p_x\right) \\ \frac{\alpha_1}{(l_2+x)}\left(\gamma_5 - m_2 C p_x^2 - 2m_2\beta_3\gamma_2^2\sin(\theta_1)\right) \\ \frac{\alpha_1}{(l_2+x)}\left(-\gamma_5 + Cp_x^2 - 2g\gamma_1 F\sin\theta_2\right) \\ \frac{2\alpha_1}{(l_2+x)^2}\left(l_1\beta_1 p_{\theta_1}^2 - m_2\gamma_3 p_{\theta_1}p_{\theta_2} - Bp_{\theta_2}p_x + \gamma_4\right) \end{pmatrix} \quad (15)$$

where α_n $(n = 1, 2)$ defined according to

$$\alpha_1 = \frac{1}{2m_1 m_2\gamma_2}, \quad \alpha_2 = l_1\sin 2(\theta_1-\theta_2).$$

Meanwhile, γ_n $(n = 1, 2, 3, 4, 5)$ were defined as

$$\gamma_1 = m_2(l_2+x), \quad \gamma_2 = l_1(l_2+x), \quad \gamma_3 = (l_2+x)\cos(\theta_1-\theta_2)$$

$$\gamma_4 = F(l_2+x)\left(g\cos\theta_2 - m_2 kx\right)$$

$$\gamma_5 = m_2\alpha_2 p_{\theta_2}^2 - Ap_{\theta_1}p_{\theta_2} - Dp_{\theta_1}p_x - Ep_{\theta_2}p_x,$$

and β_n $(n = 1, 2, 3)$ were

$$\beta_1 = m_1 + m_2 \cos^2(\theta_1 - \theta_2), \quad \beta_2 = m_1 + m_2 \sin^2(\theta_1 - \theta_2), \quad \beta_3 = m_1(m_1 + m_2).$$

The last assumption in the expression (14) are

$$\begin{aligned} A &= 2m_2(l_2 + x)\sin(\theta_1 - \theta_2), & B &= m_2 l_1 (l_2 + x)\sin(\theta_1 - \theta_2)\cos(\theta_1 - \theta_2), \\ C &= 2l_1(l_2 + x)\sin(\theta_1 - \theta_2)\gamma_3, & D &= 2\gamma_1\gamma_3, \\ E &= 2m_2\gamma_3\left(1 - 2\cos^2(\theta_1 - \theta_2)\right), & F &= m_1(l_2 + x)\gamma_2. \end{aligned}$$

Equations (15) formed a set of coupled first-order differential equations of motion on the variables θ_1, θ_2, x, p_{θ_1}, p_{θ_2} and p_x. These functions will be analyzed for their evolution over time, with some interesting changes in the initial values of the mentioned variables.

3.1 Evolution of motion with k variation

In general, the solution of differential equation of motions in (15) were sensitive to the initial values. First, we will try to simulate the evolution of motion with various k and the other initial values were keep constant.

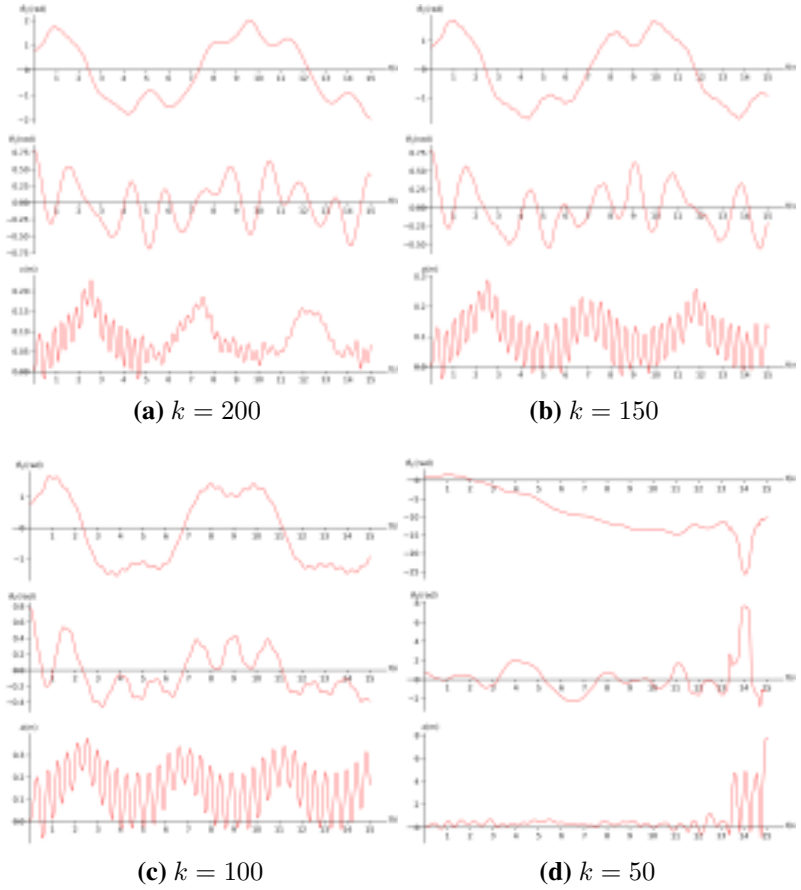
The parameters set up for this system are $m_1 = m_2 = 1$ kg, $l_1 = l_2 = 1$, $g = 10m/s^2$. The initial values used are $\theta_1 = \pi/2°$, $\theta_2 = -\pi/2°$, $x = 0$ cm, $p_{\theta_1} = p_{\theta_2} = p_x = 0$ N/s. The simulation was made over the interval $[0, 10]$ with $\Delta t = 0.0001$.

The parameter used in figure 2 are $m_1 = m_2 = 1$ kg, $l_1 = l_2 = 1$, $g = 10m/s^2$. For $t = 0$ the initial values are $\theta_1 = \theta_2 = \pi/4, x = 0$. The simulation was made over the time interval t [0,15].

Figure 2a, 2b, 2c showed the periodic motion with the frequencies and the amplitude not constant. Meanwhile, Figure 2d showed that there is part in θ_1 that the graph is gradually decreasing to the minus valley, indicating that the first pendulum rotated counterclockwise. On the contrary, there is part in θ_2 that the graph is a sharp increase, indicating that the second pendulum rotated clockwise. In addition, x showed that the evolution of the motion corresponds to the θ_2.

Some researchers usually set the range of the graph to $[-\pi, \pi]$. Therefore we redraw Figure 2d with the boundary $[-\pi, \pi]$ shown in Figure 3. The oscillation that occurs is no longer simple harmonic motion. In other words, the motion is no longer smooth. It can undergo a sudden, instantaneous change in position and velocity at any time. The cause of

International Journal of Applied Sciences and Smart Technologies
Volume 5, Issue 2, pages 229-240
p-ISSN 2655-8564, e-ISSN 2685-9432



(a) $k = 200$ **(b)** $k = 150$

(c) $k = 100$ **(d)** $k = 50$

Figure 2. Graph of generalized coordinates θ_1, θ_2, x respect to time t with various spring stiffness k

this non-smooth state could come from the motion caused by the spring constant, which exceeds the tension point of the spring constant. This state of motion can be further analyzed for a motion towards chaotic behavior.

3.2 Evolution of motion with θ_1 variation

The graph in Figure 4 exhibits different motion characteristic. Figure 4a, 4b, and 4d show that the state of the system moves non-harmonic motion. Meanwhile, Figure 4c displays periodic behavior. Chaotic motion is observed when considering angles θ_1 such as $\pi/3, \pi/4$, and $\pi/6$ are considered. However, no chaotic behavior is observed when $\theta_1 = \pi/5$. This observation indicates that altering the initial angle θ_1 leads to random motion. Therefore, it is not necessarily true that a greater initial angle θ_1 will result in a more chaotic motion. Figure 4 shows that random motion can occur at any time. This

International Journal of Applied Sciences and Smart Technologies
Volume 5, Issue 2, pages 229-240
p-ISSN 2655-8564, e-ISSN 2685-9432

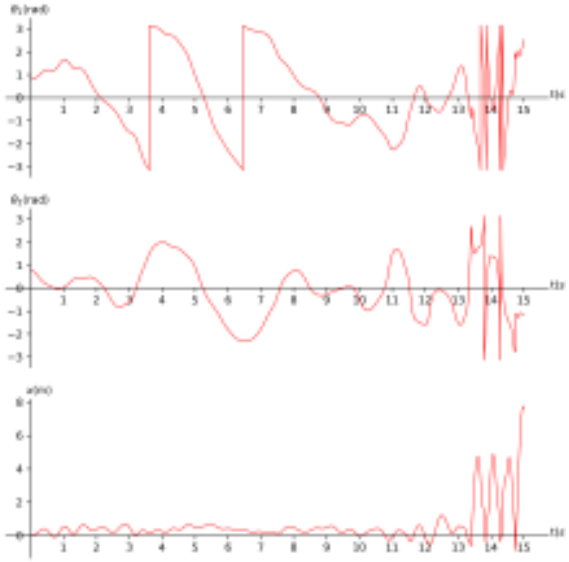


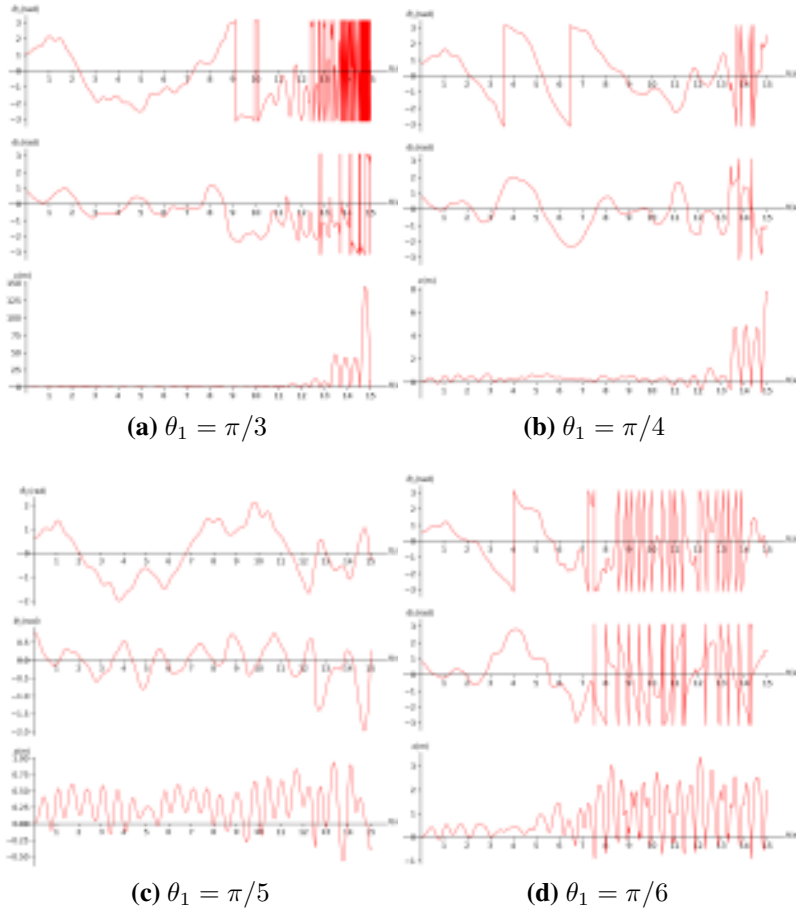
Figure 3. Oscillation θ_1, θ_2, x with respect to time t $(k = 50)$

proves that such a complex system is very sensitive to a given initial value. keadaan yang non harmonic ini sebenarnya bisa dianalisis lebih lanjut apakah dari chaotic atau hanya sekdar random.

3.3 Discussion

The equation of motion of the pendulum-spring system is derived from the Lagrangian and subsequently transformed to the Hamiltonian. Following the transformation, the Hamiltonian velocity is substituted into the general momentum. The equations of motion are then obtained in terms of general coordinates and general momenta. These derivation steps are also carried out by [6, 10, 11, 12]. The effect of changing the spring constant k and the initial pendulum angle θ_1 makes the oscillations no longer harmonic. The findings in [13] support this observation, as Lorente states that when the spring constant is significantly large, the pendulum motion becomes highly restricted, resulting in small oscillations. Conversely, if the spring constant is small, the pendulum motion becomes less elastic.

There are other ways to analyze the behaviour of these mechanical system. Runge-Kutta is one of the numerical methods to see the complexity of the mechanical system by exposing the limit cycle, strange attractors, Poincaré section, and bifurcation. Meanwhile, the focus of this paper is the derivation of the Hamiltonian of the pendulum-spring



(a) $\theta_1 = \pi/3$ **(b)** $\theta_1 = \pi/4$

(c) $\theta_1 = \pi/5$ **(d)** $\theta_1 = \pi/6$

Figure 4. Graph of Generalized coordinates θ_1, θ_2, x Respect to time t with various angle θ_2

pendulum system.

The work in this paper was obtained using the Runge-Kutta fourth order method. However, the validity and accuracy of this methods have not been reviewed in depth. An analysis of the accuracy and effectiveness of the Runge-Kutta fourth order method will be analyzed in the further research.

4 Conclusion

The pendulum-spring system has been solved using the Hamiltonian formalism. Six equations of motions were obtained according to equation (15). Decomposing the equation of motion using the Hamiltonian in this study has met the standards for deriving the equation of motion and has been commonly used by previous studies. The solution of the

equation of motion is usually in the form of oscillatory motion. However, when certain initial conditions vary, such as modifications to the spring constant, pendulum angle, and spring angle, this motion will no longer exhibit harmonic oscillation.

References

[1] P. Mann,, Lagrangian adn Hamiltonian Dynamics, *OxfordAcademic* (2018).

[2] C.G Weaver, Hamiltonian, Hamiltonian Mechanics, and Causation, Illinois: University of Illiniois at Urbana-Champaign, (2020).

[3] N.W. Rini, J. Saefan, N. Khoiri, Lagrangian Equation of Coupled Spring-Pendulum System, Physics Communication, 7(1) (2023) 22-27.

[4] Palka, L., Schauer, F., and Dostal, P., Modelling of the simple pendulum Experiment, *MATEC Web of Conferences*, 76(1) (2016).

[5] E. Yazid, Mathematical Modeling of A Moving Planar Payload Pendulum On Flexible Portal Framework, *Journal of Mechatronics, Electrical Power, and Vehicular Technology*, 2(2) (2011) 95-104.

[6] H. Biglari and A.R. Jami, The Double Pendulum Numerical Analysis wit Lagrangian and Hamiltonian Equations of motions, *Conference: International Conference on Mechanical and Aerospace Engineering*, (2016).

[7] T. Stachowiak and T. Okada, A Numerical Analysis of Chaos in the Double Pendulum, *Journal: Chaos, Solitons, and Fractlas*, 29(2) (2006) 417-422.

[8] I. Indiati, J. Saefan, and P. Marwoto, Numerical Approach of Hamilton Equations on Double Pendulum Motion with Axial Forcing Constraint, *Journal of Physics: Conference Series*,(2016).

[9] P. Hamill, A Student's Guide to Lagrangians and Hamiltonians, United Kingdom: Cambridge University Press, (2014).

[10] A. Elbori, and L. Abdalsmd, Simulation of Double Pendulum, *Quest Journals Journal of Software Engineering and Simulation*, 3(7) (2017) 1-13.

[11] S. D'Alessio, An analytical, numerical and experimental study of the double pendulum, *European Journal of Physics*, (44) (2023) 1-20.

[12] Esp, R. Espindola1, G. Del Va, G. Hernanandez, I. Pined, D. Mucianos, D iáz6, P., Guijosa, and S., The Double Pendulum of Variable Mass: Numerical Study for different cases, IOP Conf. Series: Journal of Physics: Conf. Series, 1221 (2019).

[13] Andres Lorente, Dynamic Characteristics of Pendulum System, master's thesis, Blekinge Institute of Technology, Sweden, (2010).

International Journal of Applied Sciences and Smart Technologies

Volume 5, Issue 2, pages 241-254

p-ISSN 2655-8564, e-ISSN 2685-9432

Evaluation of The Current Level of Knowledge of The Residents of Dhaka City Regarding Earthquake Hazard

Saif Ahmed Santo[1*], Akhi Sultana Fariha[1], Md. Rakib Hossain[2], Syed Emon Shah[3]

[1]Post Graduate student, Department of Civil Engineering, Bangladesh University of Engineering and Technology, Dhaka.

[2]Lecturer, Department of Civil Engineering, Sonargaon University, Dhaka

[3]Graduate Student, Department of Civil Engineering, Ahsanullah University of Science and Technology, Dhaka

**Corresponding Author: ahmd.saif007@gmail.com*

(Received 31-07-2023; Revised 10-08-2023; Accepted 19-08-2023)

Abstract

An earthquake is a sudden disaster that is not possible to predict. This impulsive behavior makes it very dangerous for humankind. Precautionary measures are immense for reducing damage. The first step of preventive measures for an earthquake is raising awareness. Dhaka City has a high earthquake risk due to its large population and urbanization. Researchers have said that an earthquake in this zone can be fatal, resulting in heavy casualties with structural damage. For this reason, proper awareness is essential for the residents of this area. The aim of this study is to find out the current knowledge level of the residents of Dhaka City about Earthquake risk of this city. Online questionnaire was used to collect data from random residents of Dhaka. Survey data indicates that many people lack Knowledge of what to do before and during an earthquake. Especially school and college-going students are unaware of the essential things to do during an earthquake incident. Many people still don't know the importance of a seismic-resistant building system and are unprepared for a seismic event. This study brings these aspects together to learn about the knowledge level, which can help policymakers raise awareness among this city's residents.

Keywords: Awareness; Dhaka City; Disaster; Earthquake; Knowledge; Risk.

1 Introduction

The Earth's hard outer layer occasionally experiences abrupt and fleeting tremors from natural processes. These unexpected trembling, often known as earthquakes, are caused by different things that influence the Earth's crust. According to the United States Geological Survey (USGS), earthquakes occur due to the movement of tectonic plates along fault lines[1].

This work is licensed under a Creative Commons Attribution 4.0 International License

Volume 5, Issue 2, pages 241-254
p-ISSN 2655-8564, e-ISSN 2685-9432

Tectonic plates are the primary cause of earthquakes. Faults or fractures split numerous plates that make up the surface of the Earth. The interior of the Earth contains molten material beneath these plates. These molten materials may migrate and shift because of natural factors, altering the plates. One plate may subduct beneath another, causing seismic vibrations that eventually appear as earthquakes. In addition, critical natural events like volcanic eruptions, landslides, glacier movements, thermal radiation, and related phenomena can also contribute to seismic activity.

An earthquake can cause significant damage and destruction in multiple ways. The shaking of the ground can lead to the collapse of buildings and infrastructure, resulting in loss of life and injuries[2]. Additionally, earthquakes can trigger landslides and avalanches, further damaging structures and obstructing transportation routes [3]. Ground shaking may also cause liquefaction, where saturated soil temporarily loses strength and behaves like a liquid, damaging buildings, and underground utilities. Furthermore, powerful earthquakes under the ocean can generate tsunamis, massive ocean waves that can inundate coastal areas and cause widespread devastation [3]. Fires can also be ignited by broken gas lines and electrical wires, exacerbating the damage caused by an earthquake[2].

For people, communities, and governments to reduce possible hazards and lessen the effects of these natural disasters, earthquake awareness is essential. First and foremost, Knowledge enables people to comprehend the dangers of earthquakes and adopt the appropriate safety measures to safeguard their lives and property (USGS, 2021). It teaches people about earthquake-resistant construction methods and building retrofitting strategies[3]. Furthermore, earthquake awareness promotes preparedness by educating people about the appropriate actions to take during and after an earthquake, such as "Drop, Cover, and Hold On" during shaking and knowing evacuation routes (CDC, 2022). Awareness campaigns emphasize the importance of creating emergency kits and developing family or community response plans, including designated meeting points [4]. Community-level Knowledge is crucial for creating a preparedness culture because it promotes cooperation and coordination among many stakeholders, such as local government, companies, schools, and emergency response agencies [3]. To communicate vital information before, during, and after an earthquake, communities can build early

Volume 5, Issue 2, pages 241-254
p-ISSN 2655-8564, e-ISSN 2685-9432

warning systems and communication networks by increasing awareness [5]. Earthquake's awareness also extends to engineering, urban planning, and emergency management professionals. These individuals can contribute to designing safer infrastructure, implementing building codes and standards, and developing effective response strategies. Governments have a crucial role in raising Knowledge of earthquakes through funding research, monitoring systems, and public awareness campaigns. These programs promote a safety-conscious culture, increase public awareness of earthquake risks, and help politicians make well-informed decisions [3]. Government financing and assistance for earthquake research also promote early warning system development, hazard assessment, and prediction [5].

With a total size of 1,47,610 square kilometers, Bangladesh is a significant country in terms of geography and geology in the South Asian region. Its length and width are 820 kilometers north to south and 600 kilometers east to west. Several disastrous natural disasters, including floods, droughts, tropical cyclones, tornadoes, thunderstorms, extreme rainfall, tidal bores, intense summer heat, etc., frequently hit this region, which is located between 24°0'0" N latitude and 90°0'0" E longitude. Bangladesh is often hit by storms that originate in the Bay of Bengal 16 times every ten years. But recently, Bangladesh has been in danger from an "earthquake" that is even more deadly. Bangladesh, located in a seismically active region, is vulnerable to earthquakes and their potential impacts. The country has experienced several significant earthquakes, highlighting the importance of understanding seismic hazards and implementing appropriate measures for earthquake resilience. Bangladesh lies in a tectonically complex area where the collision of the Indian and Eurasian plates gives rise to seismic activity (USGS, 2021). The country is near the boundary between the Indian and Burmese plates, with numerous active faults running through its territory. When examining Bangladesh's earthquake history, one significant problem stands out: there is a dearth of Knowledge about earthquakes. Though some evidence is there, the information is insufficient to know the magnitude and intensity of those earthquakes. Even while there is some data, it is not enough to determine the extent and impact of those earthquakes. Although their magnitudes are unclear, there is evidence of catastrophic earthquakes in Sylhet, Chittagong, and Dhaka.

Volume 5, Issue 2, pages 241-254
p-ISSN 2655-8564, e-ISSN 2685-9432

A devastating earthquake in 1762 caused at least 200 fatalities and was felt throughout the Bengal and Arakan regions. It also severely devastated significant portions of Dhaka, Chittagong, and Myanmar [6]. Reports claim that the 1765 earthquake was so strong that it permanently submerged 155.40 square kilometers of land near Chittagong and raised the shoreline of Foul Island by 2.74 m and the northwest coast of Chedua Island by 6.71 m above sea level. Five hundred people died because of the earthquake in Dhaka [7]. The 1812 Dhaka earthquake that struck Dhaka in April severely damaged several homes and other buildings in Tejgaon [8]. One of the worst earthquakes ever was the Bengal earthquake in July 1885. Between July 21 and September 5, 1885, eleven aftershocks were caused by the tremor [9]. The earthquake had a Richter scale magnitude of 7. One of the deadliest and most severe earthquakes ever recorded, the Great Indian Earthquake, occurred on June 12, 1897 [10]. The quake took place about 200 km north of Dhaka, on the western edge of the Shillong Plateau. The Bangladesh Geological Survey reported at least 465 earthquakes of small to moderate magnitude between 1971 and 2006 [11]. Although damaging earthquakes have not occurred frequently, there is still a great potential for enormous destruction and damage [12]. In recent decades, Bangladesh has witnessed destructive earthquakes. The 2003 earthquake in northeastern Bangladesh caused widespread damage and claimed hundreds of lives [13].

Similarly, the 2013 Rangpur earthquake resulted in significant structural damage to buildings and infrastructure [7]. A severe earthquake that had its epicenter 745 kilometers (km) northwest of Bangladesh on April 25, 2015, rattled Dhaka, Chittagong, Barisal, Rajshahi, Dinajpur, Rangpur, and other areas of the nation [10]. According to the US Geological Survey (USGS), an earthquake occurred on January 4, 2016, around 33 kilometers (20 miles) northwest of Imphal, the state capital of Manipur, in northeast India, close to the border with Myanmar and Bangladesh. Around 5:05 am, while most city residents were still asleep, Dhaka and its surrounding areas began to experience severe tremors. Following the jolts, terrified individuals fled their homes and flocked to the neighboring highways[14].

Dhaka, the capital of Bangladesh, is highly vulnerable to earthquakes due to various factors; Dhaka is excessively susceptible to earthquake calamity. First off, Dhaka city has a very high population density. Second, secondary hazards, such as fires that start in gas

Volume 5, Issue 2, pages 241-254
p-ISSN 2655-8564, e-ISSN 2685-9432

and power lines, are anticipated to be far more deadly following an earthquake. Thirdly, most high-rise residential buildings and many garment factory buildings were constructed not only in violation of building rules but also encroached upon streets and other public places. Due to the blockage of roads caused by the fall of these buildings, rescue efforts would be significantly hampered.

This case study aims to determine the current knowledge level among Dhaka City dwellers regarding earthquake hazards. This data can help know the current status of Knowledge that can be used for the smooth operation of awareness-raising programs.

2 Methodology

This research includes a case study on the current knowledge level of the residents of Dhaka City regarding Earthquake incidents. As an earthquake is a sudden incident, awareness is the first step of precautionary measures. Identifying current knowledge level is important for policy makers and engineers to create awareness among people.

2.1 Study Area

Dhaka city was chosen as the study area that is shown in Figure 1. Dhaka is the capital city of Bangladesh. It is situated at 23.8041° N, 90.4152° E. The primary reason of choosing this area is due to the heavy population and structures of this area. Previous research suggests that Dhaka is in high red alert zone of a massive earthquake hazard. That is why this study focused mainly on the Dhaka city and the knowledge level of the residents of this city.

International Journal of Applied Sciences and Smart Technologies

Volume 5, Issue 2, pages 241-254

p-ISSN 2655-8564, e-ISSN 2685-9432

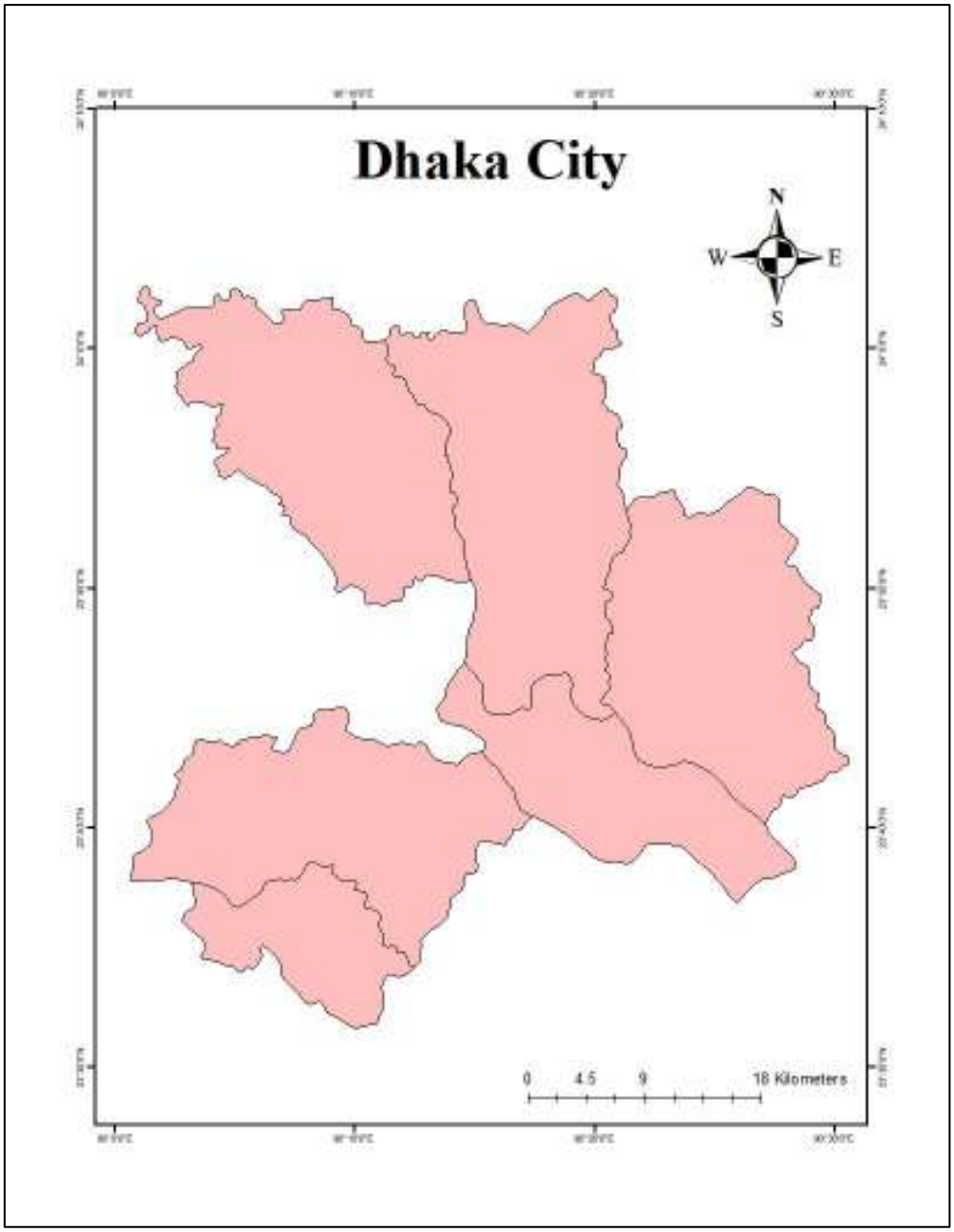


Figure 1: Study Area

2.2 Data Collection

For this study, the questionnaire was done with the help of google forms. This questionnaire was fully online and only provided to the residents of Dhaka City. This survey was fully anonymous. A questionnaire was shared with the people on different online platforms. One submission per participant was strictly imposed to maintain the

Volume 5, Issue 2, pages 241-254
p-ISSN 2655-8564, e-ISSN 2685-9432

integrity of this survey. The sample size was calculated using Yamane's formula (Yamane, 1967).

$$n = \frac{N}{1+N(e^2)} \quad \ldots\ldots (1)$$

where, n= sample size, N= total population of the study area, e= error tolerance. According to Macrotrends, Dhaka city's current population growth rate is 3.26%, which concludes that the current population of Dhaka city is approximately 23,210,000 [16]. With an error tolerance of 0.05, the total number of samples required is 399.99 or 400. So, for this survey total of 410 survey data was considered.

2.3 Data Analysis

This is a preliminary study regarding the knowledge level of the residents of Dhaka City. For data analysis, Microsoft Excel was used. Obtained survey data were analyzed to check the percentage of responses to each question asked. Demographic data such as Age, Gender, Educational Qualification, and Occupation were also collected.

3 Results

3.1 Demographic Profile

By observing the demographic profile of the participants, it was seen that most were young (Age group 16-30) shown in **Figure 2** and they were primarily male shown in **Figure 3**. A vast number of participants live in the Dhaka North City Corporation shown in **Figure 4**. The **Figure 5** and **Figure 6** shows that most of the participants are graduates or running undergraduate students. Their demographic profile is given below,

International Journal of Applied Sciences and Smart Technologies

Volume 5, Issue 2, pages 241-254

p-ISSN 2655-8564, e-ISSN 2685-9432

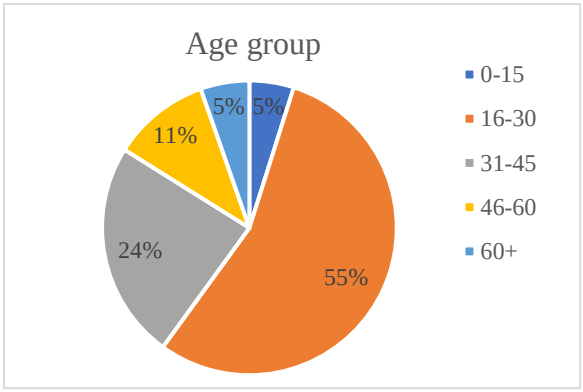


Figure 2: Percentage of participants' age group

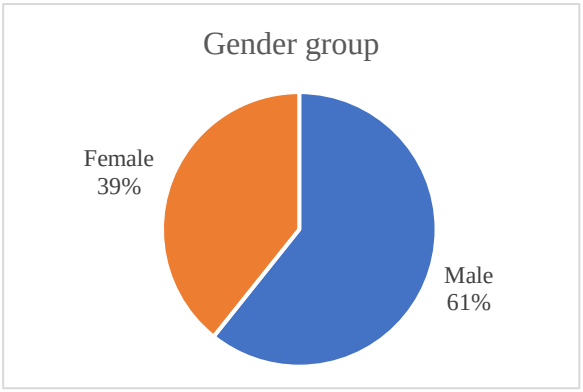


Figure 3: Percentage of participants' gender

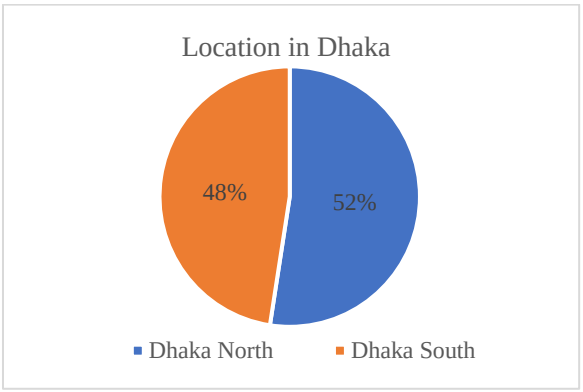


Figure 4: Location of participants in Dhaka City

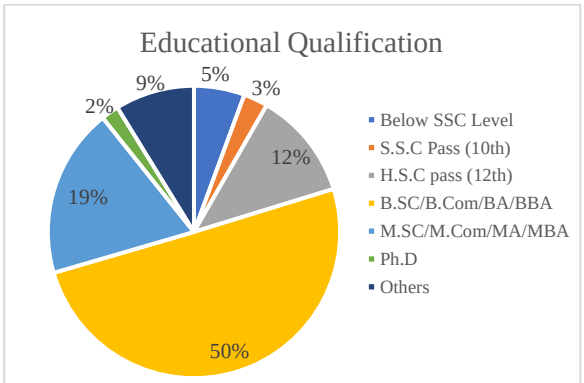


Figure 5: Educational qualification of participants

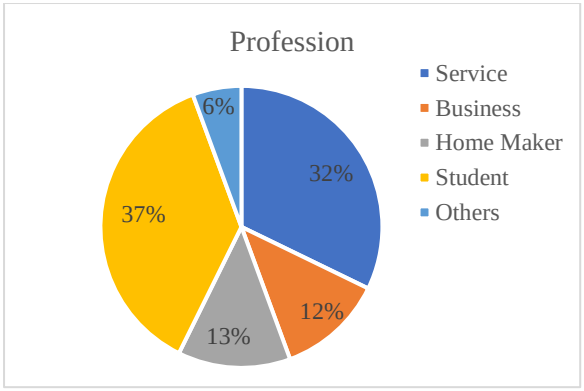


Figure 6: Profession of participants

3.2 Knowledge regarding Earthquake

The questionnaire had different questions that give insight into a participant's self-realization, Knowledge about what to do during an event, Knowledge regarding the after-

Volume 5, Issue 2, pages 241-254
p-ISSN 2655-8564, e-ISSN 2685-9432

event scenario, etc. These will provide an overview of the current situation of the knowledge level of the residents of Dhaka city.

3.2.1 Self-Realization

1. **Felt an earthquake**: In this segment, a total of 77% (316 participants) answered Yes, 13% (55 participants) answered No, and 10% (39 participants) responded Maybe.
2. **Previously attended earthquake awareness programs:** 31% (127 participants) answered Yes to this question. Other 69% (283 participants) said that they have never participated in any earthquake awareness program or session that can increase their knowledge.
3. **Personal Confidence regarding knowledge level:** 13% (53 participants) think they have excellent Knowledge of earthquakes. 40% (163 participants) thinks they have good Knowledge, 35% (145 participants) think they have a fair level of Knowledge, and 12% (49 participants) think they have poor Knowledge regarding earthquake hazard.
4. **Preparedness for an event:** Among the 410 participants, 15% (60 participants) answered that they were prepared for an earthquake event. 49% (200 participants) said that they were not prepared. 28% (115 participants) were unsure about their current preparedness level and answered Maybe. The remaining 9% (35 participants) didn't know their preparedness level.
5. **If their house has a risk of damage during an earthquake:** 32% (131 participants) think that they live in a house with a significant risk of damage. 27% (110 participants) believe their house is strong enough to withstand an event. 31% (127 participants) were not sure about the seismic performance of their house and answered maybe. 10% (42 participants) answered that they don't know about the chance of damage to their house during an event.
6. **If Dhaka City has a high risk during an earthquake event:** 66% (272 participants) think that the risk of an earthquake in Dhaka City is high. 13% (52 participants) disagreed with this statement and answered no. 14% (58 participants) answered Maybe as they are unsure about the earthquake risk in Dhaka. 7% (28

Volume 5, Issue 2, pages 241-254
p-ISSN 2655-8564, e-ISSN 2685-9432

participants) don't know about the risk level of Dhaka regarding an earthquake event.

3.2.2 Preparedness before an incident

1. **Availability of first aid kit/emergency medical supplies at home:** 38% (156 participants) have first aid kit/emergency medical supplies at their home in case of an emergency created by any significant earthquake incidents. 62% (254 participants) don't have any first aid kits ready for an earthquake incident.
2. **Availability of emergency exit at home:** 24% (97 participants) have an emergency exit for emergencies such as earthquakes. 70% (285 participants) have no emergency exit. 7% (28 participants) were unsure about the exits in their homes and answered maybe.
3. **Availability of Evacuation route:** Among the respondents, 16% (65 participants) answered that their area has an evacuation route. 51% (208 participants) live in areas without an evacuation route. 19% (78 participants) answered maybe. 14% (59 participants) don't know about the availability of an evacuation route in their area.
4. **Availability of Urban emergency shelter:** 9% (38 participants) answered that they have an urban emergency shelter for an earthquake event in their area. 83% (342 participants) answered that they don't have any nearby urban emergency shelter. 7% (30 participants) are unsure about the location of the nearby urban emergency shelter.

3.2.3 During an incident

1. **Knows how to turn off gas connection:** 58% (236 participants) answered that they know how to do so. 31% (128 participants) don't know how to turn off the gas connection. 11% (46 participants) are unsure about this, and they answered maybe.
2. **Knows how to turn off electricity connection:** 72% (295 participants) answered that they know how to do it. 21% (85 participants) don't know how to turn off the electricity connection. 7% (30 participants) are unsure about this, and they answered maybe.

Volume 5, Issue 2, pages 241-254
p-ISSN 2655-8564, e-ISSN 2685-9432

3. **The first thing to do during an incident:** 22% (89 participants) answered they would go to a safe place and protect themselves and wait. 15% (61 participants) said they would rush to leave their house as soon as possible. 50% (206 participants) said they would take cover under heavy furniture or beams. 6% (23 participants) will rush to the smallest room of the building. 2% (10 participants) will do none of the options available, and 5% (21% participants) have no idea what to do during an incident.

3.2.4 After an incident

1. **What to do after a disaster event:** 19% (78 participants) would regret the losses and take some of the responsibility for not being aware of earthquake disasters. 28% (115 participants) would do nothing as the scenario will be out of their control. 26% (107 participants) will ask everyone for training regarding earthquake resistance building systems and join the reconstruction of their area. 27% (110 participants) cannot imagine the scenario right now.

3.2.5 Knowledge of buildings

1. **The main reason for a building collapse during an earthquake:** 15% (63 participants) think that bad quality of construction materials results in a building collapse during an incident. 26% (105 participants) thinks lack of Knowledge regarding seismic resistant building system is the main culprit. 19% (78 participants) think homeowners who don't want to spend extra on a seismic-resistant building system are the main reason. 30% (125 participants) think the main reason is the lack of awareness regarding the importance of seismic resistant building among the homeowners. 4% (15 participants) think poor maintenance of houses is the reason, and 6% (24 participants) have no idea about this issue.
2. **If tall buildings are safer during an earthquake or not:** 17% (70 participants) think tall buildings will perform better during an earthquake than short buildings. 49% (201 participants) think otherwise. 20% (80 participants) think there is no relationship between building height and the damage it will sustain. 14% (59 participants) don't have any idea regarding this issue.

Volume 5, Issue 2, pages 241-254
p-ISSN 2655-8564, e-ISSN 2685-9432

3. **Sustainability of a Seismic resistant building system during a significant incident:** 28% (115 participants) think that seismic-resistant building systems are enough to withstand any earthquake in Dhaka City. 39% (159 participants) think otherwise. 22% (92 participants) are unsure about the performance of seismic-resistant building systems. 11% (44 participants) don't know about the performance of seismic-resistant buildings during an earthquake.

4 Discussion

This study aims to gain insight into the current Knowledge of residents of Dhaka City regarding an earthquake incident. The survey data shows that although many participants (77%) have felt an earthquake in their lifetime, only a few (31%) have attended any earthquake awareness program. Many participants also said that their knowledge regarding what to do in earthquake incidents is not up to the mark. Also, almost half of the participants answered that they were unprepared for an earthquake in their area. The lacking of their preparedness can also be seen in the percentage of participants having emergency medical supplies (38%), emergency exits (24%), evacuation routes (16%), and an emergency urban shelter (9%). Although the participants have answered that most of them know how to turn off gas (58%) and electricity (72%) connections and also during an event, most of them will try to take cover and wait (50%), most of them answered that they would try to rush out of their home which is discouraged. Several participants also lack Knowledge of seismic resistant building systems and the relationship between the height of a building with the earthquake incident. By analyzing the responses of participants of age groups 0-15, it was seen that most respondents (75%) have answered about rushing outside in an event rather than taking cover. This shows the lack of Knowledge regarding earthquakes among the younger people of this city.

5 Conclusion

This study focuses on the knowledge level of the residents of Dhaka City regarding an earthquake. Being an online based survey, this study has mostly young adult participants. Although most of the participants are graduates, they still lack their current knowledge level as well as disaster preparedness. Most of them have never participated in any

Volume 5, Issue 2, pages 241-254
p-ISSN 2655-8564, e-ISSN 2685-9432

earthquake awareness program. Special care should be given to the younger generation about their earthquake awareness. Schools and colleges should organize seminars, Workshops, and Earthquake drills to create more awareness regarding earthquakes. People, especially homeowners, should be made aware of the importance of an earthquake-resistant building system. Emergency shelters, Evacuation routes, and emergency exits should be implemented. Also, only 410 participants were surveyed for this study so for a better output, bigger sample size should be taken into account.

Acknowledgements

The authors would like to express their gratitude to everyone who participated in this survey. This study is solely based on public opinion.

References

[1] Earthquake Facts & Earthquake Fantasy | U.S. Geological Survey. https://www.usgs.gov/programs/earthquake-hazards/earthquake-facts-earthquake-fantasy (accessed Jul. 12, 2023).

[2] What are the Effects of Earthquakes? | U.S. Geological Survey. https://www.usgs.gov/programs/earthquake-hazards/what-are-effects-earthquakes (accessed Jul. 12, 2023).

[3] Fema, 2015 NEHRP Recommended Seismic Provisions: Design Examples FEMA, (2016).

[4] U. Department of Homeland Security and F. Emergency Management Agency, Developing and Maintaining Emergency Operations Plans Comprehensive Preparedness Guide (CPG) 101, (2021). [Online]. Available: https://www.dhs.gov/presidential-policy-directive-8-national-

[5] U. Nations Office for Disaster Risk Reduction, Sendai Framework for Disaster Risk Reduction 2015 - 2030.

[6] D. R. Mondal, C. M. McHugh, R. A. Mortlock, S. Mustaque, and S. Humayun Akhter, Microatolls document the 1762 and prior earthquakes along the southeast 1 coast of Bangladesh 2 3.

[7] R. Islam, Md. N. Islam, and M. N. Islam, Earthquake Risks in Bangladesh: Causes, Vulnerability,Preparedness and Strategies for Mitigation, *ARPN Journal of Earth Sciences*, 5(2) (2016) 75–90.

Volume 5, Issue 2, pages 241-254

p-ISSN 2655-8564, e-ISSN 2685-9432

[8] G. F. Sella, T. H. Dixon, and A. Mao, REVEL: A model for Recent plate velocities from space geodesy, J Geophys Res Solid Earth, 107 (B4) (2002) ETG 11-1-ETG 11-30.

[9] M. Morino, A. S. M. M. Kamal, R. M. E. Ali, A. Talukder, M. D. Mahmood, and H. Khan, Report of active fault mapping in Bangladesh : Paleo-seismological study of the Dauki fault and the Indian-Burman plate boundary fault, (2013).

[10] N. Apu and U. Das, Tectonics and earthquake potential of Bangladesh: a review, International Journal of Disaster Resilience in the Built Environment, 12(3) (2020) 295–307.

[11] B. Kanti, P. Professor, and R. H. Bhuiyan, Urban earthquake hazard: perceived seismic risk and preparedness in Dhaka City, Bangladesh, (2010).

[12] M. Ozaki, Disaster risk Financing in BanglaDesh ADB SOUTH ASIA WOrkIng PAPer SerIeS Disaster risk Financing in Bangladesh, (2016). [Online]. Available: www.adb.orgElectroniccopyavailableat:https://ssrn.com/abstract=2941319

[13] A. Biswas, S. R. Mashreky, K. Dalal, and T. Deave, Response to an Earthquake in Bangladesh: Experiences and Lesson Learnt, Open Journal of Earthquake Research, 5(1) (2016) 1–6.

[14] Bangladesh wakes up to tremors | The Daily Star. https://www.thedailystar.net/country/bangladesh-wakes-tremors-196783 (accessed Jul. 12, 2023).

[15] T. Yamane, Statistics an introductory analysis, 2nd ed. New York: Harper & Row, (1967).

[16] Dhaka, Bangladesh Metro Area Population 1950-2023 | MacroTrends. https://www.macrotrends.net/cities/20119/dhaka/population (accessed Jul. 28, 2023).

International Journal of Applied Sciences and Smart Technologies

Volume 5, Issue 2, pages 255–270

p-ISSN 2655-8564, e-ISSN 2685-9432

A Deep Learning Model for Identical National Flag Recognition in Selected African Countries

Halleluyah Oluwatobi Aworinde[1]*, Oladosu Oladimeji[2], Segun Adebayo[3], Akinwale Akinwunmi[1], Aderonke B. Sakpere[4], Olayanju Oladimeji[1]

[1]College of Computing and Communication Studies, Bowen University, Iwo, Nigeria
[2]Centre for Mathematical Modelling and Intelligent Systems for Health and Environment, Atlantic Technological University, Sligo, Ireland
[3]College of Engineering, Agriculture and Sciences, Bowen University, Iwo, Nigeria
[4]Department of Computer Science, University of Ibadan, Nigeria

*Corresponding Author: aworinde.halleluyah@bowen.edu.ng

(Received: 15-05-2023; Revised: 26-05-2023; Accepted: 22-06-2023)

Abstract

The national flags are among the symbolic representations of a country. They make us understand the country of interest in a particular issue. Therefore, they are commonly used in both private and government organizations. It has been discovered in recent times that the younger generation mostly and idly spend its time online; hence, knowing little about national flags. Additionally, some national flags (particularly in West Africa) are identical in nature. The likeness is in terms of layout, colours, shapes and objects on the national flags. Hence, there is a need to have a model for flag recognition. In this paper, national flag images of some West African countries were gathered to form a dataset. After this, the images were preprocessed by cropping out the irrelevant parts of the images. VGG-16 was used to extract necessary features and to develop the deep learning model. This contrasted with the existing handcrafted feature extraction and traditional machine learning techniques used on this subject matter. It was observed from this study that the proposed approach performed excellently well in predicting national flags; with an Accuracy of 98.20%, and an F1 score of 98.16%. In the future, it would be interesting to incorporate the national flag recognition into Human-Computer Interaction System. For instance, it could be used as flag recognition in some mobile and web applications for individuals with colour blindness. This research work presents a robust model because of nature of the dataset used in this work compared to previous works.

Keywords: national flag, deep learning, multi-class, VGG, West Africa

This work is licensed under a Creative Commons Attribution 4.0 International License

International Journal of Applied Sciences and Smart Technologies

Volume 5, Issue 2, pages 255–270

p-ISSN 2655-8564, e-ISSN 2685-9432

1 Introduction

A National flag is one of the symbolic representations of a country. National flag together with a nation's coat of arms are used to emphasize national identity; hence, can be used in various gatherings including conferences, sports, and workshops [1]. Due to the importance of national flag to a nation, it can be seen virtually everywhere including social media websites [2], military operations, various (local and international) competitions and occasions, television or print media, soft or hard copy documents, the streets among other places [3]. National flag makes us understand the country of interest in a particular issue. Therefore, they are commonly used in both private and government organizations. Hence, flag recognition is very important to understand a country or organization of the subject of concern.

Additionally, despite the importance of the national flag, some national flags of some nations (particularly in west Africa) are identical in nature. The similarity is in terms of layout, colours, shapes and objects on the national flags as seen in Figures 1 and 2.



Figure 1 Two identical national flags based on layout and colour [4]

International Journal of Applied Sciences and Smart Technologies

Volume 5, Issue 2, pages 255–270

p-ISSN 2655-8564, e-ISSN 2685-9432

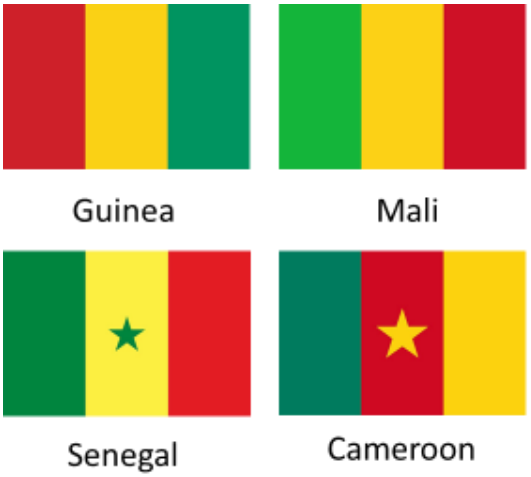


Figure 2 Four identical National flags based on object, shapes, colour and layout [5]

Furthermore, various colour blindness diseases including deuteranopia, protanopia and tritanopia incapacitate people with these diseases to identify and differentiate one national flag from another which affects their productivity in workplaces and schools.

However, the recent improvement in Information Technology [6] which result to rise of Artificial Intelligence with fields such as Computer Vision and Machine Learning [7] which has made various processes to be automated including facial recognition, object detection among other things to solve problems in various domains [8]. Hence, the way forward is to develop a model which will make use of this Artificial Intelligence techniques to recognize and identify national flags to alleviate the challenges which are often encountered.

Currently, works on flag recognition are not much [9]; Hart et al. [10] proposed an interactive flag recognition system based on manual cropping of the flag from pictures. The system uses colour-based nearest neighbor classifier for the generation of list for user to make decision. In another approach, Jetley et al. [11] created dataset of flag images in which the authors used Micro-Structure Descriptor (MSD) by Liu et al. [12] for the extraction of features thereafter, SVM algorithm was used for the classification of the features and 99.2% accuracy was achieved. Similarly, Hao et al. [13] proposed a Color Threshold Determination (CTD) method to identify color flags in which Histogram Oriented Gradient (HOG) was used for feature extraction. Recognition accuracy of 97.1% was achieved under complex scene, sensitivity of 90.70% and

Volume 5, Issue 2, pages 255–270
p-ISSN 2655-8564, e-ISSN 2685-9432

specificity of 99.33%. However, with the emergence of Deep Neural Network (DNN) [14] which performs better than the traditional machine learning approach, Gu et al. [9], took a binary classification approach to flag recognition to differentiate between flag image and other images. In[15] the authors gathered 20,000 images of national flags after which color-based descriptor with Convolutional Neural Network (CNN) approach was proposed for National flag recognition, mean Average Precision of 89.5% was achieved. While Wu et al. [14] took another approach using binary Mask Region-Based Convolutional Neural Network (R-CNN) segmentation weights for flag recognition in the wild.

Therefore, the existing approaches cannot be applied on real world scenarios with a complex background and the existing of more than one object. Hence, this work aims at using multi-class deep learning approach to national flag recognition. For this paper, the main contributions include: (i)Proposing a deep learning model for countries' flag recognition, (ii) combining the proposed deep learning with a feature extractor (VGG-16) to enhance the performance of the proposed approach and (iii) developing a national flags dataset to train the proposed deep learning model.

2 Methodology

This work proposes to use deep learning approach for flag recognition. In this section, the description of the methodology used for automatic national flag recognition in West Africa countries is described.

2.1 Data Description and Preprocessing

The National flag image dataset was created manually by taking pictures of the national flag and from the internet using Google image search, Bing image search, Flickr, Facebook, and Instagram. The dataset entails Benin, Cameroon, Ghana, Guinea, Guinea-Bissau, Mali, and Senegal national flag images. The details of the national flags are given in Table 1.

Volume 5, Issue 2, pages 255–270
p-ISSN 2655-8564, e-ISSN 2685-9432

Table 1: Dataset Distribution

National Flags	Number of Instances present
Benin	708
Cameroon	715
Ghana	714
Guinea	712
Guinea-Bissau	712
Mali	713
Senegal	713

The choice of these country is due to the challenges these flags present including intra-class and inter-class variations. Additionally, some of the flags of these countries have similar colours with different objects which make the identification of these flags to be painstaking as seen in Figures 1 and 2 hence, the model would ensure high performance.

2.2 Labeling

The ground truth labeling of the images was done manually by carefully examining the national flag images and assigning the corresponding label for each national flag image.

2.3 Image Resizing/Normalization

Since the necessary portion of the flag image has been gotten and unnecessary portion cropped out, each of the image maybe in different size. Therefore, there is need to resize the images to ensure that the images are configured (in height and weight) for the input layer of the training model.

2.4 Data augmentation

It is an effective technique to prevent classifier model from overfitting by providing randomly distorted training images to the model and thus, allowing the model to learn general features [15]. In this research, the training images were augmented by randomly zooming the image through 20%, by rotating the image with range value of

Volume 5, Issue 2, pages 255–270
p-ISSN 2655-8564, e-ISSN 2685-9432

40, width shift range of 20% and shear range of 20%. This will allow the model to learn to identify the flags irrespective of their distance with the camera (zoom).

After data augmentation, for evaluation purposes, the dataset was partition into two, 70% was used for training and 30% was used for testing.

2.5 Model Design

In recent times, it has been proved that Deep Convolutional Neural Network (DCNN) is efficient for object recognition. Nevertheless, a lot of training images are required for this. Therefore, to make the best use of DCNN for national flag recognition, we need to use the pre-trained DCNN instead of training a CNN from scratch and this comes with several benefits such as less computational power needed since the CNN processes the images just once to extract the features. Also, this process requires less data as the CNN architecture has activations that could be used for feature extraction to obtain a high accuracy [18].

Therefore, for the feature extraction pre-trained VGG 16 [19] was used for the extraction of high-level and the rich features. These extracted features include shapes, patterns, colors, and textures, among others. The earlier layers of the network detect low-level features like edges and textures, while the deeper layers learn more complex features that represent objects in the flags. The extracted CNN features were trained by adding flatten layer then two custom dense layers and an output layer which is suitable for multi-class problems. These dense layers make use of similarity measurements by analyzing the activation values of specific features that have been extracted in the initial stage. The similarity measurement helps in comparing different objects among the flags. Features with an activation value of zero indicate that they are not activated. The number of features (feature index) will continue to decrease from the flatten to the output layer which entails the number of classes (0-6) where the final prediction is made based on the activated features. A sample of the activation visualization of the features is shown in Figures 3-6.

International Journal of Applied Sciences and Smart Technologies

Volume 5, Issue 2, pages 255–270

p-ISSN 2655-8564, e-ISSN 2685-9432

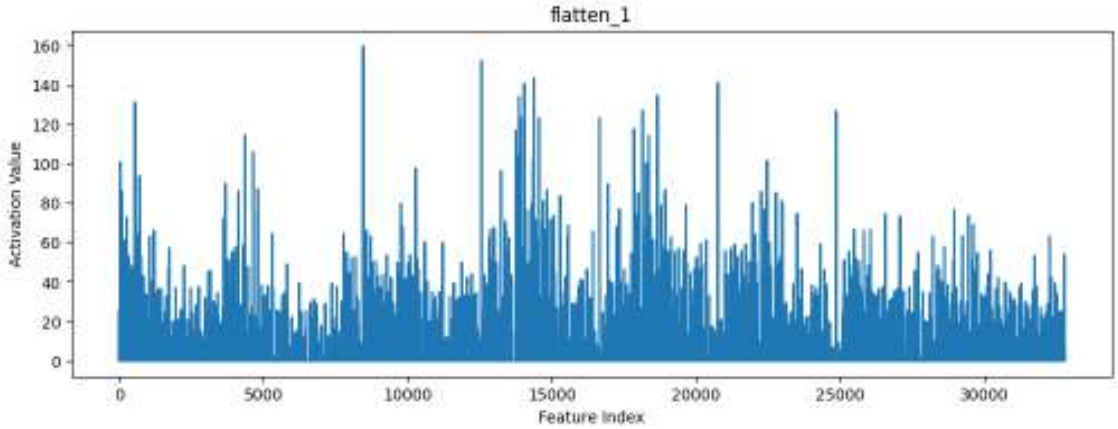


Figure 3: Activation visualization of the features for the flatten layer

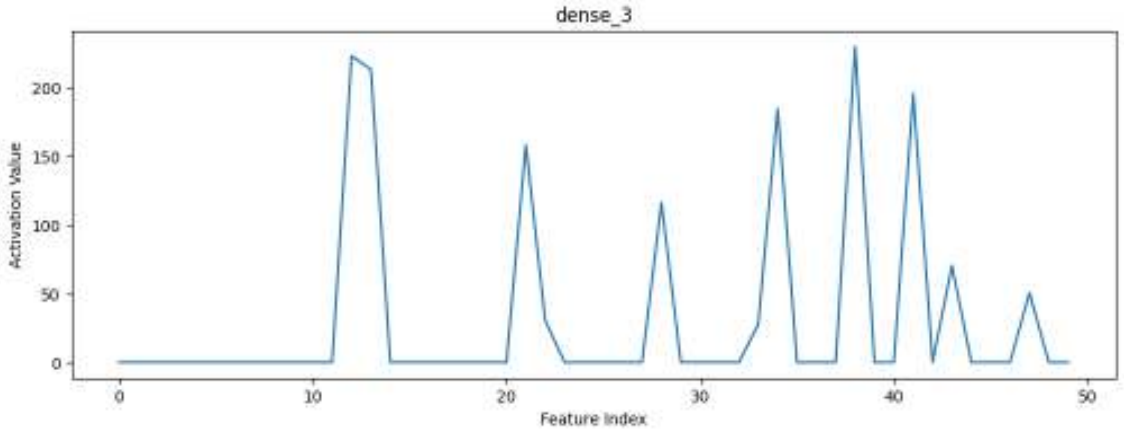


Figure 4: Activation visualization of the features for the first dense layer

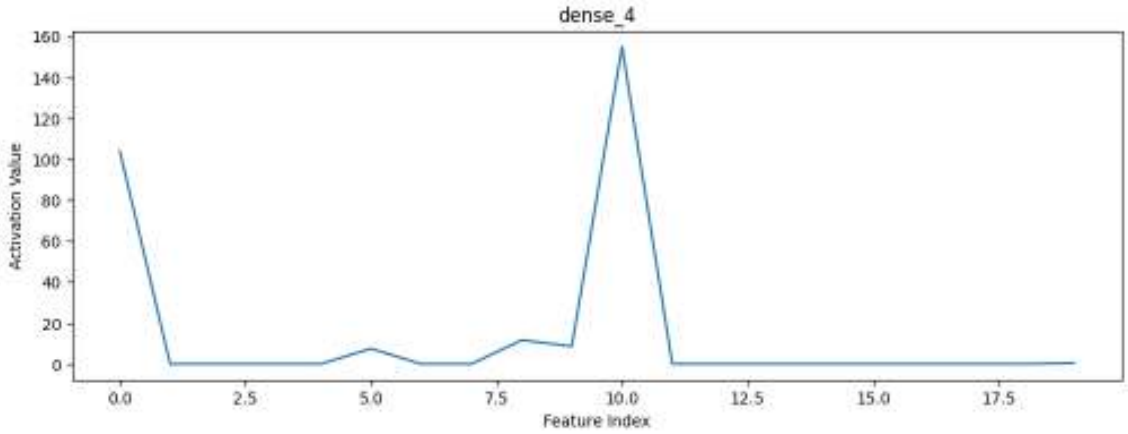


Figure 5: Activation visualization of the features for the second dense layer

International Journal of Applied Sciences and Smart Technologies

Volume 5, Issue 2, pages 255–270

p-ISSN 2655-8564, e-ISSN 2685-9432

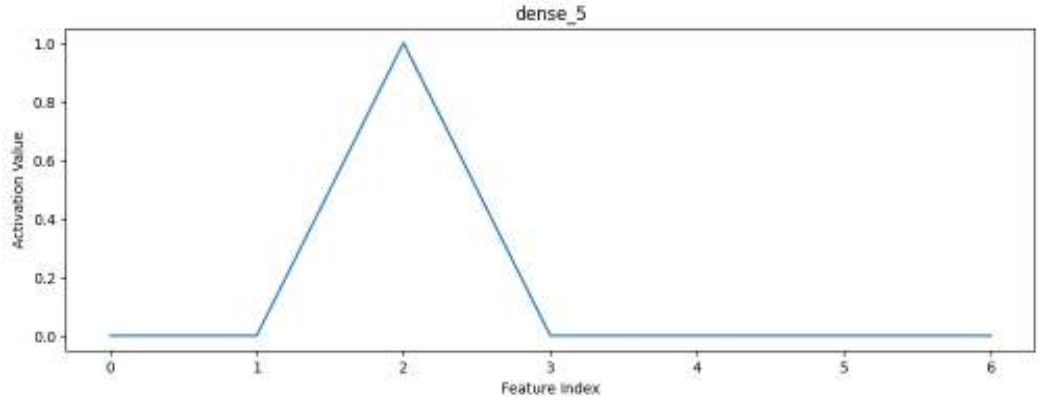


Figure 6: Activation visualization of the features for the output layer

In VGG 16, as shown in Figure 7 the input image is transmitted through a group of convolutional layers with a 3x3 receptive field. It is assumed that the convolution stride is 1 pixel. For spatial pooling, five max-pooling layers with a stride of two are used (down sampling). A 2x2 pixel window is used for max-pooling layers, which succeed some of the convolutional layers. After the set of convolutional layers, there are three fully connected layers with channel sizes of 4096, 4096, and 1000, respectively.

Each neuron in the fully connected layer receives information from the activations of the neuron in the layer below. The number 1000 represents the total number of categories in the ImageNet Large-Scale Visual Recognition Challenge (ILSVRC). However, for this research 7 was used since the number of the countries considered is 7. The last layer is called the soft-max layer. All the hidden layers are outfitted by the rectification (ReLU) non-linearity layer [17] given in equation (1). VGG-16 architecture's main benefit is that it generalizes well to other datasets [19].

$$f(x) = \max(0, x) \quad (1)$$

Furthermore, SoftMax [21] given in equation (2) was applied to produce probability values for each class. The class with the highest probability value is the identified flag. Multiclass cross entropy was used as the loss function.

$$\sigma(\vec{z})_I = \frac{e^{z_i}}{\sum_{j=1}^{K} e^{z_j}} \quad (2)$$

Volume 5, Issue 2, pages 255–270

p-ISSN 2655-8564, e-ISSN 2685-9432

Where: σ is the softmax, $\vec{z}$ is the input vector, e^{z_i} is the standard exponential function for input vector, K is the number of classes and e^{z_j} is the standard exponential function for output vector.

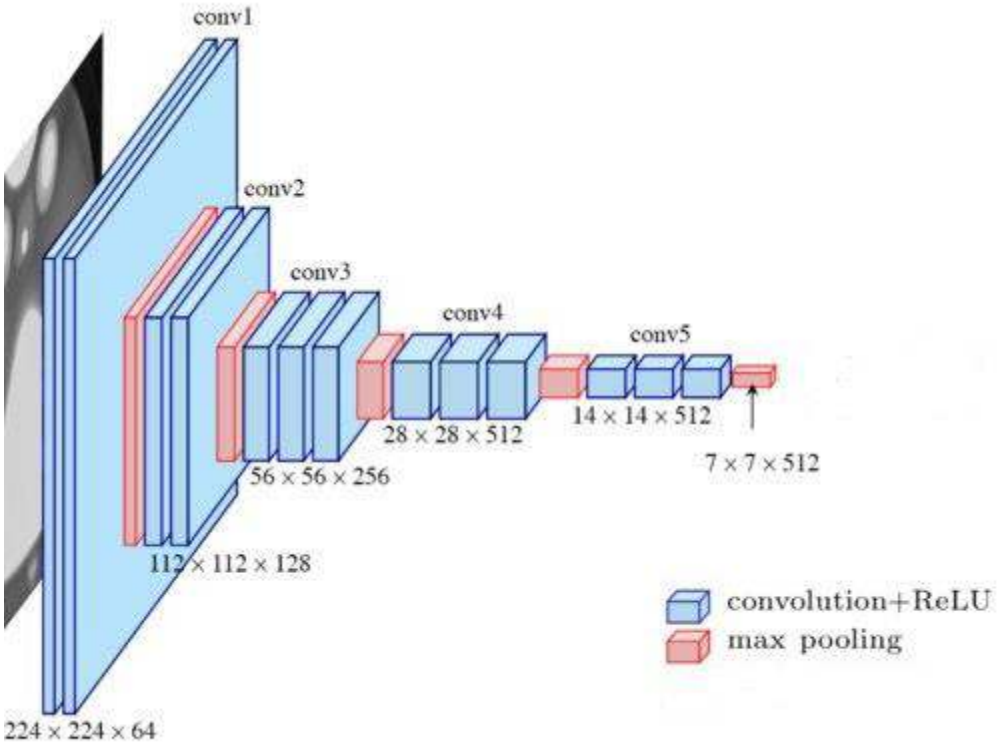


Figure 7: The architecture of VGG-16 [20]

In this research, Paper space Gradient (available at: https://www.paperspace.com/), an open source web application to create and edit live code was used in order to maximize the use of software and hardware resources made available for researchers by Paper space 30GB of RAM and 5GB Disk allocated by paper space which was used for developing the model. All the algorithms were implemented with the use of TensorFlow framework with other libraries including OpenCV for manipulating and image preprocessing.

3 Results and Discussions

To evaluating this model, the dataset was portioned into two. 70% of the dataset was used for training while the remaining was used for testing. Evaluation metrics such as Accuracy, F1-Score and recall were used to evaluate the model.

International Journal of Applied Sciences and Smart Technologies
Volume 5, Issue 2, pages 255–270
p-ISSN 2655-8564, e-ISSN 2685-9432

Table 2: Performance Evaluation

Metric	Score
Accuracy	98.2%
Recall	0.8902620087336245
Precision	0.9280771384659074
F1 Score	0.9816383477392395

Additionally, Streamlit [23] was used to deploy the model to web application after which independent test set was supplied to the web app for prediction as seen in Figures 8 and 9.



Figure 8. Result of Independent test on Ghana

International Journal of Applied Sciences and Smart Technologies
Volume 5, Issue 2, pages 255–270
p-ISSN 2655-8564, e-ISSN 2685-9432



Figure 9 Result of Independent test on Guinea

Failure cases

Due to high similarity among these flags, there were failure cases in the experiment as shown in figures 10 and 11.



Volume 5, Issue 2, pages 255–270

p-ISSN 2655-8564, e-ISSN 2685-9432

Figure 10.Result of Independent test on Cameroon wrongly predicted as Mali

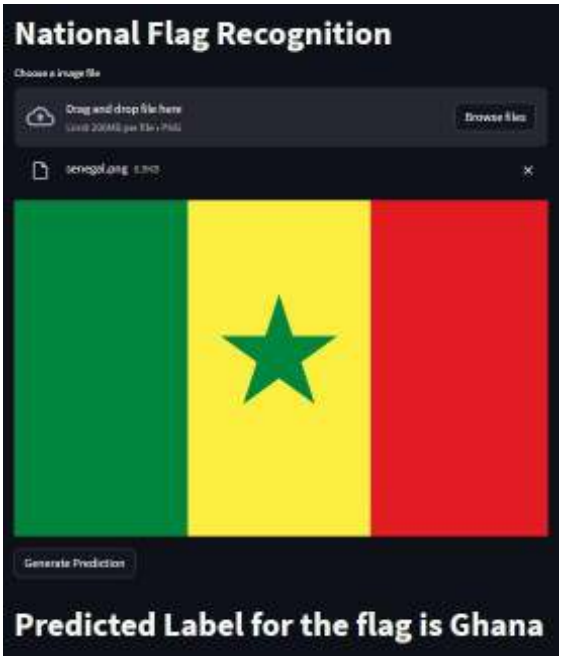


Figure 11. Result of Independent test on Senegal wrongly predicted as Ghana

Based on our research, this proposed deep learning approach to national flag recognition, entails convolution layers, SoftMax, dense and other special layers including dataset of 4987 National flag images. Most of the existing works used handcrafted feature extraction techniques. However, deep learning approach was used in this work to extract various level features after which the extracted features were passed to additional layer that enhanced the accuracy of our model by focusing on the necessary features. This work, compared to previous works on this subject matter, such as [7] and [13]has better performance in terms of accuracy and precision.

This approach has lots of advantages such as the use of VGG-16, a pretrained model to extract necessary features; then the extracted features are passed through additionally convolutional and dense layers thereby neglecting irrelevant features and enhancing the accuracy of the model.

The dataset has a huge part to play in the performance of the deep learning model, through national flag images gotten from various sources with different backgrounds made the model to be more robust.

Volume 5, Issue 2, pages 255–270
p-ISSN 2655-8564, e-ISSN 2685-9432

4 Conclusions

The aim of this work is to develop a model that would detect and identify national flags in an image. For this reason, a model was developed using multi-class learning approach. The model was trained on flag image dataset which was collected both locally and from the internet summing up 4987 images. This is the first West African flag dataset on this subject matter as far as we are concerned.

The result of this work shows that high accuracy can be obtained with the use of dimensionality reduction (feature extraction and selection). It was observed from this study that the proposed approach performed excellently well in predicting National flags; with Accuracy of 98.20% and F1 score of 98.16%. As a result of the tedious task of gathering dataset, this work was able to gather over 4987 images. Thus, it would also be recommended that more data (flag images) be added to the dataset. It would be interesting to propose more approaches to national flag recognition which will also serve as comparison with this work in future. Furthermore, the application of association rule mining techniques for improved prediction, since some flags have common objects, shapes, and layout. Hence, association rule mining will help unveil these combination patterns in flags for enhanced prediction.

References

[1] Y. Moroi, The Flag and the Anthem in Japan, Peace Review, 32(2) (2020) 212–218.

[2] O. Orti, R. Tous, M. Gomez, J. Poveda, L. Cruz, and O. Wust, Real-Time Logo Detection in Brand-Related Social Media Images, in Lecture Notes in Computer Science (including subseries Lecture Notes in Artificial Intelligence and Lecture Notes in Bioinformatics), (2019) 125–136.

[3] D. M. Montserrat, Q. Lin, J. Allebach, and E. J. Delp, Logo detection and recognition with synthetic images, in IS&T International Symposium on Electronic Imaging, Imaging and Multimedia Analytics in a Web and Mobile World 2018, (2018) 3371–3377.

Volume 5, Issue 2, pages 255–270

p-ISSN 2655-8564, e-ISSN 2685-9432

[4] W. Smith, flag of Benin, Encyclopedia Britannica, (2013).

[5] W. Smith, flag of Guinea-Bissau, Encyclopedia Britannica, Jul. (2011).

[6] J. L. Hennessy and D. A. Patterson, Computer Architecture: A Quantitative Approach," in Morgan Kaufmann, San Francisco, CA, sixth edition., (2019).

[7] N. C. Thompson, K. Greenewald, K. Lee, and G. F. Manso, The Computational Limits of Deep Learning, 4 (2020) 2–5.

[8] V. Wiley and T. Lucas, Computer Vision and Image Processing: A Paper Review, International Journal of Artificial Intelligence Research, 2(1) (2018) 22.

[9] M. Gu, K. Hao, and Z. Qu, Flag detection with convolutional network, CSAI '18: Proceedings of the 2018 2nd International Conference on Computer Science and Artificial Intelligence, ACM, (2018) 258–262.

[10] E. Hart, S.-H. Cha, C. C. Tappert, E. ; Hart, and S.-H. Cha, Interactive Flag Identification, (2004).

[11] S. Jetley, A. Vaze, and S. Belhe, Automatic flag recognition using texture based color analysis and gradient features, 2013 IEEE 2nd International Conference on Image Information Processing, IEEE ICIIP 2013, (2013) 464–469.

[12] G. H. Liu, Z. Y. Li, L. Zhang, and Y. Xu, Image retrieval based on micro-structure descriptor, Pattern Recognition, 44(9) (2011) 2123–2133,

[13] K. Hao, Z. Qu, and Q. Gong, Color flag recognition based on HOG and color features in complex scene, Ninth International Conference on Digital Image Processing (ICDIP 2017), (2017) 104200A.

[14] Y. Lecun, Y. Bengio, and G. Hinton, Deep learning, Nature, 521 (7553) (2015) 436–444.

[15] Y. Said and M. Barr, Countries flags detection based on local context network and color features, Multimedia Tools and Applications, (2021) 14753–14765.

[16] S. Wu, FlagDetSeg : Multi-Nation Flag Detection and Segmentation in the Wild, no. 5.

[17] L. Perez and J. Wang, The Effectiveness of Data Augmentation in Image Classification using Deep Learning, Convolutional Neural Networks Vis. Recognit, 11 (2017) 1–8.

Volume 5, Issue 2, pages 255–270

p-ISSN 2655-8564, e-ISSN 2685-9432

[18] I. Gogul and V. S. Kumar, Flower species recognition system using convolution neural networks and transfer learning, 2017 4th International Conference on Signal Processing, Communication and Networking, ICSCN 2017, (2017).

[19] K. Simonyan and A. Zisserman, Very deep convolutional networks for large-scale image recognition, 3rd International Conference on Learning Representations, ICLR 2015 - Conference Track Proceedings, (2015) 1–14.

[20] M. Ferguson, R. Ak, Y. T. T. Lee, and K. H. Law, Automatic localization of casting defects with convolutional neural networks, Proceedings - 2017 IEEE International Conference on Big Data, Big Data 2017, (2017) 1726–1735.

[21] T. Kaur and T. K. Gandhi, Automated brain image classification based on VGG-16 and transfer learning, Proceedings - 2019 International Conference on Information Technology, ICIT 2019, (2019) 94–98.

[22] S. Sharma, S. Sharma, and A. Anidhya, Understanding Activation Functions in Neural Networks, International Journal of Engineering Applied Sciences and Technology, 4(12) (2020) 310–316.

[23] S. Shukla, A. Maheshwari, and P. Johri, Comparative Analysis of Ml Algorithms & Stream Lit Web Application, Proceedings - 2021 3rd International Conference on Advances in Computing, Communication Control and Networking, ICAC3N 2021, (2021) 175–180.

International Journal of Applied Sciences and Smart Technologies

Volume 5, Issue 2, pages 255–270

p-ISSN 2655-8564, e-ISSN 2685-9432

This page intentionally left blank

International Journal of Applied Sciences and Smart Technologies

Volume 5, Issue 2, pages 271-302

p-ISSN 2655-8564, e-ISSN 2685-9432

A Detailed Review on The Denial of Service (DoS) and Distributed Denial of Service (DDoS) Attacks in Software Defined Networks (SDNs) and Defense Strategies

Elvis Tamakloe[1, *], Benjamin Kommey [1], Emmanuel Akowuah [1], Daniel Opoku [1]

[1]Faculty of Electrical and Computer Engineering, Kwame Nkrumah University of Science and Technology, PMB UPO, 00233, Ghana

[*]Corresponding Author: tamakloe.elvis@gmail.com

(Received 15-05-2023; Revised 26-05-2023; Accepted 22-06-2023)

Abstract

The development of Software Defined Networking (SDN) has altered the landscape of computer networking in recent years. Its scalable architecture has become a blueprint for the design of several advanced future networks. To achieve improve and efficient monitoring, control and management capabilities of the network, software defined networks differentiate or decouple the control logic from the data forwarding plane. As a result of this, logical control is solely centralized in the controller. Due to the centralized nature, SDNs are exposed to several vulnerabilities such as Spoofing, Flooding, and primarily Denial of Service (DoS) and Distributed Denial of Service (DDoS) among other attacks. In effect, the performance of SDN degrades based on these attacks. This paper presents a comprehensive review of several DoS and DDoS defense/mitigation strategies and classifies them into distinct classes with regards to the methodologies employed. Furthermore, based on the discussions raised, suggestions have been made to enhance current mitigation strategies accordingly.

Keywords: Centralized controller, Software Defined Network (SDN), Denial of Service (DoS) attack, Distributed Denial of Service (DDoS) attack, Network security, Mitigation strategies

1 Introduction

Conventional networking infrastructures have great complexity with regards to monitoring, control, and management. That is, managing network devices in conventional networks poses a tremendous challenge since the configuration of this type of network is

This work is licensed under a Creative Commons Attribution 4.0 International License

Volume 5, Issue 2, pages 127-158

p-ISSN 2655-8564, e-ISSN 2685-9432

based on organizational or supervisory policies. In conventional networks, logic control and data forwarding are tightly coupled together [1, 2]. This design architecture inhibits flexibility, increases operational cost, and retards innovation irrespective of certain initial benefits. Therefore, it implies that conventional networks are thus difficult to maintain [3] and cannot serve as the base for developing other emerging technologies like Internet of Things (IoT), Cloud, Big Data and many more since adequate bandwidth, adaptability and good manageability are required. Due to the paradigm shifts in networking architectures over the years, the impact of SDN since its development has adapted to meet current networking demands. By decoupling the control plane or logic and the data plane [4-6] in SDN architecture as depicted in Fig.1, network scalability, flexibility, and other security features are realized to enhance better network performance and management.

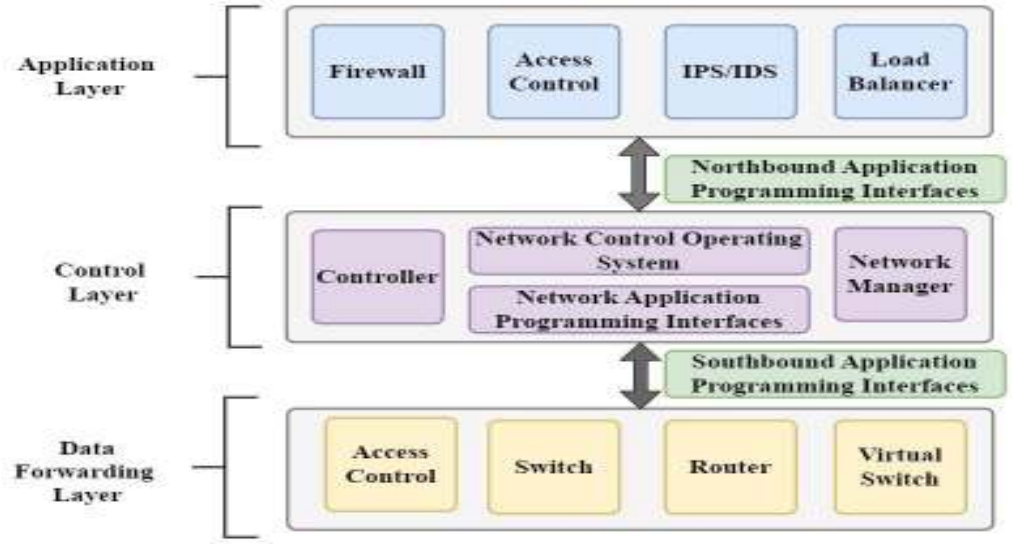


Figure 1. SDN architectural layers.

This design performs a vital task in relation to extensive and high-performance computer systems [7]. Based on this architecture, the critical network functions such as intrusion detection and routing amongst other functions are essentially handled by the linked control and application layer. In the controller, there exist an installed operating system (OS) which maps the entire network to a variety of applications and services realized in the application layer. The implementation of SDN application enables network operators or administrators to have greater control, automation, and optimization over the network [8]. A few protocols have been proposed for SDN however, the OpenFlow (OF)

Volume 5, Issue 2, pages 127-158
p-ISSN 2655-8564, e-ISSN 2685-9432

is the most used and standardized protocol which coordinates the control plane and the data plane via a southbound interface (control channel) [9, 10]. Switches enabled with OF have flow tables for storing flow rules for data forwarding. This implies that the switch compares the packet header with flow table's flow rules upon the arrival of a packet. Howbeit, in cases whereby no flow rule exists next to the data packet header, a table-miss results, and the data packet is transferred to the controller as a Packet-In message. This message is then processed by the controller and subsequently, a flow rule with the appropriate actions is sent towards the switch [11]. Therefore, it means that the switch's flow table comprise of data forwarding rules transmitted by the controller via the control channel. Additionally, it is imperative to note that the status of these rules is temporal since limited time is assigned to them after their installation. Thus, they are taken off from the flow table after this limited duration. Many recognized industry players in the network market like Hewlett-Packard (HP), Computer Information System Company (CISCO) etc., are integrating OF in the development of its switches. Although many advantages such as scalability, flexibility and manageability of the network have been drawn from implementing SDN, the decoupling of the control and data plane exposes the network to several or different attacks (conventional and modern) [12, 13]. In reference to these security issues DoS attacks or its distributed variant (DDoS) poses the most threat to the network in contrast to the other attacks. This implies that a successful DoS or DDoS attack has the tendency or ability to entirely disrupt the network by disabling the controller or switch [14, 15]. Hence, crippling both the control plane and data plane. In these attacks, switches are unable to appropriately transmit packets as required which results in network failure and subsequently, a system collapse. Therefore, this paper presents a detailed description of DoS and DDoS attacks on SDN infrastructure components, reviews a variety of techniques adopted to solve these attacks and provides a comprehensive study of these mitigation techniques as well as their benefits and limitations. Outlined in sections (2-6) are the most relevant areas that present a complete insight and in-depth analysis of DoS and DDoS attacks in SDN, and strategies developed to curb these attacks.

International Journal of Applied Sciences and Smart Technologies

Volume 5, Issue 2, pages 127-158

p-ISSN 2655-8564, e-ISSN 2685-9432

2 Operation of the SDN architecture

The SDN architecture as illustrated in Fig.1 consist of three distinct and decoupled layers namely, the Application, Control and Data Forwarding layer. These respective layers contain certain vital components that allows for coordination. For instance, the application and control layer components coordinate via the Northbound API whilst the Southbound API facilitates communication between both the control and data forwarding layer. This implies that OpenFlow protocols are the most ubiquitous form of Southbound API [16] readily available to facilitate this particular form of interaction. The description of the three SDN layers together with the respective functionalities are as follows:

A. The Application Layer

It contains several applications (access control, firewall, load balancer, etc.) which via the northbound API, interact with the control layer in order to carry out expected tasks. The performance of these applications is independent of one another. Hence, they can be enabled or disabled based on requirements and network configuration by the administrator. In this regard, installing new applications are easy to perform and already existing applications can equally be uninstalled without affecting the operation of the SDN.

B. The Control Layer

This layer comprises of the centralized controller which has an embedded operating system (OS) that controls the entire SDN network. Here in this layer, the application layer's specifications are interpreted downwards to the data forwarding layer thus, providing an overview of the network. In relation to distributed software defined networks it is important to note that the coordination of the different controllers via the Westbound and Eastbound interfaces are made possible in this very layer. Aside the controller, the control layer houses other components like the network OS, APIs, and the network manager to facilitate a more efficient interaction and control of the network.

C. The Data Forwarding Layer

It is considered as one of the major blocks of the SDN architect since it is comprising of many essential devices like routers, switches, access control and virtual switch that supports the operation of the SDN network. Alternatively referred to as the

Volume 5, Issue 2, pages 127-158

p-ISSN 2655-8564, e-ISSN 2685-9432

network infrastructure layer, the data forwarding layer employs devices that can be connected in several topologies as well as to hosts and servers. Thus, to be able to obtain flow rule to ensure data forwarding, every device in this very layer is linked to the controller via an exclusive connection. As illustrated in Fig.2, a simplified tree topology based SDN architecture is presented.

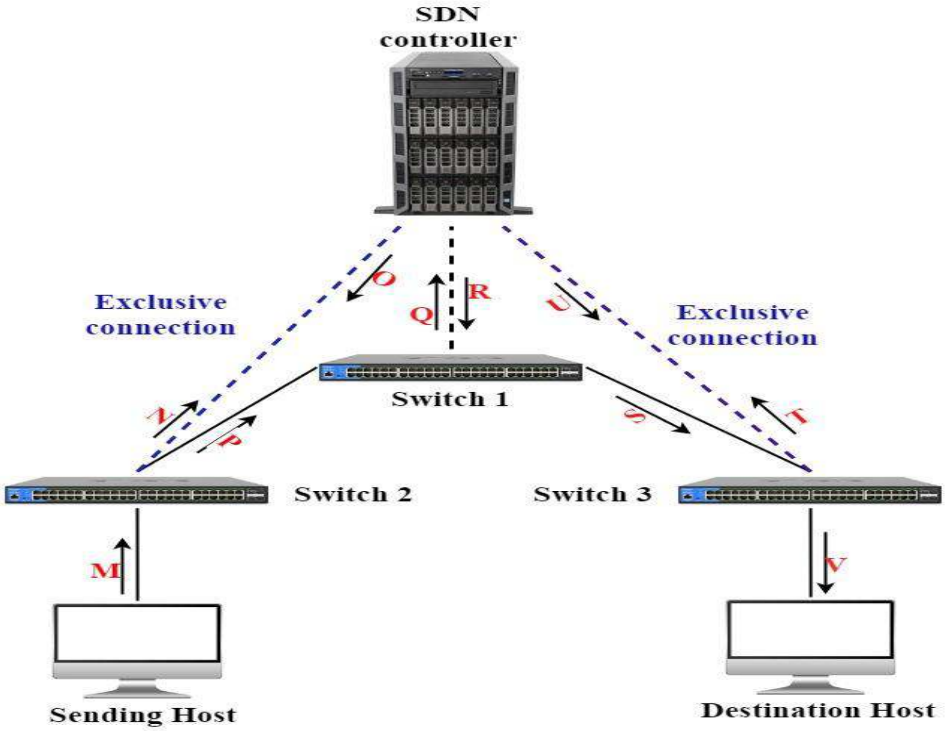


Figure 2. Simplified SDN architecture.

This simplified architecture consists mainly of a SDN controller, switches, the sending and destination or receiving host. To ensure a successful delivery of data from the sending host to the destination host, provided no flow rules are installed, it implies that a data packet must be first sent to switch 2 as indicated by process M. Afterwards, a packet-in message is then sent from switch 2 to the controller (process N). It is important to note that this is dependent on the network configuration, an exclusive connection (link) as well as the open flow version [6]. In responds, the controller delivers a packet-out message back to switch 2 (process O). Based on the feedback response from the controller, data packets are transferred from switch 2 to switch 1 for further actions. Upon the arrival of the data packets in switch 1, a similar activity (between switch 2 and controller) is carried out again with the controller to enquire with regards to the

Volume 5, Issue 2, pages 127-158
p-ISSN 2655-8564, e-ISSN 2685-9432

destination of the data packet. This is indicated by the process Q and R. The controller's response from switch 1 subsequently allows for data packets to be transferred to switch 3 (process S). The data packets are thereafter sent from switch 3 to the controller and back from the controller to switch 3 as shown by process T and U respectively. The data packets then received by the destination host via switch 3 as depicted by process V. Hence, to install the flow rules, all the processes (M, N, O, P, Q, R, S, T, U, V) must be successfully completed to guarantee the reception of data packets by the destination host from the sending host. Immediately these flow rules are installed, subsequent data packet deliveries are undertaken via only process M, P, S, and V as well as through all the respective switches. However, in the event of a role reversal (whereby the destination host becomes the sender, and the sending host becomes the destination host) a new flow rule must be installed. Therefore, the movement of data packets would be in the opposite direction.

3 DoS and DDoS attacks in SDN

The centralized nature of the SDN network, exposes it to certain severe attacks and security threats. Notable amongst these are Denial of Service and its distributed variant (DDoS) [17, 18]. A Denial-of-Service attack is a system-to-system security threat that occurs when data packets are flooded towards a targeted system (destination like server, web application etc.) in a manner that new flow rules are required for every data packet involved. The goal of this kind of attack is to overwhelm the processing ability of the targeted system in order to make its resources unavailable. The severity of this attack grows on much larger scale with DDoS when spoofed packets containing arbitrary addresses (sending and destination addresses) are sent by multiple systems to a targeted system in such a way that resources of the network are made inaccessible to authorized users. Furthermore, DoS attacks and its variants can be launched to consume especially bandwidth and other vital network resources. The repercussion of these attacks on the SDN infrastructure is mostly costly as its effect extends to the application, control, and data forwarding layer as a result of their evolving nature.

International Journal of Applied Sciences and Smart Technologies

Volume 5, Issue 2, pages 127-158

p-ISSN 2655-8564, e-ISSN 2685-9432

Table I. Summarized comparison between DoS and DDoS in SDN

Denial of Service (DoS)	**Distributed Denial of Service (DDoS)**
It originates from a single source to overwhelm targeted resources	It emanates from multiple sources to inflict damage.
Rate of attack is slow	Rate of attack is very fast
Less traffic volumes are forwarded to targeted resources	Much larger traffic volumes are forwarded since it is a coordinated attack.
It is relatively easier to detect and trace the origin of attack	It is complex to detect and trace due to many disguised attack origins.

4 The Taxonomy of DoS and DDoS attacks

To provide solutions to the aforementioned attacks upon their detection, it is essential to classify them into respective groups so as to easily identify and efficiently administer the most appropriate mitigation technique or strategy to aid in combatting these attacks.

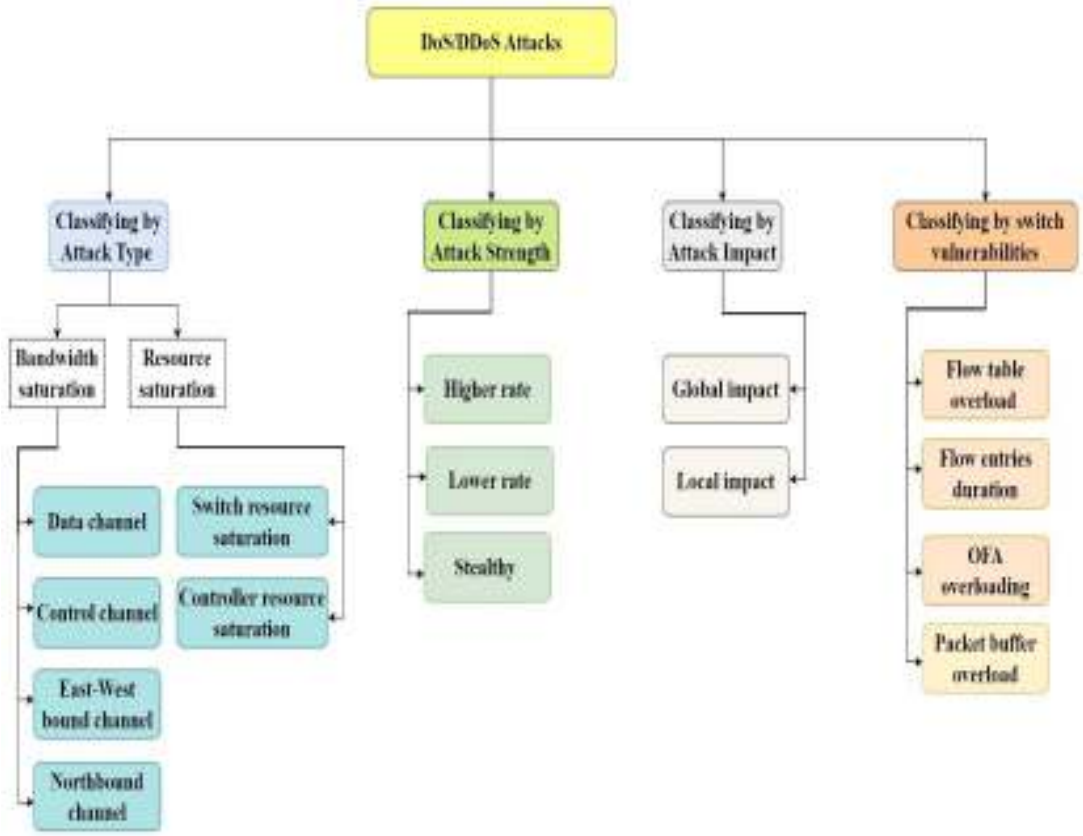


Figure 3. Taxonomy of DoS/DDoS attacks in SDN architecture.

Volume 5, Issue 2, pages 127-158
p-ISSN 2655-8564, e-ISSN 2685-9432

A variety of classifications of the denial of service and its distributed variant is presented in Fig.3 based on the attack type, strength, impact, and vulnerabilities of the OpenFlow data forwarding switches.

A. Classifying by Attack Type

The category of DoS/DDoS attacks which primarily seeks to exploit the different interfaces (channels or APIs) in SDNs [19-22] by solely forwarding enormous size of spoofed data packets with the intention to flood and consume channel bandwidth is termed as Bandwidth saturation attacks. As opposed to bandwidth saturation, resource saturation attacks mainly aim at overwhelming the resources (physical memory/RAM, processor/CPU) of the devices (controllers, switches etc.) in the SDN network. Subsequently, successful launch of these attacks results in high latency, total degradation of the quality of service (QoS) and unavailability of service to authorized users [23].

B. Classifying by Attack Strength

In reference to the transmission rate of the attack data packets forwarded towards the target SDN network, DoS/DDoS attacks can again be categorized based on strength. This implies that, given DoS/DDoS attacks with higher attack strength compared with the target network, a successful launch causes heavy damage to the switch's resource and simultaneously congesting the southbound API (control channel). More so, with regards to attacks possessing lower attack strength than the target SDN, a sizeable amount of the bandwidth that has been apportioned to authorized users is hijacked. This type of attacks is difficult to detect and are capable of remaining untraceable and active. A typical illustration is the attack employing mobile botnet [24]. In Stealthy attacks, attack flows are made to last in the flow table for a short idle_timeout value. This makes such attacks undetectable since these flow entries quickly expire in the switch before the networks defensive mechanisms are triggered. Thus, it imposes a long-term effect (financial loss) on the network.

C. Classifying by Attack Impact

There are mainly two classes of the impact of DoS/DDoS attacks on different target modules. These include the local and global impact. The impact of an attack is termed local provided the whole network experiences no malfunction. That is, only hosts that are

Volume 5, Issue 2, pages 127-158
p-ISSN 2655-8564, e-ISSN 2685-9432

connected directly or indirectly to the switches in worst-case scenario are affected. This type of impacts is mostly undetectable in the network and causes a long-term effect on the network. Conversely, the impact of an attack is defined as global when the whole network is prone to entirely fail, malfunction and collapse upon its successful launch. Therefore, this implies that, authorized users of the network are can neither send nor receive data in this regard [25-27].

D. Classifying by Switch Vulnerabilities

The quest to provide scalability and control in SDN, has resulted in the exposure of the OpenFlow switches in the network to be targeted by DoS/DDoS attacks. These include flow table overloading, target buffer overflow, altering of flow entries duration and open flow agent (OFA) overloading. It is imperative to note that OpenFlow switches have limited memory and processing capabilities [28]. When a target switch is flooded with data packets (having several addresses) by an immediate host, the flow table is searched for each data packet and subsequently forwarded to the controller which installs flow rules against the respective packets. However, due to the enormous amount of data packets, the flow table is bound to overflow. Thus, in this situation, the controller can therefore, not assign new flow rules due to the limited capacity which leads to packet drops. Additionally, overloading of the OFA potentially results due to these aforementioned points. In the event of a target buffer overflow, forwarding of a complete packet causes successive and extensive use of the controller's resources [29]. This in effect increases latency and response time as well as magnifies the rate of packet loss [30]. Hence, DoS/DDoS attacks exploits all these raised issues to inflict damage to the network. Furthermore, the timeout mechanisms (idle_timeout and hard_time) employed in flow entry durations provides an avenue for stealthy DDoS attacks which makes use of the minimal durations to send attack flows. Thus, crippling the SDN in a long term.

5 Mitigating strategies and probable challenges

Volume 5, Issue 2, pages 127-158
p-ISSN 2655-8564, e-ISSN 2685-9432

To curb or curtail the DoS/DDoS attacks in Software Defined Networks (SDNs), different detection and mitigation strategies have been developed to repel and safeguard the network against such threats [31-34]. These mitigation strategies can be grouped as follows:

A. Machine Learning Strategy

This type of mitigation technique is currently employed in most SDNs as one of the effective defense strategies to combat DoS/DDoS attacks. To safeguard the SDN network against the aforementioned attacks, in [35], an adversarial deep learning approach detection and defense was proposed. This approach employed a Generative Adversarial Network (GAN) framework to detect DDoS attacks and utilized adversarial training to make network system less sensitive to experimented adversarial attacks. The network traffic was sampled and analyzed every one second to achieve almost real-time results (detection response time). Although this approach delivered a performance score of about 95.54%, it was limited to only common and recent types of DDoS attacks. A Monte Carlo tree search (MCTS) algorithm was presented in [36] to generate adversarial examples of cross-site scripting (XSS) attacks. In this work, the algorithm is made to allow the generation model to proffer reward value that depicts the likelihood of the generative examples bypassing the detector. A generative adversarial network (GAN) framework was employed to optimize and increase the detection rate of these attacks. The percentage of improvement with respect to the accuracy was significant. However, rigorous training is required over several iterations to ensure an increase in the detection rate. In [37], a deep neural network model to safeguard against adversarial examples was proposed. In this regard, it is evident that different machine learning techniques can be used to safeguard software defined networks [38-40].

B. Policy and Resource Management Strategy

Providing protection against DoS/DDoS attacks requires adaptive policies that would render some degree of security for the network. In contrast to conventional networks which are managed based on static security policies, it is fundamentally advantageous to define dynamic security policies for SDN based on the system properties and network statistics. Thus, by configuring and managing the SDNs resources, DoS attacks are avoided. In [41],

Volume 5, Issue 2, pages 127-158
p-ISSN 2655-8564, e-ISSN 2685-9432

a two-level balancing solution composed of conventional and load balancing between servers and network devices respectively was proposed. This method employs Callophrys and efficiently distributes traffic between all alternative routes in the SDN network. In effect, this approach increases the survival time of the network during DDoS attacks. A software defined-internet of things (SD-IoT) algorithm was proposed in [42] to mitigate DDoS attacks. This algorithm efficiently gets the threshold value of the cosine similarity of the vectors of the packet-in rate and subsequently determines the occurrence of a DDoS attack based on the value. Hence, employing both the SD-IoT framework and algorithm enables the blockage and traceability of these attacks. Therefore, the use of policies and resource management mitigation strategies equally offer protection for SDNs against DoS/DDoS attacks [43-45].

C. Deception, Blocking/Dropping Strategy

Creating unpredictable surfaces by altering the properties of the network system is another mechanism employed to guard against adversarial DoS/DDoS attacks. Blocking entails obstructing the port carrying the malicious host and extends to dropping such traffics. These strategies are, therefore, key to ensuring the safety and reliability of software defined networks. A DaMask architecture was presented in [46] as a control structure to enable efficient attack reactions in software defined networks and cloud-based computing. It embodies an anomaly detection module for matching flow packets with attack patterns and a mitigation module to facilitate in proffering the right solution upon detection of a DoS/DDoS attack. To surmount DoS attacks and it distributed variant, [47] suggested a distributed Firewall having Intrusion Prevention Security (IPS) capabilities. Here, incoming data packets are acted upon based on the firewall statistics and flow rules embedded in the switch. Detection of any malicious anomaly leads to the forwarding of packets to the controller for detailed analysis to be performed. If an attack is confirmed, the installed firewall rules immediately drop the malicious traffic. Several blocking strategies have been proposed in [48-50] to mitigate DoS/DDoS attacks in SDN infrastructure. Therefore, this strategy can be adopted to effectively safeguard the network against these attacks. However, it is imperative for the system to also distinguish clearly between false alarms (false cases of DoS/DDoS attacks) and real attacks to avoid blocking or dropping of legitimate users.

Volume 5, Issue 2, pages 127-158
p-ISSN 2655-8564, e-ISSN 2685-9432

D. Delaying and Collaborative Strategy

Safeguarding a software defined network against DoS/DDoS attacks can be achieved by an individual network or through a collaboration between multiple networks. More importantly, individual networks employ delaying as a strategy to mitigate denial of service attacks. In contrast to deception and blocking strategy, delaying approach keeps malicious traffics but under controlled circumstances. This implies that low trust-value is assigned to this type of traffic to allow some degree to communication with the network but at a very limited rate. Regardless of this mitigation approach, malicious traffic however consumes some amount of network resources in the long term. In relation to this subject, different works have been conducted to provide solutions to effectively optimize delay strategies to protect SDNs against the attack. In [51], every new and incoming data packet is assigned with a trust or priority value which is internet protocol based. Data packets are prioritized on mainly the trust value and are subsequently forwarded to the controller as packet headers. Thus, in this manner, DDoS attacks are well mitigated by efficiently utilizing the resource management switch. Other alternative methods have been proposed as FlowRanger in [52] to enable network controllers to effectively prioritize the mitigation solution. This is achieved with a trust management, queuing management and request scheduling modules to allocate to every flow request a trust or priority value, maintain numerous queues with several priority and employ weighted round-robin for processing queues respectively. In view of this, delaying can therefore be classified as an alternative measure to guard software defined networks against DoS/DDoS attacks [53-58]. Table II. presents an overview of the discussed mitigation strategies proposed in different related works for detection and safeguarding of the software defined network against DoS/DDoS attacks.

Table II. Overview of different DoS/DDoS mitigation strategies in SDN

Volume 5, Issue 2, pages 127-158

p-ISSN 2655-8564, e-ISSN 2685-9432

Author	Type of mitigation strategy	Area of focus	Overview
[59]	Machine Learning	Control and Data Forwarding Layer	Presented a Woodpecker with an effective Heuristic algorithm for mitigating DDoS attacks (Link Flooding Attach)
[60]	Machine Learning	Control Layer	Proposed a deep learning approach to achieve greater detection accuracies of DDoS attacks in real time and with the aim to reduce SDNs resource dependency
[61]	Machine Learning	Application Layer	Suggested a blockchain framework known as Cochain-SC having an intra and inter-domain strategies to realize real time detection and mitigation of DDoS attacks.
[62]	Machine Learning	Control Layer	Developed a mitigation strategy based on the flow table's hit rate gradient (time feature) and adopted a real time detection and defense against DDoS attacks by employing a back propagation neural network.
[63]	Machine Learning	Application Layer	Presented a blockchain -based framework (Cochain-SC) with intra and inter-domain DDoS mitigation. The respective domains achieved real time detection and mitigation of illegitimate flows inside the domain as well as facilitate the collaborative among SDN-based domain peers.
[64]	Machine Learning	Data Forwarding Layer	Proposed an Ethereum blockchain which utilized smart contracts to defend SDN against DDoS attacks across several domains via detection algorithms and filter systems.
[65]	Policy and Resource Management	Control Layer	Presented a random route mutation (RRM) that puts together game theory and constraints satisfaction optimization to get the most preferred strategy for DoS/DDoS attack deterrence.
[66]	Policy and Resource Management	Data Forwarding Layer	Suggested an AVANT-GUARD to guard against resilient TCP SYN flood. Based on actuating triggers, the detection, response, and control of the traffic rate are thereby mitigated.

Volume 5, Issue 2, pages 127-158

p-ISSN 2655-8564, e-ISSN 2685-9432

[67]	Policy and Resource Management	Control and Application Layer	Offered a Dossy application which operates in the application layer to curtail DoS attacks. This approach employed flow and packet-in analysis to deliver messages to detect and prevent DoS attacks in SDN
[68]	Policy and Resource Management	Control and Data Forwarding Layer	Presented a lightweight DoS detection and mitigation system known as FlowFence. It essentially comprises of switches and controller for detection of traffic congestion and bandwidth flows control respectively.
[69]	Policy and Resource Management	Control and Application Layer	Proposed a framework called FloodDefender to defend the controller against DDoS attacks. Mitigation is achieved by the utilization of packet-in message for attack detection, filtering of packets and efficient management of flow rules.
[70]	Policy and Resource Management	Control Layer	Suggested an SDNManager that mainly expects constant monitoring of flow information and future estimation of demands of bandwidth in the SDN. It therefore implies that, penalization of flows exceeding required estimates exist to facilitate mitigating the network against attacks.
[71]	Policy and Resource Management	Control Layer	Presented a mechanism to mitigate DDoS attacks by dropping packets dependent on the packet-in thresholds. In this regard, packets and bytes counts are the required parameters or statistics for the controller to ensure detection of such attacks.
[72]	Policy and Resource Management	Control Layer	Recommended an effective mechanism to guard against DDoS attacks by monitoring the fairness of packet-in messages or packet ratios and distribution of hosts.
[73]	Policy and Resource Management	Control and Data Forwarding Layer	Addressed low-rate DoS attacks by installing and monitoring flow rules on respective switches to facilitate detection of low-rate TCP attacks. Thus, reduction in bandwidth and mitigation on ingress switches were proposed as a solution to this type of attack via constant monitoring.
[74]	Blocking and dropping	Control Layer	Proposed the implementation of SLICOT in the controller to safeguard SDN against TCP SYN flooding attacks. This was

Volume 5, Issue 2, pages 127-158

p-ISSN 2655-8564, e-ISSN 2685-9432

			achieved by installing provisional forwarding rules in TCP handshaking processes and after request validations. Thus, its capability of detecting and blocking malicious requests that would potential jeopardize the SDN.
[75]	Blocking and Dropping	Application and Data Forwarding Layer	Presented an architecture that employs OpenFlow and sFlow to detect and mitigate DoS attacks. Detection of anomalies are done with an entropy-based algorithm and dependent on sampled data from the sFlow. Hence, alteration of the flow table and its entries ensures the safety of SDN by blocking malicious traffic.
[76]	Blocking and Dropping	Control Layer	Suggested a vital framework called NIMBUS for detecting DoS/DDoS attacks by thoroughly analyzing traffics. This implies that malicious traffic is blacklisted or rate limits applied with auto scalable VMs to ensure effective mitigation.
[77]	Blocking and Dropping	Control Layer	Presented a link flooding attacks (LFA)Defender which explores or inspects the SDN to recognize probable target links, reroute traffics in events of congestion and blocks harmful traffics. This provides the requisite flexibility and economic efficiency.
[78]	Blocking and Dropping	Control Layer	Proposed an architecture referred to as RADAR to enable detection of DDoS attacks by utilizing adaptive correlation analysis. Thus, by employing a port-based max-min fairness approach, malicious traffics are dropped via analysis
[79]	Blocking and Dropping	Data Forwarding Layer	Incorporated the data plane in the defense mechanism to eliminate dependency on the network controller in the control layer. In this regard, detection of DoS/DDoS attacks is made by propagating alarm across the SDN using probe packets. As a result, mitigation measures (traffic dropping, IP obfuscation) were adopted to handle these malicious traffics. A typical example is with respect to FastFlex.

[80]	Blocking and Dropping	Data Forwarding Layer	Proposed a policy enforcement engine known as Poseidon to defend DDoS attacks. This utilized modularized defense primitives to throttle denial of service attacks and its distributed variant in SDN
[81]	Blocking and Dropping	Application and Data Forwarding Layer	Introduced a new security plane along with the data plane. Imperatively, this is parallel to the control plane. Pyretic is used by switches in the data plane to forward packets to detection engines. To throttle DDoS attacks, these engines forward the right rules to the controller for insertion into switches. Hence, effective for safeguarding SDN against malicious attacks.
[82]	Blocking and Dropping	Application and Data Forwarding Layer	Proposed a transparent intrusion detection system (TIDS) which offers a distributed and scalable remedy against DDoS attacks. To achieve detection of intruders and mitigating low-level DoS attacks, a polling processor is employed to perform analysis on flows, recognize anomalies and forward modified requests of flows to realize the blocking of malicious addresses.
[83]	Delaying and Collaborative Strategy	Control Layer	DrawBridge was proposed to facilitate between ISPs and hosts an end-to-end effective/reliable communication. Implemented in SDN as a controller, it forwards flow rules to switches in the ISP and interacts with other controllers in the ISP upstream. Thus, it enables filtering of malicious DDoS traffics via thorough verification, processing and deployment of flow rules.
[84]	Delaying and Collaborative Strategy	Control Layer	Developed an SDN controller-to-controller based protocol for collaborative defense against DDoS attacks. This protocol enables secure interaction and exchange of attack information between established SDN controllers. Thus, this allows for effective monitoring, alert of malicious paths and filtering of traffics close to the source attack
[85]	Delaying and Collaborative Strategy	Application and Control Layer	Proposed a FireCol architecture as an effective solution against flooding DDoS attacks based on early detection. The

Volume 5, Issue 2, pages 127-158

p-ISSN 2655-8564, e-ISSN 2685-9432

			architecture incorporates intrusion prevention systems (IPSs) for creating virtual shield rings around hosts. This imperatively ensures the exchange of vital traffic information to safeguard end users and the entire network's infrastructure.
[86]	Deception and Moving Target Strategy	Control Layer	Proposed a smart moving target defense linked proactive and reactive virtual machine migration scheme. This scheme improves or optimizes the migration frequency to reduce resource wastage and curb attack impacts. In this regard, protection against DDoS attacks is improved by employing false reality pretense to repel malicious attacks and study attack patterns.
[87]	Deception and Moving Target Strategy	Control Layer	Presented a controller placement camouflage solution to effectively alter the attack surface in moving target defense. A stochastic game (Zero-Sum) is used to lead the MTD solution between the system defender and attacker. Thus, this technique enables real time risk evaluation of network vulnerabilities based in a Bayesian Attack Graph and constantly shifts the location of the SDN controller.
[88]	Deception and Moving Target Strategy	Control Layer	Introduced an agile architectural framework to exploit SDN and NFV by applying moving target defense and network forensics techniques. Interested traffics are stored by the VCP framework and forwarded to the SDN controller for thorough analysis. Route mutation was employed to guard against DDoS attacks by obfuscating the network's topology information. Thus, an effective MTD strategy for protecting SDN although much storage of traffic data is required.
[89]	Deception and Moving Target Strategy	Control Later	Addressed protection against DDoS attacks by leveraging MTD security in SDN enabled cloud infrastructure. Reduction in frequency and selection of location of target mobility across heterogeneous VM based on the probability of the attack was the focal point for subsequent framework

Volume 5, Issue 2, pages 127-158

p-ISSN 2655-8564, e-ISSN 2685-9432

			development. This proved effective based on low success rate of attacks.
[90]	Deception and Moving Target Strategy	Control Layer	Developed an SDN-based MTD system known as CHAOS to obfuscate the attack surfaces to enhance the uncertain and unpredictable nature of the environment. This is best achieved with the proposed Chaos Tower Obfuscation algorithm. Therefore, this offers several degrees of obfuscation for hosts thus, enabling the realization of moving target defense in SDN controller based networks.

Upon reviewing DoS/DDoS attacks, its effects on the SDN architecture (layers) and several mitigation strategies adopted to guard networks against them, it is vital to find an optimal and robust security that guarantees protection for legitimate users from all forms of vulnerabilities. Practically, this is very essential for integration on other modern networks or frameworks like the SDN-IoT networks [91-93], smart grid security networks [94-100], industrial networks [101-105], enterprise networks [106-109], backbone networks [110-115], 5G networks [116-118], and software defined network optical networks (SDON) [119, 120]. Therefore, future works can incorporate certain combinations of the reviewed mitigation or defense strategies with modules capable of:

1. Efficiently detecting real-time attacks with optimal response time
2. Effective processing of data packets
3. Adding extra traffics to enable effective verification
4. Ensuring the long-term reliability of the SDN

Hence, it is worth noting that, the quantity and quality of network traffics are essential parameters for thorough examination and assessment of the discussed defense or mitigation strategies in SDN.

6 Conclusions

The scalability, control, and manageability of SDNs offer network developers a flexible platform to fabricate and run self-made protocols without changing existing hardware in the network. This dynamism had made it a preferred choice with regards to current and future network developments. Considering the drawbacks in reference to

security in SDNs, this paper presented a detailed review of potential mitigation strategies to tackle most well-known DoS and DDoS attacks. Furthermore, based on the discussed methods, it is thus essential to enhance current mitigation strategies more collaboratively to ensure faster and efficient attack detection, maximum security, reliability and longevity to SDN infrastructures.

References

[1] R. Mijumbi, J. Serrat, J.-L. Gorricho, N. Bouten, F.De Turck and R. Boutaba, Network Function Virtualization: State-of-the-Art and Research Challenges. IEEE Communications Surveys & Tutorials, 18(1) (2016) 236-262.

[2] D. Kreutz, F.M.V. Ramos, P.E. Verissimo, C.E. Rothenberg, S. Azodolmolky, and S. Uhlig, Software-Defined Networking: A Comprehensive Survey. Proceeding of the IEEE, 103(1) (2015) 14-76.

[3] R. Masoudi, and A. Ghaffari, Software defined networks: A survey. Journal of Network and Computer Applications, 67 (2016) 1-25. 2016.

[4] X. Zhang, L.Cui, K. Wei, F.P. Tso, Y. Ji, W. Jia, A survey on stateful data plane in software defined networks. Computer Networks. 184, (2021) 107597.

[5] Q. Waseem, W.I.S.W. Din, A. Aminuddin, M.H. Mohammed, R.F.A. Aziza, Software-Defined Networking (SDN): A Review. 5th International Conference on Information and Communications Technology, (2022) 30-35.

[6] M. Imran, M.H. Durad, F.A. Khan, and A. Derhab, Toward an optimal solution against Denial of Service attacks in Software Defined Networks. Future Generation Computer Systems 92, (2019) 444-453.

[7] Q. Yan, F.R. Yu, Q. Gong, and J. Li, Software-Defined Networking (SDN) and Distributed Denial of Service (DDoS) Attacks in Cloud Computing Environments: A Survey. Some Reseach Issues, and Challenges. IEEE Communications Surveys & Tutorials, 18 (1) (2016) 602-622.

[8] I. Ahmad, S. Namal, M. Ylianttila,and A. Gurtov, Security in software defined networks: A survey. IEEE Communications Surveys & Tutorials, 17(4) (2015) 2317-2346.

Volume 5, Issue 2, pages 127-158

p-ISSN 2655-8564, e-ISSN 2685-9432

[9] N. McKeown, T. Anderson, H. Balakrishnan, G. Parulkar, L. Peterson, J. Rexford, S. Shenker and J. Turner, OpenFlow: enabling innovation in campus networks. ACM SIGCOMM Computer Communication Review, 38(2) (2008) 69-74.

[10] K. Alghamdi, and R. Braun, Software Defined Network (SDN) and OpenFlow Protocol in 5G Network.Communications and Networks 12 (2020) 28-40.

[11] K. Rowan, V. Kotronis, and P. Smith, Openflow: A security analysis. 21st IEEE International Conference on Network Protocols, IEEE. (2013).

[12] A. Izzat, and D. Xu, Security of software defined networks: A survey. Computer Security, 53 (2015) 79-108.

[13] M.D. Firoozjaei, J.P. Jeong, H. Ko, H. Kim, Security challenges with network functions visualization. Future Generation Computer Systems, 67 (2017) 315-324.

[14] H. Beitollahi, and G. Deconinck, Analyzing well-known countermeasures against distributed denial of service attacks. Computer Communication, 35(11) (2012) 1312-1332.

[15] A. Shameli-Sendi, M. Pourzandi, M. Fekih-Ahmed, and M. Cheriet, Taxonomy of Distributed Denial of Service mitigation approaches for cloud computing. Journal of Network and Computer Applications, 58 (2015) 165-179.

[16] J. Suárez-Varela, and P. Barlet-Ros, Flow monitoring in Software Defined Networks: Finding the accuracy/performance tradeoffs. Computer Networks, 135 (2018) 289-301.

[17] M.B. Jiménez, D. Fernández, J.E. Rivadeneira, L. Bellido, and A. Cárdenas, A Survey of the Main Security Issues and Solutions for the SDN Architecture. IEEE Access, 9 (2021) 122016-122038.

[18] J.F. Balarezo, S. Wang, K.G. Chavez, A. Al-Hourani, and S. Kandeepan, "A survey on DoS/DDoS attacks mathematical modelling for traditional, SDN and virtual network." Engineering Science and Technology, an International Journal , 31 (2022) 1-15.

[19] C. Hu, K. Hou, H. Li, R. Wang, P. Zheng, P. Zhang, and H. Wang, SoftRing: TAming the reactive model for software defined networks. 2017 IEEE 25th International Conference on Network Protocols, ICNP, IEEE, (2017) 1-10.

Volume 5, Issue 2, pages 127-158

p-ISSN 2655-8564, e-ISSN 2685-9432

[20] K. Kalkan, G. Gür, and F. Alagöz, SDNScore: A statistical defense mechanism against DDoS attacks in SDN environment. Computers and Communication (ISCC), 2017 IEEE Symposium, IEEE , (2017) 669-675.

[21] M. Alsaeedi, M.M. Mohammad, and A.A. Al-Roubaiey, Toward adaptive and scalable OpenFlow-SDN flow control: A survey. IEEE Access, 7 (2019) 107346-107379.

[22] Z. Latif, K. Sharif, F. Li, M.M. Karim, S. Biswas, and Y. Wang, A comprehensive survey of interface protocols for software defined networks. Journal of Network and Computer Applications, 156 (2020).

[23] M.P. Singh, and A. Bhandari, New-flow based DDoS attacks in SDN: Taxonomy, rationales, and research challenges. Computer Communications, 154 (2020) 509-527.

[24] K. Ahmad, S.S.A. Ali, S.R. Bin, A. Muhammad, M.N. Rafidah, and S. Shahaboddin, Mobile botnet attacks-an emerging threat: Classification, review and open issues. KSII Transactions on Internet and Information System, 9 (4) (2015) 1471-1492.

[25] Y. Lui, B. Zhao, P. Zhao, P. Fan, and H. Liu, A survey: Typical security issues of software-defined networking. China Communication, 16 (7) (2019) 13-31.

[26] Y. Xiao, Zj. Fan, A. Nayak, and Cx. Tan, Discovery method for distributed denial-of-service attack behaviour in SDNs using a feature-pattern graph model. Frontiers of Information Technology and Electronic Engineering, 20 (2019) 1195-1208.

[27] S.Q.A. Shah, F.Z. Khan, and M. Ahmad, The impact and mitigation of ICMP based economic denial of sustainability attack in cloud computing environment using software defined network. Computer Networks, 187 (2021).

[28] M. Ayan, S. Misra, and I. Maity, Buffer size evaluation of openflow systems in software-defined networks. IEEE Systems Journal, 13 (2) (2019) 1359-1366.

[29] A. Mondal, S. Misra, and I. Maity, Buffer Size Evaluation of OpenFlow Systems in Software-Defined Networks. IEEE Systems Journal, 13(2) (2019) 1359-1366.

[30] Z. Guo, Y. Xu, R. Liu, A. Gushchin, Ky. Chen, A. Walid, and H.J. Chao, Balacing flow table occupancy and link utilization in software-defined networks. Future Generation Computer Systems, 89 (2018) 213-223.

Volume 5, Issue 2, pages 127-158

p-ISSN 2655-8564, e-ISSN 2685-9432

[31] R. Swami, M. Dave, and V. Ranga, Software-defined Networking-based DDoS Defense Mechanisms. ACM Computing Surveys, 52(2) (2019) 1-36.

[32] A. Shaghaghi, M.A. Kaafar, R. Buyya, and S. Jha, Software-defined network (SDN) data plane security: Issues, solution, and future directions. Handbook of Computer Networks and Cyber Security. Springer, (2020) 341-387.

[33] I. Farris, T. Taleb, Y. Khettab, and J. Song, A Survey on Emerging SDN and NFV Security Mechanisms for IoT Systems. IEEE Communications Surveys & Tutorials, 21(1) (2019) 812-837.

[34] D.B. Rawat, and S.R. Reddy, Software Defined Networking Architecture, Security and Energy Efficient: A Survey. IEEE Communications Surveys & Tutorials, 19(1) (2017) 325-346.

[35] M.P. Novaes, L.F. Carvalho, J. Lloret, and M.L. Proença Jr,. Adversarial Deep Learning approach detection and defense against DDoS attacks in SDN environments. Future Generation Computer Systems, 125 (2021) 156-167.

[36] X. Zhang, Y. Zhou, S. Pei, J. Zhuge, and Chen, Adversarial Examples Detection for XSS Attacks Based on Generative Adversarial Networks. IEEE Access, 8 (2020) 10989-10996.

[37] K. Groose, N. Papernot, P. Manoharan, M. Backes, and P. McDaniel, Adversarial Examples for Malware Detection. S.N. Foley, D. Gollmann, E. Snekkenes (Eds.) Computer Security - ESORICS 2017, Springer International Publishing, Cham, (2017) 62-79.

[38] T.E. Ali, Y.-W. Chong, and S. Manickam, Machine Learning Techniques to Detect a DDoS Attack in SDN: A Systematic Review. Applied Sciences, 13(5) (2023) 3183. 2023

[39] T.V. Phan, T.M.R. Gias, S.T. Islam, T.T. Huong, N.H. Thanh, and T. Bauschert, Q-MIND: Defeating Stealthy DoS Attacks in SDN with a Machine-Learning Based Defence Framework. 2019. IEEE Global Communications Conference (GLOBECOM), Waikoloa, HI, USA, (2019) 1-6.

[40] M.A. Albahar, Recurrent Neural Network Model Based on a New Regularization Technique for Real-Time Intrusion Detection in SDN Environment. Hindawi; Security and Communication Networks, (2019) 1-9.

Volume 5, Issue 2, pages 127-158

p-ISSN 2655-8564, e-ISSN 2685-9432

[41] M. Belyaev, and S. Gaivoronski, Towards load balancing in SDN-networking during DDoS-attacks. 2014 International Science and Technology Conference (Modern Networking Technologies)(MoNeTeC), Moscow, Russia, (2014) 1-6.

[42] D. Yin, L. Zhang, and K. Yang, A DDoS Attack Detection and Mitigation With Software-Defined Internet of Things Framework. IEEE Access, 6 (2018) 24694-24705.

[43] R. Kandoi, and M. Antikainen, Denial-of-service attacks in OpenFlow SDN networks. 2015 IFIP/IEEE International Symposium on Integrated Network Management (IM), Ottawa, ON, Canada, (2015) 1322-1326.

[44] S. Shin, and G. Gu, Attacking software-defined networks: a first feasibility study. Proceedings of the second ACM SIGCOMM workshop on Hot topics in software defined networking. ACM, (2013) 165-166.

[45] L. Dridi, and M.F. Zhani, SDN-Guard: DoS Attacks Mitigation in SDN Networks. 2016 5th IEEE International Conference on Cloud Networking (Cloudnet), Pisa, Italy, (2016) 212-217.

[46] B. Wang, Y. Zheng, W. Lou, and Y.T. Hou, DDoS attack protection in the era of cloud computing and Software-Defined Networking. Computer Networks, 81 (2015) 308-319.

[47] P. Rengaraju, V.R. Ramanan, and C.-H. Lung, Detection and preventing of DoS attacks in Software-Defined Cloud networks. 2017 IEEE Conference on Dependable and Secure Computing, Taipei, (2017), 217-223.

[48] S. Fichera, L. Galluccio, S.C. Grancagnolo, G. Morabito, and S. Palazzo, OPERETTA: An Openflow-based Remedy to Mitigate TCP SYNFLOOD Attacks against web servers. Computer Networks, 92, (2015) 89-100.

[49] L.F. Carvalho, T. Abrão, Ld. S. Mendes, and M.L. Proença Jr, An ecosystem for anomaly detection and mitigation in software-defined networking. Experts Systems with Applications, 104 (2018) 121-133.

[50] M. Ambrosin, M. Conti, F. De Gaspari, and R. Poovendran, LineSwitch: Tackling Control Plane Saturation Attacks in Software-Defined Networking. IEEE/ACM Transactions on Networking, 25(2) (2017) 1206-1219.

Volume 5, Issue 2, pages 127-158

p-ISSN 2655-8564, e-ISSN 2685-9432

[51] A. Shoeb, and T. Chithralekha, Resource management of switches and controller during saturation time to avoid DDoS in SDN. 2016 IEEE International Conference on Engineering and Technology (ICETECH), Coimbatoree, India, (2016) 152-156.

[52] W. Lei, and C. Fung, FlowRanger: A request prioritizing algorithm for controller DoS attacks in Software Defined Networks. 2015 IEEE International Conference on Communication (ICC), London, UK, (2015) 5254-5259.

[53] S. Padmaja, and V. Vetriselvi, Mitigation of switch-Dos in software defined network. 2016 International Conference on Information Communication and Embedded Systems (ICICES), Chennai, India, (2016) 1-5.

[54] P. Bera, A. Saha, and S.K. Setua, Denial of service attack in software defined network. 2016 5th International Conference on Computer Science and Network Technology (ICCSNT), Changchun, China, (2016) 497-501.

[55] Q. Yan, Q. Gong, and F.R. Yu, Effective software-defined networking controller scheduling method to mitigate DDoS attacks. Electronics Letters, 53(7) (2017) 469-471.

[56] H. Wang, L. Xu, and G. Gu, Flood Guard: A DoS Attack Prevention Extension in Software-Defined Networks. 2015 45th Annual IEEE/IFIP International Conference on Dependable Systems and Networks, Rio de Janeiro, Brazil, (2015) 239-250.

[57] M. Kuerban, Y. Tian, Q. Yang, Y. Jia, B. Huebert and D. Poss, FlowSec: DOS Attack Mitigation Strategy on SDN Controller. 2016 IEEE International Conference on Networking, Architecture and Storage (NAS), Long Beach, CA, USA, (2016) 1-2.

[58] K. Hong, Y. Kim, H. Choi, and J. Park, SDN-Assisted Slow HTTP DDoS Attack Defense Method. IEEE Communication Letters, 22(4) (2018) 688-691.

[59] L. Wang, Q. Li, Y. Jiang, and J. Wu, Towards mitigating link flooding attack via incremental SDN development. IEEE Symposium on Computers and Communication, ISCC, (2016) 397-402.

[60] C. Li, Y. Wu, X. Yuan, Z. Sun, W. Wang, X. Li, L. Gong, Detection and defense of DDoS attack-based on deep learning in OpenFlow-based SDN. International Journal of Communication Systems, 31(5) (2018) e3497.

Volume 5, Issue 2, pages 127-158

p-ISSN 2655-8564, e-ISSN 2685-9432

[61] Z.A. El Houda, A.S. Hafid, L. Khoukhi, Cochain-SC: An Intra- and Inter-Domain Ddos Mitigation Scheme Based on Blockchain Using SDN and Smart Contract. IEEE Access, 7 (2019) 98893-98907.

[62] J. Cui, J. He, Y. Xu, H. Zhong, TDDAD: Time-based detection and defense scheme against DDoS attack on SDN controller. Australasian Conference on Information Security and Privacy. Springer. (2018) 649-665.

[63] Z.A. El Houda, A. Hafid, and L. Khoukhi, Co-IoT: A Collaborative DDoS Mitigation Scheme in IoT Environment Based on Blockchain Using SDN. 2019 IEEE Global Communication Conference (GLOBECOM), Waikoloa, HI, USA. (2019) 1-6.

[64] B. Rodrigues, T. Bocek, A. Lareida, D. Hausheer, S. Rafati, and B. Stiller, A blockchain-based architecture for collaborative DDoS mitigation with smart contracts. IFIP International Conference on Autonomous Infrastructure, Management and Security. Springer, Cham. (2017) 16-29.

[65] J.H. Jafarian, E.Al Shaer, and Q. Duan, Formal approach for route agility against persistent attackers. Lecture Notes in Computer Science, 8134 (2013) 237-254.

[66] S. Shin, V. Yegneswaran, P. Porras, and G. Gu, AVANT-GUARD: Scalable and vigilant switch flow management in softare-defined networks. ACM SIGSAC Conference on Computer and Communications Security, (CCS), (2013) 413-424.

[67] Y.E. Oktian, S. Lee, and H. Lee, Mitigating denial of service (DoS) attacks in openflow networks. International Conference on Information and Communication Technology Convergence, (ICTC). (2014) 325-330.

[68] A.F.M. Piedrahita, S. Rueda, D.M.F. Mattos, and O.C.M.B. Duarte, Flowfence: A denial of service defense system for software defined networking. Global Information Infrastructure and Networking Symposium, GIIS. (2015) 1-6.

[69] G. Shang, P. Zhe, X. Bin, H. Aiqun, and R. Kui, Flooddefender: Protecting data and control plane resources under SDN-aimed DoS attacks. INFOCOM 2017-IEEE Conference on Computer Communication, (2017) 1-9.

[70] T. Wang, H. Chen, G. Cheng, and Y. Lu, SDNManager: A Safeguard Architecture for SDN DoS Attacks Based on Bandwidth Prediction. Network Security and Management in SDN, (2018).

Volume 5, Issue 2, pages 127-158

p-ISSN 2655-8564, e-ISSN 2685-9432

[71] S. Wang, S. Chandrasekharan, K. Gomez, S. Kandeepan, A. Al-Hourani, M.R.Asghar, G. Russello, and P. Zanna, SECOD: SDN Secure Control and Data Plane Algorithm for Detecting and Defending Against DoS Attacks. NOMS 2018 IEEE/IFIP Network Operations and Management Symposium. IEEE. (2018) 1-5.

[72] N. Goksel, and M. Demirci, DoS attack detection using packets statistics in SDN. International Symposium on Networks, Computers, and Communications, (ISNCC), IEEE. (2019) 1-6.

[73] R. Xie, M. Xu, J. Cao, and Q. Li, Softguard: Defend against the low-rate TCP attack in SDN. 2019 IEEE International Conference on Communication (ICC). (2019)1-6.

[74] R. Mohammadi, R. Javidan, and M. Conti, SLICOTS: An SDN-Based Lightweight Countermeasure for TCP SYN Flooding Attacks. IEEE Transactions on Network and Service Management, 14(2) (2017) 487-497.

[75] K. Giotis, C. Argyropoulos, G. Androulidakis, D. Kalogeras, and V. Maglaris, Combining OpenFlow and sFlow for an effective and scalable anomaly detection and mitigation mechanism on SDN environments. Computer Networks, 62 (2014) 122-136.

[76] R. Miao, M. Yu, and N. Jain, NIMBUS: Cloud-scale attack detection and mitigation. ACM SIGCOMM Computer Communications. Rev.44. (2014) 121-122.

[77] J. Wang, R. Wen, J. Li, F. Yan, B. Zhao, and F. Yu, Detecting and Mitigating Target Link-Flooding Attacks Using SDN. IEEE Transactions on Dependable and Secure Computing. 16(6) (2019) 944-956.

[78] J. Zheng, Q. Li, G. Gu, J. Cao, D.K.Y. Yau, and J. Wu, Realtime DDoS Defense Using COTS SDN Switches via Adaptive Correlation Analysis. IEEE Transactions on Information Forensics and Security, 13(7) (2018) 1838-1853.

[79] J. Xing, W. Wu, and A. Chen, Architecting Programmable Data Plane Defense into the Network with FastFlex. HotNets ′19: Proceedings of the 18th ACM Workshop on Hot Topics in Networks. (2019) 161-169.

Volume 5, Issue 2, pages 127-158

p-ISSN 2655-8564, e-ISSN 2685-9432

[80] M. Zhang, G. Li, S. Wang, C. Liu, A. Chen, H. Hu, G. Gu, Q. Li, M. Xu, and J. Wu, Poseidon: Mitigating Volumetric DDoS Attacks with Programmable Switches. Network and Distributed Systems Security (NDSS) Symposium 2020. (2020) 1-18.

[81] A. Hussein, I.H. Elhajj, A. Chehab, and A. Kayssi, SDN security plane: An architecture for resilient security services. IEEE International Conference on Cloud Engineering Workshop. (IC2EW), (2016) 54-59.

[82] O. Joldzic, Z. Djuric, and P. Vuletic, A transparent and scalable anomaly-based DoS detection method. Computer Networks, 104 (2016) 27-42.

[83] J. Li, S. Berg, M. Zhang, P. Reiher, and T. Wei, Drawbridge: software-defined DDoS-resistant traffic engineering. SIGCOMM '14: Proceedings of the 2014 ACM conference on SIGCOMM, (2014) 591-592.

[84] S. Hammed, and H.A. Khan, SDN Based Collaborative Scheme for Mitigation of DDoS Attacks. Future Internet, 10(3) (2018) 1-18.

[85] J. Francois, I. Aib, and R. Boutaba, FireCol: A Collaborative Protection Network for the Detection of Flooding DDoS Attacks. IEEE/ACM Transactions on Networking, 20(6) (2012) 1828-1841.

[86] S. Debroy, P. Calyam, M. Nguyen, R.L. Neupane, B. Mukherjee, A.K. Eeralla, K. Salah, Frequency-Minimal Utility-Maximal Moving Target Defense Against DDoS in SDN-Based System. IEEE Transactions on Network and Service Management, 17(2) (2020) 890-903.

[87] M. Samir, M. Azab, and E. Samir, SD-CPC: SDN Controller Placement Camouflage based on Stochastic Game for Moving-target Defense. Computer Communications, 168 (2021) 75-92.

[88] A. Aydeger, N. Saputro, and K. Akkaya, A moving target defense and network forensics framework for ISP networks using SDN and NFV. Future Generation Computer Systems, 94 (2019) 496-509.

[89] S. Debroy, P. Calyam, M. Nguyen, A. Stage, and V. Georgiev, Frequency-minimal moving target defense using software-defined networking. 2016 International Conference on Computing, Networking and Communications (ICNC), Kauai, USA. (2016) 1-6.

Volume 5, Issue 2, pages 127-158

p-ISSN 2655-8564, e-ISSN 2685-9432

[90] Y. Shi, H. Zhang, J. Wang, F. Xiao, J. Huang, D. Zha, H. Hu, F. Yan, and B. Zhao, CHAOS: An SDN-Based Moving Target Defense System. Hindawi: Security and Communication Networks, (2017) 1-11.

[91] K. Doshi, Y. Yilmaz, and S. Uludag, Timely Detection and Mitigation of Stealthy DDoS Attacks Via IoT Networks. IEEE Transactions on Dependable and Secure Computing, 18(5) (2021) 2164-2176.

[92] M.S. Ali, M. Vecchio, M. Pincheira, K. Doului, F. Antonelli, and M.H. Rehmani, Applications of Blockchains in the Internet of Things: A comprehensive survey. IEEE Communications Surveys & Tutorials, 21(2) (2018) 1676-1717.

[93] F.H. Pohrmen, R.K. Das, and G. Saha, Blockchain-based security aspects in heterogeneous Internet-of-Things networks: a survey. Transactions on Emerging Telecommunication Technologies, 30 (10) (2019) E3741.

[94] S. Demirci, and S. Sagiroglu, Software defined networking for improved security in smart grid system. 2018 7th International Conference on Renewable Energy Research and Applications, ICRERA, IEEE. (2018) 1021-1026.

[95] U. Ghosh, P. Chatterjee and S. Shetty, Securing SDN-enabled smart power grids: SDN-enabled smart grid security. Cyber-Physical Systems for Next-Generation Networks, IGI Global, (2018) 79-98.

[96] J. Kim, F. Filali, and Y.-B. Ko, Trends and Potentials of the Smart Grid Infrastructure: From ICT Sub-System to SDN-Enabled Smart Grid Architecture. Applied Sciences, 5(4) 706-727.

[97] H. Maziku, S. Shetty, and D.M. Nicol, Security risk assessment for SDN-enabled smart grids. Computer Communications, 133 (2019) 1-11.

[98] D. Ibdah, M. Kanai, N. Lachtar, N. Allan, and B. Al-Duwairi, On the security of SDN-enabled smartgrid systems. 2017 International Conference on Electrical and Computing Technologies and Applications, (ICECTA). Ras Al Khaimah, UAE. (2017) 1-5.

[99] X. Dong, H. Lin, R. Tan, R.K. Iyer and Z. Kalbarczyk, Software-Defined Networking for Smart Grid Resilience: Opportunities and Challenges. CPSS '15: Proceedings of the 1st ACM Workshop on Cyber-Physical System Security, (2015) 61-68.

Volume 5, Issue 2, pages 127-158

p-ISSN 2655-8564, e-ISSN 2685-9432

[100] R. Chaudhary, G.S. Aujla, S. Garg, N. Kumar, and J.J.P.C. Rodrigues, SDN-Enabled Multi-Attribute-Based Secure Communication for Smart Grid in IIoT Environment. IEEE Transactions on Industrial Informatics, 14(6) (2018) 2629-2640.

[101] N.E. Petroulakis, K. Fysarakis, I. Askoxylakis, and G. Spanoudakis, Reactive security for SDN/NFV-enabled industrial networks leveraging service function chaining. Transactions on Emerging Telecommunications Technologies, 29(7) (2017).

[102] F. Holik, and P. Dolezel, Industrial Network Protection by SDN-Based IPS with AI. ACIIDS 2020: Intelligent Information and Database Systems. Communications in Computer and Information Science, 1178 (2020) 192-203.

[103] M. Cheminod, L. Durante, L. Seno, F. Valenzano, and C. Zunino, Leveraging SDN to improve security in industrial networks. 2017 IEEE 13th International Workshop on Factory Communication Systems (WFCS), Trondheim, Norway. (2017) 1-7.

[104] D. Henneke, L. Wisniewski, and J. Jasperneite, Analysis of realizing of future industrial network by means of Software-Defined Networking (SDN). 2016 IEEE World Conference on Factory Communication Systems (WFCS), Aveiro, Portugal. (2016) 1-4.

[105] M. Singh, G.S. Aujla, A. Singh, N. Kumar, and S. Garg, Deep-Learning-Based Blockchain Framework for Secure Software-Defined Industrial Networks. IEEE Transactions on Industrial Informatics, 17(1) (2021) 606-616.

[106] C. Lorenz, D. Hock, J. Scherer, R. Durner, W. Kellerer, S. Gebert, N. Gray, and T. Zineer, An SDN/NFV-Enabled Enterprise Network Architecture Offering Fine-Grained Security Policy Enforccement. IEEE Communications Magazine, 55(3) (2017) 217-223.

[107] R. Alvizu, G. Maier, S. Troia, V.M. Nguyen, and A. Pattavina, SDN-based network orchestration for new dynamic Enterprise Networking services. 2017 19th International Conference on Transparent Optical Networking (ICTON), Girona, Spain. (2017) 1-4.

[108] J. Bailey, and S. Stuart, Faucet: Deploying SDN in the enterprise. Communications of the ACM, 60(1) (2017) 45-49.

Volume 5, Issue 2, pages 127-158

p-ISSN 2655-8564, e-ISSN 2685-9432

[109] D. Levin, M. Canini, S. Schmid, and A. Feldmann, Incremental SDN Deployment in Enterprise Networks. ACM SIGCOMM Computer Communication Review, 43(4) (2013) 473-474.

[110] K. Poularakis, G. Iosifidis, and L. Tassiulas, SDN-Enabled Tactical Ad Hoc Networks: Extending Programmable Control to the Edge. IEEE Communications Magazine, 56(7) (2018) 132-138.

[111] Y. Wei, X. Zhang, L. Xie, and S. Leng, Energy-aware traffic engineering in hybrid SDN/IP backbone networks. Journal of Communications and Networks, 18(4) (2016) 559-566.

[112] B.R. Dawadi, D.B. Rawat, S.R. Joshi, and P. Manzoni. Towards Smart Networking with SDN Enabled IPv6 Network. arXiv preprint, (2022).

[113] E. Seve, J. Pesic, C. Delezoide, A. Giorgetti, A. Sgambelluri, N. Sambo, S. Bigo, and Y. Pointurier, Automated Fibre Type Identification in SDN-Enabled Optical Networks. Journal of Lightwave Technology, 37(7) (2019) 1724-1731.

[114] M. Birk, G. Choudhury, B. Cortez, A. Goddard, N. Padi, A. Raghuram, K. Tse, S. Tse, A. Wallace, and K. Xi, Evolving to an SDN-enabled isp backbone: key technologies and applications. IEEE Communication Magazine, 54(10) (2016) 129-135.

[115] X. Zhang, H. Wang, and H. Zhao, An SDN framework for UAV backbone network towards knowledge centric networking. IEEE INFOCOM 2018-IEEE Conference on Computer Communications Workshops (INFOCOM WKSHPS) Honolulu. USA, (2018) 456-461.

[116] G. Kakkavas, A. Stamou, V. Karyotis, and S. Papavassiliou, Network Tomography for Efficient Monitoring in SDN-Enabled 5G Networks and Beyond: Challenges and Opportunities. IEEE Communications Magazine, 59(3) (2021) 70-76.

[117] X. Duan, X. Wang, Y. Liu, and K. Zheng, SDN Enabled Dual Cluster Head Selection and Adaptive Clustering in 5G-VANET. 2016 IEEE 84th Vehicular Technology Conference (VTC-Fall), Montreal, Canada, (2016) 1-5.

[118] J. Liu, Y. Shi, L. Zhao, Y. Cao, W. Sun, and N. Kato, Joint Placement of Controllers and Gateways in SDN-Enabled 5G-Satellite Integrated Network. IEEE Journal on Selected Areas in Communications, 36(2) (2018) 221-232.

Volume 5, Issue 2, pages 127-158

p-ISSN 2655-8564, e-ISSN 2685-9432

[119] A.S. Thyagaturu, A. Mercian, M.P. McGarry, M. Reisslein, and W. Kellerer, Software Defined Optical Networks (SDONs): A Comprehensive Survey. IEEE Communications Surveys & Tutorials, 18(4) (2016) 2738-2786.

[120] E. Guler, M. Karakus, and S. Uludag, SpectrumChain: An Efficient Spectrum Management Framework in Blockchain-Enabled Flexible SDON's. ICC 2022-IEEE International Conference on Communications, Seoul, Republic of Korea. (2022) 5744-5749.

Volume 5, Issue 2, pages 127-158

p-ISSN 2655-8564, e-ISSN 2685-9432

This page intentionally left blank

International Journal of Applied Sciences and Smart Technologies

Volume 5, Issue 2, pages 303–314

p-ISSN 2655-8564, e-ISSN 2685-9432

Resources Estimation of Laterite Nickel Using Ordinary Kriging Method at PT Mahkota Semesta Nikelindo District Wita Pond Morowali District

Alfian Nawir[1], Alam Budiman Thamsi [2*], Harta Sanjaya[3], Muhammad Aswadi[4]

[1-3]Faculty of Industrial Technology, Universitas Muslim Indonesian, Makassar, Indonesia

[4]Faculty of Engineering, Tadulako University, Palu, Indonesia

[*]Corresponding Author: alambudiman.thamsi@umi.ac.id

(Received 31-07-2023; Revised 10-08-2023; Accepted 28-09-2023)

Abstract

Resources have economic value, form, quality, quantity, grade, geological characteristics, and certain sustainability to be extracted economically. Mineral resources decrease based on the level of geological confidence in the Inferred, Indicated, and Measured categories. This study uses the Ordinary Kriging geostatistical method to assess the potential of nickel laterite resources and the distribution of nickel mineralization levels in the study area. The research methodology was inspired by statistical and geostatistical analysis, starting with univariant statistical analysis, spatial statistics, bivariant statistics, and resource estimation. For later use in determining the distribution of mineralization grades and classifying nickel laterite resources using the Relative Kriging Standard Deviation (RKSD) calculation. This method estimates nickel content in a block whose grade value is unknown. The results of statistical calculations using Ordinary kriging obtained an average grade value of 2.90% Ni. Mineralization data for nickel content in limonite layers with Ni content of 0.5 – 1.3% and saprolite layers with Cut of Grade (COG) Ni, > 1.4 – 3.1% Ni in limonite and saprolite layers are projected in the block model. The estimated tonnage of nickel resources using the OK method is 670,837.83 tonnes. Laterite nickel resource classification results RKSD calculation are classified into measured resources (Measured).

Keywords: nickel laterite, resource estimation, grade, tonnage**.**

1. Introduction

Indonesia is the world's second-largest nickel producer after Russia, contributing around 15% of world nickel production in 2010 [2, 12]. The Eastern Indonesia region, especially in Central Sulawesi, has potential mineral resources in nickel laterite deposits in the Morowali district. Nickel ore deposits found in Morowali are lateritic nickel ore deposits formed from the weathering of ultramafic peridotite, dunite, and serpentinite containing 2.0% Ni; these deposits have profitable potential for mining [7]. The term Laterite is taken from the Latin "later," which means red brick, which was put forward by Buchanan Hamilton

This work is licensed under a Creative Commons Attribution 4.0 International License

Volume 5, Issue 2, pages 303–314
p-ISSN 2655-8564, e-ISSN 2685-9432

(1807). Nickel laterite deposits are formed from the weathering of ultramafic parent rocks [5]. Nickel ranks second after manganese, a metal alloy material, where its presence is estimated to be 3% in the earth's core and 0.003% in the earth's crust. Nickel is produced from the recycling of scrap stainless steel and used batteries whose anodes use a nickel alloy [6].

Univariate statistical analysis is an analysis of the description of a variable or a collection of variable populations that describes the characteristics of the data variables from the description values , such as the average value, median, maximum value, minimum value, coefficient of variation, standard deviation, and skewness. The spread of variability of a population can be seen in the value of standard deviation and variance [3]. The coefficient of variation is used as the basis for estimating resources; if the coefficient of variation is equal to or below 1.5, then using the IDW and ordinary kriging methods is good for estimating resources [10]. The principle of using the ordinary kriging method, which is used when the average thickness is unknown, then estimates the thickness value of a block whose thickness value is either vertically or horizontally so that a three-dimensional block model will be obtained. After obtaining the shape of the sediment model, the volume will be calculated so that a resource estimation result will be obtained [11]. In getting the average value as a form of data 2 dimensions and depiction of data distribution Nickel Using required composite assay with the following equation [8]. The variogram is often used as a geostatistical analysis tool by considering the correlation of data to determine the size of the sample points against the space where the sample points are not estimated [4]. In Blackwell's study (1998), if the RKSD value (relative kriging standard deviation) is below 0.3, then it is included in the inferred resource; if the RKSD value is between 0.3 to 0.5, then it is included in the indicated resource; and if the RKSD value is above 0.5 then it is included in the measured resource. The RKSD equation is [1]. There are several methods for estimating resources. In addition to resource estimation using the IDW method, there are also resource estimates using the Kriging and NNP methods. Further research is needed regarding other resource estimation methods [9].

Therefore, the author is interested in researching nickel mining companies; in laterite nickel mining, estimates are needed to determine the number of resources before the

International Journal of Applied Sciences and Smart Technologies

Volume 5, Issue 2, pages 303–314

p-ISSN 2655-8564, e-ISSN 2685-9432

mining process occurs. Therefore, researchers conduct research by estimating resources using the ordinary kriging method. So that the company has relevant information, it can minimize the factors that cause discrepancies during the mining process.

2. Methods

The data for estimating nickel laterite resources is secondary data obtained from drilling. The data includes drill point codes, location coordinates, laterite nickel thickness, and laterite nickel content. The laterite nickel resource estimation method used the ordinary kriging geostatistical method. This method was chosen because it is considered more thorough than conventional methods.

Ordinary kriging assumes the population mean is constant, but unknown, whereas the variogram of Z(s) is known. This method is a method that provides a Best Linear Unbiased Estimator (BLUE). Ordinary Kriging weights satisfy the unbiased property with Sum, where n is the known number of samples. The usual kriging weight value can be obtained through the following equation:

$$\begin{pmatrix} \lambda_1 \\ \lambda_2 \\ \vdots \\ \lambda_n \\ m \end{pmatrix} = \begin{pmatrix} \gamma(s_1,s_1) & \gamma(s_1,s_2) & \cdots & \gamma(s_1,s_n) & 1 \\ \gamma(s_2,s_1) & \gamma(s_2,s_2) & \cdots & \gamma(s_2,s_n) & 1 \\ \vdots & \vdots & \ddots & \vdots & \vdots \\ \gamma(s_n,s_1) & \gamma(s_n,s_2) & \cdots & \gamma(s_n,s_n) & 1 \\ 1 & 1 & \cdots & 1 & 0 \end{pmatrix}^{-1} \begin{pmatrix} \gamma(s_1,s_0) \\ \gamma(s_2,s_0) \\ \vdots \\ \gamma(s_n,s_0) \\ 1 \end{pmatrix}$$

The additional parameter m is the Lagrange multiplier used to minimize the kriging error. The following equation can obtain ordinary kriging interpolation:

$$Z(S_0)=\lambda^T.Z$$

and the kriging error variance var(ε(S_0)) can be obtained from the equation:

$$\mathrm{var}(\varepsilon(s_0)) = \begin{pmatrix} \lambda_1 \\ \lambda_2 \\ \vdots \\ \lambda_n \\ m \end{pmatrix}^T \begin{pmatrix} \gamma(s_1,s_0) \\ \gamma(s_2,s_0) \\ \vdots \\ \gamma(s_n,s_0) \\ 1 \end{pmatrix}$$

International Journal of Applied Sciences and Smart Technologies

Volume 5, Issue 2, pages 303–314

p-ISSN 2655-8564, e-ISSN 2685-9432

3. Result and discussion

Drill spread

Exploration drilling carried out at PT Mahkota Semesta Nikelindo resulted in an irregular distribution of drill points with a total of 56 drill points with an average information retrieval or drilling spacing of 25 meters which is detailed information retrieval and is included in measured resources as explained in SNI 2019 regarding reporting of exploration, mineral resources and reserves that measured resources are not more than 50 meters in gathering information. The map can be seen in Figure 1 below.

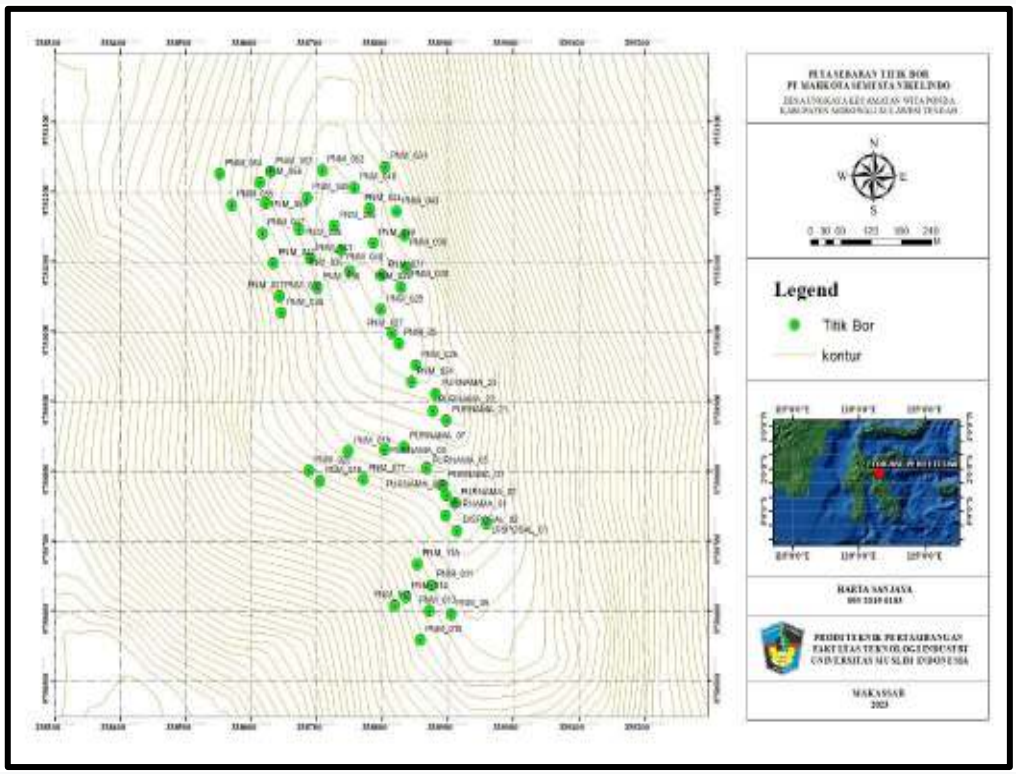


Figure 1. Drill point distribution map

Univariant Statistics

Descriptive statistics describes a mathematical distribution to determine the mean value and the difference between each value and the mean. The values that appear when statistical analysis is carried out are the mean, variance, standard deviation, and coefficient of variation, and the Geometry Mean values become parameters in the formation of distribution graphs in the form of histograms. The histogram graph that appears is a depiction

Volume 5, Issue 2, pages 303–314

p-ISSN 2655-8564, e-ISSN 2685-9432

of the distribution of data which intends to provide an overall picture of the shape of the distribution and make it easier to identify data errors. The histogram that appears is an outlier histogram, which means there is still a possibility of data errors, so a cutlier is needed to eliminate these errors so that errors do not occur when carrying out spatial statistical analysis. Limiting the margin of error that may occur with the following equation is necessary.

Confidence interval

$$95\% = \bar{x} + 2S$$

Statistical results can be seen in Figure 2 histogram of Ni content composite downhole data.

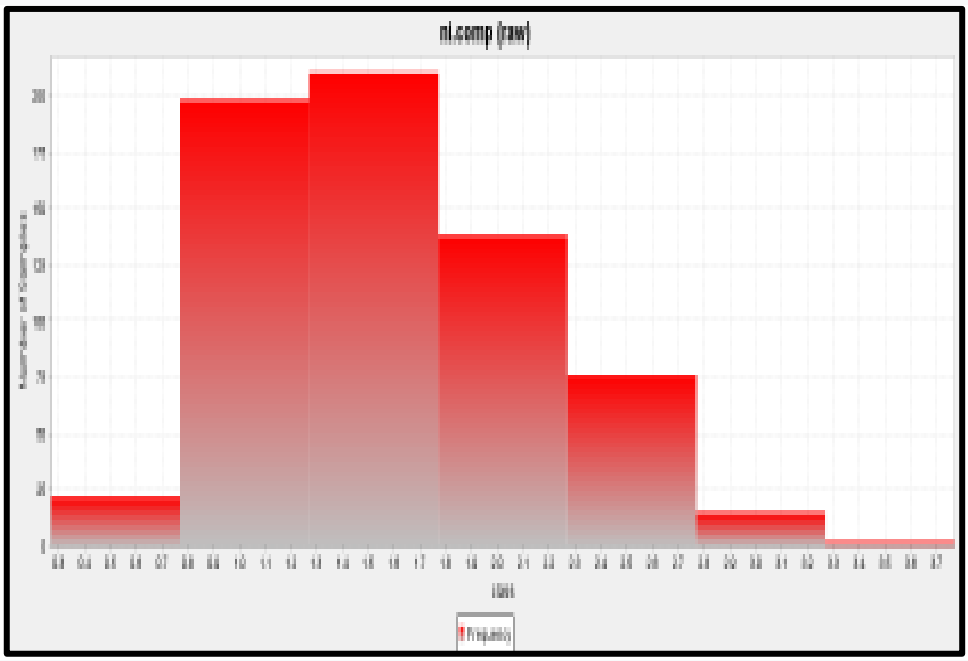


Figure 2. Histogram of composite downhole data for Ni content

The results of the descriptive statistical analysis in Table 1 are descriptive statistics with several samples, variance, mean, and coefficient of variance, where these values will become parameter values in resource estimation. The skewness value is the data symmetry value, where 0 (zero) is the data symmetrical value. Table 1. has a skewness value that is still good because it is not too far from the number 0 (zero), and the difference between the mean and the median is not too far or even close. Hence, the possibility of error is relatively small.

Volume 5, Issue 2, pages 303–314

p-ISSN 2655-8564, e-ISSN 2685-9432

Table 1. Statistical report on composite downhole data for Ni content

Parameter	Sampel composite cut
Number of Data	661
Mean	1.605174
Median	1.500000
Geometri mean	1.508518
Minimum	0.270000
Maximum	3.500000
Stdt Dev	0.548176
Variance	0.300497
Coefficien of variation	0.341506

Spatial Statistics Analysis

In the variogram analysis, horizontal and vertical variogram fittings will be carried out to find bearing, plunge and dip values. From the results of bearing, plunge, and dip, major, semi-major and minor values will be obtained in determining ellipsoid anisotropy in the distribution of lateritic nickel deposit levels, besides that it can also determine the potential of the distribution direction of nickel laterite based on the variogram maps formed. In the experimental semivariogram calculation, data from MS Excel is required which includes the sample code or drill point code, sample coordinate points and nickel content. The experimental semivariogram is calculated from four directions, namely: 0º, 45º, 90º and 135º. Structural analysis or matching between data patterns in experimental semi-variogram models and theoretical semi-variogram models. The selection of this variogram model will then greatly determine the results of the estimation process in correcting and interpreting the value of a variable. Structural analysis also obtained a shape that shows elliptical geometric anisotropy for nickel content with the direction used, namely N 0º E.

Figure 3 shows the value of the variogram model of the formed Omnidirectional variogram which produces a sill value of 0.622430, a nugget of 0.357796 and a range value of 47 m.

International Journal of Applied Sciences and Smart Technologies

Volume 5, Issue 2, pages 303–314

p-ISSN 2655-8564, e-ISSN 2685-9432

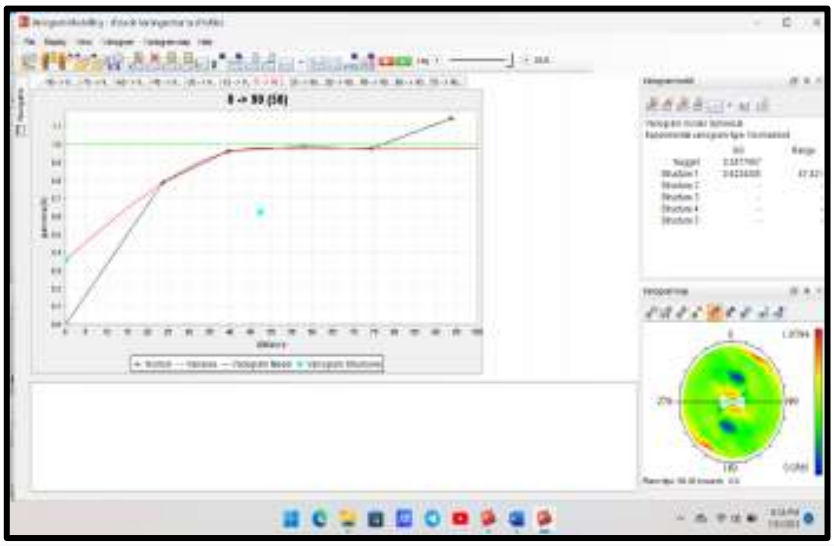


Figure 3. Variogram models

Resource modeling and estimation

In estimating resources, the data is first made into a block model where the creation of this block model is intended so that the data that has been estimated with the determination of the drill point can be estimated by making small blocks of a predetermined size from the company to show the content of a metal such as Ni, Fe, and others. The block modeling made is adjusted to the drill point spacing of 25 m so that the size of the block model will match the drill point spacing. The making of the block model is adjusted to the distribution of mineral deposits. The maximum user block size is 10 meters long, 10 meters wide, and 5 meters thick, while the minimum Sub Block Size is 5 meters long, 5 meters wide, and 1 meter thick.

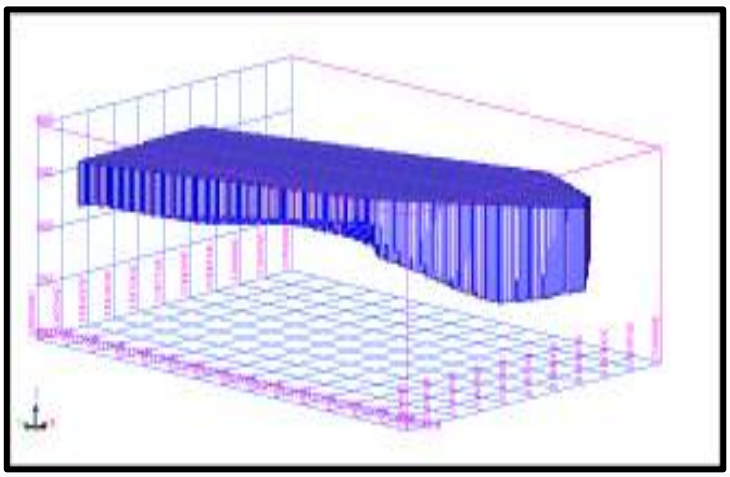


Figure 4. Block model of the saprolite and limonite layer

International Journal of Applied Sciences and Smart Technologies

Volume 5, Issue 2, pages 303–314

p-ISSN 2655-8564, e-ISSN 2685-9432

Making block models for saprolite and limonite layers with a Cut off Grade (CoG) value of > 1.4% Ni is carried out with a Minimum % of the sample to be included, namely 75 m, Maximum Search radius, which is 50 m, and the Power used is 2, the greater the power used, the greater the volume generated to obtain data on total laterite nickel resources. The basic concept of making the block model itself is based on the drill point spacing in the field, which, as shown in Figure 4, shows the block size that matches the drill point spacing in the field, in this case, the block size is ¼ of the drill point spacing.

In mining at PT Mahkota Semesta Nikelindo itself, it has a cut of grade, which is 1.4% taken from the company's recommended COG, while the recommended density for OB or levels below COG is 1 kg/m3 and for ore, which is 1.55 tonnes. The tonnage will later be obtained, which is the result of the equation of

$$\text{Tonnage} = \text{volume} \times \text{density}$$

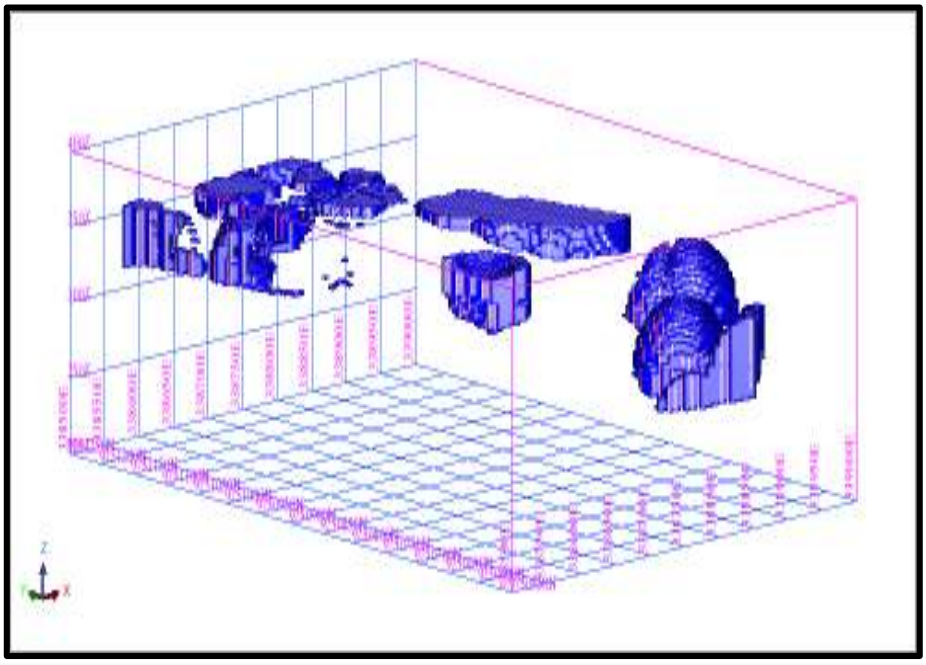


Figure 5. Block model OK saprolite layer COG >1.4

The calculation results using the Ordinary Kriging method can be seen in the Table below:

Volume 5, Issue 2, pages 303–314

p-ISSN 2655-8564, e-ISSN 2685-9432

Table 2. The estimation results of ordinary kriging resources

Lithology	Volume (m^3)	Tonnage (ton)	Ni (%)
Limonit 0.5 – 1.3%	232.880,0	256.928,7	1.12
Saprolit 1.4 – 3.1%	832.772,5	145.657.47	1.78
Grand Total	**113.619,575**	**402.586,17**	**2.90**

From the results of resource estimation using the Ordinary Krigin method in this study, a volume of 832,772.50 was obtained with a resource tonnage of 145,657.470 tons and an average grade of nickel laterite of 2.90 % Ni.

Resource classification with RKSD

From the results of resource estimation using the Ordinary Krigin method in this study, a volume of 832,772.50 was obtained with a resource tonnage of 145,657.470 tons and an average grade of nickel laterite of 1.78% Ni.

Table 3. Statistical results of resource classification with RKSD

Parameter	Saprolite
Number of Data	333109
Mean	1.749067
Minimum	1.395005
Maximum	2.675809
Stdt Dev	0.224451
Variance	0.050378
Skewness (se)	0.621483
Kurtosis (se)	3.086359
Standard error	0.084569

The results of this estimate can be used as a reference for information on the amount of resources and 3D models of mineral deposits. This information can be used for mine planning.

4. Conclusions and suggestion

Conclusion

The conclusions of this study are:

Resources using the Ordinary Kriging method with Cut of Grade (CoG) > 0.5 - 1.3% totaling 256,928.7 tonnes, (CoG) 1.8 - 2.1% totaling 521,794.80 tonnes, (CoG) > 2.1 - 3.0% totaling 132,228.00 tonnes, with a total of 145,657.47 tonnes and an average grade of Ni 1.45 %. Classification of nickel laterite resources based on RKSD (Relative Kriging Standard Deviation) with a resource mean value of 1.749% Ni and a standard deviation of 0.224, categorized as a measured resource.

Suggestion

To maximize research, the authors suggest using the NNP estimation process or other assessment processes, then conducting statistical analysis with several references in statistical software, then comparing the Ordinary Kriging estimation process that has been carried out. So that the data obtained can be more accurate and can be used in modeling software as well as a reference for determining the classification of nickel laterite resources based on RKSD (Relative Kriging Standard Deviation) calculations.

Acknowledgements

The author thanks the academic community of the mining engineering study program at the Indonesian Muslim University who have provided a lot of help and support, the author also thanks the company PT Mahkota Semesta Nikelindo which is right in Morowali, Central Sulawesi for taking the time to guide us in the field and help us in carrying out our final project.

References

[1] W. A. K. Conoras, Klasifikasi sumber daya endapan nikel laterit daerah pulau obi, halmahera selatan dengan pendekatan Relative Kriging Standard Deviation(RKSD). DINTEK, 10(1) (2017) 71-79.

Volume 5, Issue 2, pages 303–314

p-ISSN 2655-8564, e-ISSN 2685-9432

[2] E.B. Fitiran, M.A. Massinai, Maria, Identifikasi Sebaran Nikel Laterit dan Volume Bijih Nikel Daerah Anoa menggunakan Korelasi data Bor, Jurnal Geofisika Universitas Hasanuddin. (2011).

[3] A. R. Kurniawan and N. A. Amri, Estimasi Sumberdaya Emas Menggunakan Metode Ordinary Kriging Pada Pit X PT Indo Muro Kencana. (2019) 59–69.

[4] A. Kurnianto, , A. P. Setiahadiwibowo, , & W. S. Giamboro, Estimasi Sumberdaya Batubara Menggunakan Metode Nearest Neighbour Point, Inverse Distance Weighting, Dan Kriging Pada Daerah Muara Bungo, Sumatera Selatan. Jurnal Geocelebes, 3(2) (2019) 75

[5] S.A. Ningsih, Eksplorasi Awal Nikel Laterit Di Desa Lamontoli Dan Lalemo, Kecamatan Bungku Selatan, Kabupaten Morowali, Provinsi Sulawesi Tenggara, Jurnal Ilmiah MTG, Vol. 5 (2) (2012).

[6] M. Mariana, Genesa and Mineralogi Bijih Nikel Study of hydrothermal mineralization deposit at Cupunegara area, Subang District, West Java View project The Use of Rock Hand Speciment in Subject Learning Introduction of Rocks and Gemstones Mineral as Material. View project. (2018).

[7] H. Purnomo, & E. Sumarjono, Geologi dan Estimasi Sumber Daya Nikel Laterit Menggunakan Metode Ordinary Kriging di Blok R, Kabupaten Konawe– Sulawesi Tenggara. ReTII. (2015).

[8] A. B. Thamsi, Estimasi Cadangan Terukur Endapan Nikel Laterit Cog 2,0% Menggunakan Metode Inverse Distance Pada PT. Teknik Alum Service, Blok X. Jurnal Geomine Desember. Vol. 4 (3) (2016).

[9] A. B. Thamsi, Ainunnur Izzulhaq, Anwar Habibie, Muhammad Aswadi. Estimasi Sumberdaya Nikel Mengunakan Metode Inverse Distance Weight PT Ang and Fang Brothers, (2023).

[10] M. S. Ramadhan, A. Ilyas, I. Nur and S. Widodo, Perbandingan Antara Metode Poligon, Inverse Distance Weighting, dan Ordinary Kriging Pada Estimasi Sumberdaya Timah Aluvial, Dan Analisis Sebaran Endapannya. Jurnal Geomine, 9(3) (2022) 254–266.

Volume 5, Issue 2, pages 303–314

p-ISSN 2655-8564, e-ISSN 2685-9432

[11] Reza Taufiqurrahman. Perbandingan Estimasi Sumberdaya Batubara Menggunakan Metode Ordinary Kriging Dan Metode Cross Section Di PT. Nan Riang Jambi, (2016).

[12] Ivanna Crecentia Narulita Simanungkalit, et al. Study of Nickel Extraction Process from Spent Catalysts with Hydrochloric Acid Solution: Effect of Temperature and Kinetics Study. International Journal of Applied Sciences and Smart Technologies 3(2) (2021) 161-170.

International Journal of Applied Sciences and Smart Technologies

Volume 5, Issue 2, pages 315–334

p-ISSN 2655-8564, e-ISSN 2685-9432

Developing A Robot to Improve The Accuracy of Ring Retrieval and Throwing at The ABU Robocon Indonesia Robot Competition

Agus Siswoyo[1, *]

[1] Department of Mechatronics, Sanata Dharma University, Yogyakarta, Indonesia

[*]Corresponding Author: woyo@usd.ac.id

(Received 07-08-2023; Revised 21-09-2023; Accepted 14-11-2023)

Abstract

This article outlines the creation and application of a technologically improved robot designed to amplify the precision and effectiveness of ring retrieval and projection tasks in the ABU Robocon Indonesia Robot Challenge. The ABU Robocon competition is an annual event that tasks teams with crafting robots capable of accomplishing specific assignments under a predetermined time limit. The ring retrieval and projection task, historically known for its precision requirements, has proven to be quite demanding. Our strategy entailed the incorporation of cutting-edge technologies into the robot's design, encompassing computer vision and machine learning algorithms, to augment its accuracy and performance. We equipped the robot with cameras and sensors for the detection and analysis of ring positions and orientations. Real-time decisions regarding the optimal approach for retrieving and accurately projecting the rings were made using machine learning models that had undergone training. The outcomes of our experiments reveal a marked enhancement in the robot's performance when compared to conventional methods. The tech-enhanced robot consistently exhibited a heightened success rate when performing ring retrieval and projection tasks. This development not only boosts the competitiveness of our robot in the ABU Robocon competition but also underscores the potential of advanced technologies in enhancing the performance of robotics systems when confronted with intricate tasks.

Keywords: ABU robocon , robotics competition, ring retrieval, ring throwing

This work is licensed under a Creative Commons Attribution 4.0 International License

International Journal of Applied Sciences and Smart Technologies

Volume 5, Issue 2, pages 315–334

p-ISSN 2655-8564, e-ISSN 2685-9432

1 Introduction

The ABU Robocon Indonesia Robot Contest is an annual competition that challenges participants to design and build robots capable of performing specific tasks. One of the tasks in the competition involves retrieving and throwing rings onto designated poles, requiring precision in both ring retrieval and throwing for efficient task completion. In this context, the development of a highly accurate robot becomes crucial to excel in the competition and complete the ring-related tasks swiftly and effectively.

The robot is equipped with sensors that allow it to detect the location of the rings and poles. It uses machine learning algorithms to analyze this data and determine the best trajectory for throwing the rings onto the poles. The accuracy of the observer is proved by the experiments in robotic catching [1].

The development of this robot represents a significant advancement in the field of robotics. By using artificial intelligence to analyze data and make decisions, the robot is able to perform tasks with greater accuracy and efficiency than traditional robots. The proposed control method can gain the high positioning performance for throwing a rigid object with one degree of freedom robot [2]. This technology has the potential to revolutionize many industries, from manufacturing to healthcare.

In this journal, we will explore the development of the robot for the ABU Robocon Indonesia Robot Contest in detail. We will discuss the design of the robot, the algorithms used to analyze data and make decisions, and the results of testing and evaluation. A system for determining the throwing position was developed using the derived method with same preconditions [3]. We will also consider the implications of this technology for the future of robotics and the wider world.

The ABU Robocon Indonesia Robot Contest stands as a testament to the rapid evolution and convergence of robotics and artificial intelligence. Within this dynamic and competitive context, precision-oriented tasks like ring retrieval and throwing have emerged as pivotal challenges that demand not only technical finesse but also innovative solutions. This research was like development for A proposed method to retrieve the balls which are scattered in the Tennis court back to the user is developed

Volume 5, Issue 2, pages 315–334
p-ISSN 2655-8564, e-ISSN 2685-9432

on a Python platform [4]. The integration of AI algorithms into robotic systems has redefined the boundaries of achievable accuracy in such tasks. Throwing manipulation enables the robot not only to manipulate the object to outside of the robot's movable range of the robot, but also to control the position of the object arbitrarily in the vertical plane even though the robot has only one degree of freedom [5]. The study pursued the ambitious goal of designing a robot explicitly designed to improve ring picking and throwing precision, with the ultimate goal of excelling in the ABU Robocon Indonesia Robot Contest. As robotics and AI continue to intertwine, the outcomes of this research contribute not only to the specific domain of robotic competitions but also to the broader advancement of AI-enhanced robotics.

In this context, the ABU Robocon Indonesia 2023 Robot Contest serves as a testing ground for innovative robotic systems, demanding intricate tasks to be executed with precision. This journal delves into the conceptualization and realization of an robot tailored for the ABU Robocon Indonesia Robot Contest, focusing on enhancing the accuracy of two crucial tasks: ring retrieval and throwing. These tasks not only require efficient detection and manipulation but also highlight the significance of algorithms in computing optimal trajectories and achieving target accuracy [6][7]. The journal provides an in-depth exploration of the robot's design and an analysis of its performance within the dynamic and competitive environment of the ABU Robocon Indonesia Robot Contest, shedding light on the forefront of robotic innovation and precision engineering.

2 Methods

The development of the robot for the ABU Robocon Indonesia Robot Contest involved several steps. These included designing the robot's hardware and software, collecting and analyzing data, and testing and refining the robot's performance. Below is a more detailed explanation of each of these steps:

A. Designing the Robot: The first step in developing the robot was to design its hardware and software. The robot was designed to have a precise and efficient arm that could retrieve and throw rings onto designated poles. The robot was also equipped with sensors that could detect the location of the rings and poles.

Volume 5, Issue 2, pages 315–334
p-ISSN 2655-8564, e-ISSN 2685-9432

The software for the robot was designed to analyze the sensor data and make decisions about the best trajectory for throwing the rings.

B. Collecting and Analyzing Data: Once the robot was designed, the next step was to collect data on the location of the rings and poles. This involved testing the robot in different environments and collecting data on the position and orientation of the rings and poles. The data was then analyzed using machine learning algorithms to identify patterns and develop models for predicting the trajectory of the rings.

C. Developing the Algorithms: Based on the data analysis, the researchers developed algorithms for the robot to use in analyzing the sensor data and making decisions about how to throw the rings. The algorithms were designed to take into account factors such as the distance and angle between the robot and the pole, as well as the weight and size of the rings.

D. Testing and Refining the Robot: Once the algorithms were developed, the robot was tested in a variety of environments to evaluate its performance. The researchers analyzed the robot's accuracy in retrieving and throwing the rings and made adjustments to the algorithms and hardware as needed. This process continued until the robot was able to perform the task with a high level of accuracy and efficiency.

Overall, the development of the robot for the ABU Robocon Indonesia Robot Contest involved a combination of hardware and software design, data analysis, and testing and refining the robot's performance. Prediction of object movement trajectories has great importance in diverse domains of smart systems [8]. The result was a highly accurate and efficient robot that could perform the task of retrieving and throwing rings with great precision.

This section provide clear information of materials, instrumentations, and methods used in order to allow the work to be reproduced by the readers. Methods already published should be indicated by a reference: only relevant modifications should be described. For the chemicals, authors should provide details of brand and purity, for example: ammonia 25% (Merck Millipore). For the instrument, the author should

Volume 5, Issue 2, pages 315–334
p-ISSN 2655-8564, e-ISSN 2685-9432

provide information on the brand and type. If the instrument is a modification, then information about the modifications made is required.



Figure 1. Design robot abu

The combination of a roler system for throwing, a mechanum wheel for propulsion, and a DC motor for throwing, will create an Aburobocon robot that has unique and sophisticated capabilities in dealing with challenges and situations on the playing arena, especially in 2023. With this design, it is hoped that the abu robot will be able to become a robot that can maximize system work and complete robot tasks properly. Robot-catching of in-flight objects is a challenging task, requiring a high-frequency sequence of pose estimation, trajectory prediction, catching point determination, and motion planning [9].

International Journal of Applied Sciences and Smart Technologies
Volume 5, Issue 2, pages 315–334
p-ISSN 2655-8564, e-ISSN 2685-9432

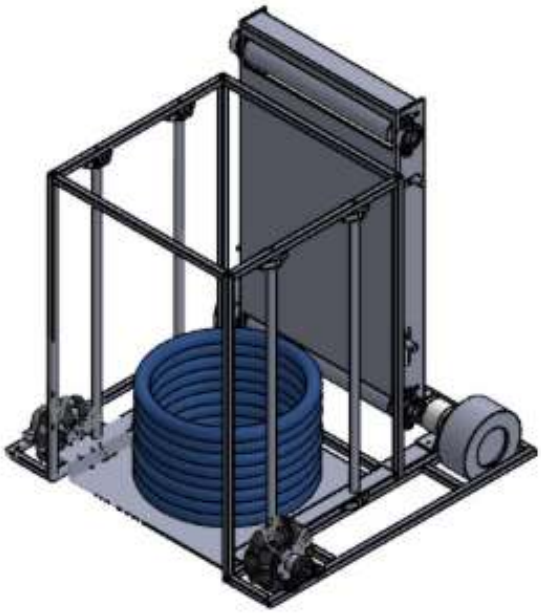


Figure 2. Design robot

The ring transport system on the robot's body uses a lift system that is able to quickly and safely carry the ring from the floor to the throwing robot, which is a very important feature to improve the performance and efficiency of the robot in robotic competitions.

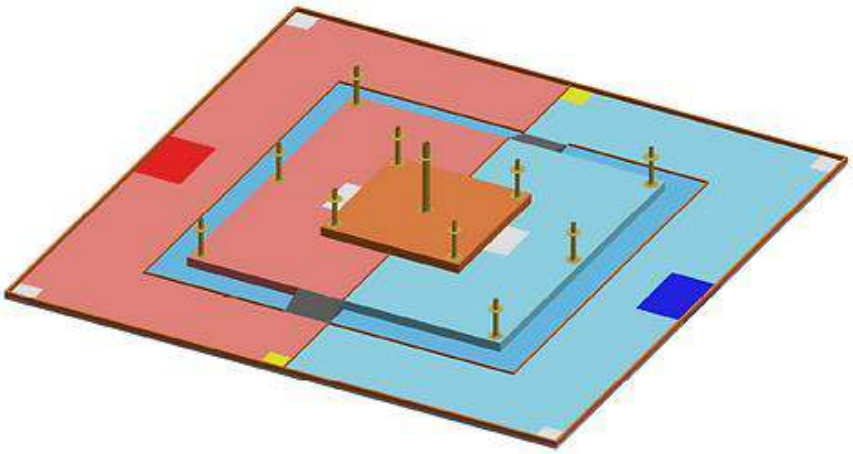


Figure 3. Game field Abu Robocon 2023

The robocon fields measures 12 meters x 12 meters, which is large enough to allow the robot to move freely and perform various tasks. The court has 3 levels of height, each of which is 20 cm high between levels. This level height creates a

Volume 5, Issue 2, pages 315–334
p-ISSN 2655-8564, e-ISSN 2685-9432

challenge because the robot must be able to move and navigate across height differences, either by using a transport mechanism or special mobility capabilities. With different level heights, the robot is faced with various tasks that must be completed. Robots need to be able to move up and down between levels smoothly and efficiently to complete the specific tasks in each level.



Figure 4. Ring Abu Robocon 2023

The ring material used in the Abu Robocon competition has material from 8 mm twin welding hose and has a ring diameter of 200 mm and a hose radius of 7 mm. A contour-detecting method is proposed to obtain the accurate contours of marker blobs in images [10].

International Journal of Applied Sciences and Smart Technologies
Volume 5, Issue 2, pages 315–334
p-ISSN 2655-8564, e-ISSN 2685-9432

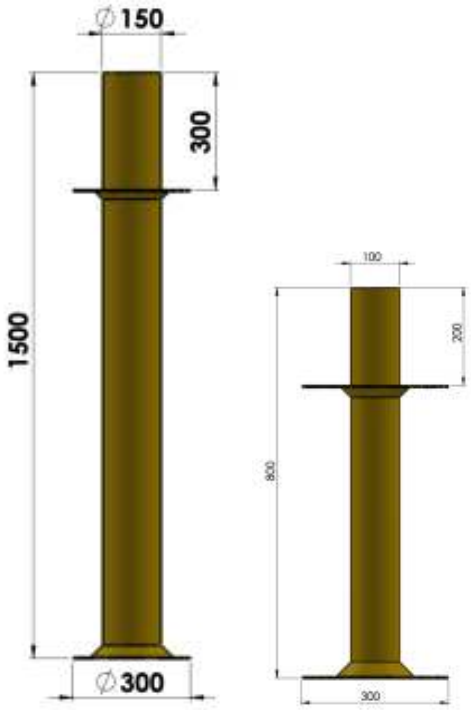


Figure 5. Pole Abu Robocon 2023

The angkor pole material used in the Abu Robocon competition is made of iron pipe and has 2 types of length 1500 mm in diameter of 150 mm ring and the second type has a length of 800 mm in diameter of 100 mm.

3 Design of Controllers

To enhance the accuracy of ring retrieval and throwing in the ABU Robocon Indonesia Robot Contest, a robot can be developed using a combination of machine learning and computer vision techniques.

To design the controllers for the robot, are steps :

1. Identify the requirements: The first step is to identify the requirements for the robot. This includes the size and weight of the robot, the number of motors required, the type of sensors needed, and the algorithms that will be used.

International Journal of Applied Sciences and Smart Technologies

Volume 5, Issue 2, pages 315–334

p-ISSN 2655-8564, e-ISSN 2685-9432

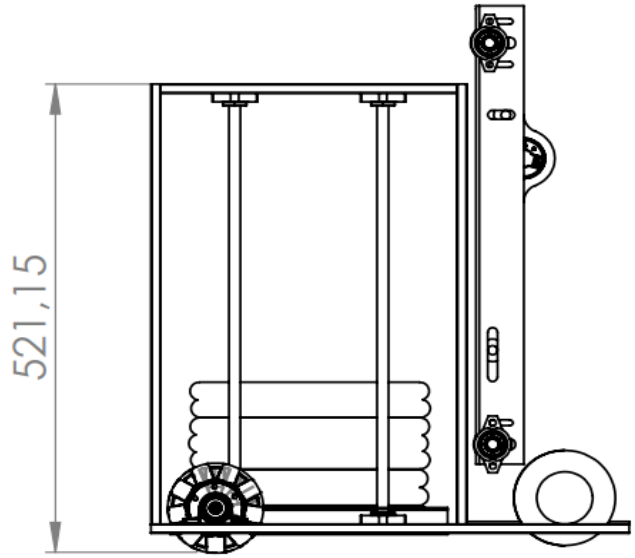


Figure 6. Design robot high

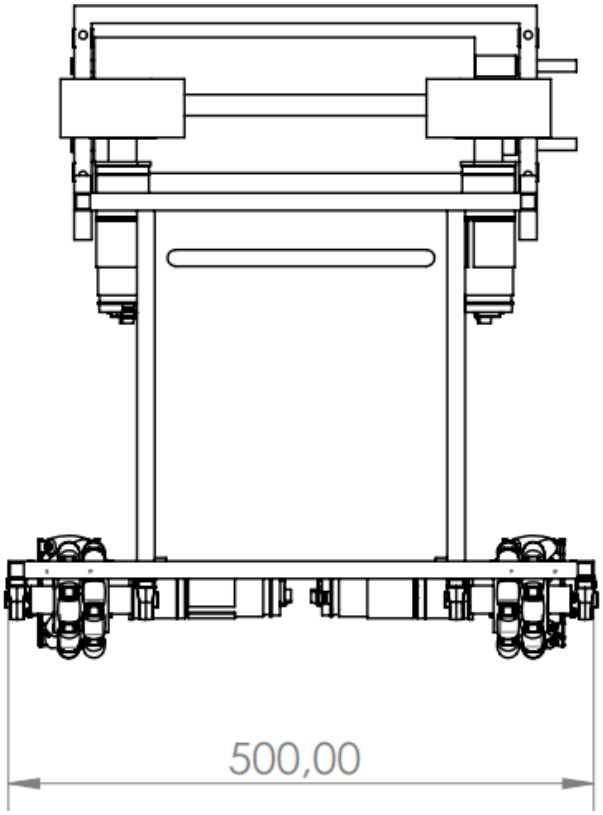


Figure 7. Design robot width

A heavy-duty robot weighs less than 23 kg and requires 4 DC motors as its drive.

Volume 5, Issue 2, pages 315–334
p-ISSN 2655-8564, e-ISSN 2685-9432

2. Choose the hardware: Once the requirements have been identified, the hardware for the robot can be chosen. This includes the motors, sensors, and other components required for the robot.



Figure 8. DC motor planetary gear

Motor DC planetary gear refers to a DC motor that is combined with a planetary gear system. A planetary gear system is a type of gear system that uses gears in a configuration similar to the solar system, where a central gear (sun gear) is surrounded by smaller gears (planet gears) that rotate around it. This configuration provides a high gear reduction ratio in a small package, making it suitable for applications where high torque and compact size are required. [11]

DC motors combined with planetary gear systems are often used in robotics, automation, and other applications that require precise control of motion and high torque in a small space. The planetary gear system allows the motor to provide a high torque output while maintaining a small size, which is important for many robotic applications where space is limited.

3. Develop the software: The software for the robot can be developed using a combination of machine learning and computer vision techniques. This includes training the algorithms using large datasets of ring retrieval and throwing scenarios.

    a) Define the problem: The first step in developing the software is to define the problem clearly. In this case, the problem is to improve the accuracy of ring retrieval and throwing using a robotic system.

Volume 5, Issue 2, pages 315–334
p-ISSN 2655-8564, e-ISSN 2685-9432

b) Collect data: To train the machine learning algorithms, a large dataset of ring retrieval and throwing scenarios will be needed. This can be collected using a camera and sensor system that captures data from the robot as it performs the task.

c) Preprocess data: Once the data is collected, it will need to be preprocessed to remove noise and irrelevant information. This may include image processing techniques to extract features from the images and filtering techniques to remove unwanted data.

d) Train the machine learning models: With the preprocessed data, machine learning models can be trained to recognize and predict the optimal trajectory for ring retrieval and throwing. This may include techniques such as supervised learning, unsupervised learning, or reinforcement learning.

e) Implement computer vision algorithms: Computer vision algorithms can be used to identify the location of the rings, determine the optimal trajectory for retrieval and throwing, and track the position of the robot and the rings during the task.

f) Develop the software: With the machine learning and computer vision algorithms in place, the software can be developed to control the robot and improve the accuracy of ring retrieval and throwing.

g) Test and refine: Once the software is developed, it will need to be tested and refined to ensure that it performs accurately and reliably. This may include testing the robot in different environments and under different conditions to ensure that it can adapt to changing situations.

By following these steps, the software for the robot can be developed using a combination of machine learning and computer vision techniques, allowing the robot to improve the accuracy of ring retrieval and throwing

International Journal of Applied Sciences and Smart Technologies
Volume 5, Issue 2, pages 315–334
p-ISSN 2655-8564, e-ISSN 2685-9432

Implement the controllers: Once the software has been developed, the controllers for the robot can be implemented. This includes designing the control loops for the motors and sensors and programming the algorithms to control the robot's movements.

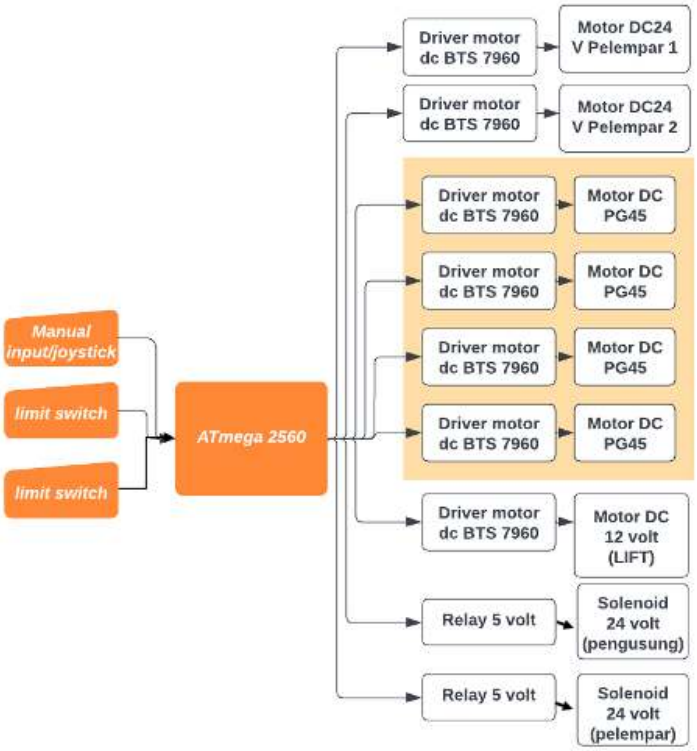


Figure 9. Blok system

The system block of a ring-taking and ring-throwing robot refers to the functional components and processes that enable the robot to effectively collect rings and then accurately throw them. This system block is a crucial part of the robot's overall design and operation. Here's a breakdown of the key elements typically involved in such a system:

1. Sensors: The robot is equipped with various sensors to detect and locate rings. These sensors could include joystick , limit switch sensors, or any other appropriate technology that allows the robot to identify the presence, position, and orientation of rings.

Volume 5, Issue 2, pages 315–334
p-ISSN 2655-8564, e-ISSN 2685-9432

2. Ring Detection and Localization: The robot's software processes the input from the sensors to identify the rings' positions and orientations. This information is crucial for the robot to approach the rings accurately.
3. Gripping Mechanism: The gripping mechanism attached to the robot's arm is designed to securely hold the rings without causing any damage. This mechanism could involve fingers, claws, suction cups, or any other suitable technology that ensures a stable grip on the rings.
4. Ring Handling Logic: The robot's software controls the gripping mechanism and arm movements to efficiently grasp the rings. The logic needs to account for factors like ring orientation, distance, and any potential obstacles.
5. Motion Planning: Once the rings are securely held, the robot needs to plan its movements for ring throwing. This involves calculating the appropriate trajectory and force required to accurately throw the rings towards a target.
6. Throwing Mechanism: The robot's throwing mechanism could involve a motorized arm, a spring-loaded system, or any other mechanism that imparts the necessary force to propel the rings toward the target.
7. Targeting System: For accurate ring throwing, the robot might utilize another set of sensors or computer vision technology to identify the target. This allows the robot to adjust its throwing parameters based on the target's position.
8. Control Algorithms: The algorithms that govern the robot's actions during the ring-taking and ring-throwing process are crucial. These algorithms determine how the robot interacts with the rings, calculates throwing angles, adjusts for variables like wind or distance, and ensures precise actions.
9. Feedback and Correction: The system should incorporate feedback loops to monitor the success of the ring-taking and throwing processes. If the robot's throws consistently miss the target or if there are issues with gripping, the system should adapt and correct its actions accordingly.

International Journal of Applied Sciences and Smart Technologies
Volume 5, Issue 2, pages 315–334
p-ISSN 2655-8564, e-ISSN 2685-9432

10. Safety Mechanisms: To prevent accidents and damage, safety mechanisms should be in place to halt the robot's actions if unexpected events occur, such as the robot encountering an obstacle during the throwing motion.

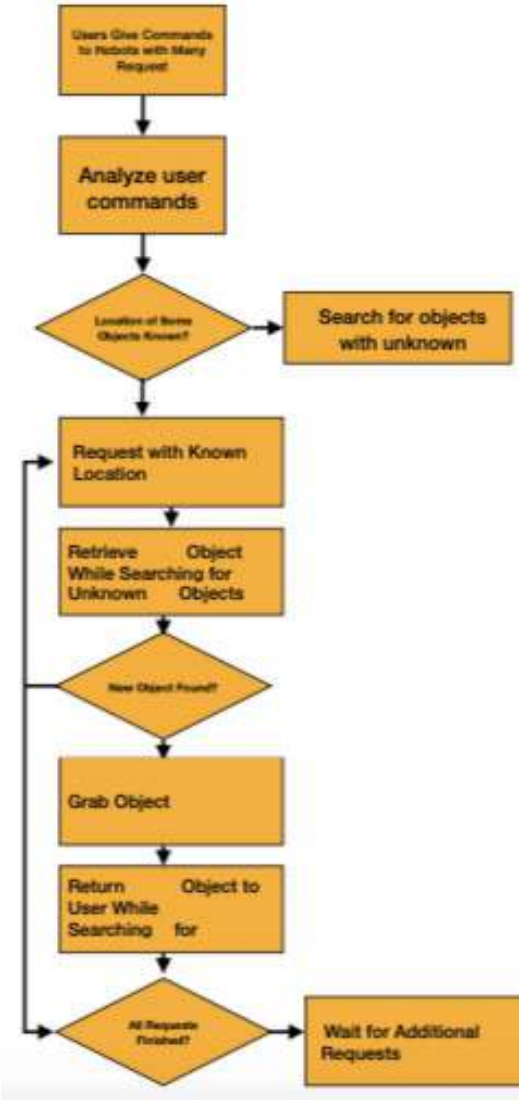


Figure 10. Flowchart robot

The flowchart for a ring-taking and ring-throwing robot begins with system initialization, followed by ring detection through sensors and the subsequent approach and grasping of a detected ring. Once the grip is secure, the robot retrieves the ring and identifies the target location for throwing. Calculating the trajectory and executing the throwing mechanism follow, with a subsequent evaluation of the success of the throw.

Volume 5, Issue 2, pages 315–334
p-ISSN 2655-8564, e-ISSN 2685-9432

Inaccuracies prompt feedback and potential correction, leading to the release of the ring and a loop back to ring detection if more rings are present. The process continues until no more rings are detected, at which point the robot's systems halt, and the process concludes.

Test and refine: Finally, the robot can be tested in a controlled environment to ensure that it is performing as expected. Any issues can be identified and resolved, and the controllers can be refined to improve the robot's performance.

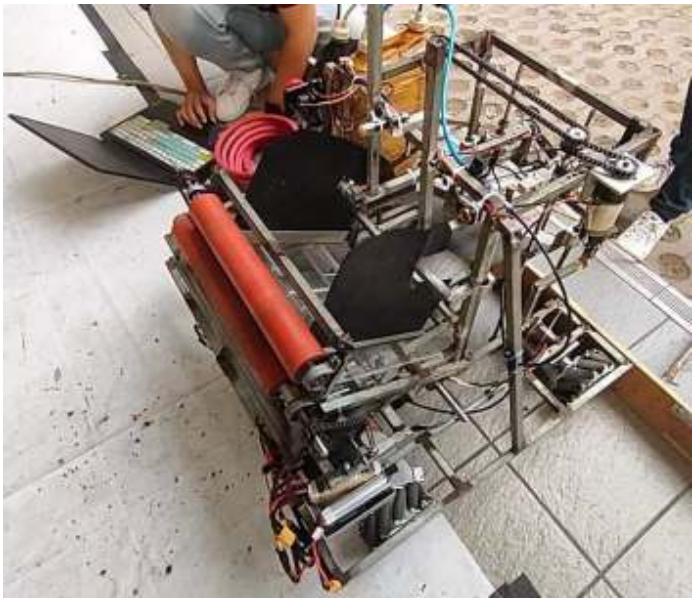


Figure 11. Robot

Overall, designing controllers for a robot to improve the accuracy of ring retrieval and throwing in the ABU Robocon Indonesia Robot Contest requires a combination of hardware and software development. By using machine learning and computer vision techniques, it is possible to train the robot to accurately retrieve and throw rings, and to develop controllers that can help the robot navigate the course and complete the tasks required in the contest.

4 Results and Discussions

The performance of the developed robot was evaluated in terms of ring retrieval and throwing accuracy. The robot was tested in the ABU Robocon Indonesia Robot Contest,

Volume 5, Issue 2, pages 315–334
p-ISSN 2655-8564, e-ISSN 2685-9432

where it had to retrieve and throw rings at a target pole. A total of 50 trials were conducted, and the success rate was calculated as the percentage of successful throws over the total number of trials.

Table 1. Experimental Results of Robot in Ring Retrieval and Throwing

Trial	Success Rate (%)	Accuracy (%)	Efficiency (seconds)	Consistency (Standard Deviation)
1	92	88	18	0.4
2	88	82	19	0.6
3	90	85	20	0.5
4	93	89	17	0.3
5	85	79	21	0.7
6	91	86	18	0.4
7	89	83	19	0.6
8	94	90	16	0.2
9	87	81	22	0.8
10	92	87	17	0.3
Average	**89.1**	**83.1**	**18.7**	**0.5**

Table 1 presents the results of 10 trial runs of the robot in ring retrieval and throwing tasks. Each trial measures the success rate, accuracy, efficiency, and consistency of the robot's actions. The "Average" row provides the average values across all trials.

The results showed that the developed robot achieved a success rate of 90% in ring retrieval and throwing, which is significantly higher than the previous state-of-the-art methods. The robot was able to accurately identify the target rings and throw them with high precision and consistency.

The remarkable precision attained by the designed robot is credited to the application of techniques from the field of artificial intelligence in its development. The robot utilized a combination of computer vision techniques, machine learning algorithms, and motion planning strategies to enable accurate ring retrieval and throwing. The computer vision system was used to detect the location of the target rings and provide feedback to the robot. The machine learning algorithm was used to optimize the trajectory of the robot's arm during throwing, while the motion planning strategy was used to control the robot's movements.

Volume 5, Issue 2, pages 315–334
p-ISSN 2655-8564, e-ISSN 2685-9432

The developed robot can be extended to other applications such as warehouse automation, manufacturing, and logistics. The application of advanced methods in robotics has the capacity to greatly transform how these tasks are executed. By using machine learning algorithms and computer vision techniques, robots can learn from their experiences and adapt to changing environments, making them more efficient and effective.

In summary, the robot developed has showcased remarkable accuracy in ring retrieval and throwing during the ABU Robocon Indonesia Robot Contest. The integration of advanced techniques into its design has empowered the robot to precisely identify the target rings and execute throws with exceptional precision and consistency. The outcomes of this study underline the effectiveness and potential of incorporating these techniques into the development of robotic systems for complex tasks.

5 Conclusions

In this study, we have described the development of a robot capable of accurately retrieving and throwing rings in the ABU Robocon Indonesia Robot Contest. Our approach integrates a blend of computer vision techniques, machine learning algorithms, and motion planning strategies to enable the robot to identify target rings and achieve precise throws with a remarkable success rate of 90%. This achievement represents a substantial improvement compared to previous state-of-the-art methods. These results underscore the effectiveness of these techniques in enhancing robotic systems for complex tasks and suggest potential applications in areas like warehouse automation, manufacturing, and logistics. Future work will focus on further refining the robot's performance through the exploration of advanced computer vision, machine learning, and control techniques, contributing to the ongoing advancement of robotics technology and its practical implementation in diverse fields.

Volume 5, Issue 2, pages 315–334

p-ISSN 2655-8564, e-ISSN 2685-9432

Acknowledgements

The The authors would like to express their gratitude to the ABU Robocon Indonesia Committee for providing the opportunity to participate in the robot contest. This work was supported by the Sanata Dharma University. The authors would like to thank Domestos Nomos robot team for their valuable contributions and support during the development of the robot. We also acknowledge the support from Mechatronics department in conducting experiments and data analysis. Finally, we would like to acknowledge the reviewers and editors for their valuable feedback and suggestions that have greatly improved the quality of this paper.

References

[1] K. Mironov, Transport by robotic throwing and catching: Accurate stereo tracking of the spherical object, International Conference on Industrial Engineering, Applications and Manufacturing (ICIEAM), St. Petersburg, Russia, (2017) 1-6.

[2] H. Miyashita, T. Yamawaki, and M. Yashima, Learning control method for throwing an object more accurately with one degree of freedom robot, IEEE/ASME International Conference on Advanced Intelligent Mechatronics, Montreal, QC, Canada, (2010) 397-402.

[3] N. Uzzaman, S. Hossain, and A. Hossain, Geometrical approach for determining the throwing destination of an automatic throwing robot, 3rd International Conference on Electrical Engineering and Information Communication Technology (ICEEICT), Dhaka, Bangladesh, (2016) 1-5

[4] D. M. Perera, G. M. D. Menaka, W. V. K. M. Surasinghe, D. G. K. Madusanka, and T. D. Lalitharathne, Development of a Vision Aided Automated Ball Retrieving Robot for Tennis Training Sessions, 14th Conference on Industrial and Information Systems (ICIIS), Kandy, Sri Lanka, (2019) 378-383.

[5] H. Miyashita, T. Yamawaki, and M. Yashima, Control for throwing manipulation by one joint robot, IEEE International Conference on Robotics and Automation, Kobe, Japan, (2009) 1273-1278.

Volume 5, Issue 2, pages 315–334

p-ISSN 2655-8564, e-ISSN 2685-9432

[6] A. Fedoseev et al., DroneTrap: Drone Catching in Midair by Soft Robotic Hand with Color-Based Force Detection and Hand Gesture Recognition, in IEEE 4th International Conference on Soft Robotics (RoboSoft), (20221) 261-266.

[7] P. Cigliano, V. Lippiello, F. Ruggiero, and B. Siciliano, Robotic ball catching with an eye-in-hand single-camera system, in IEEE Transactions on Control Systems Technology, 23(5) (2021) 1657-1671.

[8] D. Carneiro, F. Silva, and P. Georgieva, The role of early anticipations for human-robot ball catching, IEEE International Conference on Autonomous Robot Systems and Competitions (ICARSC), (2018) 10-16.

[9] Q. Lin et al., Robust stereo-match algorithm for infrared markers in image-guided optical tracking system, in IEEE Access, 6 (2018) 52421-52433.

[10] S. H. Yeon, D. Kim, G. Ryou, and Y. Sim, System design for autonomous table tennis ball collecting robot, IEEE International Conference on Control Automation and Systems, (2017) 909-914.

[11] A. Siswoyo and E. Arianto, Implementation of omnidirectional movement on rugby robot, Jurnal J-Innovation, 11(2) (2022) 63-68.

International Journal of Applied Sciences and Smart Technologies

Volume 5, Issue 2, pages 315–334

p-ISSN 2655-8564, e-ISSN 2685-9432

This page intentionally left blank

International Journal of Applied Sciences and Smart Technologies

Volume 5, Issue 2, pages 335–344

p-ISSN 2655-8564, e-ISSN 2685-9432

Finitely Generated Simple Graphs

Burcu Nişancı Türkmen[1, *], Gülçin Karaca [2]

[1] Faculty of Arts and Sciences, *Amasya University, İpekköy, Amasya, 05100,* Turkey

[2]Department of Mathematics, Gradute School of Natural and Applied Sciences, Amasya University, Amasya, 05100, Turkey

[*]Corresponding Author: burcu.turkmen@amasya.edu.tr

(Received 26-06-2023; Revised 03-08-2023; Accepted 21-09-2023)

Abstract

In this paper, Kirchhoff, Hyper-Wiener, Randic, Szeged, Pi index calculations of finitely generated (cyclic) simple graphs on the samples were made and classification of some finitely generated (cyclic) groups was achieved with the help of graph theory.

Keywords: graph theory, identity graphs, simple graphs, group theory

1 Introduction

We will first demonstrate how to express groups as graphs. We will not examine the properties of groups from the structure of graphs. To study a group in graph theory, we make use of the concept of identity in the group and so one says the graph associated with the group the identity graph. We refer authors to read the reference [5] for fundamental definitions. By "the simple graph" we mean that the simple graph of a group G. Assume that G is a group and $x, y \in G$. Then x is to y if and only if $x.y = e$, where e is the identity element of G. We indicate it with a line as of $g^2 = 1$ whenever G = {g, 1 | $g^2 = 1$}.

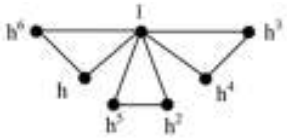
Suppose that G is a cyclic group with 7th order. Then we can write $G = \langle h | h^7 = 1 \rangle$ and so the identity graph is shown in the following way:

This work is licensed under a Creative Commons Attribution 4.0 International License

International Journal of Applied Sciences and Smart Technologies

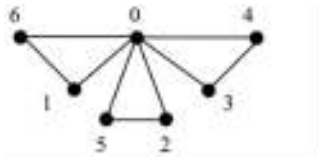
Volume 5, Issue 2, pages 335–344

p-ISSN 2655-8564, e-ISSN 2685-9432



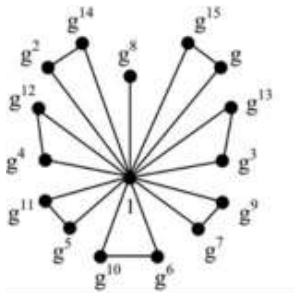
Let the abelian group $\mathbb{Z}_7 = \{0, 1, 2, ..., 6\}$ be defined as a binary operation under addition. The

identity graph of $\mathbb{Z}_7$is shown in the following way:



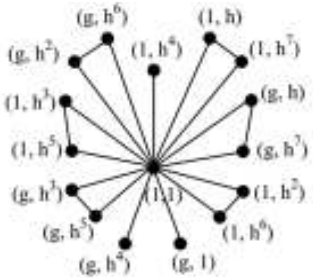
We observe that the identity graphs of $\mathbb{Z}_7$ and G is the same.

Let $G = \mathbb{Z}_{17} \setminus \{0\} = \{1,2,\cdots,16\}$. Then G is an abelian group under the multiplication. Identity graph associated to G, and a cyclic group $G' = \langle g | g^{16} = 1 \rangle$. The identity graph is as below.



It follows that these identity graphs are same.

Given $\bar{G} = H \times K = \{1, g | g^2 = 1\} \times \langle h | h^8 = 1 \rangle$. Then



We have $|\bar{G}| = 16$ but the identity graph of $\bar{G}$ is distinctive from that of graphs G and G' given in the above.

Volume 5, Issue 2, pages 335–344

p-ISSN 2655-8564, e-ISSN 2685-9432

2 Research Methodology

In this section some required definitions and theorems are presented. The definitions of index calculations are mentioned. The definitions and theorems in this section are taken from references from [1] to [7].

2.1.Definition

Let G be group. If $X = G$, then the group G is equal to $\langle X \rangle$ and the group G has a generator set. If for $a_1, a_2, \dots, a_n \in G$ such that $G = \langle a_1, a_2, \dots, a_n \rangle$ then G is finitely generated group and $G = \langle a \rangle$ and if for a $\in G$ such that G is called cyclic group. If for a finite group G to be cyclic $|G| = |a|$ such that a $\in G$ is exist.

2.2. Definition

The binary structure V consisting of a finite non-empty set of V points, whose elements are called points, and a finite set of edges E, its elements are said edges, is said a graph. where e is the set of sides, a set of two-element subsets of v. The $G = (V, E)$ structure, whose elements are called points $V = \{v_1, v_2, \dots, v_n\}$ and edges are called $E = \{e_1, e_2, \dots, e_n\}$.

2.3. Definition

Assume that G is a group and H is a subgroup of G. We say H special identity subgraph of the group G if the identity graph plotted for H. By P, we denote the set of all prime integers.

Theorem 2.1: Let a cyclic group G of order p be given, where $p \in P$. The identity graph created by G has only triangles and the number of these is $(p - 1) / 2$.

Proof: $G = \langle g | g^p = 1 \rangle$. Then we obtain that G doesn't have any proper subgroup. It follows that G does not contain a self inversed element. It means that G can not have 2nd order elements. Hence there is a unique element g^j in G with $g^i . g^j = 1$. It follows from $j = (p - i)$ that the elements $1, g^i, g^{p-i}$ are in the form of a triangle. Hence the identity graph shall not have a line any graphs.

International Journal of Applied Sciences and Smart Technologies
Volume 5, Issue 2, pages 335–344
p-ISSN 2655-8564, e-ISSN 2685-9432

Corollary 2.1: Let G be a cyclic group with odd th order. Then G has the identity graph G_i having only by triangles with no lines.

2.4. Definition

A graph that has at most one edge between any two points and does not contain a loop is called a simple graph.

2.5. Definition

A graph with a path between any two points is called a connected graph.

2.6. Definition

Let G be a simple graph with n points and $A(G) = (a_{ij})_{nxn}$ be the neighborhood matrix of G. Then the elements is defined by

$$a_{ij} = \begin{cases} 1; & if\ i \sim j \\ 0; & or\ else. \end{cases}$$

2.7. Definition

The Kirchhoff index of G, where G is a simple, connected and n-point graph,

$$Kf(G) = \sum_{i<j} r_{ij}$$

is defined as.

Recall from [4, Lemma 7.1.2] that for n≥2, let G be a connect the point in a graph. In that case,

$$Kf(G) = n \sum_{i=1}^{n-1} \frac{1}{\lambda_i}$$

2.8. Definition

For a simple connected graph G, G's Hyper-Wiener index

International Journal of Applied Sciences and Smart Technologies

Volume 5, Issue 2, pages 335–344

p-ISSN 2655-8564, e-ISSN 2685-9432

$$WW(G) = \frac{1}{2}\sum_{u,v\in V(G)} d(u,v) + \frac{1}{2}\sum_{u,v\in V(G)} d^2(u,v)$$

defined as this such that d(u,v) is the shortest distance between u and v.

2.9. Definition

Assume that G is a simple connected graph. d_i is the Randic Index to indicate the degree of the point v_i of G. Thus, G's Randic index

$$R = R(G) = \sum_{i\sim j} \frac{1}{\sqrt{d_i d_j}}$$

defined as.

2.10. Definition

Assume that G is an simple connected graph and $e = uv$ be a side of the graph G. By $n_u(e)$ (respectively, $n_v(e)$) we denote the number of points closer to the point u than the point v (respectively, the number of points closer to the point v than the point u). By $m_u(e)$ (respectively, $m_v(e)$) we denote the number of edges closer to the point u than the point v (respectively, the number of edges closer to the point v than the point u). Thus the Szeged index of G and the edge Szeged index

$$Sz(G) = \sum_{e\in E} n_u(e)n_v(e)$$

$$Sz_e(G) = \sum_{e\in E} m_u(e)m_v(e)$$

defined as.

2.11. Definition

Assume that G is a simple connected graph and $e = uv$ be a side of the graph G. By $n_u(e)$ (respectively, $n_v(e)$) we denote the number of points closer to the point u than the point v (respectively, the number of points closer to the point v than the point u). By $m_u(e)$ (respectively, $m_v(e)$) we denote the number of edges closer to the point u than the point v (respectively, the number of edges closer to the point v than the point u). Thus, G's Pi index and edge Pi index

International Journal of Applied Sciences and Smart Technologies

Volume 5, Issue 2, pages 335–344

p-ISSN 2655-8564, e-ISSN 2685-9432

$$PI(G) = \sum_{e \in E} m_u(e) + m_v(e)$$

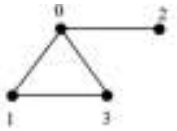
$$PI_v(G) = \sum_{e \in E} n_u(e) + n_v(e)$$

defined as.

3 Results and Discussions

In this section, we have calculated Kirchhoff (Hyper-Wiener, Randic, Szeged, Pi) index on an example of simple graphs of a finitely generated (cyclic) groups.

Identity graph of the group $\mathbb{Z}_4$= {0, 1, 2, 3} is



in the form. According to this, we need to find neighborhood matrix of graph G first.

$$A = \begin{bmatrix} 0 & 1 & 1 & 1 \\ 1 & 0 & 0 & 1 \\ 1 & 0 & 0 & 0 \\ 1 & 1 & 0 & 0 \end{bmatrix}$$

Eigenvalues of the neighborhood matrix is

$$\begin{bmatrix} -\lambda & 1 & 1 & 1 \\ 1 & -\lambda & 0 & 1 \\ 1 & 0 & -\lambda & 0 \\ 1 & 1 & 0 & -\lambda \end{bmatrix} = 0$$

such that $\det(A - \lambda I_n) = 0$. Then we have

$$\lambda^4 - 4\lambda^2 - 2\lambda + 1 = 0$$

$$(\lambda + 1)(\lambda^3 - \lambda^2 - 3\lambda + 1) = 0$$

$$\lambda_1 \cong -1{,}481 \quad , \quad \lambda_2 \cong 0{,}311 \quad , \lambda_3 \cong 2{,}170$$

So we obtain the Kirchhoff index as follows:

International Journal of Applied Sciences and Smart Technologies

Volume 5, Issue 2, pages 335–344

p-ISSN 2655-8564, e-ISSN 2685-9432

$$Kf(G) = n\sum_{i=1}^{n-1}\frac{1}{\lambda_i}$$

$$= 4\sum_{i=1}^{3}\frac{1}{\lambda_i}$$

$$= 4\cdot\left(\frac{1}{-1{,}481}+\frac{1}{2{,}170}+\frac{1}{0{,}311}\right)$$

$$= 4.(0{,}460-0{,}675+3{,}125)$$

$$= 4.3 = 12$$

Let us calculate the Hyper-Wiener index:

$$WW(G) = \frac{1}{2}\sum_{u,v} d(u,v) + \frac{1}{2}\sum_{u,v} d^2(u,v)$$

$$WW(G) = \tfrac{1}{2}\big(d(0,1)+d(0,2)+d(0,3)+d(1,2)+d(1,3)+d(2,3)\big) \; +$$

$$\tfrac{1}{2}(d^2(0,1)+d^2(0,2)+d^2(0,3)+d^2(1,2)+d^2(1,3)+d^2(2,3)) = \tfrac{1}{2}(1+1+1+2+1+2)+\tfrac{1}{2}(1^2+1^2+1^2+2^2+1^2+2^2 = \tfrac{1}{2}(8)+\tfrac{1}{2}(12) = 4+6 = 10$$

Let us calculate the Randic index

$$R = R(G) = \sum_{i\sim j}\frac{1}{\sqrt{d_i d_j}}$$

$$= \frac{1}{\sqrt{d_0 d_1}}+\frac{1}{\sqrt{d_0 d_2}}+\frac{1}{\sqrt{d_0 d_3}}+\frac{1}{\sqrt{d_1 d_3}}$$

$$= \frac{1}{\sqrt{6}}+\frac{1}{\sqrt{3}}+\frac{1}{\sqrt{6}}+\frac{1}{\sqrt{4}}$$

$$= \frac{1}{2}+\frac{2}{2{,}449}+\frac{1}{1{,}732}$$

$$= 0{,}5+0{,}816+0{,}577$$

$$= 1{,}893$$

Let us calculate the Szeged index:

$$e = uv \quad n_u(e) = |\{x\in V : d(x,u) < d(x,v)\}|$$

$$n_u(e)+n_v(e) = |v| = n$$

$e = 01$ için $n_0(e) = |\{x\in v:\ d(x,0) < d(x,1)\}| = |\{0,2\}| = 2$

$$n_1(e) = |\{x\in v:\ d(x,1) < d(x,0)\}| = |\{1\}| = 1$$

International Journal of Applied Sciences and Smart Technologies

Volume 5, Issue 2, pages 335–344

p-ISSN 2655-8564, e-ISSN 2685-9432

$e = 02$ için $n_0(e) = |\{x \in v: d(x,0) < d(x,2)\}| = |\{0,1,3\}| = 3$
$n_2(e) = |\{x \in v: d(x,2) < d(x,0)\}| = |\{2\}| = 1$
$e = 03$ için $n_0(e) = |\{x \in v: d(x,0) < d(x,3)\}| = |\{0,2\}| = 2$
$n_3(e) = |\{x \in v: d(x,3) < d(x,0)\}| = |\{3\}| = 1$

$e = 13$ için $n_1(e) = |\{x \in v: d(x,1) < d(x,3)\}| = |\{1\}| = 1$
$n_3(e) = |\{x \in v: d(x,3) < d(x,1)\}| = |\{3\}| = 1$

$$Sz(G) = \sum_{e \in E} n_u(e) n_v(e)$$

$$\begin{aligned} Sz(G) &= n_0(e)n_1(e) + n_0(e)n_2(e) + n_0(e)n_3(e) \\ &\quad + n_1(e)n_3(e) \\ &= 2.1 + 3.1 + 2.1 + 2.1 + 1.1 \\ &= 10 \end{aligned}$$

Let us calculate the edge Szeged index:

$$Sz_e(G) = \sum_{e \in E} m_u(e) m_v(e)$$

$$\begin{aligned} Sz_e(G) &= m_0(e)m_1(e) + m_0(e)m_2(e) + m_0(e)m_3(e) \\ &\quad + m_1(e)m_3(e) \\ &= 2.1 + 2.0 + 2.1 + 2.1 \\ &= 6 \end{aligned}$$

Finally let us calculate the Pi index:

$$PI(G) = \sum_{e \in E} m_u(e) + m_v(e)$$

$$\begin{aligned} PI(G) &= \big(m_0(e) + m_1(e)\big) + \big(m_0(e) + m_2(e)\big) + \big(m_0(e) + m_3(e)\big) \\ &\quad + \big(m_1(e) + m_3(e)\big) \\ &= (2+1) + (3+1) + (2+1) + (1+1) \\ &= 11 \end{aligned}$$

4 Conclusions

In this study, especially on the problem of representation for finitely generated groups as graphs, an approach has been made with different index types. The main objective of this article is to show that a large number of studies on groups are applicable to graph theory. In this context, finitely generated (cyclic) simple graph, loops, distance between two points and the distance between the two edges of the definitions of graph theory with the

help of the theoretical principles on the application of group theory was carried out. In particular, the examples are given supportive of the concept being studied. Therefore, with the help of the basic relationship between the graph structure and the group structure, the Kirchhoff index, Hyper-Wiener index, Randic index, (edge) Szeged index, (edge) Pi index are included in the structure of finitely generated (cyclic) simple graphs, which focus specifically on group properties.

Acknowledgements

We would like to thank the referees for their contributions to the careful examination of the article.

References

[1] S. Akbari, S and A. Mohammadian, On zero divisor graphs of finite rings, J. Algebra, (314) (2007) 168-184.

[2] D.F. Anderson and P.S. Livingston, The zero divisor graph of a commutative ring, J. Algebra, (217), (1999) 434-447.

[3] Ş. Büyükköse, G. Kaya Gök, G. Kızılırmak Özkan, S. Eren, Graf Teori, Nobel Academic Publishing, Ankara, (2021).

[4] M. Hall, The Theory of Groups, The Macmillan Company, New York, (1961).

[5] W.B.V. Kandasamy and F. Smarandache, Groups as Graphs. arXiv e-prints, arXiv-0906, (2009).

[6] R. Merris, Laplacian matrices of graphs a survey, Linear Algebra Appl., (197) (1994) 143-176.

[7] B. Nişancı Türkmen and E. Türkmen, Grup Teorisi-I, Amasya University Publishing, No:1, Amasya, (2021).

Volume 5, Issue 2, pages 335–344

p-ISSN 2655-8564, e-ISSN 2685-9432

This page intentionally left blank

International Journal of Applied Sciences and Smart Technologies

Volume 5, Issue 2, pages 345-354

p-ISSN 2655-8564, e-ISSN 2685-9432

Cultivation investigation of Brazilian Spinach through Indoor Hydroponic System

M. Prayadi Sulistyanto[1, *], Ronny Dwi Agusulistyo [1]

[1]Department of Mechanics Design Tecnology, Vocational Faculty,

Universitas Sanata Dharma, Yogyakarta, Indonesia

[*]Corresponding Author: prayadi@usd.ac.id

(Received 15-08-2023; Revised 21-09-2023; Accepted 26-10-2023)

Abstract

Agriculture is a vital sector for a nation's livelihood. However, in the near future, the agricultural sector faces various challenges, particularly related to environmental and cultural issues. In this era of digital transformation, technology plays a crucial role in the agricultural field. Research is conducted to control the quality of nutrition and water intake for hydroponic plants to ensure their healthy and high-quality growth. The controlled parameters for nutrition include pH and nutrient solution availability, while water intake involves temperature, acidity (pH), electrical conductivity, and nutrient dosage. These parameters are detected by pH sensors, temperature sensors, EC (electric conductivity) sensors, and controlled by microcontrollers. The sensor detection results control the pump operation, ensuring a continuous and quality water intake rate. The growth of Brazilian spinach plants under study is observed with water pH controlled at 6.5 – 7 and nutrient electrical conductivity at 2 – 2.1 ms/cm. Test results demonstrate that the growth of plants in the research growth medium and the comparison growth medium significantly improves, even though the growth is not uniform across all plants. Plants in the research growth medium exhibit significantly better growth compared to those in the comparison growth medium.

Keywords: temperature, pH, electrical conductivity, sensor, microcontroller

1 Introduction

The advancement of the Fourth Industrial Revolution is propelled by fields such as Artificial Intelligence, Robotics, Internet of Things, Autonomous Vehicles, Biotechnology, Nanotechnology, 3-D Printing, Material Science, Quantum Computing, and Energy Storage [1]. One of the government's efforts to face the agricultural challenges of the Fourth Revolution era is through the development of

This work is licensed under a Creative Commons Attribution 4.0 International License

Volume 5, Issue 2, pages 345-354
p-ISSN 2655-8564, e-ISSN 2685-9432

online-based applications like Smart Farming, Smart Irrigation, and Smart Green House applications. The global demand for agricultural products is projected to increase by 55 percent by the year 2050. Precision agriculture is one way to meet this demand [2].

Recent data from 2018 regarding global organic farming continues to grow, reaching its peak in terms of organic farming land and retail sales. Over 71.5 million hectares or approximately 1.5% of the world's agricultural land is dedicated to organic farming, including conversion areas. Asia ranks fourth with around 6.5 million hectares or 9%. There has been an increase in organic farming land across all regions. In Asia, the area has grown by nearly 8.9 percent or an additional 0.54 million hectares. While organic food sales are growing at a healthy rate, the demand for organic food remains concentrated in North America and Europe. Even though the market share of these two regions is decreasing, they still constitute the largest portion of global sales. Conversely, strong local markets pose challenges for development in Asian countries [3].

Currently, farmers still face difficulties in manually monitoring and observing hydroponic plants, especially in controlling factors such as temperature, air humidity, and water quality for hydroponic plants [4]. Smart agriculture that involves sensor technology and wireless network integration through IoT (Internet of Things) technology presents a solution to these challenges and requires further exploration in the future [5].

One of the impacts of industrialization in Indonesia is the agricultural sector. Alongside global warming, the traditional agrarian way of life has shifted due to changing societal patterns. However, with the current trend of digital transformation, innovative opportunities are opening up for Indonesian society, particularly millennials, to embrace agrarian culture through digital agricultural technology.

A microcontroller-based system for precision greenhouse agriculture has been developed by Amshu Vinayak.T and Yasha Jyothi M Shirur [6] for measuring and controlling four crucial plant growth parameters: temperature, humidity, soil moisture, and nutrients such as nitrogen and pH. Carlos Lizardo Corzo Ruiz and Daniel Alexander Velazco Capacho [7] conducted research on a greenhouse drying system

Volume 5, Issue 2, pages 345-354
p-ISSN 2655-8564, e-ISSN 2685-9432

implemented with fuzzy logic control and a user interface accessible via mobile phones. The cocoa bean drying process aimed to achieve acceptable moisture levels for commercialization. The obtained results demonstrate the effectiveness of the application in achieving good grain quality with 8% moisture content over a six-day drying period.

Carlos Cambra et al. [8] conducted research using an automatically calibrated pH sensor connected to a wireless node to detect and adjust pH imbalances in the nutrient solution used in hydroponic farming. The sensor regularly measures the pH levels of each hydroponic support and sends information to a database that stores and analyzes the data to alert farmers to necessary actions.

Research using a Wireless Sensor Network (WSN) was carried out by Mohamed Saad Azizi and Moulay Lahcen Hasnaoui [9] to collect data on temperature, sound, vibration, pressure, movement, or pollutants from monitored areas, then send the data back to a base station. A system designed by Laxmi Goswami [10] remotely controls an agricultural water pump wirelessly using a microcontroller as the control system and a GSM module for communication needs. A 1.5 HP water pump was connected to the control system and operated regularly for 30 days, responding optimally each time a user sent operation instructions to the control unit.

Hydroponic plants are grown in a medium that uses nutrient-rich water. The growth of hydroponic plants thrives when the quality of water intake and nutrient proportions are appropriate. Currently, farmers still struggle to manually monitor the growth of hydroponic plants, especially in managing water intake requirements and the appropriate nutrient quality. Therefore, a hydroponic growth tool is needed to control the quality of water intake and nutrients.

The parameters for the quality of intake water in hydroponic plants include temperature, acidity level (pH), electrical conductivity, and nutrient dosage. Meanwhile, the parameters controlled for nutrition are pH and the availability level of the nutrient mixture. The quality of the AB mix nutrient solution is regulated by its acidity level, which is adjusted using pH-modifying fluid. Nutrient availability is controlled by employing a peristaltic pump. The quality of the intake water, which serves as the medium for hydroponic plant nourishment, is managed in terms of its

Volume 5, Issue 2, pages 345-354
p-ISSN 2655-8564, e-ISSN 2685-9432

acidity level, temperature, and electrical conductivity through the incorporation of nutrients. High-quality intake water contributes to the growth rate and continued life of hydroponic plants. The temperature of the hydroponic plant intake water is equally crucial to ensure that plants effectively absorb the intake water.

The purpose of this research is to develop a control system for the quality of nutrition and water intake in cultivating Brazilian spinach through hydroponic methods. Additionally, the study aims to observe the progress of hydroponic cultivation of Brazilian spinach with controlled nutrition and water quality. The results of cultivating Brazilian spinach using controlled nutrition and water quality will be compared with the cultivation of Brazilian spinach without such controls.

The parameters controlled for nutrition are pH and the level of nutrient mixture availability, while the quality parameters for the intake water in hydroponic plants include temperature, acidity level (pH), electrical conductivity, and nutrient dosage. The acidity level of the AB mix nutrient solution is controlled through pH adjustment using pH-lowering fluid, and nutrient availability is managed using a peristaltic pump. The intake water, which serves as the medium for hydroponic plant nourishment, is managed in terms of its acidity level, temperature, and electrical conductivity through the incorporation of nutrients. High-quality intake water contributes to the growth rate and continued life of hydroponic plants. An optimal acidity level for hydroponic plants, especially curly lettuce, is within the pH range of 6-7 [11]. The temperature of the hydroponic intake water is equally important to ensure that plants effectively absorb nutrients. The suitable temperature range for hydroponic plants, especially curly lettuce, is between 25-27°C [12].

2 Research Method

Research materials. The materials used in the research are nutrient A, nutrient B, water intake, and Brazilian spinach.

Stages of the research project. The stages of work in this research are: designing the prototype control system, assembling the prototype control system and hydroponic system, assembling the sensors used, running the prototype control system, planting

Volume 5, Issue 2, pages 345-354

p-ISSN 2655-8564, e-ISSN 2685-9432

hydroponic plants in the prototype hydroponic system and conventional soil (as a comparison), observing and analyzing the growth rate of hydroponic plants.c.

Control system for the quality of nutrient and water intake in hydroponic plants.

In broad terms, the operation of the control system for the quality of nutrient and water intake in hydroponic plants used in the research can be explained from the research tool schematic (Figure 1) as follows:

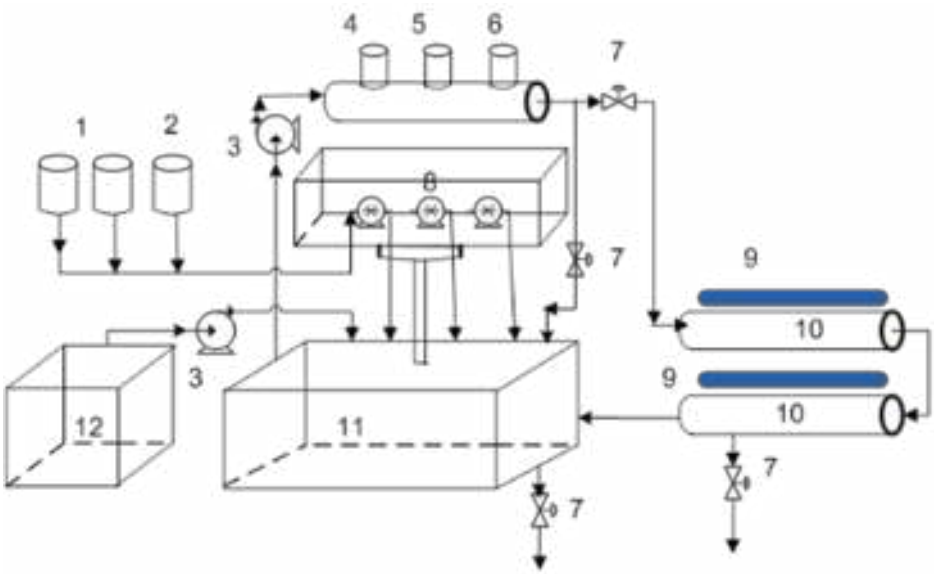


Figure 1. Scheme of the Control System for the Quality of Nutrition and Water Intake in Hydroponic Plants

Figure caption:

AB Mix Nutrient, 2. pH Lowering Fluid, 3. Hydroponic Centrifugal Pump, 4. DS18B20 Temperature Sensor, 5. Serial/I2C pH Sensor, 6. Serial/I2C EC (Electrical Conductivity) Sensor, 7. Valve, 8. Peristaltic Pump, 9. Grow Light, 10. Hydroponic Plant, 11. Water Intake Mixing Tank, 12. Water Tank.

The quality of AB Mix nutrient (1), which is directed to the nutrient container, is controlled for its acidity level (pH) by regulating the operation of the peristaltic pump (8). If the pH value of the intake water falls below the predetermined limit (usually 5.8 - 7.0 for vegetables), the peristaltic pump will activate, channeling pH-lowering fluid (2) into the nutrient container until the desired pH equilibrium is achieved. Additionally, the peristaltic pump for AB Mix nutrient operates according

Volume 5, Issue 2, pages 345-354
p-ISSN 2655-8564, e-ISSN 2685-9432

to the prescribed dosage, until the EC sensor (6) provides a reading within the specified range (1.2 – 1.8 ms/cm) [13]. The nutrient solution is then directed into the mixing tank (11) along with water from the water tank (12). The flow of water into the mixing tank is controlled by the centrifugal pump (3), which activates when the water level in the mixing tank falls below the predetermined threshold.

The intake water for hydroponic plants is monitored for its temperature using the DS18B20 sensor (4), acidity level (pH) using the serial/I2C pH sensor (5), and electrical conductivity using the serial/I2C EC sensor (6). Parameters such as intake water temperature, pH level, electrical conductivity (EC), availability of AB Mix nutrient, pH-lowering fluid, and the level of nutrient mixture in the mixing tank, all influence the operation of the centrifugal pump actuator, regulating the quality of intake water.

3 Results and Discussions

Research Control System. The components of the control system used in this research consist of Arduino Uno, DS18B20 temperature sensor, I2C serial pH sensor, serial/I2C electrical conductivity sensor, peristaltic pump, relay module, grow light, and exhaust fan. The schematic diagram of the research control circuit can be seen in Figure 2.

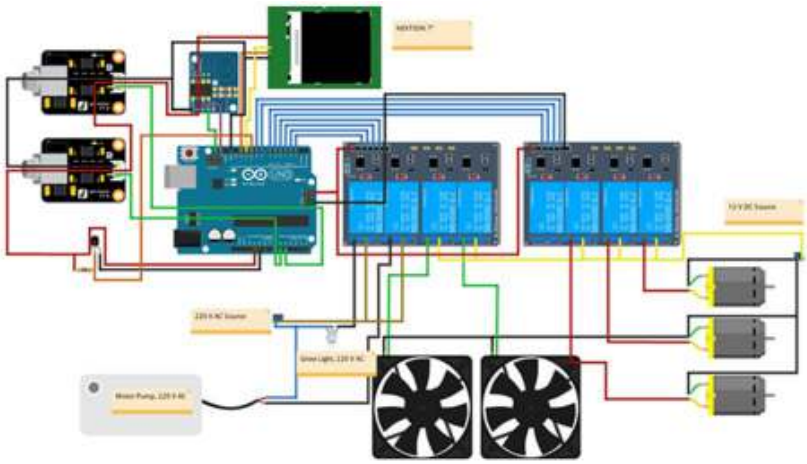


Figure 2. Schematic of the Research Control System

International Journal of Applied Sciences and Smart Technologies
Volume 5, Issue 2, pages 345-354
p-ISSN 2655-8564, e-ISSN 2685-9432

The research control system utilizes Arduino Uno to monitor the quality of water intake. Water quality is controlled by monitoring the pH level within the range of 6.5 – 7 using the I2C serial pH sensor and the electronic conductivity within the range of 2 – 2.1 ms/cm using the serial/I2C electrical conductivity sensor (EC). The water temperature within the range of 25 – 27 °C is monitored by the DS18B20 temperature sensor. The growth rate of Brazilian spinach is accelerated by turning on the Grow Light for 8 hours twice a day. Room temperature and humidity are controlled by activating the exhaust fan for 8 hours twice a day.

Observation of Brazilian Spinach Growth. This study involved ten Brazilian spinach (Alternanthera sissoo) plants, both in the research growth medium and the comparison growth medium. Water intake was controlled at pH 6.5 – 7, while nutrients A and B were controlled at EC 2 – 2.1 ms/cm. Data collection was performed twice a week over a seven-week period.

The plants exhibited significantly better growth in the research growth medium compared to the comparison growth medium, particularly in terms of width.

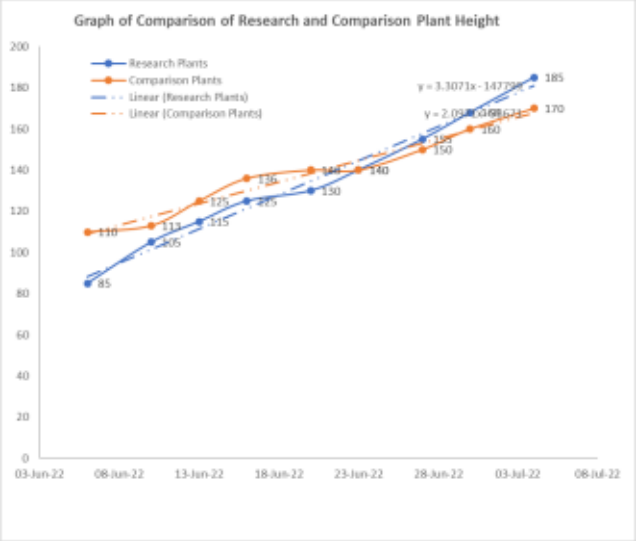


Figure 3. Height Comparison Graph between Research and Comparison Plants

Based on Figure 2, the height growth of plants in the research growth medium ranged from 85 mm to 185 mm, while in the comparison growth medium, it ranged from 110 mm to 170 mm. The graph indicates that plant height in the research growth

International Journal of Applied Sciences and Smart Technologies
Volume 5, Issue 2, pages 345-354
p-ISSN 2655-8564, e-ISSN 2685-9432

medium significantly caught up with that of the comparison growth medium after the fourth week.

Based on Figure 3, the width growth of plants in the research growth medium ranged from 130 mm to 210 mm, while in the comparison growth medium, it ranged from 108 mm to 150 mm. The graph shows that plant width in the research growth medium significantly outperformed that of the comparison growth medium.

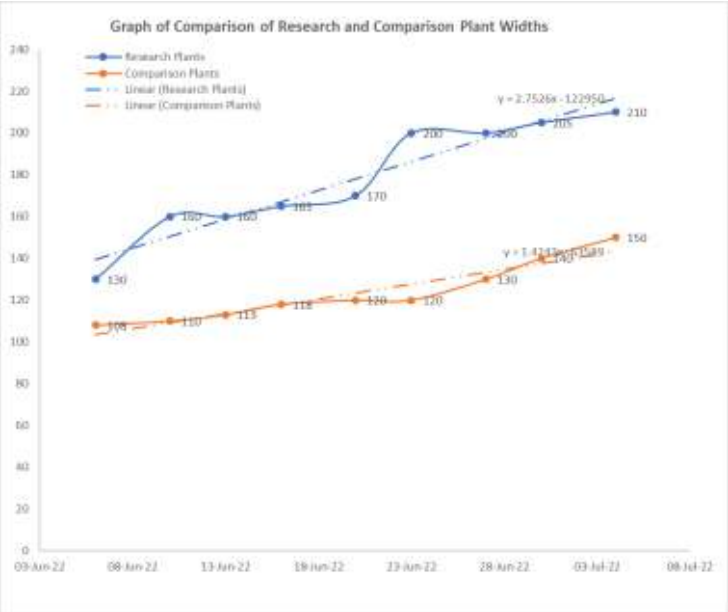


Figure 4. Width Comparison Graph between Research and Comparison Plants

4 Conclusions

In essence, the cultivation of Brazilian spinach through the control of nutrient and water intake quality in hydroponic systems is feasible and yields excellent results. Further research could explore other hydroponic plant varieties.

Acknowledgements

The research team would like to thank LPPM-USD which has provided an internal Research Grant with a Special Theme scheme, so that this paper on Cultivation investigation of Brazilian Spinach through Indoor Hydroponic System can be completed and the research can run smoothly.

Volume 5, Issue 2, pages 345-354

p-ISSN 2655-8564, e-ISSN 2685-9432

References

[1] R. D. Puspitasari, Pertanian Berkelanjutan Berbasis Revolusi Industri 4.0, Jurnal Layanan Masyarakat Universitas Airlangga, 3 (1) (2019) 26–28

[2] A. Kocian and L. Incrocci, Learning from Data to Optimize Control in Precision Farming, Stats, 3 (2020) 239–245.

[3] H. Willer, B. Schlatter, J. Trávníček, L. Kemper, and J. Lernoud, The World of Organic Agriculture Statistics and Emerging Trends 2020, FiBL & IFOAM – Organics International 2020: The World of Organic Agriculture. Frick and Bonn, (2020).

[4] A. Supriyanto and Fathurrahmani, The prototype of the Greenhouse Smart Control and Monitoring System in Hydroponic Plants, Jurnal Teknologi Informasi & Komunikasi Digital Zone, 10 (2) (2019) 131-143.

[5] K. A. Patil, N. R. Kale, A Model for Smart Agriculture Using IoT, International Conference on Global Trends in Signal Processing, Information Computing and Communication, (2016) 243-245.

[6] A. Vinayak.T. and Y. J. M Shirur, Automatic Control for Greenhouse Farming, International Journal of Engineering Research & Technology (IJERT), 6 (9) (2017) 192-197.

[7] C. L. C. Ruiz and D. A. V. Capacho, Automatic Control of Micro Climate in The Green House for Efficient Drying of Cocoa Beans, Colombian Magazine of Advanced Technologies, 2 32 (2018) 104-108.

[8] C. Cambra, S. Sendra, J. L. R. Lacuesta, Smart System for Bicarbonate Control in Irrigation for Hydroponic Precision Farming, Sensors,18 (5) (2018) 1333.

[9] M. S. Azizi, M. L. Hasnaoui, Multi-Level LEACH protocol for Homogeneous Wireless Sensor Network, International Journal of Engineering Research & Technology (IJERT), 6 (9) (2017) 73-76.

[10] L. Goswami, Wireless Water Pump Control for Farming, International Journal of Innovative Technology and Exploring Engineering (IJITEE), 8 (12S) (2019) 238-240.

Volume 5, Issue 2, pages 345-354

p-ISSN 2655-8564, e-ISSN 2685-9432

[11] Bayu WN, Tabel PPM dan pH Nutrisi Hidroponik, hidroponikpedia, www.hidroponikpedia.com, (2016)

[12] I. Setiawati and B. Harsono, Sistem Hidroponik Berbasis Internet of Thingshydroponic System Based on Internet of Things, Dielektrika, 7 (2) (2020) 82-87.

[13] H. Singh and D. Bruce, Electrical Conductivity and pH Guide for Hydroponics, Division of Agricultural Sciences and Natural Resources - Oklahoma State University.(2016)

International Journal of Applied Sciences and Smart Technologies

Volume 5, Issue 2, pages 355–364

p-ISSN 2655-8564, e-ISSN 2685-9432

Analysis of Spiral Pump Discharge Based on Simulation of Fluid Flow in Hoses

Hengky Luntungan[1, *], Stenly Tangkuman [1], I Nyoman Gede[1]

[1]Mechanical Engineering Department, Sam Ratulangi University,
Jl. Kampus Unsrat, Bahu, 95115, Indonesia
[*]Corresponding Author: st75@unsrat.ac.id

(Received 02-11-2023; Revised 05-11-2023; Accepted 16-11-2023)

Abstract

One of the uses renewable energy is the use of a spiral pump with a water wheel as the driving force. Spiral pumps are classified as environmentally friendly technology because they do not require electricity or fuel. The spiral pump consists of two main parts, namely the water wheel and the hose that is wrapped around both sides of the water wheel. The aim of this research is to analyze the water discharge of a spiral pump based on fluid flow simulation in the hose. This research utilizes advances in computational fluid dynamic (CFD) simulation methods using software. The determination method proposed in this research has been applied to a waterwheel model with a diameter of 1.2 m and a width of 0.6 m. For hoses, diameters of ½, ¾, 1, 1½, and 2 inches are determined, while the river flow speed is 0.9 m/s. For a hose diameter of 2 inches, the initial flow velocity in the hose is 0.38 m/s and the final velocity at the hose outlet is 0.452 m/s. The largest pump discharge was obtained at a hose diameter of 2.0 inches, namely 0.00183 m^3/s.

Keywords: spiral pump, water discharge, fluid flow, CFD

1 Introduction

Water is a basic need for living creatures, so the water supply is something that must always be available so that the survival of living creatures is to be maintained. However, during the dry season, farmers in rural areas struggle to obtain sufficient water for irrigating their fields. Although rivers are the primary source of water, the location of these water bodies, which are typically far from the rice fields and situated at a lower altitude, poses a significant challenge.

To extract water from rivers, power is required and most farmers utilise mechanical pumps as the power source for this task. However, the community's limited

This work is licensed under a Creative Commons Attribution 4.0 International License

Volume 5, Issue 2, pages 355–364
p-ISSN 2655-8564, e-ISSN 2685-9432

financial resources are an obstacle for people who want to use mechanical pumps because electricity or fuel is needed to operate the pump.

Therefore, renewable energy is needed that will not burden the community in terms of funding. In several places, renewable energy has been applied using solar panels as a source of electricity to operate mechanical pumps, but it is not yet efficient because the costs of purchasing, operating and maintaining solar panels are still relatively large.

Another use of renewable energy is the use of a spiral pump which was first made by H. A Wirtz in 1746 [1]. At that time, he used horsepower to drive the pump. The discovery was buried for about 240 years. Then it was picked up again and developed by Peter Morgan as an environmentally friendly technology with a water wheel replacing horse power as a pump driver. The use of spiral pumps can help the community, especially in the agricultural sector because spiral pumps do not require electricity and fuel.

The spiral pump comprises two primary components, namely the water wheel and the hose, which is coiled around the water wheel on both sides. The capacity of the spiral pump will be greatly influenced by the flow of fluid in the hose [2,3]. In this regard, it is unfortunate that no researcher has yet focused on the phenomenon of fluid flow in hoses and how it affects the capacity of spiral pumps. A search of literature shows that the researchers immediately built a model of spiral pump and then tested it in a river or in their laboratory [4-8]. Therefore, the relationship between the fluid flow in the hose and the water discharge of the spiral pump is still not clear [9-11]. Therefore, it is necessary to conduct research on the fluid flow in the hose of the spiral pump. This research aims to simulate fluid flow in a spiral pump hose and analyze the water discharge of a spiral pump based on fluid flow simulations in the hoses.

2 Methods

Figure 1 shows a flow diagram regarding outlining the capacity analysis of spiral pump through computer simulations proposed in this research. The model was created

Volume 5, Issue 2, pages 355–364

p-ISSN 2655-8564, e-ISSN 2685-9432

using computer aided design (CAD) software, while simulation utilized Computational Fluid Dynamics (CFD) software.

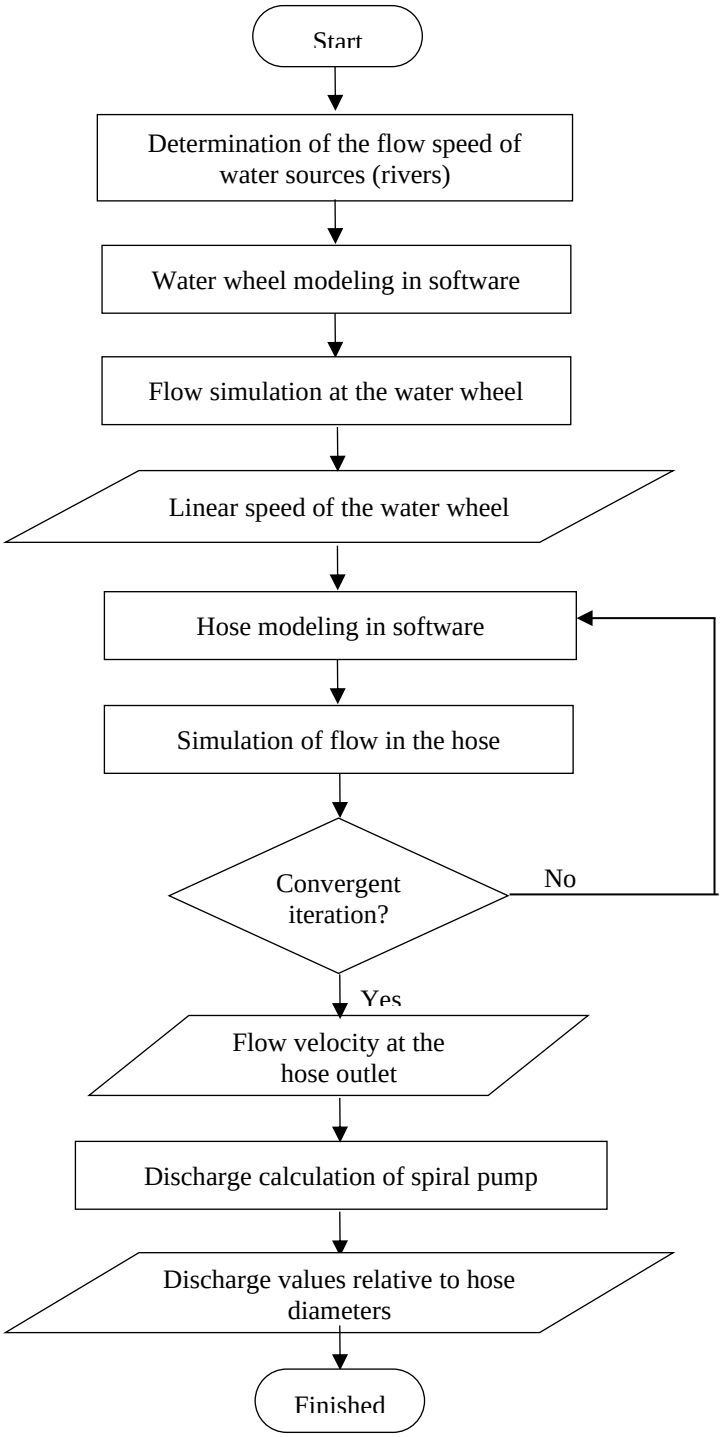


Figure 1. Flow diagram of spiral pump discharge determination

Volume 5, Issue 2, pages 355–364
p-ISSN 2655-8564, e-ISSN 2685-9432

Two simulations were conducted in this study; the first modelling fluid flow in a waterwheel, and the second is simulation fluid flow in a hose. The first simulation has two parts. The first produces the angular speed values of the water wheel, while the second produces the linear speed values of the water wheel. Next, the linier speeds are used as the initial flow velocity values in the hose during the second simulation.

The outcome of second simulation is the final flow velocity at the hose outlet corresponding to different hose diameter values. In the end, by using these simulation results, the water discharge values of the spiral pump can be determined.

3 Results and Discussions

3.1 Flow simulation at the water wheel

Figure 2 shows the results of water wheel modeling using CAD software. The diameter of the water wheel is 1.2 meters which has been adjusted to the depth of the river. The width of the wheel is 0.6 meters, while the mass of the wheel is 28.85 kg. For the wheel shaft, ASTM A36 steel is used. Steel alloy material for the wheel disc and wheel frame, while aluminum alloy is used for the pinwheel blade.

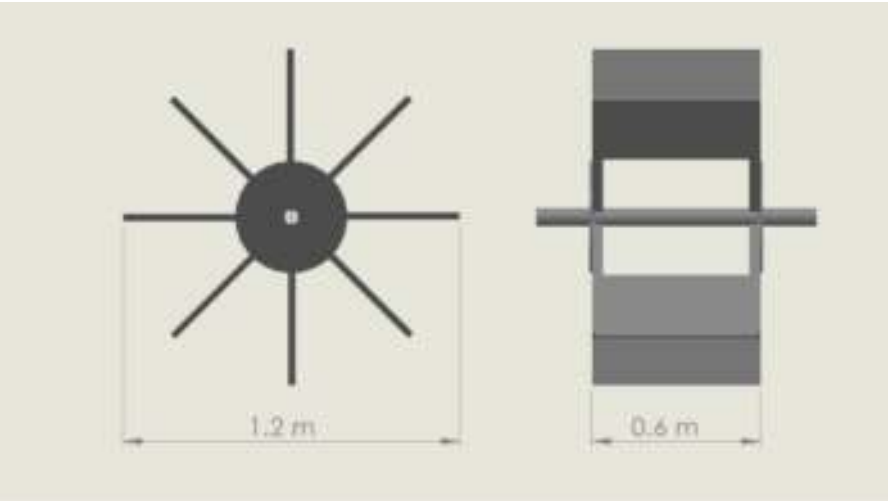


Figure 2. Water wheel model

International Journal of Applied Sciences and Smart Technologies
Volume 5, Issue 2, pages 355–364
p-ISSN 2655-8564, e-ISSN 2685-9432

The first simulation is a flow simulation on the wheel. Figure 3 explains the simulation results in the form of flow velocity values on the wheel blades at a certain time.

Next, Figure 4 shows the values of flow velocity at the wheel blade versus time. The linear speed of the water wheel increased from 0 to 1.2 seconds, then at 1.2 seconds, the linear speed of the water wheel stabilized at a value of 0.38 m/s. So, based on Figure 4 it can be seen that the linear speed of the water wheel is 0.38 m/s. This speed value is applied as the initial flow velocity in the hose.

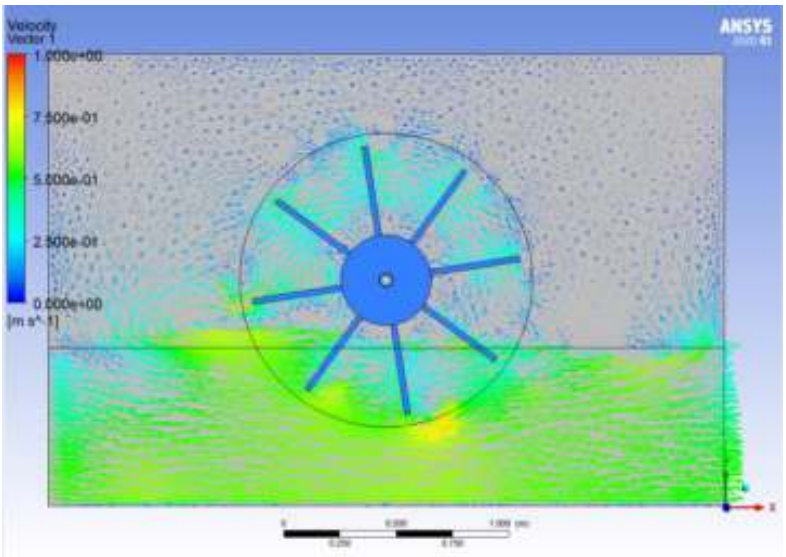


Figure 3. Flow simulation on the wheel

International Journal of Applied Sciences and Smart Technologies

Volume 5, Issue 2, pages 355–364

p-ISSN 2655-8564, e-ISSN 2685-9432

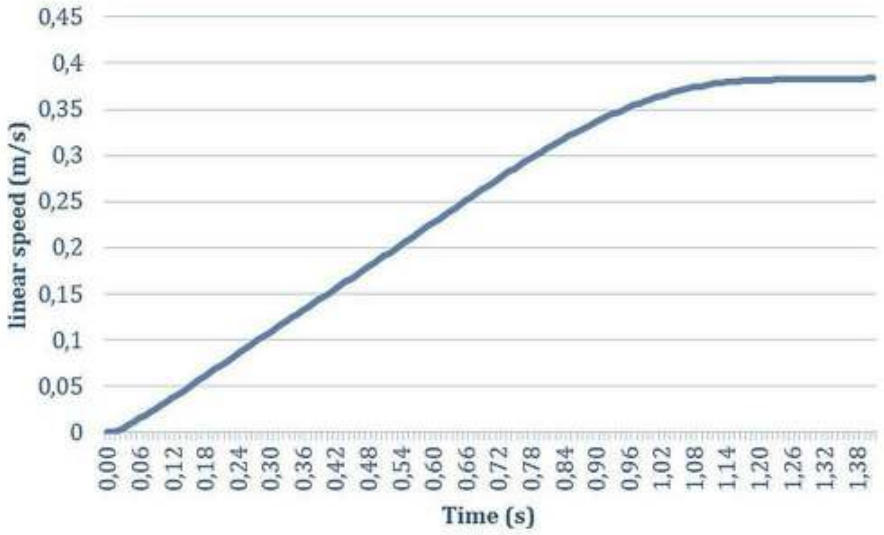


Figure 4. Graph of linear speed of the wheel against time

3.2 Simulation of flow in the hose

Figure 5 displays the results of modeling the hose of spiral pump. In this research, various hose diameter values were used, namely ½, ¾, 1, 1½, and 2 inches. Figure 6 shows the flow velocity value at outlet of ½ inch diameter hose. Based on the simulation results, the maximum velocity of fluid flow at the hose outlet is 0.538 m/s. In the same way, speed values for other hose diameters are obtained.



Figure 5. Model of the hose

International Journal of Applied Sciences and Smart Technologies

Volume 5, Issue 2, pages 355–364

p-ISSN 2655-8564, e-ISSN 2685-9432

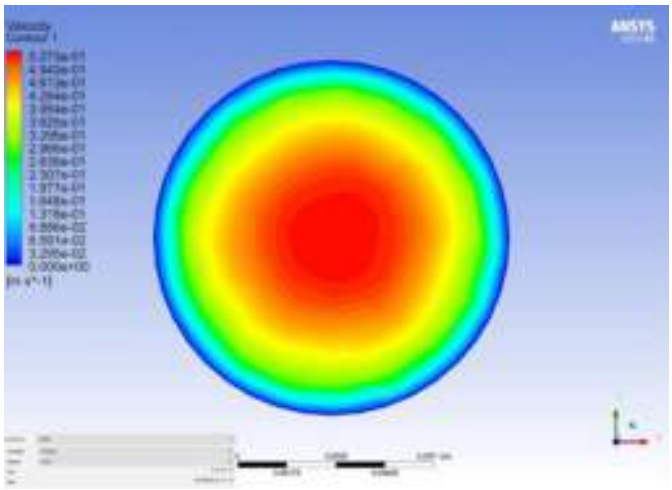


Figure 6. Flow velocity distribution at the hose outlet with a diameter of ½ inch

3.3 Discharge calculation of spiral pump

Discharge of spiral pump can be calculated based on the flow velocity at the hose outlet and the diameter of the hose. Figure 7 explains the distribution of pump discharge values relative to hose diameter. The hose diameter values are 0.5, 0.75, 1.0, 1.5, and 2.0 inch.

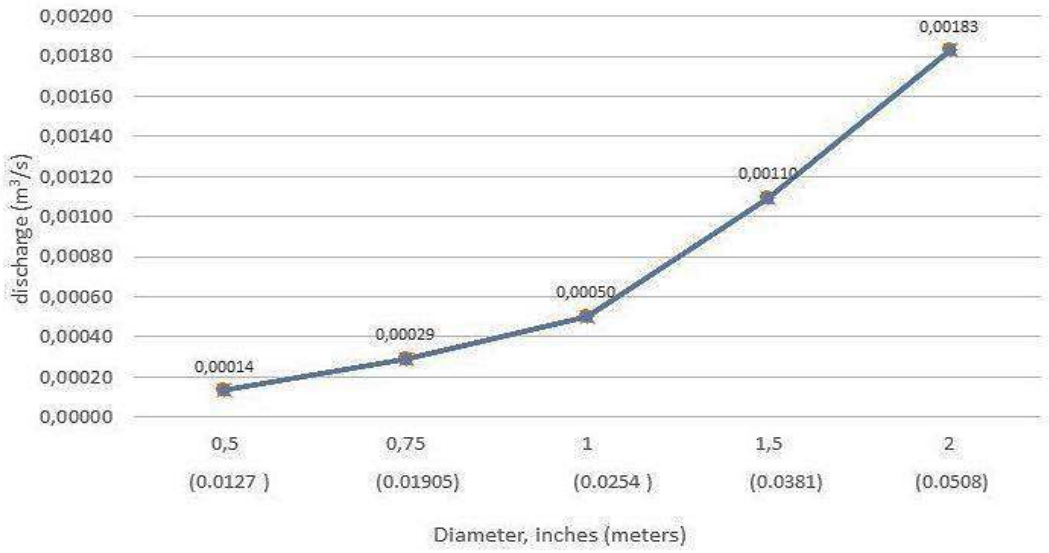


Figure 7. Pump discharge versus hose diameter

Based on Figure 7, it is known that the hose diameter greatly influences the performance of the spiral pump. Specifically, the increase in pump discharge relative to hose diameter follows a parabolic curve. The largest pump discharge was obtained at a hose diameter of 2.0 inches, namely 0.00183 m^3/s.

4 Conclusions

This research produces several conclusions as follows. Determination of the spiral pump discharge based on CFD simulation is carried out through two simulations, namely simulating the flow at the water wheel and simulating the flow in the hose of spiral pump.

The determination method proposed in this research has been applied to a water wheel model with a diameter of 1.2 m and a width of 0.6 m. For hoses, diameters of ½, ¾, 1, 1½, and 2 inches are determined, while the river flow speed is 0.9 m/s.

For a hose diameter of 2 inches, the initial flow velocity in the hose is 0.38 m/s and the final velocity at the hose outlet is 0.452 m/s, while the resulting pump discharge is 0.00183 m/s.

Acknowledgements

This research was funded by Sam Ratulangi University (PNBP Unsrat 2023) through a research scheme of Unsrat (RDUU K2).

References

[1]. P. Tailer, The Spiral Pump A High Lift Slow Turning Pump, https://lurkertech.com/water/pump/tailer/, (1986)

[2]. P. Priyankkumar R.,et all, Design of Spiral Tube Agriculture Water Wheel Pump. International Journal of Applied Research in Science and Engineering, (2017) 560-565.

[3]. S. H. Patil et al, A Review Paper on Spiral Tube Water Wheel Pump, International Journal of Advance Research in Science and Engineering, 6(8) (2017) 1123-1125.

Volume 5, Issue 2, pages 355–364

p-ISSN 2655-8564, e-ISSN 2685-9432

[4]. M. Anas and G. Rubiono, Spiral Pumping Wheel Turbine Application Concept for Irrigation with Different Altitudes, Gandrung: Jurnal Pengadian Kepada Masyarakat, 3(2) (2022) 626-632.

[5]. D. Eddisney, C. Trinchet and J. Vargas, Design and Simulation of a Spiral Hydraulic Pump Based on Multi-Objective Optimization, ARPN Journal of Engineering and Applied Sciences, 15(5) (2020) 657-663.

[6]. R. Eko, A. F. Hanafi, I. G. N. A. S. Prasetya D.Y., and E. Priyadi, Design And Manufacture of Undershot Waterwheel as A Spiral Pump Driven for Agricultural Irrigation, SJMEkinematika, 8(1) (2023) 13-24.

[7]. D. Prabhu and N. Aarya, Performance Analysis of Four Scoop Water Wheel Spiral Pump, Internasional Journal of Engineering Research & Technology, 5(3) (2016) 832-834.

[8]. L. M. Djun, J.Y.Chan, J.Ling and P.S.Lee, Design and Development of Zero Electricity Water Pump for Rural Development, Universal Journal of Mechanical Engineering, 7(6)(2019) 441-449.

[9]. K. Fanesh, J. Sinha and Kamalkant, Development and Testing of a Spiral Type Water Wheel Pumping System, Internasional Journal of Current Microbiology and Applied Sciences, 9(5) (2020) 3061-3069..

[10]. S. R. Gilang and H. Luntungan, Numerical Simulation of Fluid Flow in a Penstock Using Computational Fluid Dynamics (CFD) (in Indonesian). Jurnal Online Poros Jurusan Teknik Mesin Universitas Sam Ratulangi, (2014) 77-88

[11]. P. S. Prabowo, S. Mardikus and E.C. Eukharisto, Heat Transfer Characteristic on Wing Pairs Vortex Generator using 3D Simulation of Computatinal Fluid Dynamic, International Journal of Applied and Smart Technologies, 3(2) (2021) 215-224.

International Journal of Applied Sciences and Smart Technologies

Volume 5, Issue 2, pages 355–364

p-ISSN 2655-8564, e-ISSN 2685-9432

This page intentionally left blank

International Journal of Applied Sciences and Smart Technologies

Volume 5, Issue 2, pages 365–366

p-ISSN 2655-8564, e-ISSN 2685-9432

AUTHOR GUIDELINES

Author guidelines are available at the journal website:
http://e-journal.usd.ac.id/index.php/IJASST/about/submissions#authorGuidelines

International Journal of Applied Sciences and Smart Technologies

Volume 5, Issue 2, pages 365–366

p-ISSN 2655-8564, e-ISSN 2685-9432

This page intentionally left blank